Investigating the effect of a 3D physical microenvironment on hepatocyte structure, function, and adhesion signalling

CHHATWAL, ALISHA,KAUR

School of Biological and Biomedical Sciences

Investigating the Effect of a 3D Physical Microenvironment on Hepatocyte Structure, Function and Adhesion Signaling

Alisha Chhatwal

A thesis submitted for the degree of Doctor of Philosophy

2015

Abstract

Presenting cells with a two-dimensional (2D) substrate, as is the case with traditional cell culture, causes them to aberrantly flatten out, and lose their characteristic cell shape. With the case of liver cells, their cuboidal cell shape is vital to cell-specific functions, such as xenobiotic metabolism. Accordingly, culturing hepatocytes in 2D may produce results that do not accurately reflect the behavior of such cells *in vivo*. Cells *in vivo* are in constant contact with the ECM across three dimensions whereas culturing cells in 2D monolayers will alter the geometry of the cell leading to cytoskeletal remodeling and aberrant polarisation. As the cytoskeleton is physically and biochemically linked to the nucleus, this change in cell shape will in turn change the gene expression profile of the cell, leading to differences in cell behaviours such as proliferation, differentiation, and tissue-specific function. Mammalian cells respond to changes in the chemical composition and dimensionality of their microenvironment through complex signalling events at adhesion sites along their membrane. Changes in the microenvironment can result in up/down regulation of integrins, and changes in signalling downstream of adhesion.

Using a commercially available highly porous polystyrene scaffold, a method was developed to propagate cells continually in 3D. This model has been used to analyse how long-term growth under 3D conditions affects cytoskeletal organisation and whether adhesion signalling differs between 2D and 3D maintained cells. Cells maintained in 3D show significant cytoskeletal re-organisation, and significant changes in cell morphology. 3D maintained cells generally adopt a more physiological morphology than 2D counterparts. These changes are amplified the longer the cells are maintained and propagated in 3D. In addition, these cells show a significant decrease in the phosphorylation of Focal Adhesion Kinase (FAK) and higher levels of α5β1.The differences in morphology and adhesion signaling between 2D and 3D maintained cells appear to lead to enhanced hepatic functionality. Under the conditions tested, 3D maintained HepG2s showed higher drug resistance to model xenobiotics, as well as generally higher levels of albumin, urea and glucose metabolism. 2D and 3D maintained cells also showed different levels of gene expression of key metabolic enzymes. As such, it could be argued that 3D propagation results in cells i*n vitro* more closely reflecting the activity of their counterparts *in vivo.*

Acknowledgments

I would like to acknowledge funding from the Biotechnology and Biological Sciences Research Council (BBSRC) and ReproCELL Reinnervate Ltd for funding this thesis.

I would also like to thank the following people:

My supervisor, Professor Stefan Przyborski, for supervision, support and guidance throughout the last 4 years;

Joanne Robson and Tim Hawkins for all their help and support with high-resolution imaging and microscopy;

All the members of both Lab 234 in Chemistry and Lab 4 in Biology who have made my PhD experience both enjoyable and highly memorable; including Bridie for all the support in the early years, Eleanor and Rosie for listening to my endless vents and passing over the wine, and Neil and Cole for providing endless comic relief and potentially hazardous distractions during ridiculously late evenings in the lab. Thank you all for keeping me sane.

Finally, thanks to my family and friends for going out of their way to provide whatever help and support they could, and for putting up with me during the whole process.

Declaration

The work described herein was carried out in the School of Biological and Biomedical Sciences or the Department of Chemistry, University of Durham, between October 2011 and September 2015. All of the work is my own, except where specifically states otherwise. No part has been previously submitted for a degree at this or any other university.

Statement of Copyright

Publications arising from this work

Chhatwal, A. & Przyborski, S. (2014) The effect of long-term 3D culture on cell morphology and behavior. In eCM 28(s4), page 22 (published abstract)

Chhatwal, A., Mold, R. & Przyborski, S. (2012). Continual propagation of cells in three- dimensional culture. In eCM 23 (s4), page 75 (published abstract)

Oral presentations:

The impact of a 3D growth environment on cytoskeletal organisation and focal adhesion signalling (2014) 16th Annual White Rose Biomaterials and Tissue Engineering Work in Progress Meeting, Sheffield, UK

The effect of long term 3D cell culture on cell morphology and behaviour (2014) Tissue and Cell Engineering Society conference, Newcastle, UK

The effect of long term 3D cell culture on cell morphology and behaviour (2014) Tissue Engineering and Regenerative Medicine International Society (EU COngree), Genoa, Italy

The effect of 3D propagation on cell morphology and behaviour (2013) 15th Annual White Rose Biomaterials and Tissue Engineering Work in Progress Meeting, Sheffield, UK

Poster presentations:

European Society of Biomaterials; Krakow, Poland (Aug 2015)

Gordon Research Conference (GRC): Fibronectin and Integrins, and Related Molecules; Tuscany, Italy (May 2015)

Quasi-Vivo Users Group Meeting: Advances in *in vitro* cell and tissue culture; Liverpool, UK (May 2013)

Cell Control in a Petri Dish Meeting; Nottingham, UK (Nov 2012)

Tissue and Cell Engineering Society National Conference, Liverpool, UK (Jul 2012)

White Rose Progress-in-Work Meeting; Sheffield, UK (Dec 2011)

Table of Contents

List of Abbreviations

2D	Two Dimensional
3D	Three Dimensional
5-FU	5 Flurouracil
APAP	Acetaminophen
ATCC	American Type Culture Collection
BSA	Bovine Serum Albumin
Col I	Collagen Type I
CYP450	Cytochrome P450
DAPI	4',6-diamidino-2-phenylindole
DMEM	Dulbecco's Eagle's Medium
DNA	Deoxyribonucleic Acid
DSF	Dorsal Stress Fibre
ECACC	European Collection of Cell Cultures
EDTA	Ethylenediaminetetraacetic Acid
ECM	Extracellular Matrix
ECN	Extracellular Matrix-Cytoskeleton-Nucleus
FA	Focal Adhesion
FAK	Focal Adhesion Kinase
FBS	Fetal Bovine Serum
FN	Fibronectin
GST-1	Glutathione-S-Transferase 1

H&E	Haematoxylin & Eosin
LD50	Lethal Dose 50
LSCM	Laser Scanning Confocal Microscopy
MEM	Minimum Eagle's Medium
MTT	3-(4,5-dimethylthiazol-2-yl)-2,5-diphenyltetrazolium bromide
NGS	Normal Goat Serum
PBS	Phosphate Buffered Saline
PDL	Poly-D-Lysine
PFA	Paraformaldehyde
pFAK	phosphorylated Focal Adhesion Kinase
polyHIPE	polymers made by High Internal Phase Emulsion
RNA	Ribonucleic Acid
SEM	Standard Error of the Mean
SIM	Structured Illumination Microscopy
TA	Transverse Arc
TCP	Tissue Culture Plastic
VSF	Ventral Stress Fibre

Chapter 1: Introduction

1.1 Literature Review

1.1.1 Background

Most of our current understanding of the biological mechanisms that regulate key cellular behaviours such as proliferation, differentiation and migration, has come from studies conducted on cells cultured in two dimensions (2D) – usually glass of plastic surfaces. However, in the last few decades, cell biologists have come to realize that the disparity between these artificially flat surfaces, and the complex three-dimensional (3D) topologies that cells navigate and exist in *in vivo* may lead to a parallel disparity in key observation of cellular functionality. This has led to the advent of new technologies and methodologies that enable cells to exist *in vitro* within 3D culture environments that actively mimic the microenvironment that cells experience in native tissue. As these methodologies become more widespread in biological research, it is vital that we identify exactly which features of these 3D culture systems are most significant, and specifically what mechanisms underlie the adaptation of cells to a novel 3D microenvironment. This project focuses on outlining key changes in cell morphology, adhesion and signalling brought about by 3D cell culture systems and characterising the mechanisms by which these changes result in enhanced cellular functionality.

It is well established that cells are dynamic units that adapt to their environments by responding to local biochemical and geometric cues and signals; this interaction between a cell and its microenvironment affects cell proliferation, differentiation and behaviour [1]. When cells are removed from their native *in vivo* state and cultured on conventional two-dimensional (2D) plastic-ware, they undergo cytoskeletal reorganisation and artificially flatten, divide aberrantly and lose their differentiated phenotype [2]. This change in morphology directly affects a cell's ability to function and as such can lead to artificial results far removed from the in vivo state. As well as this flattening, when cells are grown in 2D monolayers, a large proportion of their surface area is exposed to either the plastic growth substrate or the growth medium, leaving very little opportunity for cell-cell contact. Biochemical interactions between neighbouring cells is vital to most advanced tissue functions and again results in behaviours that bare little resemblance to the natural state. These consequences of cytoskeletal remodelling mean that conventional 2D biological models of health and disease

states may not be representative of physiology, thus drastically reducing their value to research.

One area of particular importance is pharmaceutical research, which relies heavily on the ability to accurately model liver functionality in order to truly appreciate drug metabolism and toxicity. Approximately 80% of the human liver volume is composed of hepatocytes, a complex cell type that is responsible for, amongst other functions, xenobiotic metabolism [3]. Thus, hepatocyte cell culture forms a large and vital part of pharmaceutical research, especially in the early stages of drug screening and discovery. It is crucial that hepatocytes are accurately modelled so that drug toxicity can be detected early on in the drug development pipeline. Hepatocytes, however, exhibit functional polarity and as such any changes in their shape will drastically affect their behaviour. When these cells are cultured in 2D, they flatten and lose their characteristic cuboidal morphology, and this leads to decreased liver-specific functionality such as albumin production and CYP450 expression.

Models that enable hepatocytes to grow in three dimensions for long culture periods would potentially allow for increased liver-specific functionality, and thus more physiological modelling of the native liver.

1.1.2 Cell culture

1.1.2.1 The history of cell culture

The process of culturing cells *in vitro* can be dated back to 1907, when Harrison explanted pre-differentiated amphibian neural tissue in a drop of lymph hanging upside down from the surface of a coverslip [4]. He reported that it was possible to use this set-up to constantly monitor tissue growth and differentiation outside of the body – this was the first time that living tissue had been grown and observed *in vitro* [5]. In 1910, Burrows adapted this method, which would become known as the 'hanging drop' method, for use with warm-blooded tissue, and along with Carrel, advanced the field of culturing cells throughout the twenties [6]. However, it wasn't until 1951 that the field truly took off. In this year, Gey cultivated the first immortal cell line, HeLa, from the biopsy of a cancer patient called Henrietta Lacks [7], and with this the idea of immortalised cell-lines was born. With the development of the first chemically defined media by Eagle in 1955 [8], cell culture as a technique for studying

biological activity was established, and the next few decades saw many rapid advances bringing us to our current standard methodology for culturing cells *in vitro*.

1.1.2.2 The current standard of 2D cell culture

Cells are typically grown as a monolayer on a flat surface, most commonly in culture flasks or sometimes Petri dishes or glass coverslips [9]. The cells are incubated with standardized medium as a source of nutrition and maintained at body temperature (37°C). Medium is often supplemented with bovine serum to aid cell growth. When cells reach appropriate confluency (which refers to the proportion of the growth surface that is covered by cells) they are sub-cultured so as to avoid complications from senescence or nutrient-exhaustion. To sub-culture, adherent cells are enzymatically cleaved from the bottom of their culture dish (typically with trypsin EDTA) and an aliquot of the cell suspension is re-seeded into a flask for continued growth of the cell line. In this way cells can be maintained indefinitely *in vitro*.

Animal cell culture has been an invaluable tool in biology and biomedical sciences, and is considered to be a reliable, robust and crucial methodology [10]. One of the areas that cell culture has been particularly useful is in the pharmaceutical industry and preclinical drug testing.

1.1.2.3 The use of cell culture methods in drug discovery

The discovery, design and development of all new drugs usually follows a predictable timeline [11], which is indicated in the pipeline in Figure 1.1. Typically a potential biological target is identified and, with the aid of *in silico* molecular modelling, lead compounds are designed, developed and optimised. Preclinical screening is then performed against large compound libraries to establish which members of the library exhibit therapeutic efficacy towards the target in question. Using *in vitro* analyses of appropriate cell line models, certain drug parameters are determined, including toxicity, pharmacokinetics, absorption, distribution, metabolism and excretion properties. This stage of testing is fundamental in determining the basic safety and potential usefulness of the drug. Molecules that successfully pass through this stage then enter animal testing, human clinical trials and eventually make it onto market.

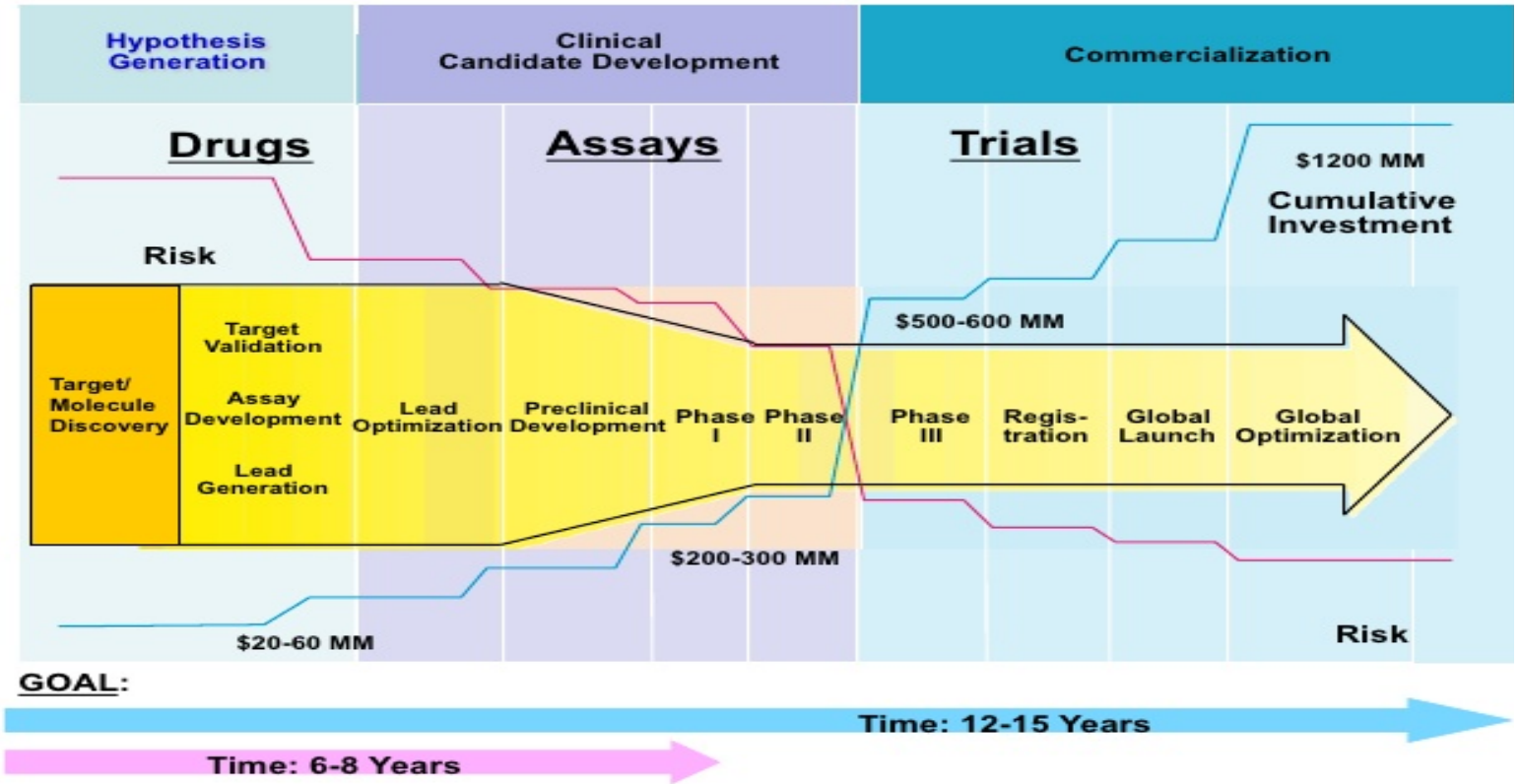

Figure 1.1 Drug discovery and development follows a characteristic pipeline of stages

Developing a new therapeutic molecule tends to follow a predictable timeline. Initial stages involve generating a hypothesis, outlining possible biological targets, and choosing the molecule with the most potential to take forward a lead compound. At these early stages, the risk is low in terms of both time and financial investment. Experiments at this level usually involve *in vitro* analyses using cell-lines or cultured primary cells. After preclinical development, studies shift to animal, and later human models. At this stage, the risk escalates, as these studies cost hundreds of millions of dollars. Eventually, once a drug has passed through these trials, it is released onto the market. At this point, for the typical drug, the process has taken roughly 12-15 years and cost roughly $1.2bn dollars. Image taken from a presentation: Doroshow, J.H., NIH, 16th Annual Drug Discovery Symposum, Northwestern University, Chicago IL, Oct 12 2011

Using anti-cancer drugs as a representative example of a pharmacological pursuit, there has been an increase in the number of potential anti-cancer agents being advanced through the drug development pipeline in the last ten to fifteen years [12]. However, the percentage of these molecules that progress successfully through to market is less than 10% [13]. Lack of clinical efficacy and unacceptable levels of toxicity are the two leading causes of drug failures during development [14,15]. Because of the high costs (up to US$1.2bn) in getting new drugs to market and the fact that many oncology drugs in particular fail during phase III human trials, which is the most expensive phase of clinical development, [16,17], it is crucial that compounds that are ineffective or toxic are dismissed as early in the testing process as possible, preferably in the initial *in vitro* stages before animal testing. It is therefore necessary to improve the accuracy of *in vitro* cell-based testing methods for more reliable prediction of drug efficacy and safety [18].

For *in* vitro assays to produce reliable and bio-medically relevant data, it is necessary that the cells accurately mimic the phenotype of cells within the target tissue [19, 20]. Conventionally, 2D cell culture is used in *in vitro* drug testing; however there are several limitations of 2D that curtail the effectiveness of these methods. These limitations include the lack of cell-cell and cell-matrix signalling that occurs in the 3D *in vivo* environment – these signals have been shown to be essential in regulating cell proliferation, differentiation, and specialised function [21, 22]. It stands to reason that 3D cellular assays would be more reflective, and thus predictive, of *in vivo* events compared to more simplified 2D cultures that may exhibit compromised signalling and specialised function [23]. The use of 3D *in vitro* systems in drug research and development has, therefore, been suggested as a potential link to bridge the gap between monolayer cultures and animal model studies [24].

In a landmark paper in 1997 [22], Bissell demonstrated that blocking antibodies against the β1 cell surface integrin subunit could reverse the malignant phenotype of human breast cancer cells in 3D cultures (Figure 1.2) and *in vivo* – a finding that had never been shown in previous studies using 2D models. In this paper, both non-malignant HMT-3522 breast cells and malignant HMT-3522 type cells were grown in 3D using Matrigel. The non-malignant cells formed organised, polarised acini, similar to those found in healthy breast tissue *in vivo*. The cancerous cells, however, formed disorganized, unstructured aggregates. Treatment of the normal cells with these inhibitory antibodies against β1

integrin (an integrin previously shown to be over-expressed in breast cancer [25]) resulted in apoptosis, but treatment of cancerous cells resulted in a reversal of the malignant phenotype back to the normal cell type, where cells appeared to re-model their cytoskeletons, adopt normal morphologies, and follow healthy growth patterns. Tumour cells were also injected into nude mice post treatment with the inhibitory antibodies and the mice showed a reduction in the number and size of tumours. This effect of blocking the β1 integrin on cancer progression has not been reproducible in 2D culture models [26], indicating that extracellular cues can affect cellular phenotype and behavior.

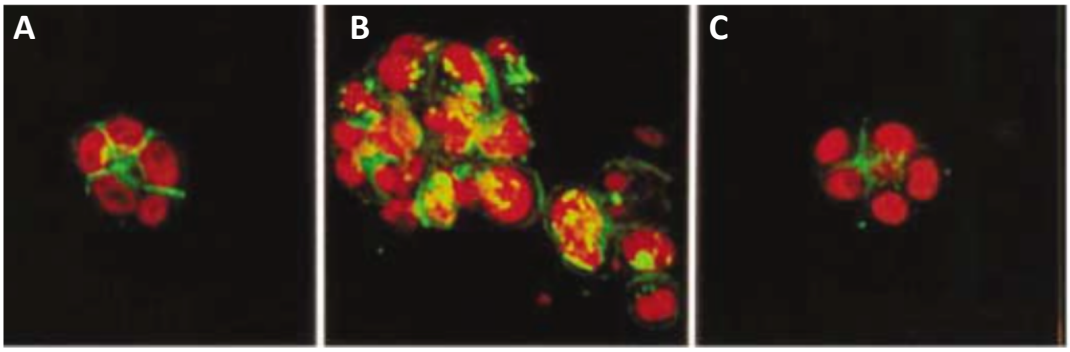

Figure 1.2 3D culture models allow for observations not seen in traditional 2D models

Bissell and colleagues grew both non-malignant (a) and malignant (b) breast carcinoma cells in 3D spheroids. Treatment of malignant cells with a blocking antibody (c) against β1 integrin resulted in a conversion back to the non-malignant state. This is a finding that was not shown in previous 2D studies and indicates how 3D cell culture is vital in accurately modelling complex cellular behaviours [22]

This paper not only demonstrates how different biological results can be seen in 2D and 3D cell culture, it also highlights how 3D culture can be beneficial in identifying possible drug targets for discovery and development – indeed integrins are now considered a major target for chemotherapeutic drugs [27]. Another example of how the difference in cell shape between 2D and 3D cells has been shown to affect drug behavior was observed in the growth of human breast carcinoma cells that overexpress HER2, an oncogene found to be overexpressed in over 25% of all breast cancers [28]. SKBR-3 cells were grown in 3D spheroids using p-HEMA-coated plates or in 2D monolayers [29]. When the cells were treated with a fixed concentration of Trastuzumab (a monoclonal antibody that targets HER2), the 2D cultured cells underwent a 16% reduction in proliferation, whereas

proliferation in 3D spheroids was reduced by 48%. HER2 is a cell surface growth receptor, and thus the observation that drugs targeting this receptor have different effects in 2D and 3D cultures would indicate that there is possibly a difference in receptor signaling caused by 3D culture. And indeed, Pickl and Ries [30] concluded that 3D cultures are more representative of the HER2 signalling pathway in tumours *in vivo*.

Using the hanging drop method to generate 3D spheroids, Tung et al. [31] showed that transfected human epithelial carcinoma cells (A431.H9) grown in 2D and 3D show differences in viability when treated with the same concentrations of 5-fluorouracil (5-FU) and tirapazamine (TPZ). Following treatment with 5-FU, 2D cultures showed a 95% drop in viability, whereas 3D cells treated with the same concentration of the drug only showed a 25% drop, indicating that the cells in spheroids were more resistant to the anti-proliferative effects of 5-FU. These data show that the manner in which cells are cultured (i.e. 2D or 3D) can substantially alter the effect of a drug on the cells.

The striking differences seen between 2D and 3D cultured cells have led to researchers designing a multitude of different technologies that enable routine 3D cell growth.

1.1.3 Overview of 3D technologies

An overwhelming number of biomaterials, technologies and advanced culture methodologies have been developed for studying 3D cellular behaviours and matrix interactions. These roughly fall into two categories: scaffold-based and scaffold-free systems. Below is an overview of some of the more widely used 3D culture methods, and their advantages and disadvantages.

1.1.3.1. Aggregates/spheroids

Aggregate culture is a simple scaffold-free 3D culture system. When cells are seeded onto non-adhesive growth substrates, cells are encouraged to cluster and adhere to each other rather than adhering artificially to the substrate. In this way, they form aggregates that are self-organised and structurally supported by their own secreted ECM proteins [32]. Aggregates can also be formed by the hanging drop method (Figure 1.5), which is the

oldest documented method of 3D cell culture [33]. In this method, cells are cultured in suspension, and a drop of this suspension is placed on the lid of a cell culture disk. The cells are unable to adhere to the substrate and thus freely form spheroids at the apex of the media drop.

Hepatocytes grown in spheroid culture exhibit enhanced differentiated function and liver-specific gene expression when compared to 2D hepatocytes [34-36]. Aggregate culture also leads to prolonged survival and increased viability [37,38].

One of the major advantages of aggregate culture is that cells within the aggregates develop strong and biochemically complex cell-cell contacts. Because cell-cell and cell-ECM contacts more closely mimic the environment experienced *in vivo,* the resultant morphologies are also more physiological. In addition, 3D spheroids are comprised of cells in different stages of the cell cycle, usually including proliferating, quiescent, hypoxic and necrotic cells [39]. This cellular heterogeneity is far more realistic than the homogeneity found in monolayer cultures [40]. These factors, along with the biochemical and gaseous gradient that cells in the inner core of the aggregates experience, combine to create a physiologically relevant microenvironment for the cell. In terms of practical feasibility, these models are very easy to set up, and do not require specialist equipment or materials. This also makes them very cost-efficient. However, their simplicity is a double edged sword – because growth is limited to individual spheroids, it is impossible to mimic the complex structures seen *in vivo.* Attempts to add complexity to aggregates include the use of multi-cell aggregates – multi-cellular tumour spheroids in particular have led to ground-breaking work in the field of cancer research [reviewed in 41-43]. Another potential disadvantage is the lack of standardisation – aggregates formed by these methods are often a heterogeneous mix of sizes and shapes, and thus this method is not always replicable.

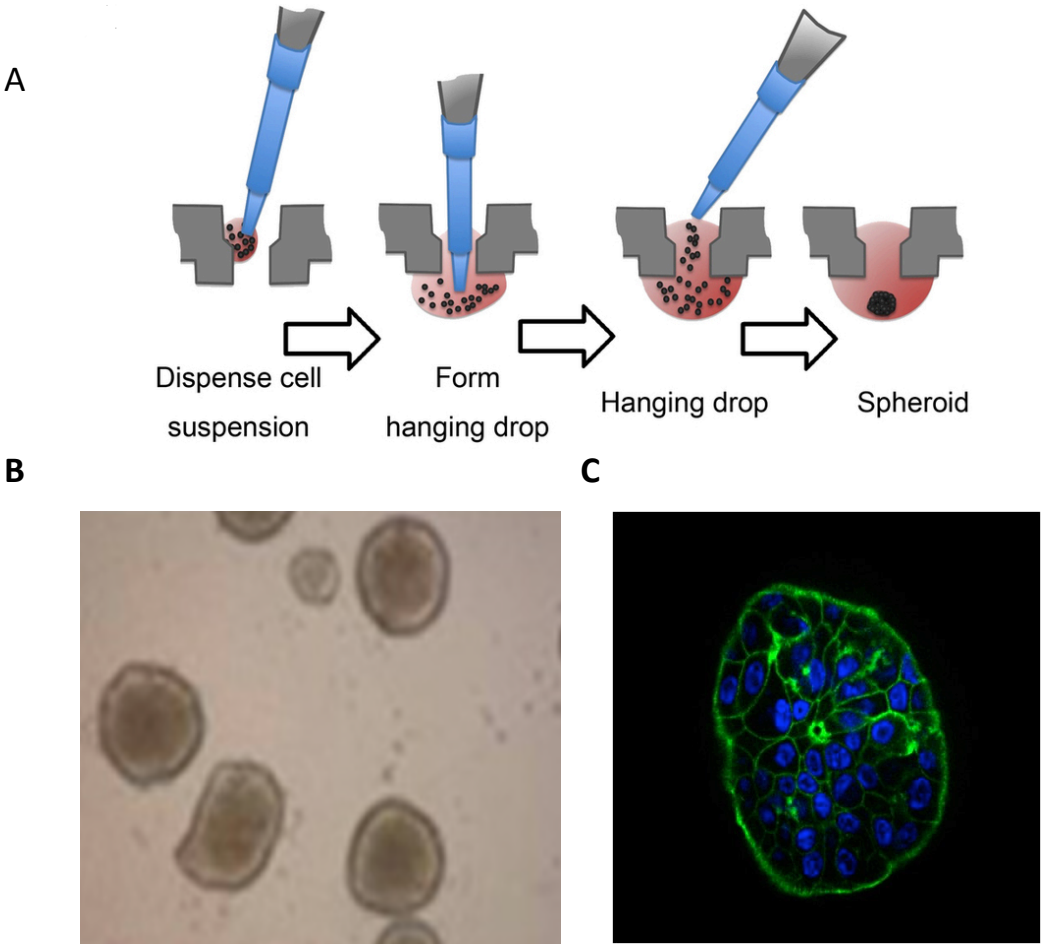

Figure 1.3 Cells can be grown in 3D as aggregates

A. The hanging drop method is one of simplest and oldest methods of 3D cell culture. Cell suspensions are left in droplet form, allowing cells to cluster as spheroids. Adapted from [44]
B. HepG2 spheroids growing in suspension. Image obtained from results of this thesis.
C. An example of human hepatocytes forming an aggregate. Green staining indicated F-Actin, and blue staining indicated individual cell nuclei. [45].

1.1.3.2 Hydrogels

Hydrogels can be derived from either natural or synthetic materials and can be used to immobilise cells within a 3D matrix that can be designed to mimic certain physical, mechanical or biochemical properties of the ECM *in vivo.* Cells are either embedded into the gel [46] or allowed to migrate into the interior zone of the gel after being seeded on top [47](Figure 1.4). Hydrogels can be composed of protein fibres or cross-linked polymer chains, and this initial ECM can be modified by the matrix that the cells themselves put out into the gel [48]. Because of their relative simplicity, hydrogels have been involved in a lot of the pioneering research into 3D culture systems. For example, Bissell and colleagues showed drastic differences in the way breast cancer cells grow in hydrogels compared to 2D monolayers [49,50]. Hydrogels continue to be a popular choice these days because they are simple and inexpensive while allowing the cells to grow in a permissive 3D environment. They are particularly useful when studying cells and tissues for which matrix stiffness is a key criterion for phenotype, e.g. osteoblasts, or for studying tissue wounding and repairing, since they closely resemble soft tissue [51]. They're also commercially available, allowing for standardisation across experiments

Agarose gels have been shown to sustain viability of primary murine hepatocytes for 3 weeks. Within these gels, hepatocytes typically form aggregates and secrete higher amounts of albumin than their 2D counterparts [52]. Shen *et al.* demonstrated that gel-entrapped hepatocytes demonstrated enhanced liver-specific functions and phase I metabolism and maintained higher intracellular ATP levels than those cultured in traditional 2D monolayer culture [53]. In addition, measurements of phase I metabolic enzymes were similar to levels found *in vivo*. Furthermore, gel entrapped cultures were able to accurately reflect hepatotoxicity in over twenty reference compounds [54].

However, mass transfer is an issue, especially in certain gels where the material is too dense for nutrient diffusion. Secondly, most hydrogels require an external change in state to induce gelation, such as a change in temperature, pH, or exposure to UV radiation. If cells are added to the material prior to gel formation, then these could all cause cell degradation, and a drop in cell viability.

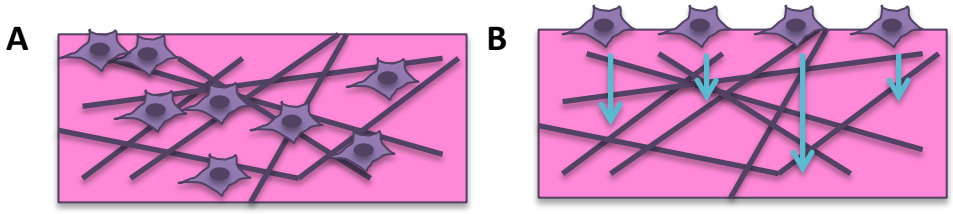

Figure 1.4 Cells can be encapsulated in hydrogels to allow for 3D growth

Hydrogels can be made from the meshwork of protein or polymer fibres. Cells can either be added to the mixture prior to gelation (A) or cells can be seeded on top of gels and encouraged to migrate through (B). Figure based on [55]

1.1.3.3 Electrospun scaffolds

Electrospinning is a technique whereby polymeric liquids from either natural or synthetic origins are converted into nanoscale fibres that intertwine to create a 3D mesh-like topography. These meshes can be formed from natural materials such as silk [56] or alginate [57], synthetic polymers like polycaprolactone [58], or a mixture of both [59]. The technique is highly versatile due to the wide range of input materials and thus can be used to create scaffolds of various compositions and architectures. The size and number of pores can be modified extensively allowing scaffolds to be designed for purpose. Biologics can also be incorporated into the polymer mixture in order to functionalise the scaffolds. This is particularly useful as a drug delivery method, and has been successfully used to control the release of antibiotics [60] and chemotherapeutic agents [61].

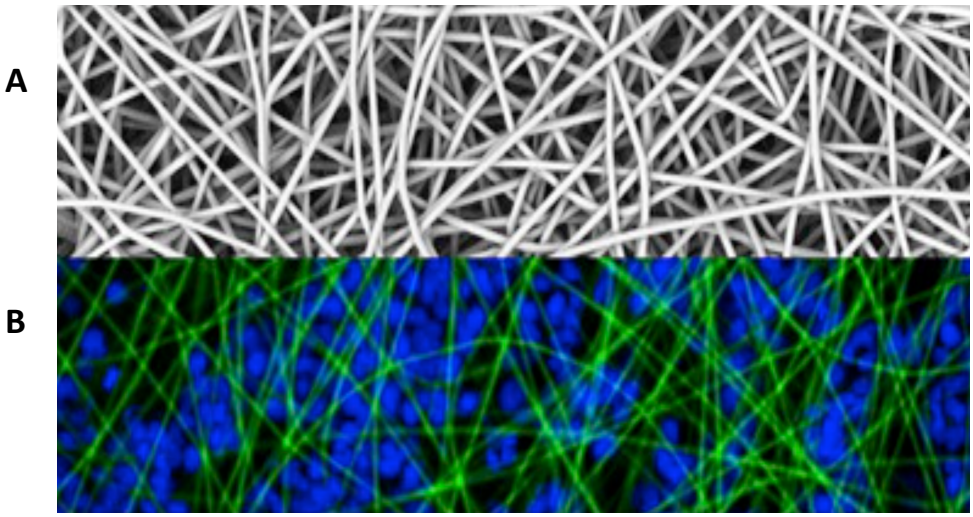

Figure 1.5 Electrospinning can be used to create a 3D mesh of fibres within which cells can grow in a 3D fashion

[A] Scanning electron microscopy can be used visualise the network of fibres that creates a complex 3D topography

[B] As an example, MCF7 breast cells within the Mimetix® electrospun scaffold. The green dye outlines the fibres, and the blue indicates the individual nuclei of cells.

Images taken from E.Hesiter, Elctrospinning Company UK (www.electrospinning.co.uk).

Hepatocytes, when cultured on scaffolds created by electrospinning, have been shown to come entrapped in the material. As such, they form spheroidal populations of hepatocytes that exibit increased cell-cell and cell-matrix interactions [62]. These scaffolds have been shown to enable enchanced hepatic functionality, such as albumin and urea synthesis and CYP450 expression [63]. These scaffolds have also been used to actively encourage stem cells down a differentiated hepatocytic lineage [64].

Finally, electrospun scaffolds can be created from biodegradable materials, using poly(lactic) acid and poly(glycolic) acid, allowing for translational biomedical research. For instance, Sun and colleagues used PLA fibres to grow human dermal fibroblasts in order to further work on human skin equivalents [65]. Electrospinning requires specialist equipment and training, however once this is set-up they are relatively easy and inexpensive to produce. However, cells can only grow at areas where fibres sufficiently overlap, and often there are large gaps between individual fibres which man that 3D growth tends to be as individual clusters dispersed throughout the material rather than consistent growth throughout the material. Although the mechanical properties of these scaffolds are occasionally poor, reducing their suitability for routine *in vitro* culture.

1.1.3.4 Porous polymer scaffolds

There are several different key ways of creating porous polymers including fibre bonding, particulate leaching, gas foaming, phase separation and emulsion templating.

Fibre bonding was one of the first methods used to create porous scaffolds. Briefly, a PLA solvent is cast over PGA fibres to create a composite. When heat is applied to this, the fibres bond at nodes of intersection, creating a mesh [66]. These scaffolds are highly porous, with large voids, and provide a physiological environment for cell growth [67]. However, the solvents used in fabrication can be toxic to cells. Also, the use of synthetic polymers adds a degree of artificiality to the surface topography.

Alternatively, in particulate leaching, a solution containing the polymeric material is cast over a mold that contains soluble beads known as porogens. Common porogens include paraffin spheres [68] and crystalline salts [69]. When the solvent is evaporated, the polymer-porogen compositive is washed to remove the porogen, leaving a porous sponge-like structure behind. Again this method produces porous material conducive to 3D cell growth. However residual salts can lower cell viability, and salt crystal size is hard to control and so void diameter is variable. Thus there is a high degree of inter-scaffold variability.

Another method of producing porous scaffolds is emulsion templating [70]. Typically, an internal droplet phase is added gradually to a monomeric continuous phase while mixing constantly, which produces an emulsion. The external phase wraps around the internal droplets to produce a polymer containing voids where the droplets originally were. During the polymerisation process, the thin external phase separating each internal phase droplet from its neighbouring droplets ruptures and these leave interconnecting holes between the voids. The resulting material is therefore highly porous and provides a complex 3D environment for cells to negotiate and invade. Usually these materials, termed polyHIPEs, are produced in monoliths, which can then be cut to size for cell culture. One such scaffold, and the material that will form the basis of the experiments in this thesis, is described by Carnachan et al [71]. The material is made from polystyrene, the same material as standard 2D culture-ware, making it directly comparable. The material is non biodegradable making it suitable for long-term *in vitro* studies, and it is commercially available under the name Alvetex® [72]. It has been used for the growth of a variety of cell types including osteoblasts [70], pluripotent stem cells [73, 74] and hepatocytes [75].

The reason that 3D culture methodologies have been so successful in drug discovery applications is because the main cells involved in metabolizing drugs in the liver, hepatocytes, exhibit specialized morphologies, as well as functional polarization. Hepatocytes grown on

plastic tend to attach poorly, show limited functionality, and die fairly quickly. This is because the cells aberrantly flatten [76]. Survival and function can be improved by growing these cells in complex 3D environments – these cultures show prolonged survival, enhanced differentiated function, and preservation of a normal near-cuboidal shape [77]. This is because these environments better reflect the native environment that hepatocytes exist in in the native liver.

1.1.4 Hepatocytes in cell culture

In order to fully understand the features of the 3D environment that reflect the native tissue, it is important to consider the anatomical context.

1.1.4.1 The Liver

The liver is the largest internal solid organ and the largest exocrine gland in the human body and it is essential for human survival. The liver is estimated to perform over 500 distinct functions. It is responsible for producing bile, which emulsifies and digests fats. It also plays a role in glucose metabolism: it converts glucose into glycogen for long-term energy storage, and converts glycogen back into glucose for immediate energy release. The liver also plays a role in immunity by removing microbes and parasites from the bloodstream, and synthesising blood plasma proteins involved in the immune response. However, its primary function is in drug/xenobiotic metabolism and detoxification [78].

1.1.4.2 Hepatocytes

The structural organisation of the liver closely mirrors its functional diversity. Hepatocytes are the functional units of the liver and exist within a complex, highly vascularised tissue architecture. Structurally, the liver is a triangular organ that is divided into four lobes: right, left, quadrate and caudate. Each lobe is made of thousands of individual lobules that are hexagonal in cross-section. At the centre of each of these repeating units is the central vein, from which extend hepatic plates that contain hepatocytes.

Within these hepatic plates, hepatocytes exist in a cuboidal geometry. They are polar epithelial cells roughly 20-40µm in size. Approximately 80% of the parenchymal volume, and 60-70% of the cell number in the liver is made of hepatocytes. The cells themselves are surrounded by a plasma membrane that is composed of specialised domains. Each hepatocyte is multi-polarised, carrying two sinusoidal (baso-lateral) and two canalicular (apical) membrane domains [79], as well as an intercellular (lateral) domain. The sinusoidal membrane exhibits 0.5µm long microvilli that project into the sinusoidal lumen to create an enhanced surface area for endogenous and exogenous nutrient uptake as well as blood exchange and waste drainage into the sinusoids.

The canalicular membrane is located at the apical pole of the hepatocyte and is roughly 15% of the entire cell membrane [80]. Invaginations of the membrane at the apex of two or three hepatocytes demarcate a specialised space termed the bile canaliculus. The primary role of these bile canaliculi is to provide a transport network for bile, but these structures also contain associated transporter proteins that play a role in the elimination of toxic metabolites created during drug metabolism. [81].

The lateral membrane extends from the bile canaliculus to the sinusoidal domain and thus represents the contact area between adjacent hepatocytes – as such it is the site for all intercellular communication between neighbouring cells. There are three main structures responsible for intercellular signalling: tight junctions, desmosomes and gap junctions. These structures are vital for maintain functional hepatic homeostasis, for instance gap junctions have been shown to play a controlling role in hepatocyte growth mechanisms [82] and inducing drug metabolising enzymes [83].

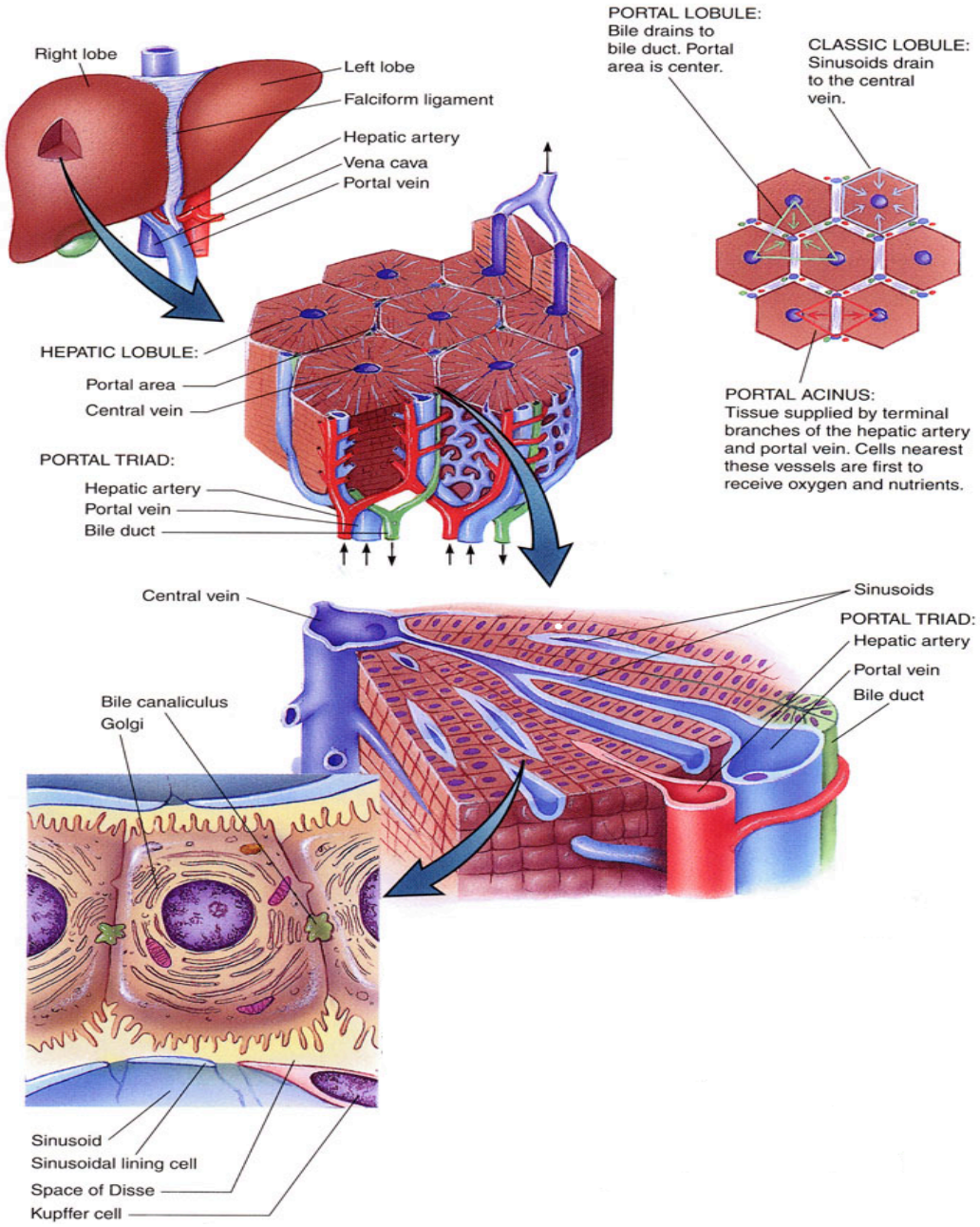

Figure 1.6 The architecture of the liver

The liver is a lobular organ made up of a right and left lobe. Each lobe is made of repeating lobules, which are hexagonal functional units that are richly vascularised. Within these lobules, the primary cell type of the liver, the hepatocyte, is arranged in thin hepatic plates, which run parallel to the sinusoids. Within each plate, the hepatocytes are cuboidal and tightly packed together in a regular conformation.

1.1.4.3 The importance of cell shape for hepatocytes

When primary hepatocytes are disaggregated from the liver and cultured *in vitro* on ECM coated substrates, or gels, cells assume a differentiated shape and express high levels of mRNA for liver-specific genes such as albumin [84, 85]. However, when hepatocytes are plated onto plastic growth substrates, they exhibit a de-differentiated, flattened shape due to the rigidity of the substrate [86]. With this flattened shape comes a sharp decrease in liver-specific gene transcription [87]. This dynamism between cell shape and function is the main concern of this thesis. In particular, how this relationship is controlled on a molecular level in a 3D culture system, and whether this can be manipulated in order to enhance liver functionality.

1.1.5 Regulation of the cell shape-function relationship

One of the most obvious differences when comparing cells grown in 2D and 3D culture systems is the drastic difference in morphology. Cells grown in a monolayer are flat, and while they are free to adhere and spread across a horizontal plane in the X and Y dimensions, they have no support to spread in the Z dimension. Consequently, they have a forced apical-basal polarity that can directly impact cell function, such as modulating the susceptibility of cells to apoptotic cell death [88]. Meyers et al., (2006) also found that artificial flattening of cells, such as in monolayer culture, alters the membrane:cytoplasm ratio of a cell, meaning that signalling from the surface is artificially propagated straight to the nucleus, since signals have a smaller distance to travel [89]. Since signalling pathways are fundamental to all cell functions, these findings show how strong the relationship is between cell shape and cell function. The dynamism between structure and function is a paradigm that can be seen across the scale of biology right down to the sub-cellular organelle level. Many specialised cells in the body require a precise structure in order to carry out their specific function. Tight regulation of the structure-function relationship is vital to a cell's continued survival. This regulation is achieved through what is termed the ECM-cytoskeleton-nucleus (ECN) axis [1]. Cells in vivo are embedded within a complex microenvironment consisting of the extracellular matrix (ECM), growth factors, and neighbouring cells. Cell adhesion to proteins in the ECM is mediated though specific cell surface receptors, including the integrin family of transmembrane proteins. Binding between these receptors and ECM proteins induces integrins to cluster into focal

adhesions. This then triggers a cascade of intracellular signalling events that cause changes in cell behaviour and gene expression (Figure 1.7).

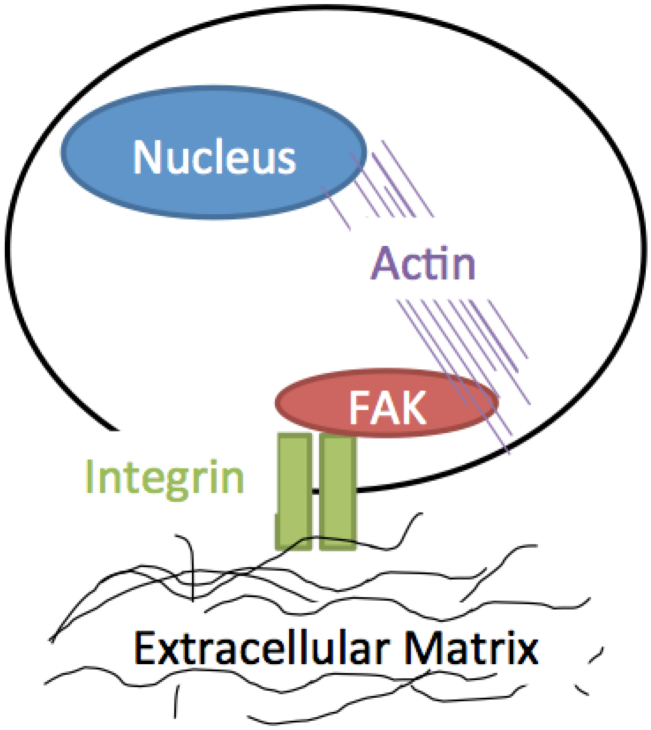

Figure 1.7 The extracellular matrix-cytoskeleton-nucleus axis

Environmental cues are translated into cellular behaviours through a physical and biochemical link mediated mostly by integrin receptors, and focal adhesion kinase (FAK) signalling. These adhesion sites provide a bridge from the cell exterior to the nucleus along the cytoskeleton, and thus they act as a control centre for regulating cell shape and function in response to cell geometry within the matrix.

1.1.5.1 The extracellular matrix (ECM)

The ECM is the non-cellular component present in all tissues, and it provides both physical scaffolding and biomechanical cues that are essential for tissue morphogenesis, cell differentiation and tissue homeostasis [90]. Though the ECM of all tissues share a generic make-up of water, proteins and polysaccharides, individual tissues and cells experience a unique ECM and topology that is generated through embryonic development. A further level of complexity is added when one considers that the ECM is also a dynamic structure that is constantly evolving and being remodelled depending on the body's state, and it's protein components are subject to a myriad of post-translational modifications. The ECM is mostly comprised of fibrous proteins, the three most significant of which are collagen, elastin, and fibronectin. Collagen is the most abundant protein in most ECMs, and most matrixes show a heterogeneous mix of different types. Collagens are responsible for mediating cell adhesion and migration, as well as directing tissue development [91], elastin provide recoil to tissues that need to undergo stretch and relax cycles [92] and fibronectin is mostly responsible for cell migration both during healthy development and tumour metastasis [91]. Fibronectin is also vitally important as a mechano-regulator, mediating changes in ECM topology [93].

Liver ECM is composed mostly of fibronectin, vitronectin, laminin, elastin and collagen type I [94]. The precise ratio of these components differs across the liver, but in the Space of Disse, which is the prime site for hepatocyte-matrix interactions, fibronectin is the predominant protein. Although ECM can be secreted by most of the cells of the liver, including hepatocytes, it is the stellate cell population that is responsible for the majority of ECM production.

Within the liver, the ECM plays a vital role in the modulation of many hepatocytic functions, including cell migration, differentiation and development. Since hepatocytes are anchorage-dependent cells, the ECM is crucial for maintaining cell structure and polarity [95,96].

The ECM directs morphological organisation of cells within a tissue through interacting with growth factors and cell surface receptors to elicit downstream signal transduction and consequently alter gene transcription. One such family of cell surface receptors are the integrins.

1.1.5.2 Integrins

The integrins are a ubiquitously distributed family of cell adhesion molecules (CAMs) that interact with a variety of ECM ligands including fibronectin, collagens and laminins. Since the ECM provides the physical microenvironment in which cells exist, it serves as a tissue scaffold, both guiding cellular migration during development and consequently ensuring that cells exist in their optimal geometry. Since integrins link the ECM to individual cells, they are involved in a range of fundamental physiological processes including embryogenesis, morphogenesis, wound repair, inflammation, and tumour-cell migration [97]. Structurally, integrins are large heterodimers of non-covalently associated larger α (120-180kD) and smaller β (90-110kD) units; in vertebrates, there are 18 different α subunits and 8 β subunits that assemble into 24 different functional receptors that exhibit different tissue distributions and varying binding affinities to different ECM proteins [98]. The α and β chains have large extracellular domains at the amino terminus that fold to form a binding pocket for their specific ligand. The chains then span the membrane through a short hydrophobic transmembrane region, and extend into the cytoplasm. The cytoplasmic tails are small, highly conserved, and interact with the actin cytoskeleton through actin linking proteins such as vinculin and talin. At sites where the carboxy-terminal of integrins interacts with the cytoplasm, there are binding sites for various signalling proteins that build up adhesion complexes after integrin clustering.

Some integrins, such as α5β1, the canonical fibronectin receptor, will only bind to one ligand in the ECM [99], whereas others have multiple binding partners [100,101]. Cells also often display multiple integrins capable of binding the same ECM ligand. In some cases, two integrins that bind to the same ligand will do so within different domains of that ligand [102], but some will actually bind the exact same region [103]. This overlapping and redundant expression, while seemingly paradoxical, is the reason that these molecules act as a control centre for cell-matrix interactions. The sheer number of possible computations of ligand-integrin complexes ensures that the cell can react to a number of different mechanical and biochemical cues from the environment, and adapt accordingly.

1.1.5.3 Adhesion sites

Focal adhesions are the sites where environmental cues are translated into intracellular biochemical signals [104]. The process by which external biomechanical cues are translated

into internal biochemical signals is called mechano-transduction, and this process is responsible for regulating all aspects of a cell's life, including proliferation, metabolism, migration, differentiation and death. Mechano-transduction occurs at adhesion sites, which are sites that build at the convergence of integrin adhesion, the actin cytoskeleton, and intracellular signalling [105]. There are three broad classes of adhesion: focal complexes, focal adhesions, and fibrillar adhesions [106]. When cells start to spread and extend lamellae, small ($<1\mu m^2$) puncta appear along the edges of lamellipodia. These integrin-mediated complexes are called focal complexes and are considered the temporal precursors to focal adhesions, which are the best-characterised and most abundant form of adhesion. Focal adhesions mediate strong adhesion to the substrate and they serve as docking sites for downstream signalling. Once focal adhesions are stable, the activated integrins translocate centripetally on lamellae towards the cell body – this translocation drives the formation of fibrillar adhesions, which apply tension to fibronectin and facilitate fibrillogensis. Focal adhesions are flat, elongated structures that are approximately $1\text{-}5\mu m^2$ and located preferentially towards the cell periphery or centrally at the end of stress fibres [107]. Structurally, these sites are large multi-protein complexes and a diverse group of signalling proteins have been found at focal adhesions – collectively these are known as the adhesome [108]. There are roughly 150 protein members of the adhesome, which share approximately 742 unique direct protein-protein interactions [109]. The sheer number and diversity of the proteins involved in these adhesion sites, and the "on/off" nature of protein-protein interaction, means that these sites allow the cell the opportunity to construct various different signalling complexes depending on the cues the cell is given, and this leads to diverse cell behaviours. Though these proteins, and their interactions are well characterised, it is unclear how the cell regulates these combinatorial interactions spatially and temporally, or how changes in the ECM composition and geometry alter the composition of these adhesion sites.

1.1.5.4 Focal Adhesion Kinase

One of the major signalling events that occur at focal adhesion sites is tyrosine phosphorylation. This phosphorylation provides docking sites for various adaptor proteins, while also blocking the binding of other sites, and as such could be viewed as the 'switch' that controls the on/off protein-protein interactions regulating cell behaviour. Within the adhesome, there are 9 kinases and 9 phosphotases that control the tyrosine phosphorylation

state of adhesion receptors, adaptors and actin-linkers [110]. One of the most significant of these kinases is Focal Adhesion Kinase (FAK), which can create docking sites for several different partners to control adhesion dynamics, cytoskeletal dynamics and cell behaviour.

Figure 1.8 Focal Adhesion Kinase

Focal Adhesion Kinase (FAK) is made of three domains: a FERM domain, a catalytic domain, and a FAT domain. These are connected by proline rich regions (PRR).

FAK is a 125kDa tyrosine kinase that localises to adhesion sites using a C-terminal FAT domain (Figure 1.8). This localisation is necessary for it's signalling function – FAK mutants that lack this targeting domain show limited auto-phosphorylation and limited kinase activity in response to integrin clustering [111]. FAK also contains an N terminal FERM domain that interacts with the β tail of certain integrins to control auto-inhibition. This domain is also important for mediating several key protein-protein interactions, and there is some evidence that the FERM domain also supports information transfer between the cell cortex and nucleus, thus controlling the link between the ECM and gene expression [112]. Additionally, FAK also has two proline-rich motifs that allow FAK to bind to the SH3 domain of p130Cas [113] and the LD2 domain of paxillin [114], both of which are phosphorylated following integrin binding and interact strongly with the actin cytoskeleton [115].

FAK is activated upon integrin engagement with ECM ligands, and this activation occurs through auto-phosphorylation at Tyrosine 397 (Y397). As integrins begin to cluster, FAK is targeted to these clusters by the FAT domain, and clustering of FAK then amplifies auto-phosphorylation at Y397. This site is a binding site for Src kinase, which phosphorylates FAK at two further tyrosine sites, Y576 and Y577, which activate FAK kinase activity [25]. Src also phosphorylates Y861 and Y925, which provide docking sites for SH2 domains. One of the most important SH2-bearing molecules is Grb2, which, once bound to FAK, activates Ras, which is turn activates Raf and thus links adhesion sites to the central MAP Kinase pathway [116]. This

pathway is a vital intracellular signalling pathway responsible for, amongst other cellular and tissue behaviours, embryogenesis, morphogenesis, cell differentiation, proliferation, and programmed cell death through apoptosis [117].

However, the signalling events at focal adhesion sites are a lot more complicated than it would seem on the surface. Although canonically, integrin-mediated phosphorylation of FAK and Src kinase appears to be the trigger event for the initiation of adhesion signalling, knock-out studies have shown that neither of these events is necessary for focal adhesion assembly. Genetic deficiencies of either protein do not prevent the formation of focal adhesions, but rather result in enlarged adhesions [118,119], suggesting that both proteins play a vital role in adhesion turnover, a necessary step for cell locomotion. From this it would appear that Src-FAK-mediated phosphorylation has dual, and seemingly conflicting, roles in regulating focal adhesion dynamics. The mechanism behind this is still unclear, but there is some evidence that suggests a role for Rho kinase (ROCK) and the RhoA pathway [120].

1.1.5.5 Adhesions in 3D matrices

Focal adhesions have been well characterised and extensively studied, but the majority of these studies have investigated cells plated on 2D tissue culture plastic-ware such as coverslips, culture flasks, well plates, and culture dishes. This is clearly a very different physiological environment than cells encounter *in vivo*. The major differences that are relevant in any discussion of adhesions sites are:

1) 2D plastic-ware is a much more rigid growth substrate than experienced within tissues, and as such there is often exaggerated adhesion [121]
2) Typical cells in tissue have almost 100% of the surface area exposed to either other cells or the matrix; in contrast, cells in 2D have approximately 50% of their surface area exposed to either growth media or the plastic-ware of the flask/dish [122]
3) Since cells in 2D grow in monolayers, they are only exposed to cells on two sides. Contrastingly cells in tissues share cell-cell contacts around their

entire perimeter, and as such these interactions are more numerous and complicated than those seen in 2D [123].

4) Growing cells in 2D, such as on coverslips or culture dishes imposes a different topology on cells, and thus the biophysical environment is different than experienced in tissue

The fact that focal adhesions have been characterised without considering these differences raises a significant question: do focal adhesions even exist *in vivo*, or are they simply artefacts of tissue culture? A paper in 2010 challenged the existence of any detectable cell adhesion structures in 3D collagen gels [124]. However, despite the existence of focal adhesions *in vivo* being questioned, research has shown that these structures do exist in tissue, but they're different to the sites characterised in the literature in several key ways. *In vivo* adhesion occurs when cells attach themselves to three-dimensional mesh-like fibrous networks, rather than 2D rigid plastic, which is relatively restraint-free. In 3D environs, cells have to negotiate, remodel and/or proteolytically cleave the physical scaffold in order to spread and extend. Thus cell spreading, takes hours, or even days, rather than the minutes it takes for a call to flatten in 2D settings [125]. Another key difference observed between 2D and 3D cellular adhesion is in the spatial and temporal distribution of integrin-mediated adhesions. One study used sandwich culture techniques to seed fibroblasts between two ECM mimetic gels so as to engage both dorsal and ventral integrin engagement [126]. The result was a loss of lamellipodia and an adoption of stellate-like phenotype with rich linearised extensions, much like the fibroblast morphology observed *in vivo*. There was also a reduction in the number and size of adhesions across the cell surface, and a reduction in the cell migration rate. The fact that these major changes were seen using the simplest of 3D systems shows that dimensionality alone can alter cellular responses. Focussing specifically on adhesion structures, there is now a growing body of evidence indicating that the composition, shape, and location of adhesion structures in 3D cells is drastically different to those seen in 2D cells. A landmark paper by Cukierman and colleagues [127] took human foreskin fibroblasts (HFF) and grew them on a variety of substrates including tissue- and cell- derived 3D matrices, 2D substrates coated with ECM substrates such as fibronectin and Collagen I, and mechanically compressed 3D matrices. They then probed these populations for key molecules found in 2D focal adhesions such as the integrin αvβ3, paxillin, vinculin, FAK, as well as those that define fibrillar adhesions such as α5β1 and tensin. They found that within the 3D cell systems, paxillin and α5β1 co-localised to unusual cell-matrix attachments, that neither fit the criteria for focal complexes, adhesions or

fibrillar adhesions. They thus proposed that there is a fourth type of adhesion that occurs exclusively in 3D systems – 3D matrix adhesions. The biggest differences between 2D and 3D adhesions they characterised were a shift in main integrin composition from αvβ3 to α5β1, and a lack of positive $pFAK^{Y397}$ staining localised to adhesion sites in 3D matrices. These changes are outlined in the schematic in Figure 1.9.

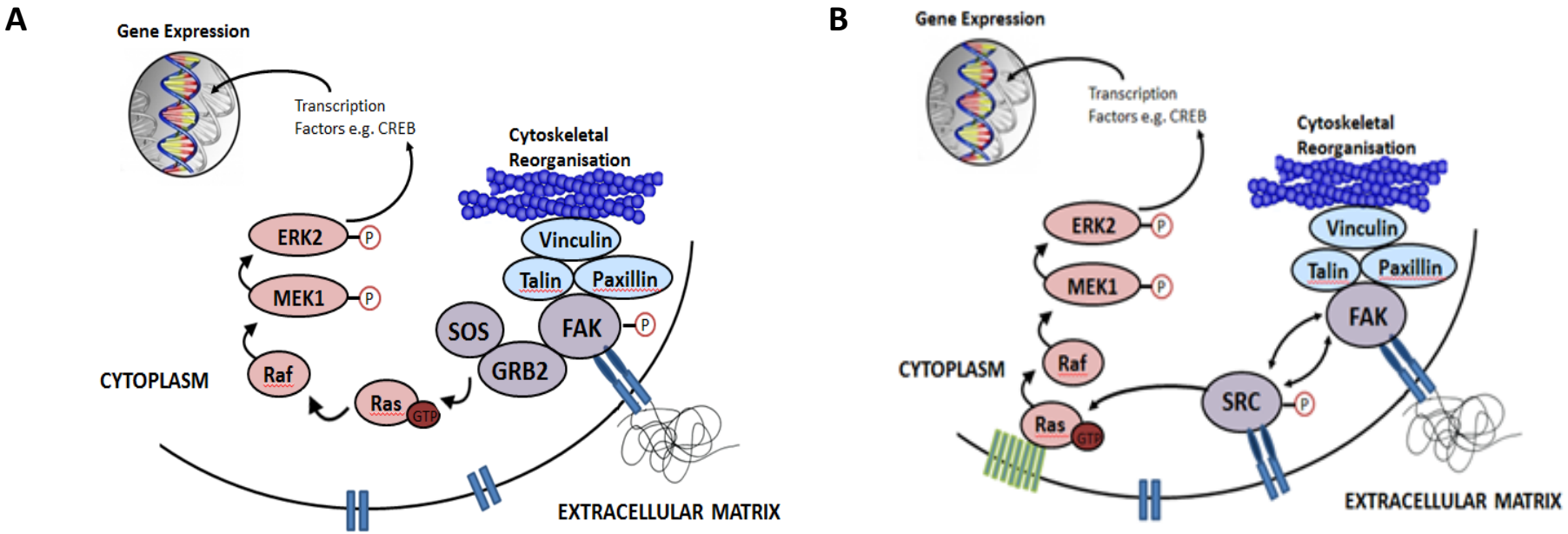

Figure 1.9 Focal Adhesion signalling may differ in significant ways between 2D and 3D culture systems

Focal Adhesion signalling is one of the key pathways in regulating cell shape and function, and is especially relevant when looking at how cells adapt to changes in their physical microenvironment. This is because information about the ECM is relayed through integrins to Focal Adhesion Kinase (FAK), which then recruits different proteins from the adhesome depending on the signals it receives. Differences in how this complex is built affects both the cytoskeleton through actin-linking proteins such as Paxillin, and gene expression through other intracellular signalling pathways including the MAP Kinase pathway as depicted above. Much of what we know about this complex is derived from studies in 2D (A). However, it has been suggested that changes in how FAK is phosphorylated in 3D cells may alter the complexes behaviour and thus explain how the change in cell geometry bought about by 3D systems results in observable differences in cell behaviour (B).

However, an additional issue when considering 3D adhesions is the wide variety of different substrates and topographies found within different 3D culture systems. Hakkinen et al. [128] addressed this issue by directly comparing the adhesions formed by HFF cells on the four most commonly used 3D matrices: collagen gels, fibrin gels, basement membrane extract (BME), and cell-derived matrix (CDM) from fibroblasts. For direct controls, they grew the same cells on coverslips coated in collagen, fibrinogen, or BME, or mechanically compressed fibroblast-derived 3D matrix. They found that although there were several factors in common between the adhesions found on each of these matrices, namely a lack of classical focal adhesions and stress fibres and an increased area of the cell surface devoted to other types of adhesion structure, each matrix exhibited slightly different adhesion behaviours in terms mostly of dynamics and axial ratio. This highlights that, although dimensionality is a very important determinant of adhesion structure and kinetics, there are also other factors such as chemical composition of the matrix and the degree of fibril alignment. The main determinants for the differences in 2D and 3D cellular adhesions are shown in Figure 1.10.

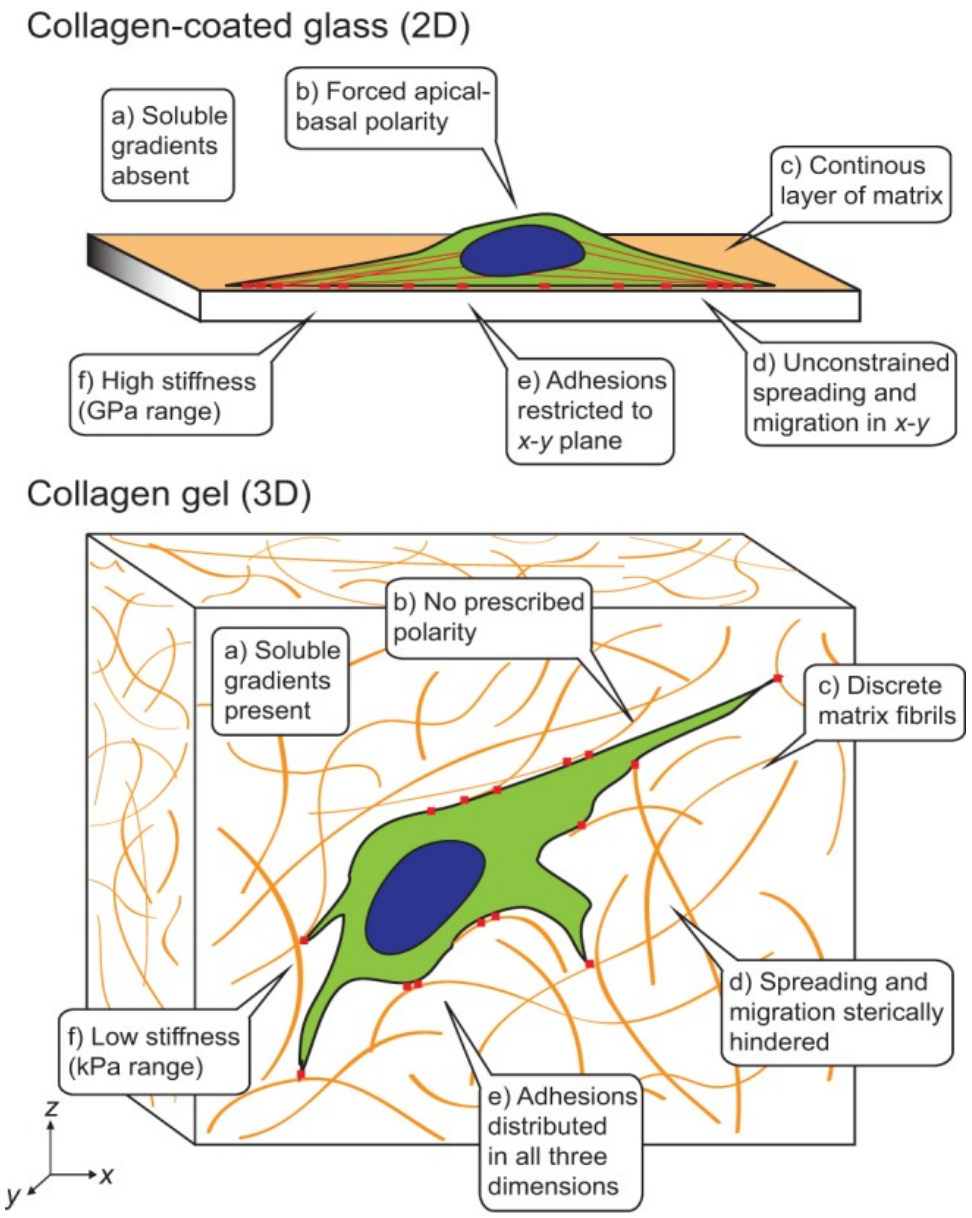

Figure 1.10 Cells grown in 2D and 3D experience different mechanical and biological cues

The environmental cues encountered by a cell are drastically different between an glass or plastic surface (2D) and a typical 3D cell system, such as collagen gels. These cues include mechanical differences, such as stiffness, biological cues such as polarity and adhesions, and chemical cues such as gradients of soluble nutrients. These differences all come together to control the shape and function of the cell, and underlies the main differences in observable behaviours between cells grown in 2D and 3D systems. Figure taken from [129].

1.1.6 The need for long term 3D hepatocyte models

Given the large body of research presented thus far that demonstrates the differences between cells maintained in 2D and 3D, and given the importance of *in* vitro hepatocyte models in drug discovery and development, it follows that there is a need for 3D hepatocyte models that display prolonged viability and hepatic functionality. Although there are currently a wide variety of 3D technologies that have been used to grow hepatocytes, these models do not currently allow for cells to be continually maintained in 3D conditions in the long-term. This is important when considering the adaptability of cells, and the changes that they undergo when placed in a novel environment, as outlined in Section 1.1.5. Namely, if cells that are naïve to a 3D microenvironment are placed into 3D models just prior to toxicology studies, they will undergo adaptation events that could cloud observable function. The cells will already be under stress due to the change in their environment, and so then further stressing them with a drug may lead to artificial findings of drug resilience. Thus, it would beneficial to be able to maintain cells in 3D conditions for a period of time prior to their use in drug assays, so as to allow the cells to fully adapt to the environment, and become 'primed'. Therefore, this project is concerned with developing a model that would allow hepatocytes to be primed to a 3D microenvironment.

1.2 Aims and Objectives

1.2.1. Hypothesis

The primary hypothesis of this work is that hepatocytes propagated in 3D will show morphologies closer to those seen in native liver tissue, allowing for enhanced liver-specific functionality *in vitro*. Furthermore, it is hypothesised that this enhanced morphology and function will be mechanistically coupled to changes in adhesion signalling.

1.2.2 Aims

The biological question at hand for this project is what is the mechanism by which cells adapt to changes in their physical microenvironment over long periods of culture *in vitro*. To answer this, the experimental design will involve sampling cells from the two populations created at various stages along the adaptation process, and assessing differences in cellular morphology and cytoskeletal organisation. These cells will then be analysed for changes in cellular functionality. Finally, these cells will be probed for key signaling molecules involved in adhesion signaling in order to determine whether these pathways are responsible for controlling and regulating cell adaptation to the microenvironment. Together this body of work will aim to provide vital information on the impact of 3D cell culture on observable cell function, which will have lead to a better understanding of key physiological processes such as morpho-and organo-genesis and tissue formation, damage and repair. In particular, this project will focus on the case of hepatocytes *in vitro*, exploring how 3D technologies can be used to maintain cells in 3D prior to use in toxicity studies, thus allowing cells to be 'primed'. This priming should enable researchers to differentiate between behaviours that are due to adaptation to the environment and behaviours that are due to toxicological attack.

1.2.3 Objectives

- Develop and optimise a methodology for cell retrieval and re-passage from a porous polystyrene scaffold
- Establish a model using this methodology to create populations of 2D and 3D maintained cells
- Determine the effects of long term propagation on cell proliferation and viability
- Characterise, if any, the changes 3D propagation causes in cellular morphology and cytoskeletal organisation
- Assess the degree to which changes in morphology lead to changes in cell metabolism and function
- Characterise, if any, the changes in adhesion signaling between cells maintained in 2D and 3D

Chapter 2: Materials and Methods

2.1 Cell Culture

2.1.1 2D cell culture

2.1.1.1 Maintenance of Met4 cells

The squamous cell carcinoma cell-lines Met1 to Met4 were derived from a clinical progression of an epidermal tumour; Met4 cells (ATCC, US patent 8,309,315) were cultured from a distant metastatic lesion [130] They were cultured in high glucose Dulbecco's modified Eagle Medium (DMEM, SLS LZBE12-614F12), supplemented with 10% heat-inactivated Foetal Bovine Serum (FBS, Fisher VX16010159), 2mM L-Glutamine (SLS, LZBE17-605F) and 100U/ml Penicillin/Streptomycin (SLS, LZDE17-602F; sDMEM). Cells were plated into a T25 cell culture flask (Nunc), which was placed in a humidified incubator at 37°C at 5% CO_2 until they reached 80% confluency (see Fig 2.1A). Cells were then passaged using 0.25% Trypsin-EDTA for 5 minutes, and split 1:3 into 3 T75 cell culture flasks (Nunc) every 3-4 days. Cells were maintained between passage numbers 40 and 60.

2.1.1.2 Maintenance of HepG2 cells

The hepatocellular carcinoma cell-line HepG2 (ECACC, Cat No. 85011430) was derived from a liver tumour in a paediatric patient [131]. They were cultured in high glucose Minimum Essential Medium (MEM, SLS LZBE12-125F12), supplemented with 10% heat-inactivated FBS, 2mM L-Glutamine and 100U/ml Penicillin/Streptomycin (sMEM). Cells were plated into a T25 cell culture flask, which was placed in a humidified incubator at 37°C at 5% CO_2 until they reached 90% confluency (see Fig 2.1C). Cells were than passaged using 0.25% Trypsin-EDTA for 10 minutes, and split 1:4 into 4 T75 cell culture flasks every 4-5 days. Cells were maintained between passage numbers 20 and 40.

2.1.1.3 Cryopreservation of cells

HepG2 and Met4 cells were suspended as single cells in freezing medium (10% DMSO in FBS) and split 1:3 into cryovials. These were placed in Mr Frosty containers for 24 hours (Fisher, CRY-120-010T) to allow cells to cool slowly at a rate of 1°C/minute. At this point, cells were transferred to -140°C for long-term storage.

Cells were thawed rapidly from -140°C in a 37°C water bath. Cells were then added drop-wise to a Falcon tube containing 10ml warm media. Cell suspensions were centrifuged at 1000rpm for 3 or 5 minutes, depending on the cell type, and the DMSO-containing media was carefully aspirated. Cell pellets were then re-suspended and plated as described above.

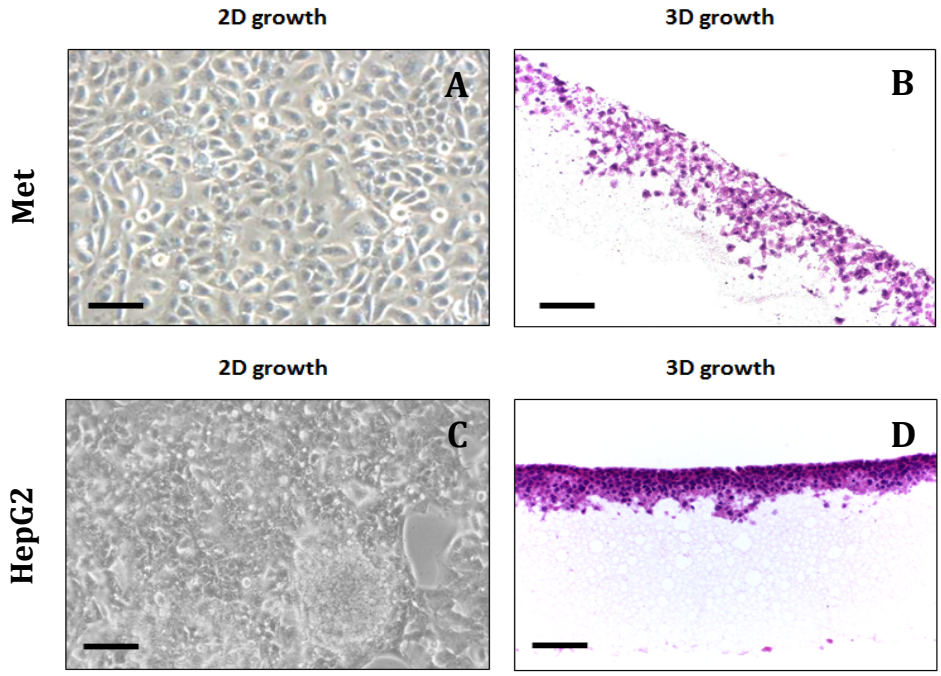

Figure 2.1 Met4 and HepG2 cells can be grown in 2D and 3D systems.

Phase contrast (A,C) and brightfield (B,D) microscopy images of Met4 and HepG2 cells grown in 2D (A,B) and in 3D on Alvetex® Scaffold (C,D). Scale bars = 50µm.

2.1.2. 3D cell culture

2.1.2.1 Alvetex®Scaffold

Alvetex® Scaffold is a commercially available, inert polyHIPE scaffold produced through water in oil (w/o) emulsion [132]. The polystyrene material is highly porous, and each void is connected to neighbouring voids through numerous interconnects (see Fig 2.4C). The average pore size is 40µm, and the average interconnect size is 13µm. The resulting material is sectioned into 200 µm thick sheets, which are cut into discs and placed into plastic inserts, allowing the scaffold to be readily compatible with existing tissue culture plasticware. Unless stated otherwise, Alvetex® Scaffold was used in the 6 well insert format.

2.1.2.2 Plasma treatment of Alvetex®Scaffold

Plasma treatment is used to create a hydrophilic surface for cell adhesion. Alvetex®Scaffold was used in the 6 well insert format, unless otherwise stated. The inserts were sterilised in 70% ethanol and left to dry overnight in a laminar flow hood. The inserts were then plasma-treated using the Emitech K1050X Plasma Asher (see Fig 2.2). The following parameters were selected for optimal coating:

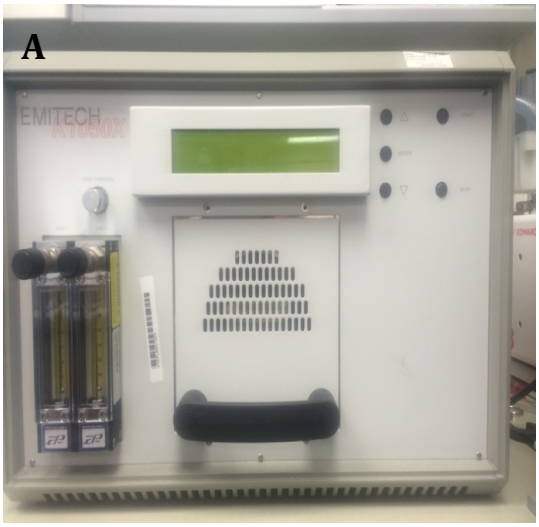

B

- RF power level – 40 watts
- Ashing time – 5 minutes
- Bleed delay – 15 seconds
- Process gas – as appropriate
- Vent value – unrestricted
- Restrict vent time – 120 seconds
- Pump spin down time – 15 seconds
- Vent hold time – 0 seconds
- Gas shutoff time – 10 seconds
- Turbo pumping enabled - 0

Figure 2.2 A Plasma Asher can be used to pre-treat Alvetex®scaffolds

Alvetex®Scaffolds can be treated using a plasma asher in order to allow for cell adhesion (A). (B) shows an example of precise settings typically used.

2.1.2.3 Ethanol treatment of Alvetex®Scaffold

The inserts were sterilised and prepared for cell adhesion by a wash in 70% ethanol, followed by 2 washes in sterile Phosphate Buffered Saline (PBS, SLS LZ17-512F24). The scaffolds were left in PBS until the cell suspension was added.

2.1.2.4 Met4 cell seeding on Alvetex®Scaffold

Prior to seeding onto inserts, MET4 cells were removed from T75 cell culture flasks by incubation in 0.25% Trypsin-EDTA (SLS, LZBE17-161F) for 5 minutes at 37°C and 5% CO_2.

MET4 cells were centrifuged at 1000rpm for 3 minutes and seeded dispersedly onto either Scaffold or Strata (see Fig 2.3). For dispersed seeding, the required number of cells per scaffold was re-suspended in 8ml of media, which was then added to each well of a 6 well plate containing the insert. This allows cells to settle evenly across the scaffold. Media was changed every 2 days.

2.1.2.5 Alvetex® Strata

Alvetex® Strata is a commercially available, inert polyHIPE scaffold produced through water in oil (w/o) emulsion, as with Scaffold. However, Strata differs from Scaffold by having smaller pores and interconnects (see Fig 2.4D). The average pore size is 13µm and the average interconnect size is 5µm. This smaller pore size allows average sized cells to grow on top of the membrane in a scaffold-free 3D manner.

2.1.2.6 Ethanol treatment of Alvetex®Strata

The inserts were sterilised and prepared for 3D cell culture by a wash in 70% ethanol, followed by 2 washes in sterile PBS. The scaffolds were left in PBS until the cell suspension was added.

2.1.2.7 Growth of cells on Alvetex®Strata

A variety of cell-lines were grown on Alvetex®Strata in order to investigate the effect of smaller pore sizes on cell growth. Table 2.1 shows the cell-types and the growth conditions used. As opposed to the dispersed seeding method used for the Met4 cells on Alvetex®Scaffold, in the concentrated seeding method, the required number of cells per scaffold was re-suspended in 100µl of media, which was added directly the centre of the scaffold disc in a droplet. These inserts were then incubated for 30 minutes at 37°C at 5% CO_2, before the addition of 8ml of media to each well (see Fig 2.3). For each cell-type, cells were seeded at a density of $1x10^6$ cells per membrane.

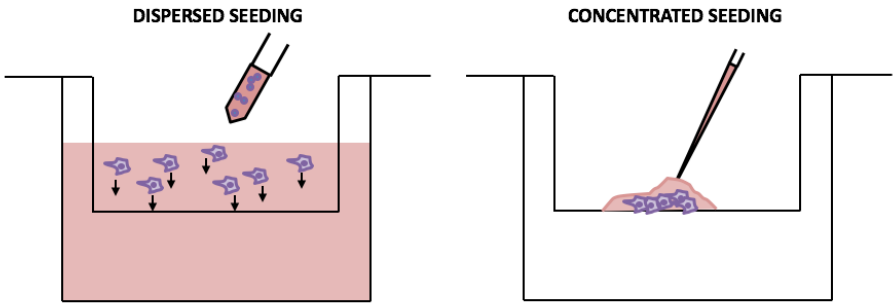

Figure 2.3 Cells can be seeded on Alvetex®Scaffold in two distinct ways.

There are two methods of seeding cells when using Alvetex®Scaffold. In the disperse seeding method, 5ml of culture media is added to the well containing scaffold. The cell suspension is diluted in 4ml of culture media and added drop wise across the entire surface of the scaffold, allowing cells to settle evenly over the surface. In the concentrated seeding method, cells are concentrated in a 100µl droplet which is added directly to the centre of the scaffold, allowing cells to rapidly penetrate the material. Cells are incubated for 15 minutes at 37°C to allow attachment before 8ml of culture media is added.

2.1.2.8 HepG2 cell seeding on Alvetex®Strata

Prior to seeding onto inserts, HepG2 cells were removed from T75 cell culture flasks by incubation in 0.25% Trypsin-EDTA (SLS, LZBE17-161F) for 10 minutes at 37°C and 5% CO_2. HepG2 cells were centrifuged at 1000rpm for 5 minutes and seeded in a concentrated manner onto Strata. This allows cells to share close cell-cell contact throughout the culture period. Media was changed every 3 days.

2.1.2.9 Suspension culture and growth of aggregates

A suspension culture of $1x10^6$ HepG2 cells was re-suspended in 15ml of sMEM and incubated overnight in an untreated 90mm Petri dish (Fisher, FB51504) to allow cells to form aggregates. Passaging of aggregates was achieved by transferring the suspension into a 50ml falcon tube, and leaving the aggregates to settle for 20 minutes. After this period,

the old media was aspirated carefully to avoid disturbing the aggregates. Fresh sMEM was added and the aggregates were re-suspended by gently swirling the tube. This suspension was then placed in a fresh Petri dish and incubated overnight at 37°C and 5% CO_2.

Cell Type/s	Source	Media Type	Seeding Method	Growth Period
SW480	Human colorectal adenocarcinoma	DMEM	Concentrated	4 days
SW620	Human colorectal adenocarcinoma	DMEM	Concentrated	4 days
HepG2	Human hepatocellular carcinoma	MEM	Concentrated	4 days
LN229	Glioblastoma	MEM	Concentrated	4 days
NIH-3T3	Mouse embryonic fibroblast	DMEM	Disperse	4 days
HaCaT	Human keratinocyte	DMEM	Disperse	4 days
GFP-NIH-3T3	Mouse embryonic fibroblast	DMEM	Disperse	4 days
Caco-2	Human colorectal adenocarcinoma	MEM	Disperse	4 days
MCF-7	Human breast ductal carcinoma	MEM	Disperse	4 days
MDA-MB-231	Human breast cancer (pleural effusion)	L15	Disperse	4 days
PC3	Human prostate cancer	Hams F12	Disperse	4 days
A549	Human alveolar adenocarcinoma	Hams F12	Concentrated	4 days
BT-474	Human breast ductal carcinoma	RPMI 1640	Concentrated	4 days
Tera2.sp12	human pluripotent embryonal carcinoma stem cell line	DMEM	Disperse	4 days

Table 2.1 The growth parameters for different cells that were grown on Alvetex®Strata

A variety of physiologically diverse and commonly used cell-lines were grown on Strata in order to characterise cell growth on the material. Thw growth period was kept constant across all the cell-lines tested to allow for direct comparison, but media and

2.2 Cell Viability

2.2.1 MTT Assay

To assess cell viability using an MTT assay, scaffold discs were removed from the plastic inserts, and placed into fresh 12 well plates. To each well containing a scaffold, plus an empty control well, 1ml of a 1mg/ml MTT solution (Sigma, M5655) was added. Plates were covered in foil to protect from light exposure, and placed in an incubator at 37°C and 5% CO_2 for an hour. After the incubation period, the insoluble purple-coloured formazan salts were solubilised using 1ml acidified isopropranol, and left on a rotating platform set to 45rpm for 10 minutes at room temperature. The resulting solution on each scaffold and in the control well, was diluted 1:20 and 200µl of the diluted solution was placed in a well of a 96 well plate. For 2D cultures, the method is similar, except that the cell culture media is removed before the addition of fresh media containing MTT solution. Absorbance was measured at 570nm using a BioTek ELx800 microplate reader, and the data captured using Gen5 1.10.

2.2.2 Trypan Blue Exclusion Assay

To assess cell viability using a Trypan Blue Exclusion Assay, cells were retrieved from scaffold discs by incubation with 0.25% Trypsin EDTA for 15 minutes at 37°C and 5% CO_2. 2D cells were incubated with 0.25% Trypsin EDTA for 5 minutes at 37°C and 5% CO_2. Cells were centrifuged at 1000rpm for 3 minutes (MET4 cells) or 5 minutes (HepG2 cells) respectively, and re-suspended in 10ml media. A 10µl aliquot was taken and diluted 1:1 with Trypan Blue (Sigma, T8154). A 10µl aliquot of the diluted cell suspension was placed in the chamber of a haemocytometer and observed under a light microscope (Nikon Eclipse T5100). Live cells appear colourless, whereas dead cells are stained dark blue due to the dye penetrating through broken cell membranes. The ratio of live:dead cells is taken as a measure of cell viability.

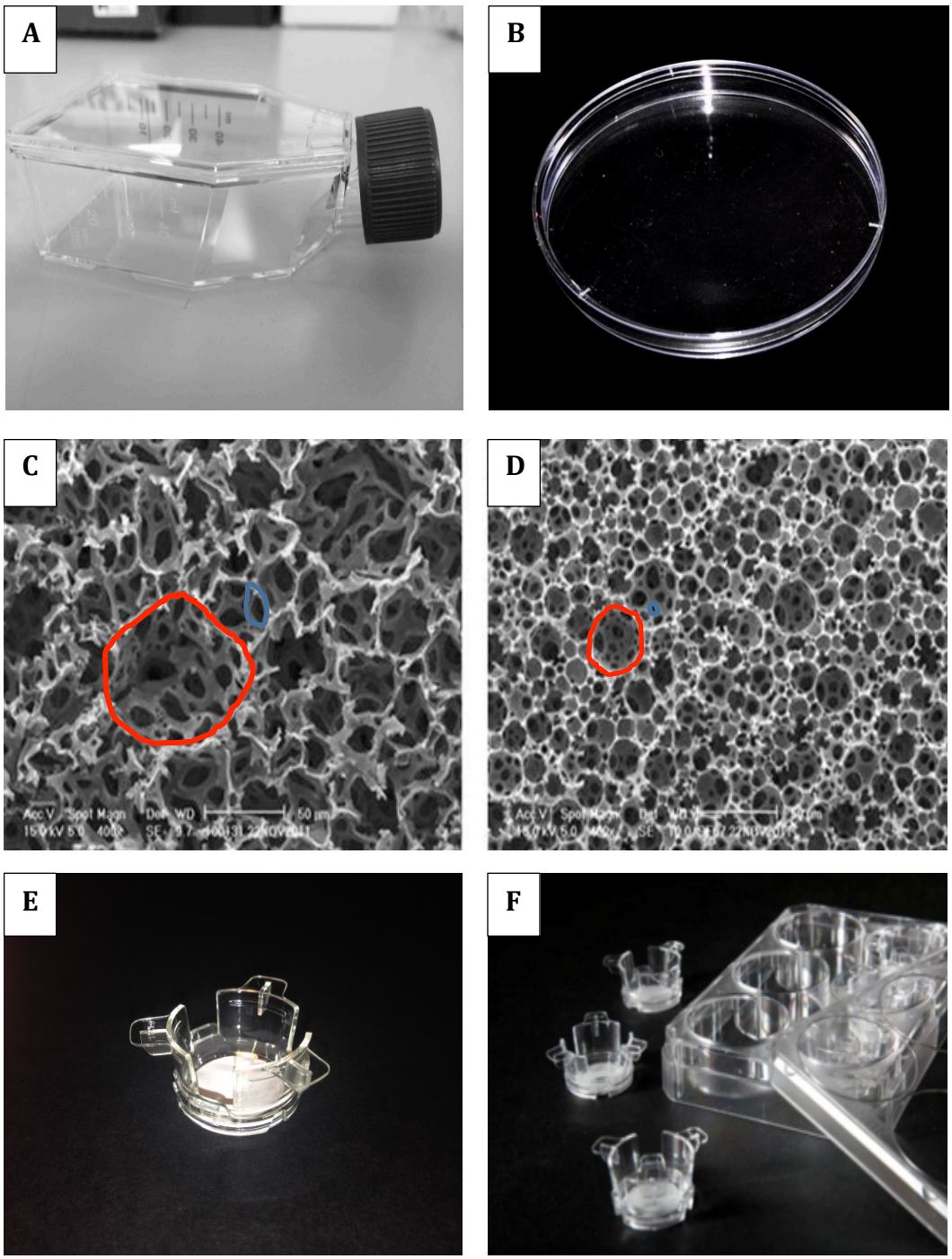

Figure 2.4 Growth substrates used for 2D and 3D cell culture.

Cells grown in 2D were grown in tissues culture flasks (A), and aggregates in untreated culture dishes (B). SEM images show that Alvetex Scaffold (C) has average pore sizes (red) of 40µM and average interconnects (blue), of 13µm, whereas Strata (D) has average pore sizes of 13µm and interconnects of 5µm. Both Strata and Scaffold were used in the 6 well insert format (E-F).

2.3 Histology

2.3.1 Dehydration and Embedding of samples

Scaffold discs were removed from plastic inserts, fixed in 4% Paraformaldehyde (PFA; Sigma P6148) overnight, and then washed in PBS three times. Cells were dehydrated through a series of ethanols – 30%, 50%, 70%, 80%, 90%, 95%, and finally 100% - each for 15 minutes. After dehydration, scaffolds were cut in half, and transferred to Histoclear (National Diagnostics, HS-200) for 15 minutes, and then to a 1:1 paraffin wax:Histoclear mixture at 60°C for 30 minutes. Following a final incubation in wax at 60°C for an hour, half scaffolds were embedded in cassettes with the cut edge placed perpendicular to the bottom of the cassette, and left to solidify at room temperature overnight.

2.3.2. Dehydration and Embedding of primary murine tissue

All procedures involving mice were conducted in accordance with guidelines and permission granted by the Institution and the Home Office, UK. Mice were euthanized and the liver dissected out. The liver was roughly cut into quarters to obtain pieces of tissue approximately $2mm^2$. These were fixed in 4% PFA at 4°C for 24 hours. The fixative was then poured off, and the tissue washed in dH_2O three times for 10 minutes each to remove all traces of fixative. The tissue was then left in 30ml of 70%, 80%, 90%, 95% and 100% ethanols for 2 hours each, before being transferred to a fresh falcon of 30ml 100% dry ethanol for 24 hours. Liver samples were then left in Histoclear for 24 hours, followed by a 1:1 paraffin wax:Histoclear mixture at 60°C for 4 hours. Over the next 48 hours, tissue samples were transferred through three changes of warm wax at 60°C before embedding overnight.

2.3.3 Sectioning

Sections of scaffold between 8µm and 10µm were cut using a microtome (Leica, RM2125RT) and transferred to electrostatically charged SuperFrost+ (Fisher, 10149870) slides by floatation in a 40°C water bath. Slides were left overnight on heat-racks to dry prior to staining. Sections of tissue between 6µm and 8µm were cut using a microtome, transferred to slides by floatation, and left to dry overnight as above.

2.3.4 Haematoxylin & Eosin (H&E) staining

Scaffolds were stained using H&E staining in order to visualise the cells. Haematoxylin binds to basophilic cell components, and thus stains nuclei blue. Eosin binds to acidophilic cell components, and thus stains cytoplasm pink. Sections were deparaffinised in Histoclear for 5 minutes, and then rehydrated through a series of ethanols: 100% ethanol (2 minutes). 95% ethanol (1 minute) and 70% ethanol (1 minute), before being transferred to distilled water (dH_2O) for a minute.4. Nuclei were stained using Mayer's Haematoxylin (Sigma MH532-1L) for 5 minutes, washed for 30 seconds in dH_2O, and subsequently blued in alkaline ethanol (30ml Ammonia: 970ml 70% Ethanol) for 30 seconds. Sections were dehydrated through 70% and 95% ethanol for 30 seconds each, before being stained in Eosin Y solution (Sigma HT 110232-1L; 5g in 1L 70% Ethanol) for 45 seconds. Sections were washed twice in 95% ethanol for 10 seconds each, and then twice in 100% ethanol for 15 seconds and 30 seconds. Finally, slides were cleared twice in Histoclear for 3 each time, and mounted in DPX (Fisher D/53 19/05), before being covered in a glass coverslip and allowed to dry.

2.4 Immunostaining

2.4.1 Immunohistochemistry of 3D cultures and primary murine tissue

Scaffolds were fixed, embedded and sectioned as previously described. Sections were then deparaffinised in Histoclear for 5 minutes, and hydrated through a series of ethanols: 100% ethanol for 2 minutes, followed by 90% and 70% ethanol for one minute each. If antigen retrieval was necessary for the antibody being used, this was achieved by placing slides in 200ml of a 10mM citrate buffer solution (pH 6) and microwaving (800 W) for 3 x 2 minutes. Slides were left in warm buffer and allowed to cool outside the microwave for 20 minutes, before being treated with 0.1% (v/v) Triton-X 100 (Fisher, BPE-151-100) in PBS for 20 minutes in order to permeablise the cell membranes. Cells were blocked for 30 minutes using a blocking buffer made of 1% Normal Goat Serum (NGS, Sigma G6767) and 0.1% Tween-20 (Sigma, P9416) in PBS. Primary antibodies and cell stains at appropriate dilutions (see Table 2.2 and 2.3 respectively) in blocking buffer were added to slides, which were incubated at 4°C in a humidified chamber overnight, and then washed 3 times in blocking buffer for 5 minutes each, on a rotating platform set to 40rpm. Fluorescence conjugated secondary antibodies were diluted 1:600 in blocking buffer, along with the nuclear stain

Hoechst 33342 (Molecular Probes, H3570) and then added to sections for one hour in the dark at room temperature. Stained sections were then washed as before for 3 x 5 minutes and mounted onto slides in Vectashield (Vector Labs, H-1000); glass coverslips were attached using nail varnish. The slides were kept in the dark until ready to be observed using fluorescent microscopy.

For the staining of primary murine liver samples, slides were stained using a DAB-HRP kit (Millipore, DAB500). Slides were deparaffinised and placed in citrate buffer for antigen retrieval as before. Using a PAP pen (Fisher, VX08877), a hydrophobic barrier was drawn around the section. A few drops of a 3% hydrogen peroxide solution (v/v; Sigma, 216763) were added to the sections, which were then left in a humidified chamber at room temperature for 20 minutes. Sections were then rinsed three times in rinse buffer (diluted twenty fold from a stock provided in kit), and blocked using a blocking buffer (provided in kit) for 30 minutes at room temperature. Slides were washed as before in rinse buffer, and incubated with primary antibodies at the correct dilutions (Table 2.2) for one hour at room temperature. Slides were rinsed and incubated with a few drops of secondary antibody (provided in kit) for an hour before being rinsed again. A few drops of Streptavidin-HRP conjugate (provided in kit) was added to each section for 15 minutes. The Chromagen A and B reagents provided in the kit were mixed at a 1:25 ratio, and a few drops of this mixture were added to the slides for 10 minutes. Slides were rinsed and incubated with a few drops of the nuclear counterstain haematoxylin (provided in kit) for 2 minutes, before being rinsed in deionised water and mounted in DPX.

2.4.2 Immunocytochemistry of cultured cells

2.4.2.1 Preparation of glass coverslips

For imaging and staining of cells, Ø16mm circular Borosilicate glass coverslips with a thickness between 0.13 and 0.17mm (Fisher, 12313138) were sterilised with 70% ethanol and then washed twice in PBS before being placed in 12 well culture plates.
These coverslips were then coated with the following: Poly-D Lysine (1µl/ml; Sigma P7405), Rat tail Collagen I (5µg/ml SLS, 354236), or Fibronectin (0.5µg/ml, Sigma, F1141) overnight at room temperature in a laminar flow hood. These were then washed twice in PBS, and left in PBS until cell seeding.

Antibody	Dilution	Secondary antibody	Supplier
FAK	1:200	Alexa fluor 488 goat anti-rabbit IgG (Fisher)	Abcam (ab40794)
Paxillin	1:500	Alexa fluor 488 goat anti-mouse IgG (Fisher)	Abcam (ab3125)
pFAK^{Y397}	1:200	Alexa fluor 488 goat anti-rabbit IgG (Fisher)	Abcam (ab4803)
Vinculin	1:100	Alexa fluor 488 goat anti-mouse IgG (Fisher)	Abcam (ab18058)
α Tubulin	1:2500	Alexa fluor 488 goat anti-mouse IgG (Fisher)	Abcam (ab18281)

Table 2.2 Primary antibodies used in immunohistochemistry

The table shows the optimal dilutions of the primary antibodies used in immunohistochemical analyses in this thesis. As well as this, the supplied of the antibody and the secondary antibody used is listed for each primary antibody.

Stain	Dilution	Supplier
Hoechst 33352	1:1000	Molecular Probes (H3570)
Phalloidin	1:150	Universal Biologicals (PHDG1-A)

Table 2.3 Cell stains used in immunohistochemistry

The table shows the optimal dilutions and suppliers of the two cell stains used in this thesis. Hoechst 33352 was used as a nuclear stain, and Phalloidin as a cytoskeletal marker.

For high-resolution microscopy, high precision square 22x22mm Borosilicate glass coverslips with a thickness of 0.17mm (VWR, MARI0107052) were sterilised as above, and coated with PDL overnight.

2.4.2.2 Seeding and fixing of cells

Cells were seeded at low confluency ($5x10^4$) to allow for single cell imaging, and incubated in 4ml sMEM at 37°C and 5% CO_2 for 3 hours to allow adhesion without cell flattening. At this point, the media was aspirated, and cells were washed twice with PBS before being left to fix in 4% PFA for an hour at room temperature. After fixation, the coverslips were washed twice in PBS before staining.

For imaging of the entire monolayer, cells were seeded at higher confluency ($2x10^6$) and incubated in 5ml sMEM at 37°C and 5% CO_2 for 4 days, with phase contrast images taken at various time-points every day.

2.4.2.3 Staining of coverslips

Cells were immuno-stained in a similar way to that described above for tissue and scaffold samples. Cells were permeabilised with 0.1% (v/v) Triton X100 for 15 minutes; in In the case of antibodies to cell membrane proteins (FAK, pFAK^{Y397}, and α5β1) this step was bypassed in order to maintain the integrity of the cell membrane. Cells were then left in blocking buffer (0.1% Tween-20 and 1% NGS in PBS) for 30 minutes before being washed 3 times for 5 minutes each on a rotating platform at 40rpm. Primary antibodies at appropriate dilutions

in PBS (see Table 2.4) were added to cells for an hour on ice. Coverslips were then washed as described before. Fluorescence conjugated secondary antibodies were diluted 1:600 in blocking buffer, along with the nuclear stain Hoechst 33342 and then added to cells for one hour in the dark on ice. Immuno-stained cells were than washed as before, mounted cell-side down in 50µl Vectashield onto slides and sealed with nail varnish.

When staining cells for the cytoskeletal marker Phalloidin, a dye that specifically binds F-Actin, the cells were incubated in the dark at room temperature for an hour in 200µl of a Phalloidin:Hoechst 33522 mixture (1.3µl Phalloidin and 0.2µl Hoechst 33522 in 200µl blocking buffer). The cells were then washed 3 times for 5 minutes each on a rotating platform at 40rpm, mounted cell-side down in 50µl Vectashield onto slides and sealed with nail varnish.

Antibody/stain	Dilution	Secondary antibody	Supplier
FAK	1:100	Alexa fluor 488 goat anti-rabbit IgG (Fisher)	Abcam (ab40794)
Paxillin	1:250	Alexa fluor 488 goat anti-mouse IgG (Fisher)	Abcam (ab3125)
pFAK^{Y397}	1:100	Alexa fluor 488 goat anti-rabbit IgG (Fisher)	Abcam (ab4803)
Vinculin	1:50	Alexa fluor 488 goat anti-mouse IgG (Fisher)	Abcam (ab18058)
α Tubulin	1:2500	Alexa fluor 488 goat anti-mouse IgG (Fisher)	Abcam (ab18281)
α5β1	1:150	Alexa fluor 488 goat anti-mouse IgG (Fisher)	Millipore (MAB1969)
αVβ3	1:200	Alexa fluor 488 goat anti-mouse IgG (Fisher)	Abcam (ab78289)

Table 2.4 Primary antibodies used in immunocytochemistry

The table shows the optimal dilutions of the primary antibodies used in immunocytochemical analyses in this thesis. As well as this, the supplied of the antibody and the secondary antibody used is listed for each primary antibody.

2.5 Microscopy

2.5.1 Brightfield microscopy

For imaging of H&E stained slides, a Leica ICC50 high definition camera mounted onto a Leica microscope was used, with the following objective lenses: HI PLAN 10x/0.25 PH1, HI PLAN 20x/0.40 PH1 and HI PLAN 40x/0.65 PH 2 (Leica). Images were captured and analysed using the LAS EZ software suite.

2.5.2 Phase-contrast microscopy

For imaging of cells under phase-contrast conditions, such as for scratch wound assays, the following microscope was used:
Leica DFC 310FX with digital camera DMI 3000B. Objectives: HI PLAN 10x/0.25 PH1, HCX PL FLUOTAR 20x/0.40 PH1, N PLAN 40x/0.55 PH2 and HI PLAN 100x/1.25 OIL PH3 (Leica). Filters: DAPI and 488nm.
Images were captured and analysed using the LAZ 3.7 software suite.

2.5.3 Fluorescence microscopy

For capturing of immuno-stained cells and phase contrast images, the following two microscopes were used:
1. Leica DFC 310FX with digital camera DMI 3000B. Objectives: HI PLAN 10x/0.25 PH1, HCX PL FLUOTAR 20x/0.40 PH1, N PLAN 40x/0.55 PH2 and HI PLAN 100x/1.25 OIL PH3 (Leica). Filters: DAPI and 488nm.
Images were captured and analysed using the LAZ 3.7 software suite.
2. Nikon DIAPHOT 300 fluorescence microscope with camera DMX 1200. Objectives: PlanApo 100/1.40 OIL. Filters: DAPI, 488nm.
Images were captured and analysed using ACT-1 software.

2.5.4 High Resolution microscopy

The advanced imaging facility at Durham University allows for high resolution imaging of cells and materials. The following microscopes were used in the work contained in this thesis.

2.5.3.1 Laser-Scanning Confocal Microscopy (LSCM)

To obtain high resolution images, the Zeiss 510 Meta Confocal Laser Scanning Microscope was used on the 63x oil immersion objective. Images were captured using AxioVision software

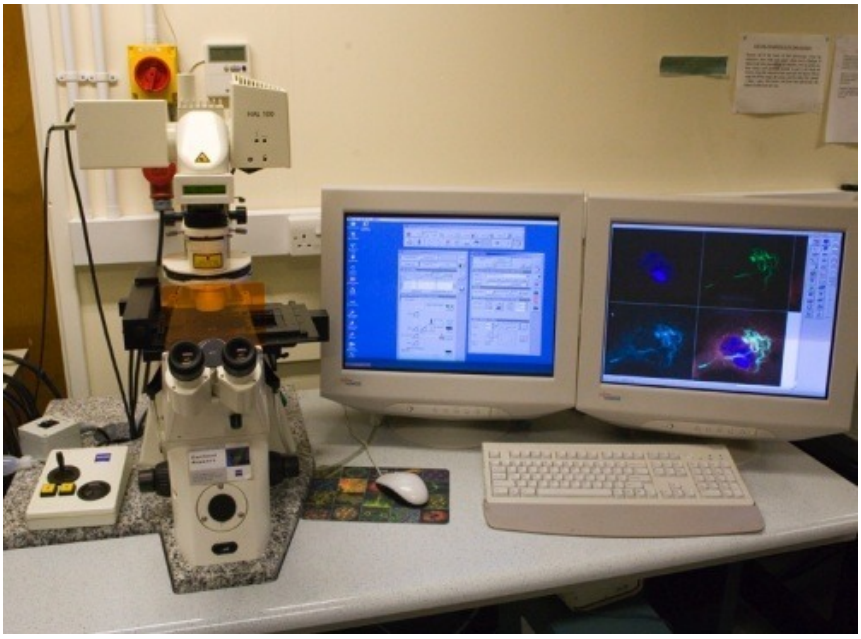

Figure 2.5 Zeiss 510 Meta Confocal Laser Scanning Microscope

Laser Scanning Confocal Microscopy (LSCM) can be used to obtain high-resolution images.

2.5.3.2 Structured Illumination Microscopy (SIM)

For single-cell imaging, a super resolution Delta Vision OMX V4 microscope (Applied Precision GE Healthcare systems) was used. This microscope is capable of generating wide-field and SIM images. Structured Illumination (SI) is a wide-field technique in which a grid

pattern is generated through interference of diffraction orders; the grid is superimposed on the specimen while capturing images and is rotated in degrees between the capture of each image set. This spatially structured excitation causes normally unreachable high-resolution information to become encoded into the observed image. This information is computationally extracted and mathematically transformed through an algorithm to generate a three-dimensional reconstruction with twice as high resolution, in all three dimensions, as is possible in a conventional wide-field microscope, or a standard laser scanning confocal microscope such as the Zeiss 510 described above (see Fig 2.7).

2.5.3.3 Calibrating and Optimisation of image capture using OMX

Images were captured using the standard Olympus Plan-Apo 60X, 1.42 NA PSF "A" quality objective lens. For each sample, the optimal oil was chosen from the kit provided. Each oil provides a different refractive index, and this can be calibrated to the particular sample by viewing the image on the orthogonal viewer, and choosing immersion oil that produces a symmetrical flare of light that extends equally in both directions (see Fig 2.6A). This can be further optimised by calibrating the section thickness (see Fig 2.6B). Setting these parameters allows for the capture of sharp, defined and super-resolution images.

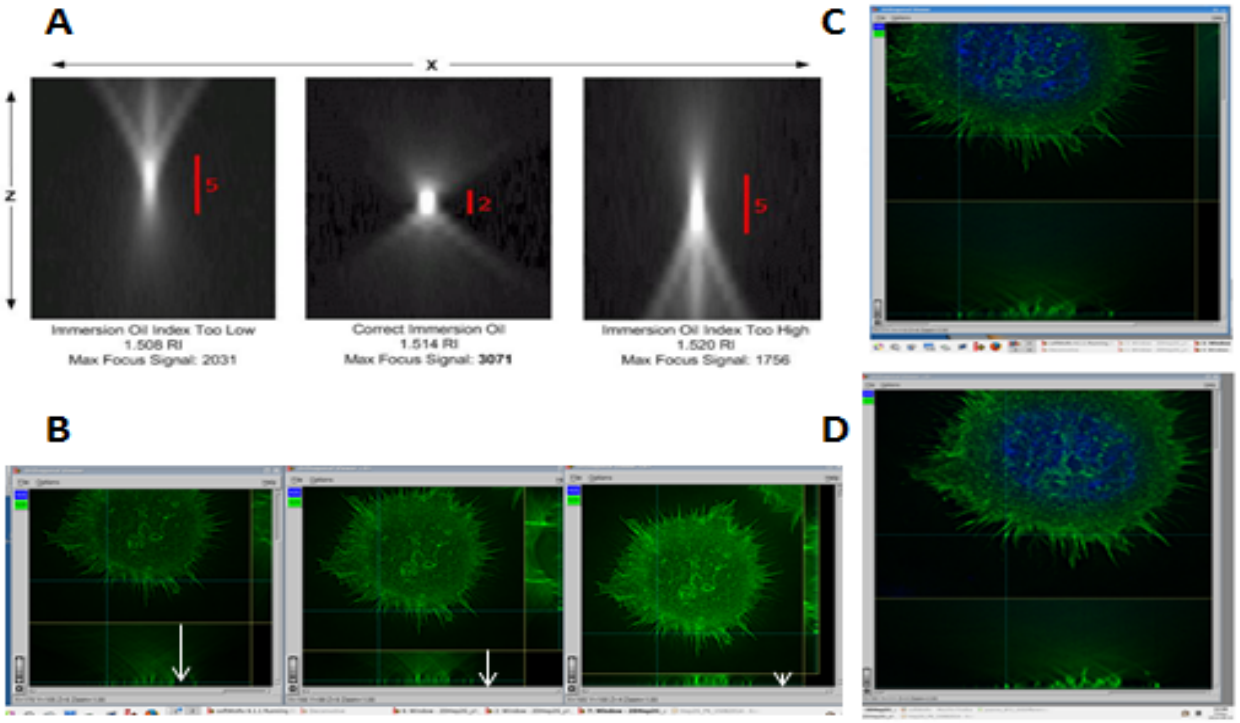

Figure 2.6: The parameters for image capture on the OMX Super Resolution Microscope need careful optimization

A) The panel of images show the flare of light when the orthogonal viewer is focussed on a specific point in a sample using three different immersion oils. The middle image shows a symmetrical flare, with the first showing an upwards flare when the oil is too low, and the third a downwards flare when the oil is too high. B) shows a decrease in the asymmetrical upwards flare when the section thickness is decreased. Changing these two parameters can have a significant effect on the resolution of the image produced. C) An image before optimisation and D) the same cell post-optimisation.

Laser Scanning Confocal Microscopy

Structured Illumination

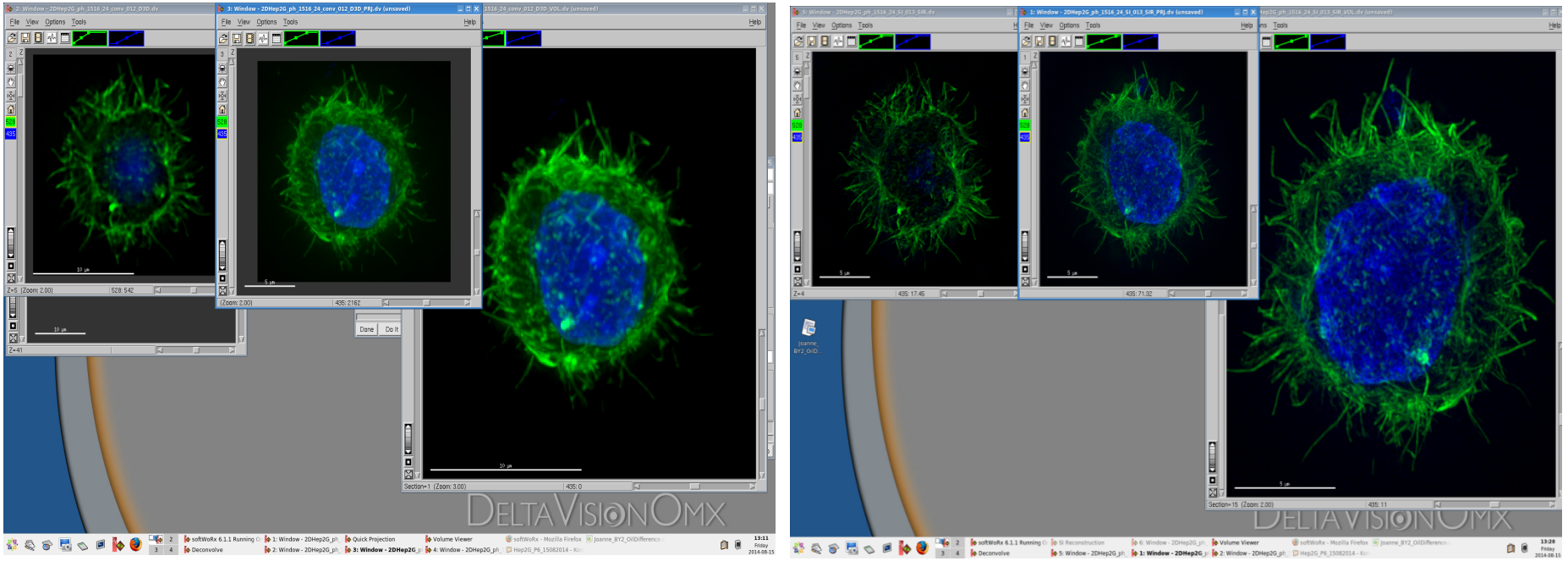

Figure 2.7: A side-by-side comparison of the same cell, stained with Phalloidin and Hoechst 33352 and imaged using the OMX Blaze in conventional mode (akin to LSCM) and in SIM mode shows clear differences in the two methods of image capture.

The image captured in SIM mode is clearly of a higher resolution, with individual actin fibres being distinguishable. The background staining is significantly reduced and the staining is more well-defined. This leads to a much sharper image.

2.6 Flow Cytometry

2.6.1 Preparation of samples for quantification of cell surface markers

Cells for cytometric analysis were retrieved from culture flasks, counted using a haemocytometer and re-suspended in 1ml blocking buffer (0.1% w/v Bovine Serum Albumin (BSA) in PBS) to create a single cell suspension of $5x10^5$ cells. 200µl of this suspension was added to each well of a U-bottomed 96 well untreated flow cytometry plate. The plate was then centrifuged at 1000rpm for 5 minutes at 4°C, and the plate inverted to remove the supernatant.

2.6.2 Preparation of samples for quantifying intracellular markers

As before, a single cell suspension was created through trypsinisation. This suspension was transferred to a 15ml falcon tube and cells were allowed to settle for 10 minutes. 2ml of 4% PFA was added and pelleted through centrifugation at 1000rpm for 5 minutes at 4°C. At this stage, the pellet was re-suspended in 4% PFA and left to fix on ice for 20 minutes. During this time the tube was gently swirled periodically to prevent the cells sticking together. Cells were centrifuged as before and washed twice with PBS. The cell pellet was then re-suspended in 2ml 0.1% Triton X100 and left on ice for 15 minutes to permeablise the cells. Cells were washed three times as before and the pellet re-suspended in 1ml of blocking buffer (0.1% w/v BSA in PBS) to create a single cell suspension of $5x10^5$ cells. 200µl of this suspension was then plated into the wells of a U-bottomed 96 well plate and centrifuged to pellet cells.

2.6.3 Detection of antigens

The pellet was then re-suspended in 50µl of the primary antibody appropriately diluted as described in Table 2.1 and incubated on ice for an hour. P3X IgM (mouse; Developmental Studies Hybridoma Bank) was used as a negative control, at a 1:10 dilution, and detected with a FITC-conjugated goat-anti-mouse IgM (µ-chain specific) secondary (Sigma, F9259) diluted 1:100 in blocking buffer. Unbound excess antibody was removed by adding 100µl of the BSA blocking solution and centrifuging at 1000rpm for 5 minutes at 4°C. Cells were washed twice by addition of 180µl blocking buffer and centrifugation. Cells were then

incubated with 50µl of diluted secondary antibodies for an hour on ice in the dark. Cells were washed as before and re-suspended in 200µl blocking buffer for analysis

2.6.3 Setting up the Flow Cytometer and capturing data

Prior to analysis, a quality control step using the Guava Check kit (Millipore, 4500-0020) was performed on the cytometer (Millipore GuavaCyte Plus Flow) to determine whether the system required calibration. This involves using beads of known size, shape and fluorescence to determine a % coefficient of variance (CV); this should ideally be less than 5%. Plates were then read and the mean fluorescence was detected by the Guava technologies EasyCyte system.

Debris and cell clumps were removed from the data set by optimising the forward and side scatter parameters, ensuring that any detected fluorescence was from single cells (see Fig 2.8). A negative control is run in order to determine the gate settings for background– this is done by placing a horizontal bar designated M1 over the region encompassing no signal in the resulting histogram for the negative control (Fig 2.8A). This bar then designates the fluorescence levels that will be counted as positive events. These settings are then applied to the histograms for samples, and only the fluorescence covered by the M1 bar is counted in the final percentage of positive cells.

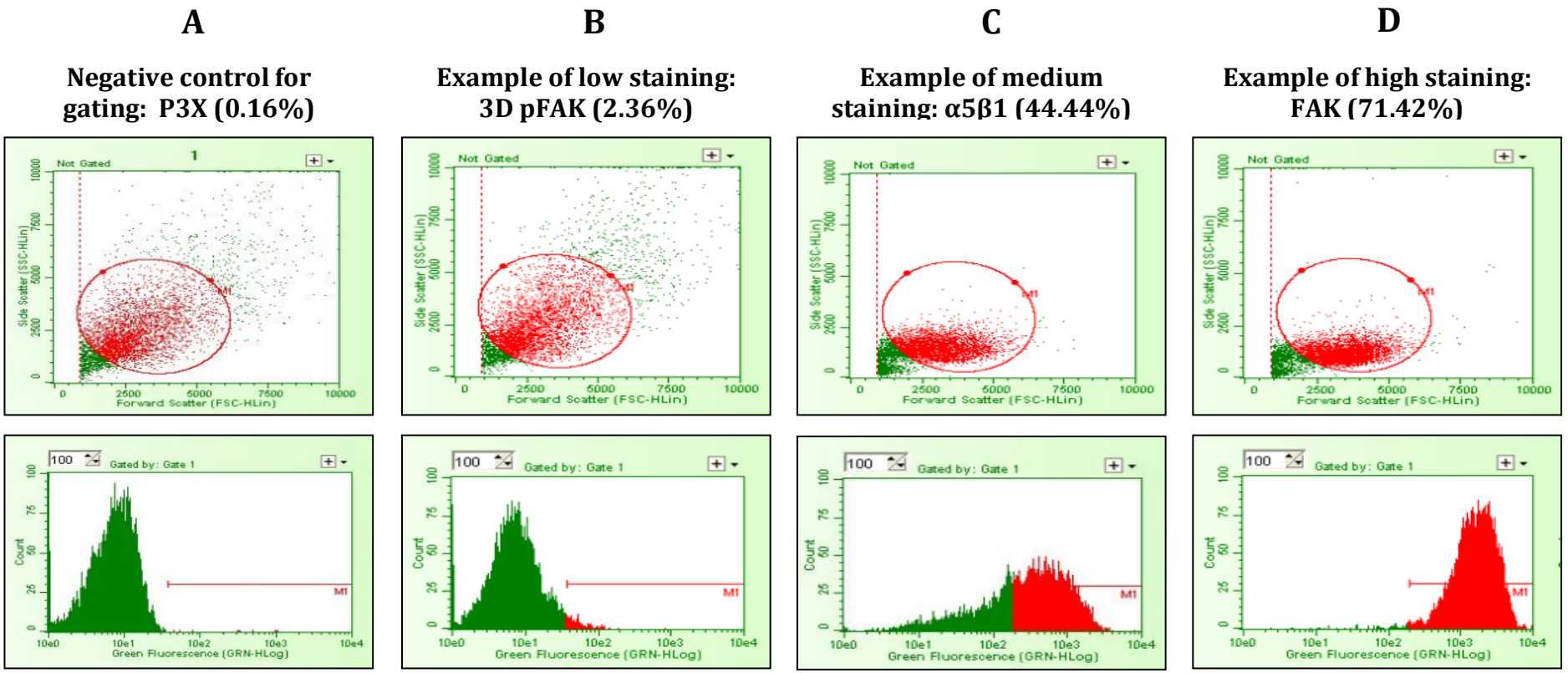

Figure 2.8 Flow Cytometry requires gating to ensure accurate data capture.

The trace obtained for P3X (A) was used as a negative control to gate the histogram so that the percentage number of positive cells was close to zero (0.16%). Using these gating parameters, other antibodies were tested in control and experimental conditions. Traces B-D show representative examples of low (B), mid-range (C) and high (D) expression traces. The histograms below are used to obtain the mean percentage positive cells.

Chapter 3: Developing a methodology for the 3D propagation of mammalian cells

3.1 Introduction

3.1.1 Adaptation of cells to a 3D microenvironment

Research has found that cells cultured in a 3D culture system differ morphologically and physiologically from cells cultured in traditional 2D culture systems [133-135]. Arguably, it is the additional Z dimensionality of 3D cultures that is the crucial feature leading to the differences in cellular responses because not only does it influence the spatial organization of the cell surface receptors engaged in interactions with surrounding cells, but it also induces physical constraints to cells. These biomechanical aspects of 3D culture affect the signal transduction from the exterior to the interior of cells, and ultimately influence gene expression and cellular behavior.

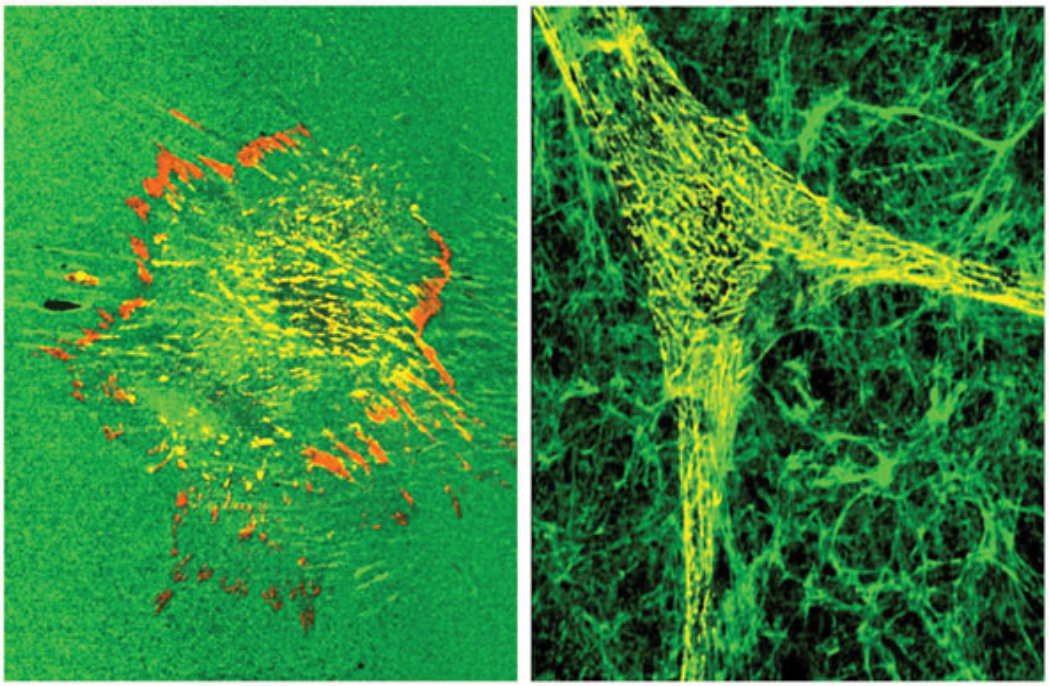

Figure 3.1 Cells grown in 2D and 3D show drastically different morphologies

Fibroblasts grown on 2D substrates tend to spread onto the substrate in a flattened morphology (left panel), whereas cells attaching to 3D matrices rapidly assume an elongated morphology (right panel) that tends to mimic shapes of fibroblastic and mesenchymal cells *in vivo* [235].

These changes are due to a process called mechano-transduction, by which mechanical cues form the environment are translated into chemical cues within the cell. This translation event allows the cell to fully adapt to the environment in which it is growing. While we know the main players in this process, in terms of signalling molecules, we don't know how they come together in terms of a 3D context. There is also a gap in our current knowledge on the temporal aspects of this adaptation. A key question that needs to be asked here is how long does it take for cells to fully adapt to a 3D topography? One of the main hypotheses behind this project is that there are two main stages of cell adaptation to the environment: short-term dynamism controlled by signalling events, and long-term priming controlled by changes in gene expression. It is likely that these longer-term events will require longer periods of culture in 3D systems. Chang et al. [136] found that there were large-scale global changes in gene expression between the human hepatocyte cell line HepG2 cells grown in monolayer (2D) and spheroids (3D). In this study, they demonstrated that HepG2 cells respond to differing physical environments of 2D and 3D culture with altered actin cytoskeleton structure and cell shape. Through global gene expression analysis, they showed that distinct genetic programs were triggered depending on the physical shape of the cells. Monolayer cells expressed high levels of ECM, cytoskeleton, and cell adhesion molecules. These transcripts were down-regulated in the spheroids while metabolic and synthetic functional genes were significantly up-regulated. These changes were found in cells cultured in both environments for 6 weeks.

However, the question remains whether the 6-week culture period is necessary for these changes, or indeed whether it is sufficient to see the full extent of the changes. With this in mind, it is important to be able to establish a protocol by which cells can be grown for long culture periods in 2D and 3D in parallel and then compared to each other at different passages in order to analyse any propagation-dependent differences at different time-points in 3D culture.

3.1.2 Long term cultures of hepatocytes

The advantages of 3D cell models lie in improved physiology, the ability to include different cell types in one model, and, in the case of hepatocytes, increased longevity. These three aspects together have the potential to significantly improve biological relevance of *in vitro* assays and increase the chances that drug-induced toxicities, generation of a potentially

toxic metabolite or accumulation-processes over time will be detected.However, the design and delivery of models that allow for long-term stability and maintained functionality remains challenging. While certain key parameters, for example, cellular viability, may remain constant for longer culture periods, other factors such as phenotypes, change. In unpublished data reviewed in [137], whole genome microarray analysis of cells grown in 3D sandwich models revealed that, after about 4 weeks, the cell model appeared to undergo physiological changes so that the pattern of expressed genes did not match that of an *in vivo* liver anymore. This example was particularly unexpected as the key liver functions, such as P450s, remained constant over the same experimental period, and thus a liver-like cellular environment and functionality would have been expected. Without careful analysis of the gene expression pattern and comparison with human liver samples, these physiological changes in the 3D culture would have remained undetected, thus probably rendering the interpretation of data from a drug assay with this culture misleading.

Studies like this are revealing because they show the need for continued understanding of the mechanisms of cell adaptation to the environment. They also highlight the need for consistency in cell models, and provide a solid argument for the need of methodologies allowing for long-term maintenance of cells in 3D without de-differentiation occurring. It is with this in mind that the first stages of this work focused on designing a protocol for the continual propagation of cells in 3D conditions.

3.2 Aims of Chapter

The aim of this chapter is to develop a model for the continual propagation of mammalian cells in 3D using a novel polystyrene scaffold. This model will require a methodology for the successful retrieval of cells from one scaffold and successful re-plating of these cells onto a fresh scaffold in order to maintain the 3D phenotype. This model will then be used to create two different populations of cells from a common pool in order to assess the effect of long-term culture in 3D.

3.3 Objectives

1. Characterise the growth of cells on a novel polystyrene scaffold and select a cell type suitable for developing 3D propagation.
2. Optimise conditions for the successful retrieval of these cells from one scaffold disc and the re-plating of these cells onto a fresh scaffold.
3. Continually propagate cells in both 2D and 3D culture over several months to produce two different cell populations.
4. Compare differences in proliferation and viability between these two populations over this period of time.

3.4 Materials and Methods

3.4.1 Cell retrieval from Alvetex®Scaffold

Scaffold discs were removed from the plastic inserts by snapping the three clips securing the base ring to the walls, and washed with brief immersion in PBS to remove traces of culture media. A pair of dissection scissors were washed in 70% ethanol solution and then used to cut scaffold discs into either halves or quarters. These were transferred to a 3ml plastic vial and incubated with 2ml of 0.25% Trypsin-EDTA solution at 37°C for between 5 and 30 minutes on either an orbital or platform shaker. The cell suspension solution was collected and placed into a fresh vial for cell counting. The remaining pieces of scaffold were washed with brief immersion in PBS and transferred to a fresh culture plate.

3.4.2 Assessing retrieval efficiency

3.4.2.1 Neutral Red staining

Neutral Red is a vital cell stain that can be used to assess cell viability, and was used in this context to assess the degree of successful cell retrieval from scaffold. Live cells incorporate the neutral red chemical into their lysosomes, but as cells begin to dye they lose their ability to incorporate the substance and dye lighter. Therefore, the darker red the cell stains the more viable the cell is. A lack of positive red staining can be taken to mean a lack of viable cells.

To assess the efficiency of cell retrieval, one disc per experiment acted as a control disc and was incubated only with PBS. Both the control and treated discs were stained with Neutral Red and the difference between the staining patterns taken to indicate the amount of cells that had been removed. Briefly, discs were incubated in 500µl of Neutral Red solution (Sigma N6264) for 5 minutes at room temperature. The discs were then placed in a deep well culture dish full of PBS on a reciprocating shaker at 100 strokes per minute for 5 minutes. To remove all excess stain, the discs were then washed twice by brief immersion in PBS. The stained scaffold pieces were placed on a microscope slide with a drop of PBS to keep them moist, cover-slipped, and studied under a microscope.

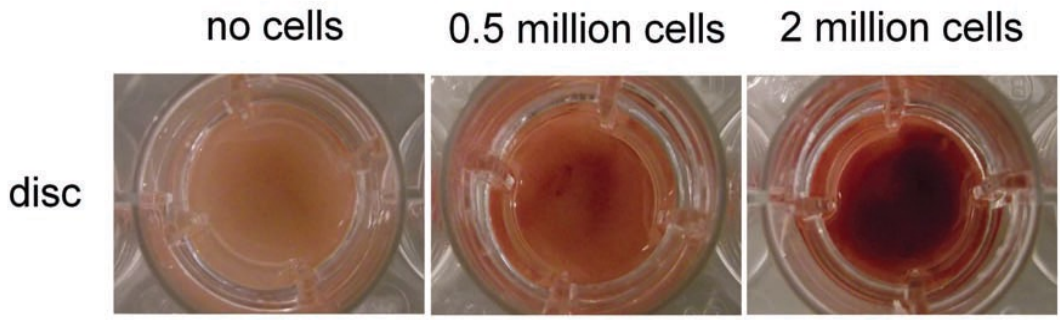

Figure 3.2 Neutral Red staining can be used to assess the amount of cells present on a disc

Neutral Red is a vital stain that is incorporated into live cells, and the degree of staining can be used to estimate the amount of cellular growth/attachment on a scaffold. Data courtesy of ReproCELL Reinnervate.

As demonstrated in Figure 3.2, a darker staining pattern is obtained when there are more cells on the scaffold, and this proportional relationship was used to obtain qualitative data on the degree of successful cell retrieval.

3.4.2.2 MTT viability assay

The full protocol for the MTT cell viability assay can be found in Section 2.2.1. In this set of experiments, the MTT assay was used to provide quantitative data on cell retrieval. To assess the efficiency of cell retrieval, one disc per experiment acted as a control disc and was incubated only with PBS. Both the control and treated discs were placed in a fresh 6 well culture plate and incubated with the MTT solution for an hour at 37°C and protected from light exposure with foil. The resultant salt was solubilised with acidified isopropanol and then diluted 10 fold in isopropanol and read at 570nm on a plate-reader. The values were normalised firstly to a blank, and then to the control disc, so that the difference in the number of viable cells in each sample could be expressed as a percentage of the untreated disc.

3.4.3 Cell retrieval from Alvetex®Strata

Scaffold discs were removed from plastic inserts as before and washed by brief immersion in PBS to remove residual traces of culture media. 2ml of Trypsin-EDTA solution was then added to each well. Plates were then transferred to a platform shaker in a 37°C incubator and left for 15 minutes to allow for enzymatic dissociation. Plates were then removed from the incubator, and placed within a sterile culture hood. Using a standard cell scraper, cells were gently scraped off the surface of each disc in a circular motion. Discs were then washed in PBS and put aside in fresh culture discs for further analysis. The cell suspensions in each well were collected in individual tubes and 2ml of culture media was added to each to neutralise the trypsin action. 10µl of each tube was sampled out for counting.

3.4.4 Assessing penetration through and growth above Alvetex®Strata

Strata discs were processed for histology as explained in section 2.3. In order to capture cellular behaviour across the entire disc, 8um sections were taken in triplicate at distances of 100µm apart. These sections were then transferred to microscope slides and stained with H&E to visualise the cells. Images were captured at 20x magnification using an inverted light microscope. Serial images were taken at each point along the entire diameter of the disc and stitched together to create a montage image. At various points along this montage, measurements were taken to assess the degree of cell growth above and through the scaffold. These numbers were averaged out across each section and then across all three sections.

3.5 Results

3.5.1 Characterisation of Alvetex®Scaffold

Alvetex®Scaffold is a porous polystyrene scaffold that is inert and non bio-degradable. Each void of the scaffold is connected to neighbouring voids via interconnects which provides a large surface area for three dimensional cell growth; this is clearly visualised in Figure 3.3A, where voids are outlined in red and interconnects in blue. SEM micrographs were analysed to determine the average void and interconnect size, which were found to be 40µm and 13µm respectively (Figures 3.3C and D respectively). The scaffold is commercially available in several formats including well inserts which are shown in Figure 3.3B. With this format, the monolith is cut into membranes that are 200µm thick and 22mm in diameter, allowing the inserts to sit in individual wells of a traditional 6 well culture plate. This insert format is also available in a smaller diameter of 16mm which is fully compatible with 12 well culture plates, for larger scale experiments. Polystyrene clips hold the membrane in place within the well so that the discs don't float when immersed in media – these clips can be easily removed using a pair of forceps, which allows the scaffold to be processed. The benefits of the insert format over a standard plate format is that the cells are fed from above and below the surface ensuring that nutrients from the growth medium fully penetrate the scaffold interior. This results in a similar growth environment for cells in the very interior zone of the scaffold to those cells growing on either surface.

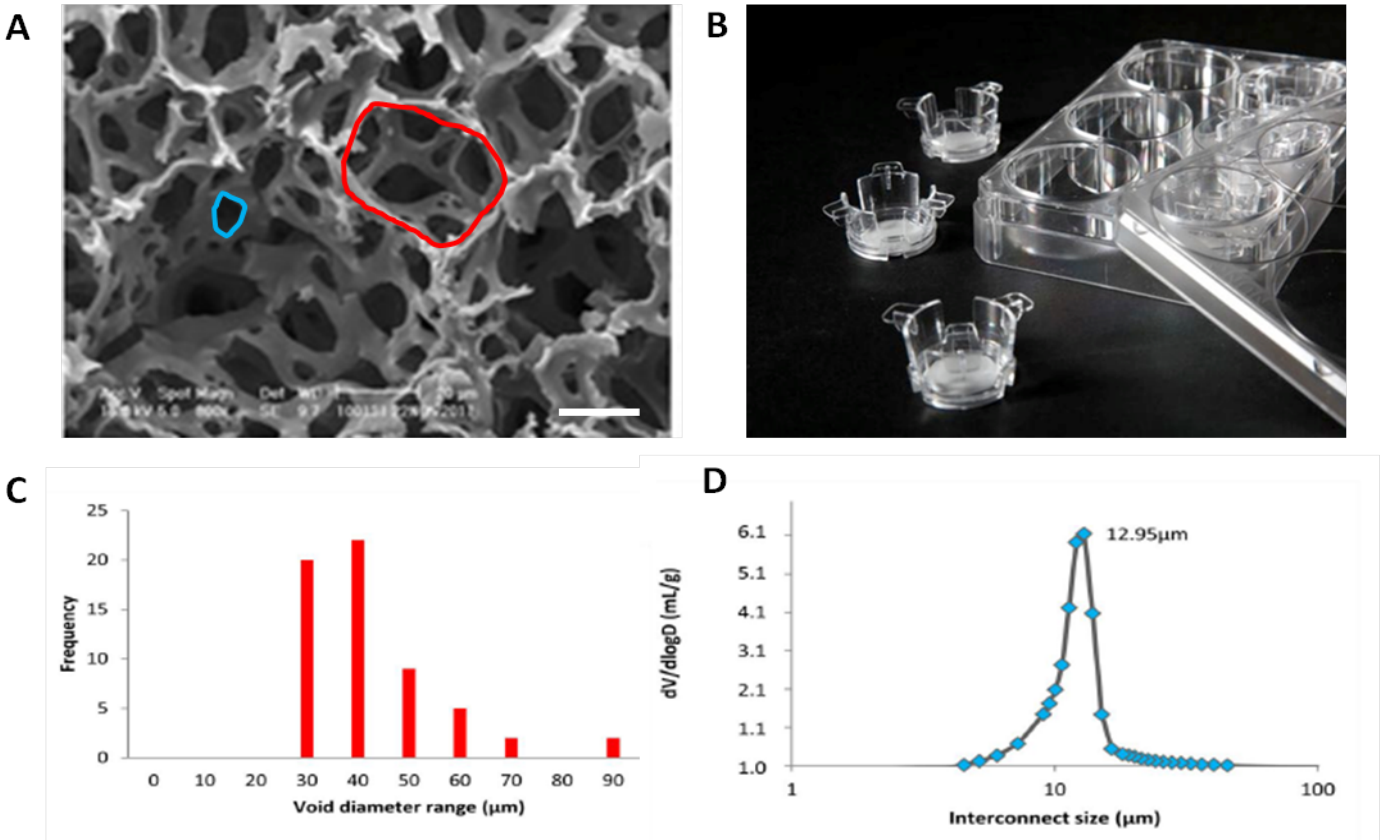

Figure 3.3 Alvetex®Scaffold is a porous polystyrene material for 3D cell growth.

Alvetex®Scaffold is a highly porous PolyHIPE polystyrene material (A) that is commercially available in formats readily compatible with existing plasticware (B); 6 well inserts are shown in this example. The scaffold has pores (outlined in red in A) of approximately 40µm and interconnects (outlined in blue in A) of approximately 13µm (C&D). Scale bar = 20µm. Data courtesy of ReproCELL Reinnervate.

3.5.2 Determination of optimal growth parameters of Met4 cells on Alvetex®Strata

Met4 squamous carcinoma cells were chosen as a model cell type for the development of a propagation methodology because they are small, invasive, and grow successfully on Alvetex®Scaffold, as demonstrated in Figure 3.4.

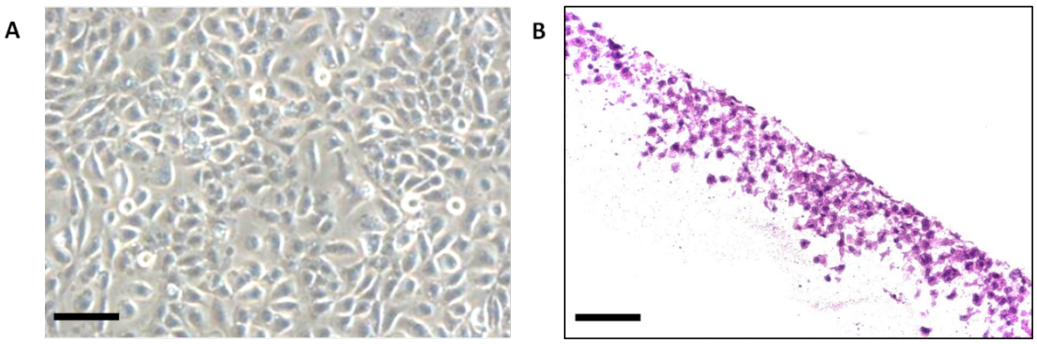

Figure 3.4 Met4 cell growth is vastly different on a gross level between 2D and 3D growth substrates.

Met4 squamous carcinoma cells were grown at a density of $1x10^6$/ml for 7 days in 2D conditions on tissue culture plastic (TCP) and in 3D conditions on Alvetex®Scaffold. Cells in 2D were photographed under phase-contrast microscopy (A) and 10µm sections of scaffold were stained with H&E to visualise cells (B). Scale bars = 50µm in A; 100µm in B

It was thought that these cells would be the most expedient cell-line to use during model development; theoretically given how easily they penetrate the scaffold, they should be easy to retrieve and re-passage. In order to start developing a retrieval protocol, the parameters for optimal cell growth had to be established. Firstly, cells were grown in parallel in 2D and 3D for 2 weeks in order to work out the optimal experimental growth period. As Figure 3.5 shows, Met4 cells show very different growth profiles in 2D and 3D, a clear sign that the environment in which a cell is placed has a direct impact on cell growth. The growth of cells in culture generally follows a well-characterised 4 phase curve consisting of a slow lag phase as well adjust to culture conditions, a short log phase of exponential growth due to an abundance of nutrients, an extended stationary phase, where nutrients become a limiting factor, and finally a death phase, where the cells begin to die due to an accumulation of toxic metabolites and by-products, as well as a lack of fresh nutrient; this is visualised in Figure 3.5A. Met4 cells largely confirm to this pattern when grown in 2D conditions, though there is a lack of an

observable stationary period. However, when placed in 3D conditions, cells remain in the lag phase for longer, probably explained by the extra adaptation required for the transition between 2D and 3D growth, as well as the period of penetration through the scaffold. This has indications for the period of cell growth allowed in 3D before experimental analysis, showing that considerations have to be made for the difference in growth dynamics between 2D and 3D.

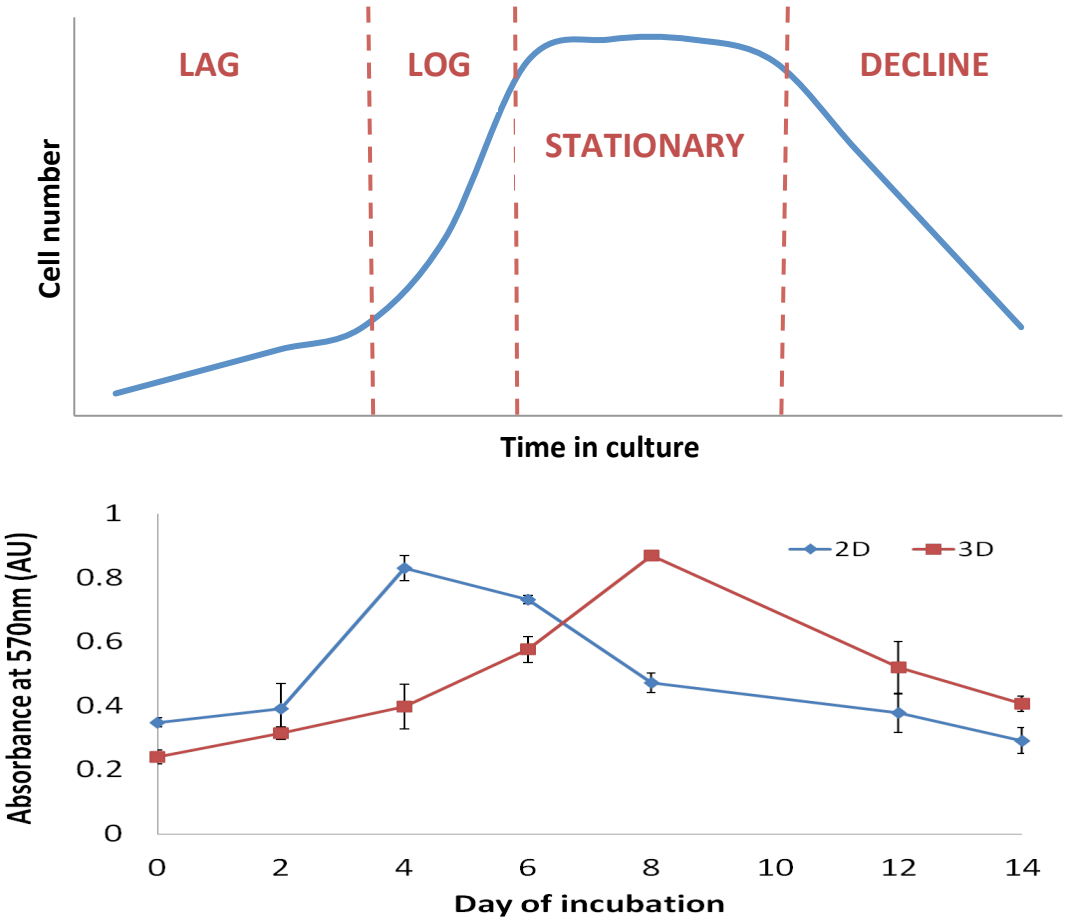

Figure 3.5 Met4 growth curve in 3D is shifted to the right, resulting in a longer lag phase, but higher viability after 2 weeks in culture.

Cell growth curves tend to show four characteristic phases: lag, log, stationary and decline (A). Met4 squamous carcinoma cells were grown on TCP or Alvetex®Scaffold for 2 weeks, and the viability tested through an MTT assay every 2 days (B). Cells grown in 3D grow slower than their 2D counterparts, reaching the exponential phase of growth 4 days later. However, cells remain viable for a longer period of time in 3D. Data presented as n = 3 ± SEM.

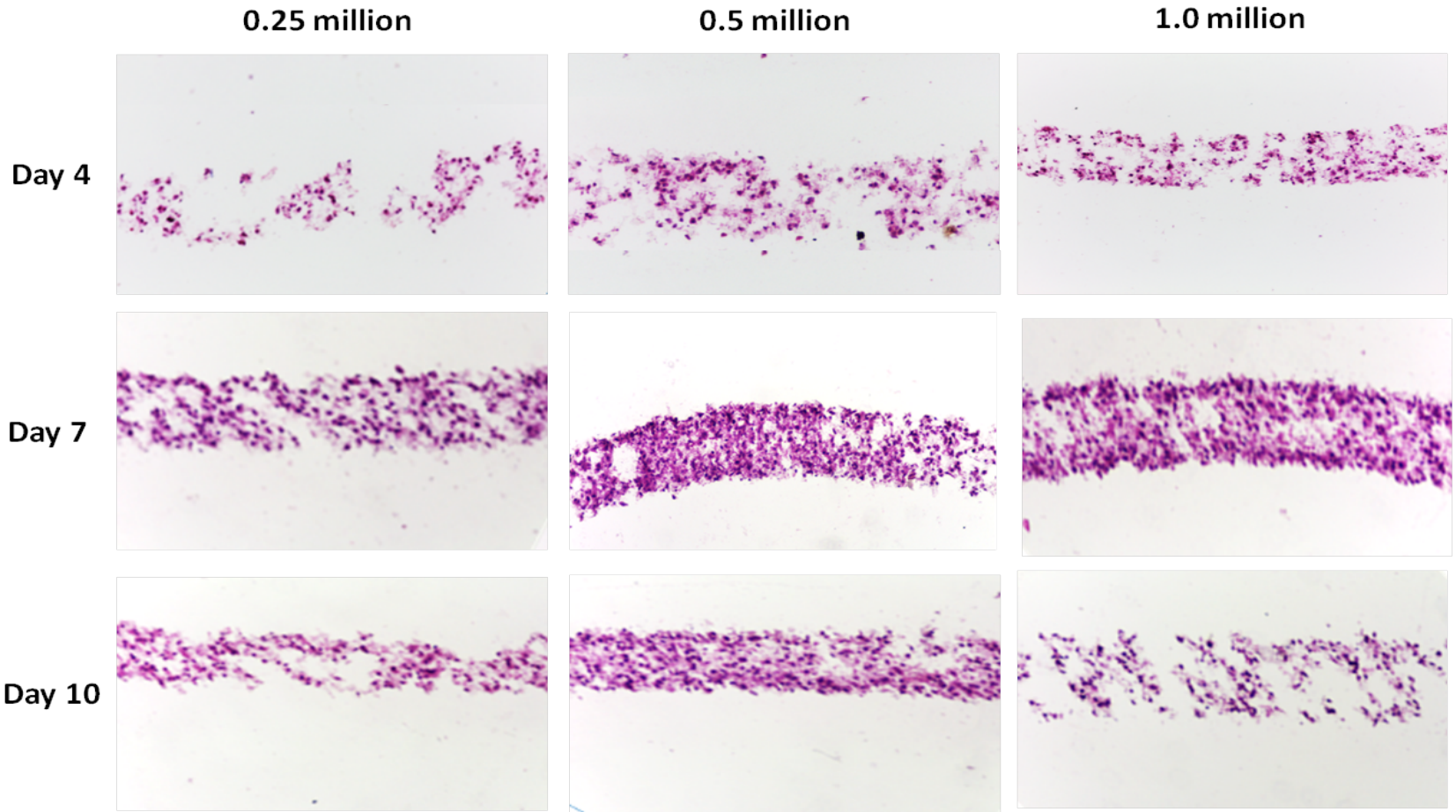

Figure 3.6 Met4 cell growth in 3D can be optimised by manipulating seeding densities and culture period.

Met4 squamous carcinoma cells were grown for either 4, 7 or 10 days at various seeding densities in order to define optimal growth conditions. Cells at 4 days (A-C) show spare growth at all seeding densities tested, whereas after 10 days in culture (G-I), cells appear to be dying. Out of the three densities tested, cells seeded at 0.5million cells/disc show the most consistently optimal penetration of the scaffold. Scale bars = 200µm.

The next parameter to be optimised was the initial seeding density for growth on Alvetex®Scaffold. Cells were grown at three different concentrations for either 4, 7 or 10 days in order to characterise penetration through the scaffold (Figure 3.6). Cells showed penetration throughout the depth of the scaffold even by 4 days, but growth was sparse at all three tested densities. By day 10, cells began to die at all three tested densities, which fits well with the growth profile established in Figure 3.5. Based on this, an experimental growth period of 7 days was determined on. Looking at Figure 3.6D-F, it is clear that cells penetrate the scaffold best when seeded at 0.5 million cells/disc (Figure 3.6E). In order to ensure that the cells were viable and healthy, an MTT assay was conducted, and as Figure 3.7 indicates, the cells are healthiest at 7 days of growth.

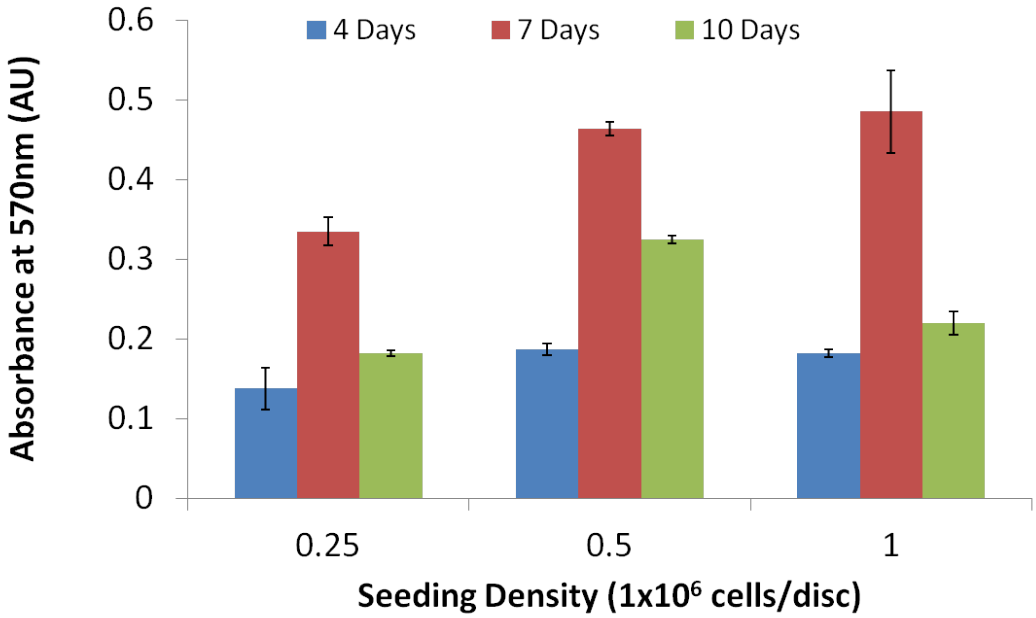

Figure 3.7 The viability of Met4 cells grown on Alvetex®Scaffold is dependent on seeding density and culture period.

Met4 squamous carcinoma cells were grown for either 4, 7 or 10 days at various seeding densities in order to define optimal growth conditions. At the end of the growth period, the cells were analysed for viability using a MTT assay. Values show absorbance at 570nm, and indicate that cells grow optimally when seeded at 0.5 million cells/disc. Data presented as n = 3 ± SEM.

Cells can be seeded onto Alvetex®Scaffold in one of two ways: dispersed or concentrated seeding, as shown in the schematic in Figure 38. The dispersed seeding method results in a

similar pattern of cell distribution to that in traditional 2D culture. Cells are seeded onto the scaffold in a suspension of the final volume of media (for 6 well plates, this is usually between 8 and 10ml) and allowed to settle evenly across the entire surface of the membrane. An alternative method of cell seeding involves concentrating the cell suspension into a 100µl droplet, which is added directly to the centre of the scaffold. This is followed by a short incubation to allow the cells to adhere prior to the addition of the final volume of culture media. This method does not result in uniform coverage, rather the cells grow in a concentrated zone at the centre of the scaffold, but cells are allowed to penetrate the entire depth of the scaffold rapidly.

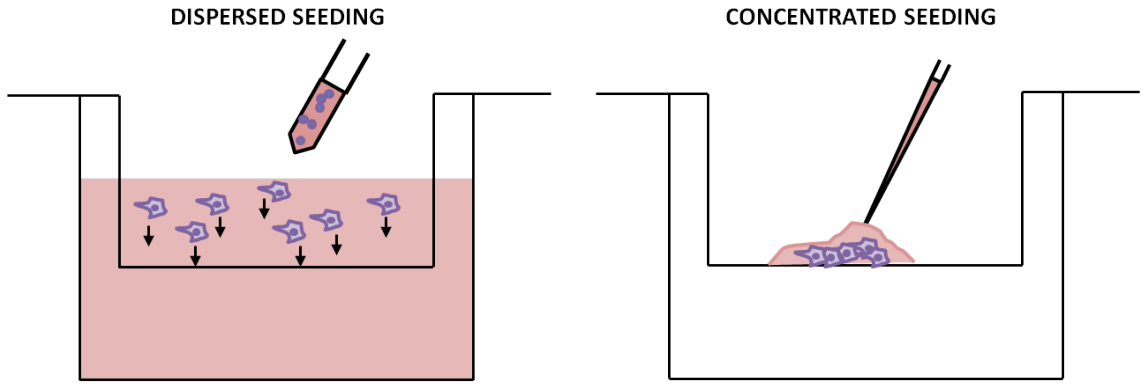

Figure 3.8 Cells can be seeded on Alvetex®Scaffold in two distinct ways.

There are two methods of seeding cells when using Alvetex®Scaffold. In the disperse seeding method, 5ml of culture media is added to the well containing scaffold. The cell suspension is diluted in 4ml of culture media and added drop wise across the entire surface of the scaffold, allowing cells to settle evenly over the surface. In the concentrated seeding method, cells are concentrated in a 100µl droplet which is added directly to the centre of the scaffold, allowing cells to rapidly penetrate the material. Cells are incubated for 15 minutes at 37°C to allow attachment before 8ml of culture media is added.

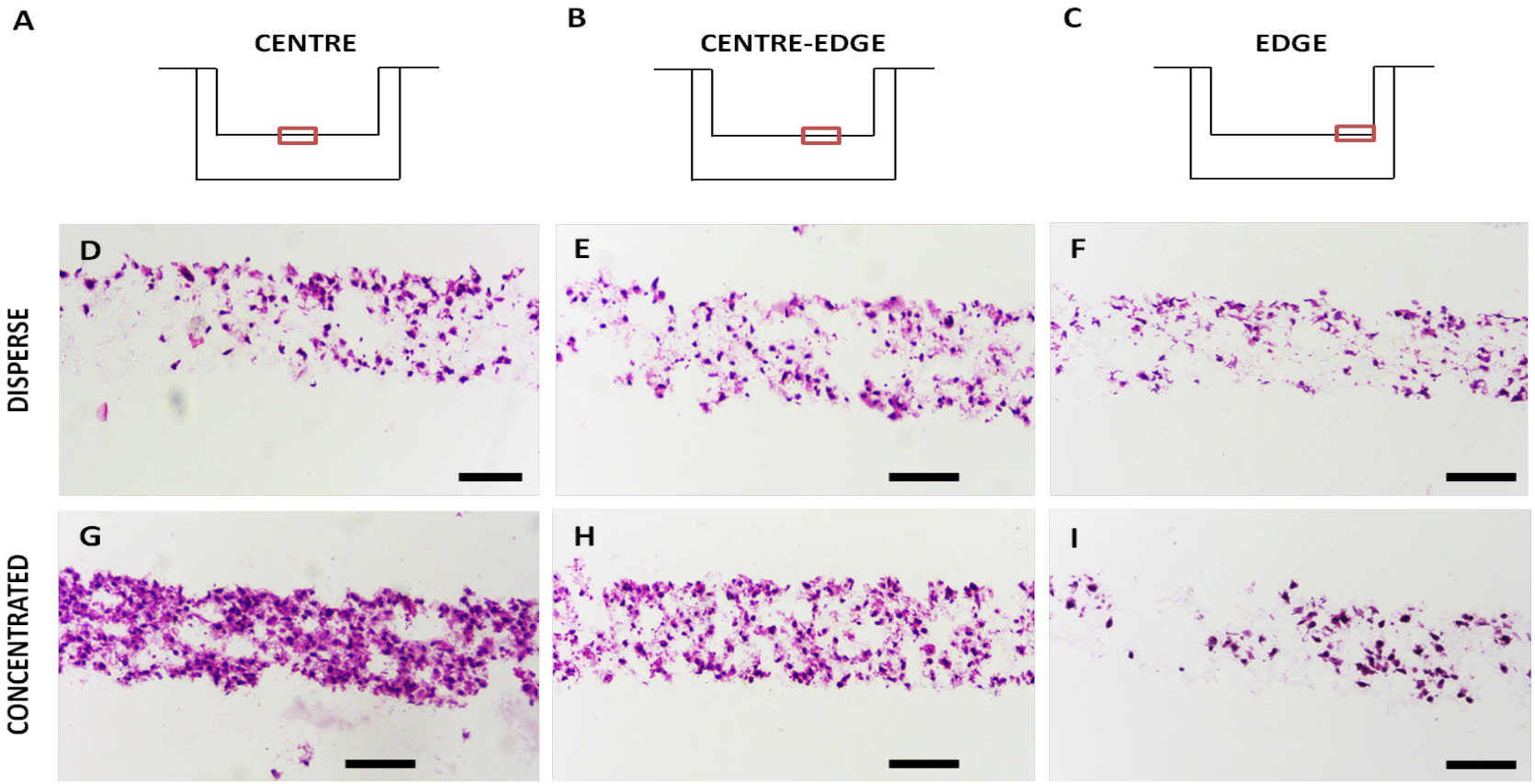

Figure 3.9 Met 4 cell growth through the scaffold differs between dispersed and concentrated seeding methods.

Met4 squamous carcinoma cells were grown for 7 days at a concentration of $0.5x10^6$ cells/disc. 10µm sections were stained with H&E for visualisation. A-C show the area of the scaffold disc that is shown in the images below. D-F show cells seeded using the dispersed method, and G-I show cells seeded using the concentrated seeding method. The images show that cells grow more evenly across the entire surface when using dispersed seeding, but share pack together when seeded using concentrated seeding. Scale bars= 100µm.

As Figure 3.9 shows, Met4 cells grow evenly across the surface of the disc when seeded dispersely (Figure 3.9D-F), but the growth is sparse, and cells occupy regions of the scaffold individually rather than in colonies. In contrast, cells grow densely and pack together tightly when seeded in a concentrated manner, sharing close cell-cell contacts. In terms of on-going experiments, cells were seeded in a concentrated manner.

3.5.2 Optimising cell retrieval from Alvetex®Scaffold

Cells were seeded using the concentrated method at 0.5 million cells/disc and grown for 7 days. They were then incubated in a weak Trypsin-EDTA solution for 5, 15 or 30 minutes in order to determine the optimal period of incubation. If cells are not incubated for long enough, the enzymatic treatment will not fully loosen the adherent cells, and the yield will be low, however if the cells are incubated too long, the trypsin will have a negative effect on cell viability. Neutral Red staining was used to determine how many cells were left on the scaffold after trypsin incubation, and Trypan Blue was used to determine how many of the released cells were still viable. As Figure 3.10 shows, the optimal period of incubation was found to be 15 minutes. However, the average cell yield was 335,000, which is significantly lower than the 500,000 cells initially seeded. In order to increase the efficacy of the retrieval protocol, two strategies were tested: cutting the discs up in order to increase the surface area available for the trypsin to act, and adding a method of agitation to ensure the entire scaffold was exposed to the trypsin solution. Cutting the scaffold into quarters prior to incubation increased the cell yield, as indicated by a lighter Neutral Red staining pattern (Figure 3.11E-F). Two methods of agitation were directly compared: a linear platform shaker and a rotary orbital shaker. These two methods did not show a significant difference when looking at samples cut into halves (Figure 3.11B-C), but there was a clear difference with the samples cut into quarters, with the rotary shaker removing more cells than the platform shaker, suggesting that a higher degree of agitation aids the detachment of cells from the scaffold.

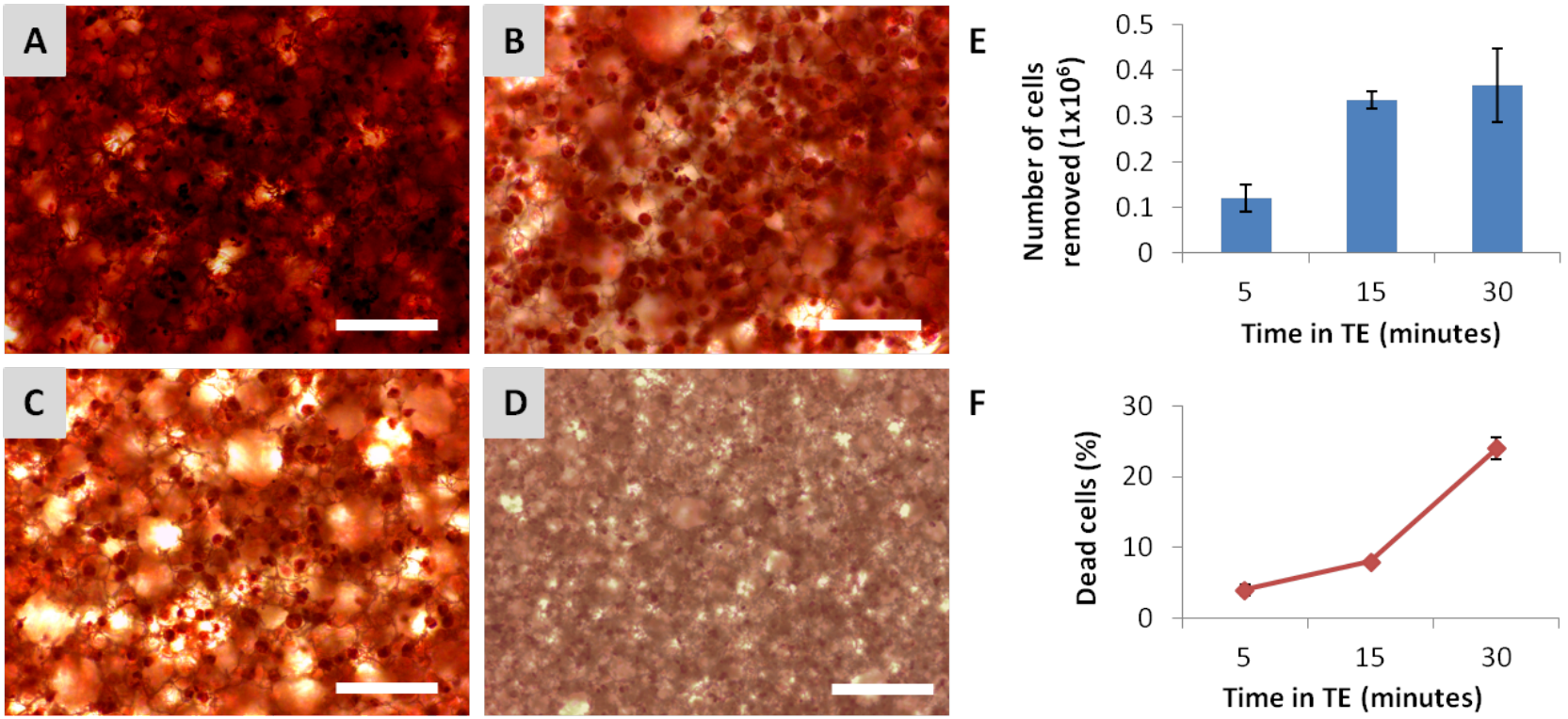

Figure 3.10 Cells can be removed from Alvetex®Scaffold through incubation with Trypsin-EDTA.

Cells were grown at $0.5x10^6$ cells/disc for 7 days and then incubated with either 4ml PBS (A) or 4ml 0.25% Trypsin-EDTA (TE) for 5 minutes (B), 15 minutes (C) or 30 minutes (D). 4ml of culture media was added to each well and triturated several times before being collected and the cells counted (E-F). The discs were stained with Neutral Red (NR) to visualise the remaining cells (A-D). Increasing trypsin incubation times results in increased cell yields, but decreased viability indicated both by Trypan Blue Exclusion Assay (F) and NR staining which shows reduced uptake of the vital stain (D). Results therefore suggest an optimal incubation time of 15 minutes. Data presented as n = 3 ± SEM. Scale bars = 100µm.

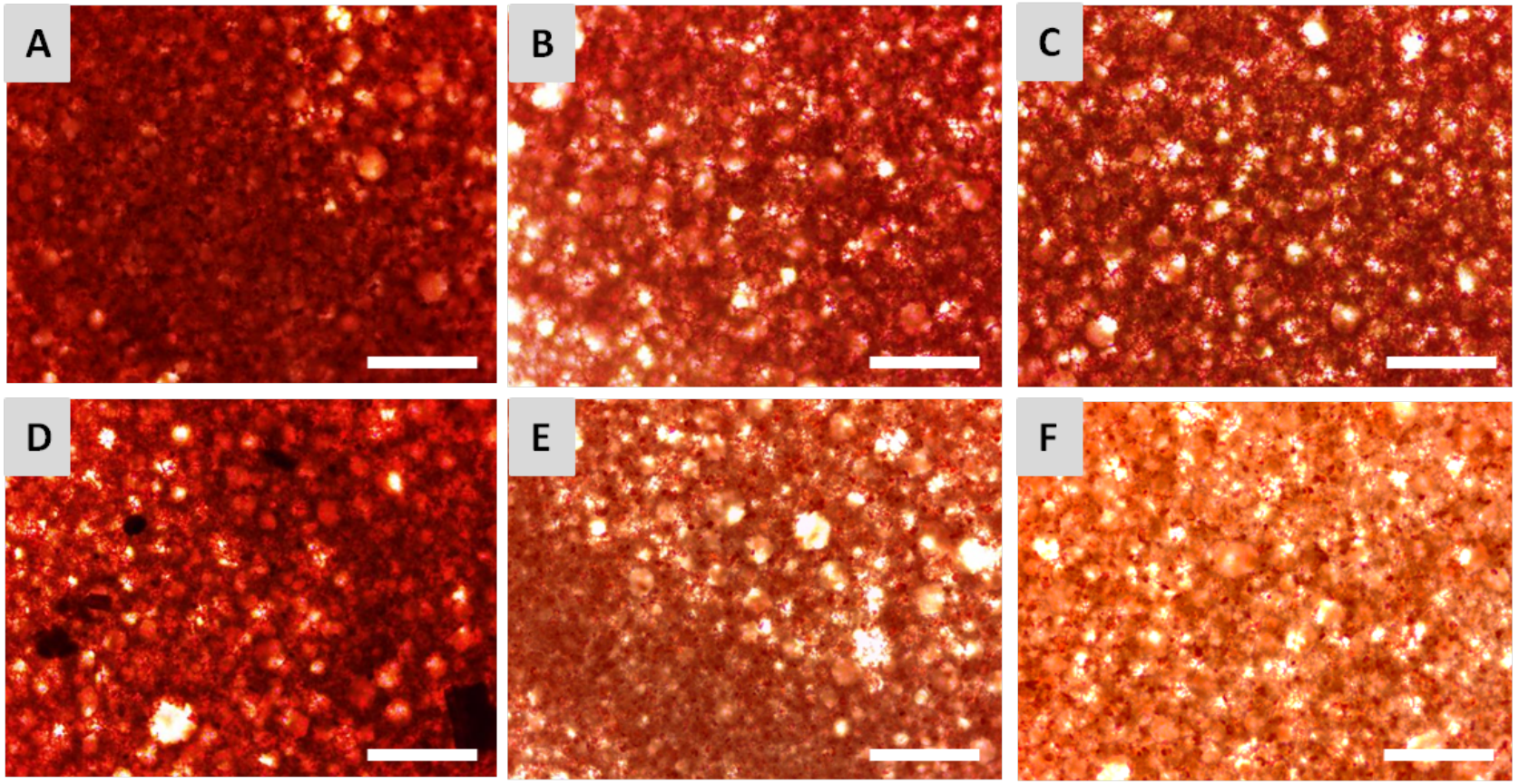

Figure 3.11 Adding agitation to the TE incubation can improve cell removal from Alvetex®Scaffold.

Cells were grown at $0.5x10^6$ cells/disc for 7 days and then incubated with either 4ml PBS (A and D) or 4ml 0.25% TE (B-C, E-F) for 15 minutes. Treated discs were cut into halves (B-C), or quarters (E-F) prior to TE incubation, and agitated using either a linear platform shaker (B&E) or a rotary orbital shaker (C&F) during TE incubation. Lighter staining indicates that there are fewer cells remaining. Results indicate that the optimal conditions are those that increase the surface area exposed to TE. Scale bars = 100µm.

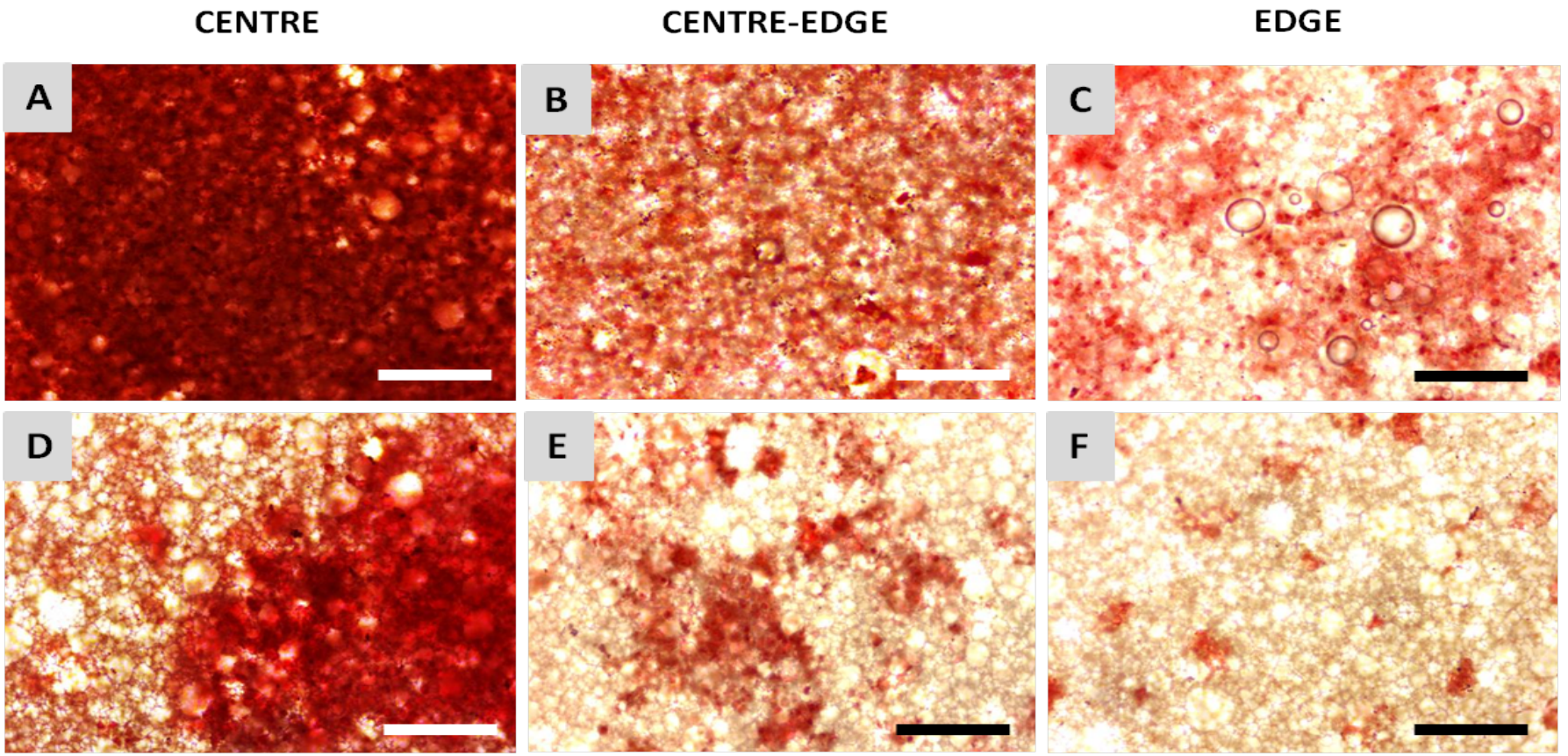

Figure 3.12 Cells that are retrieved from Alvetex®Scaffold do not proliferate or migrate as much as controls.

Cells were grown at $0.5x10^6$ cells/disc for 7 days and then retrieved using the optimised protocol designed. These cells were counted, and $0.5x10^6$ cells were then seeded onto a fresh scaffold and grown for 7 days (D-F). The same amount of cells were retrieved from a T25 and seeded in the same manner as a control (A-C). Cells that were retrieved from scaffold did not proliferate or migrate out from the central droplet as well as the control cells. Scale bars = 100µm.

3.5.3 Optimising cell passaging using Alvetex®Scaffold

Using the protocol designed in Section 3.3.2, cells were retrieved from one scaffold, counted, and seeded onto a fresh scaffold at 0.5 million cells per disc using concentrated seeding, as before (Figure 3.12). As a control, cells retrieved from 2D culture were seeded in the same way to see if there was any difference between 2D→3D and 3D→3D passaging. Cells retrieved from a 2D source grew densely in the centre of the disc, uniformly in the middle, and sparsely towards the edge, as expected. However, cells seeded from a 3D source did not migrate outwards from the central droplet and failed to populate any of the middle or edge zones of the scaffold. This was classed as an unsuccessful passage, and taken as an indication that Alvetex®Scaffold is not a suitable material for 3D propagation. This is because cells penetrate the pores and attach tightly to the walls, making it difficult to remove a sufficient number of cells to facilitate a second passage without drastically reducing the cell health.

3.5.4 Characterisation of Alvetex®Strata

3.5.4.1 Differences between Alvetex®Scaffold and Alvetex®Strata

Alvetex®Strata differs from the Scaffold format in only one viable – pore size. Whereas Alvetex®Scaffold has an average pore-size of 40µm, Strata membranes have an average pore size of 13µm, with interconnects of roughly 6µm. These differences can be seen in the SEM images in Figure 3.13A and B. Because the pore-size is smaller than the average diameter of most mammalian cells, these cells do not penetrate through the scaffold but rather grow on top of the membrane in a scaffold-free manner. As the SEM images in Figure 3.13C and D show, the cells grow in a tissue-like formation on top of the porous material. Porosity and average pore-size have been established as parameters that vastly affect the growth of cells in culture. Thus, it is unsurprising that when the same cell type is grown on both Alvetex®Scaffold and Alvetex®Strata, the resultant morphologies and cellular organisation are drastically different, as demonstrated in Figures 3.13E and F.

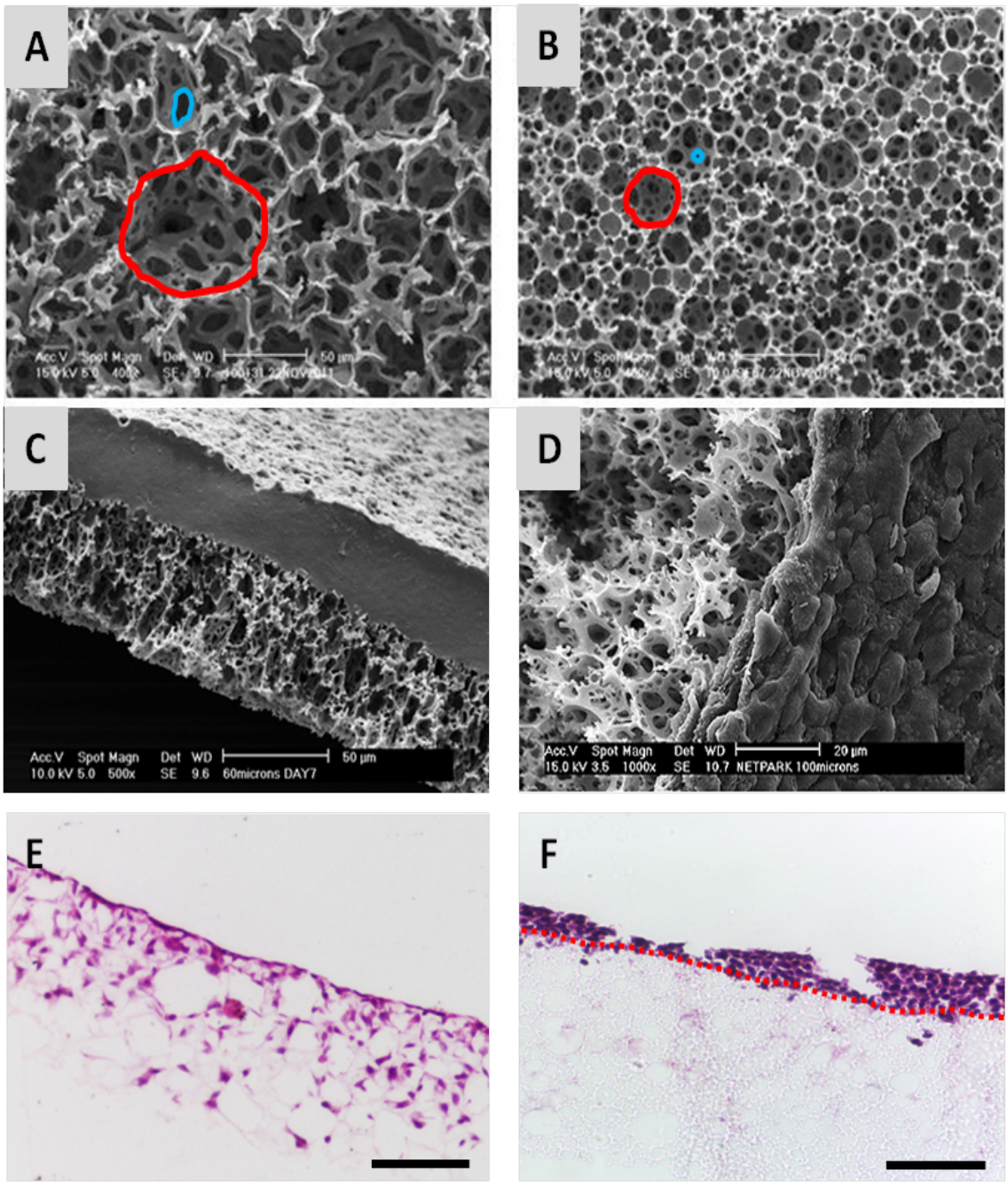

Figure 3.13 Alvetex®Strata is a novel membrane that differs from Alvetex®Scaffold in terms of pore-size.

Alvetex®Scaffold (A) and Alvetex®Strata (B) are both polyHIPE foam membranes that differ only in pore-size; as shown in the red (pore) and blue (interconnect) outlines, Strata membranes have smaller pores of approximately 13µm, compared to pores of approximately 40µm in Scaffold. The smaller pore size allows cells to grow on top of the membrane in a scaffold-free manner (C&D). E and F are H&E stained sections that show how the same cell type grows in a different way when presented with either Scaffold (E) or Strata (F). SEM images courtesy of ReproCELL Reinnervate. Scale bars = 100µm.

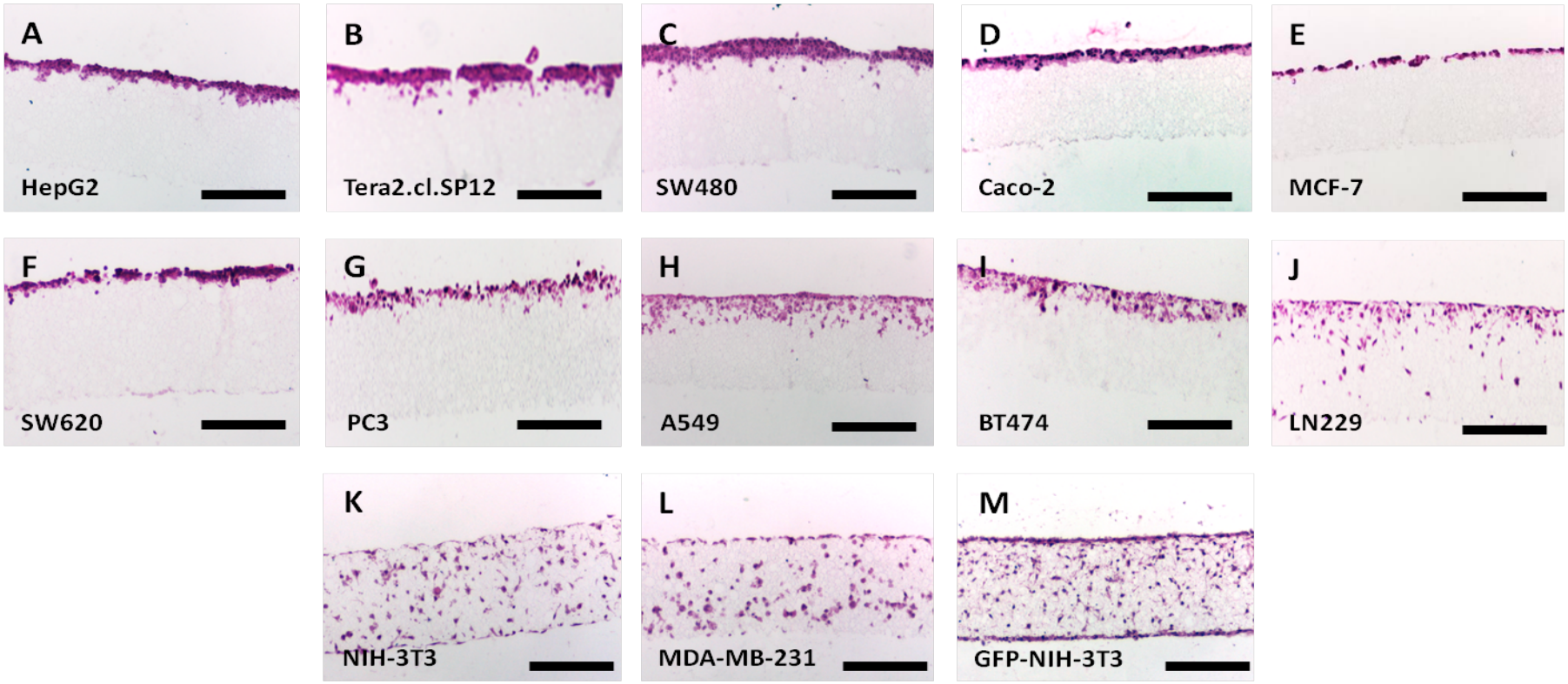

Figure 3.14 Several cell-types were grown on Alvetex®Strata to investigate the effect of a smaller pore-size on cell growth.

Several cell types were grown on Strata membranes in order to characterise different migration patterns seen on small-pore material. The cells were all seeded at $1x10^6$ cells/disc and grown for 4 days. Despite a wide variation in cell type (e.g. cancerous, non-cancerous, epidermal, mesenchymal etc...), cells approach the material in one of three characteristic ways. Some cell types grow in 2-8 cell thick layers on top of the membrane with minimal penetration (A-E), some penetrate the material partially (F-J), and some penetrate the full thickness of the material with sparse growth in the mid regions (K-M). For the purposes of optimal cell retrieval and propagation potential, cells belonging to the first class are the most promising candidates. Scale bars = 100µm.

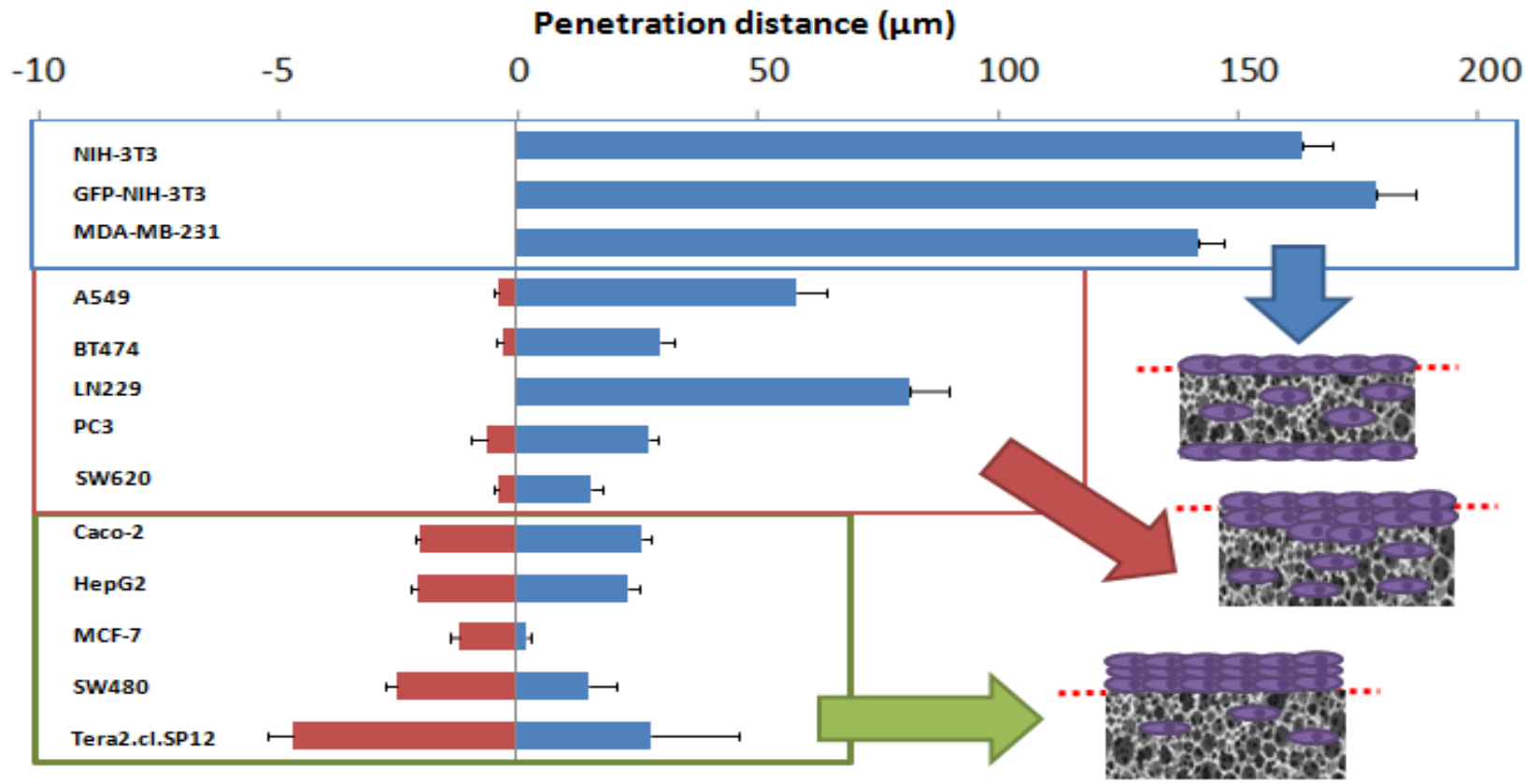

Figure 3.15 Cell types on Alvetex®Strata penetrate the material in one of three characteristic ways.

As visualised in Figure 3.13, cells types grow in one of three characteristic ways on Alvetex®Strata- minimally penetrative (green box), partially penetrative (red box), and fully penetrative (blue box). These migratory patterns can be quantified using a penetration assay, with red bars representing the thickness of the cell later above the membrane, and the blue bars showing the depth of penetration through the membrane. Data presented as n = 15 ± SEM

3.5.4.2 Characterising cell growth on Alvetex®Strata

In order to characterise how cells grow on the novel Strata material, a variety of different cell types were grown on the material for the same time period of 4 days and at the same seeding density of 1 million cells per scaffold. To ensure that a range of cellular shapes and behaviours were investigated, a pool of thirteen diverse cell lines was studied, ranging from breast carcinoma cells (MDA-MB-231) to fibroblasts (NIH-3T3) and stem cells (Tera2.cl.SP12). As expected, these cell lines all grew differently on the material, as can be seen in the H&E images in Figure 3.14. However, a pattern began to emerge – despite the wide variety of cell lines grown, the penetration patterns roughly fell into one of three classes. Some cells grew in thick layers on top of the membrane, as expected. However, some cells penetrated the top layers of the material, and others even penetrated the entire depth of the material. Presumably this is due to differences in cell size, with smaller more malleable fibroblastic cells being able to 'squeeze' through the pores. This could also be an effect of cellular organisation. Some cell types, such as HepG2 cells and Tera2.cl.SP12 cells, share very close cell-cell contacts and grow best when densely packed. This behaviour would make single cell migration highly unlikely, and thus would promote tissue-like growth on top of the material.

This behaviour was explored further using a penetration assay. Images were taken across the entire diameter of the disc and stitched together to create a montage image. At several points along this image, two distances were quantified: the distance from the top of the cell layer to the material surface, and the distance from the material surface to the furthest penetrating cell. The former was given a negative value and the latter a positive value, and the distance in microns calculated using the scale bar. These values were plotted in order to see whether the pattern observed in Figure 3.14 could be quantified (Figure 3.15). The results of the penetration assay clearly confirm the qualitative data from the H&E images. This pattern however was not seen previously with the Alvetex®Scaffold material, and thus a representative cell line from each of the 'classes' was chosen and grown in parallel on both materials using the same growth conditions. The three cell lines analysed in this way were the human invasive breast carcinoma cell line MDA MB 231, which grows throughout the material, the adenocarcinomic human alveolar basal epithelial cell line A549 which penetrates the upper depths of the material, and the human hepatocarcinoma cell line HepG2, which grows on top of the material entirely (Figure 3.16).

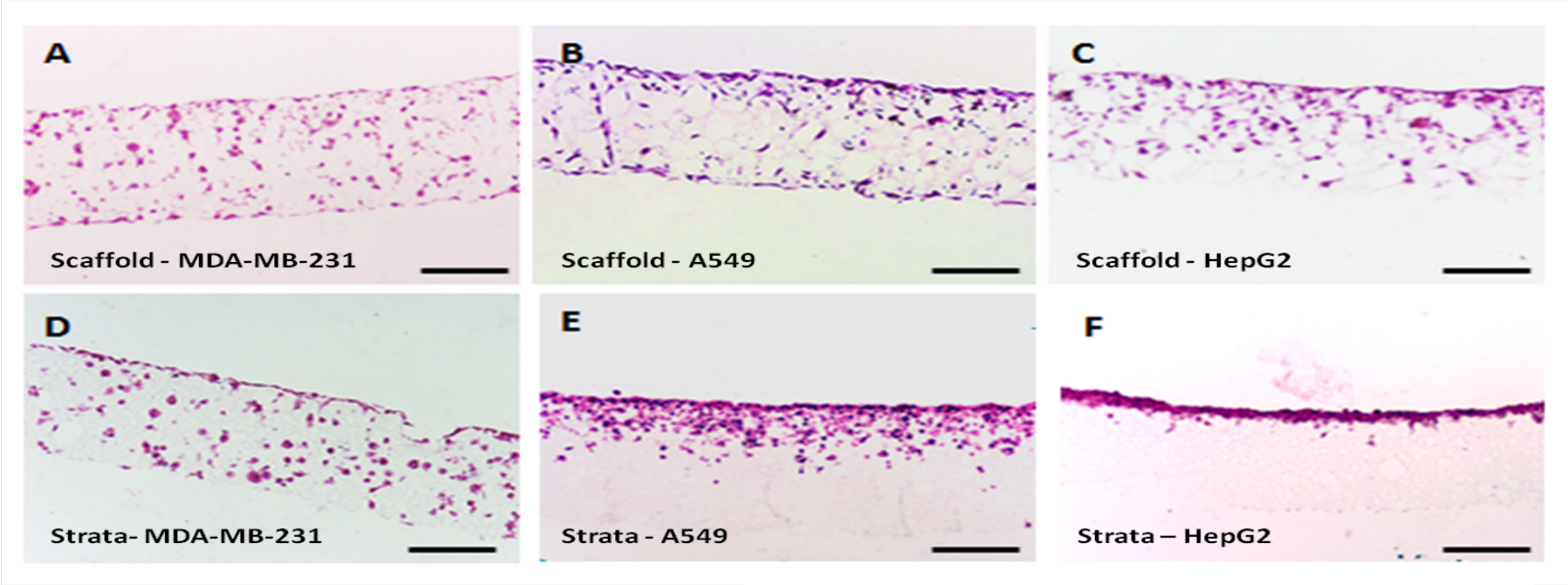

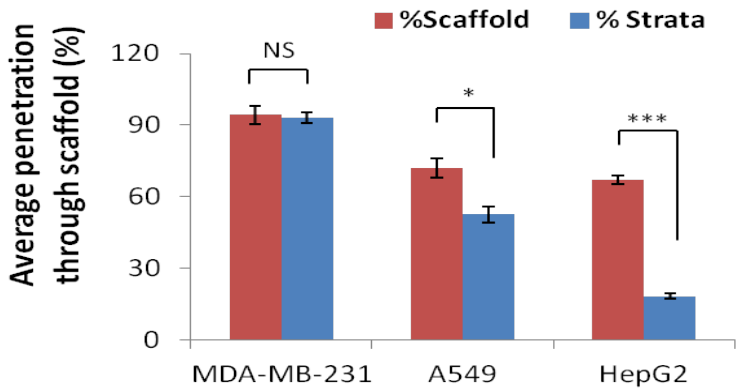

Figure 3.16 The smaller pore-size of Alvetex®Strata results in different cell growth patterns than those seen in Alvetex® Scaffold.

Representative cell types from each migratory class were grown in parallel on Scaffold and Strata in order to test whether the characteristic migration pattern was unique to the smaller-pore material. H&E images show that fully penetrative cells (A&D) show little difference between materials, whereas minimally penetrative cells grow in vastly different ways on Strata versus Scaffold (F compared to C). These differences were quantified using a penetration assay (G). Data presented as n = 15 ± SEM. Statistical significance through one-way ANOVA. Scale bars = 100µm

The MDA-MB-231 cells do not show drastic growth differences between Scaffold and Strata (Fig 3.16A and D), and the penetrative behaviour was statistically similar (Fig 3.16G). Contrastingly, the A549 cells show a more sparse growth pattern on Scaffold and penetrate the entire depth, whereas they prefer to grow in a denser 'clump' in the upper regions of the material on Strata (Fig 3.16B and E). However, the biggest difference was seen for the HepG2 cell line (Fig 3.16C and F) – the HepG2 cells are entirely restricted to the surface when grown on Strata, but grow throughout the material on Scaffold. They organise themselves differently also – the cells appear to grow in smaller colonies in Scaffold, whereas they form a single thick 'slab' of cells in Strata. This tissue-like behaviour is much more representative of the way hepatocytes organise themselves in the liver *in vivo*. Because of this, HepG2 cells were chosen to take forward into presumptive 3D cell propagation models.

3.5.5 Characterising HepG2 growth on Alvetex®Strata

HepG2 cells are an immortalised cell line originally derived from the isolated liver tissue of a well-differentiated hepatocellular carcinoma. They are epithelial in morphology when grown on 2D tissue plastic, as seen in the phase contrast image in Figure 3.17A. However, hepatocytes *in vivo* display a characteristic cuboidal morphology, indicating that these cells have gone through aberrant flattening. When these cells are grown in 3D on Strata, the cells show a more rounded spherical shape, as indicated in the H&E panel in Figure 3.17B.

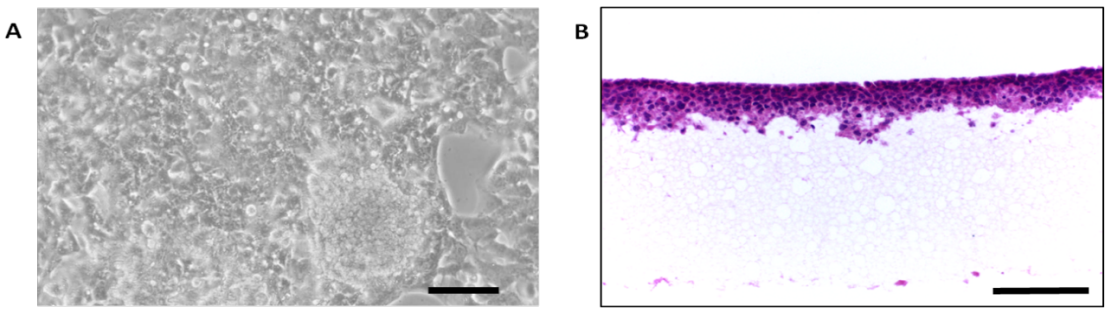

Figure 3.17 HepG2 cell growth is vastly different on a gross level between 2D and 3D growth substrates.

HepG2 hepatocellular carcinoma cells were grown at a density of $1x10^6$/ml for 7 days in 2D conditions on tissue culture plastic (TCP) and in 3D conditions on Alvetex®Strata. Cells in 2D were photographed under phase-contrast microscopy (A) and 10µm sections of Strata were stained with H&E to visualise cells (B). Scale bars = 50µm in A; 100µm in B

This clearly shows that Strata provides a permissive 3D environment for cell growth that allows cells to adopt more physiological morphologies and behaviours.

In order to characterise the cell growth of HepG2 cells in 3D compared to 2D, the cells were grown for two weeks in parallel on 2D tissue plastic and Strata (Figure 3.17). The differences in the cell cycle between 2D and 3D cells are incredibly similar to the differences seen for Met4 cells grown on tissue plastic and Scaffold in Figure 3.5B. The HepG2 cells grown in 2D show the characteristic lag, log, stationary and decline phases as expected. However the cells in 3D show a much longer lag phase and there is a noticeable absence of a discernible log phase. Instead, cells grow steadily over a longer period of time, possibly due to the extra resources being required for active adaptation to a novel three dimensional micro-environment. From the data in this graph, it would appear that the optimal growth period for cells on Strata, from a viability stand-point, is between 6 and 8 days.

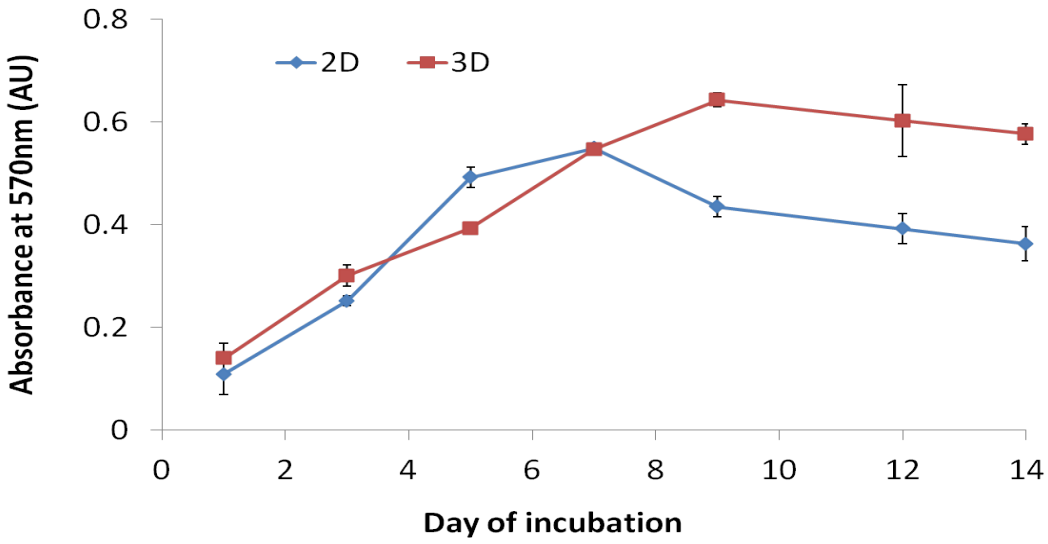

Figure 3.18 HepG2 cells show a different pattern of cell growth in 3D than they do in 2D.

HepG2 hepatocellular carcinoma cells were grown on TCP or Alvetex®Scaffold for 2 weeks, and the viability tested through an MTT assay every 2 days. Cells grown in 3D grow slower than their 2D counterparts, reaching the exponential and stationary phases of growth 2 days later. However, cells remain viable for a longer period of time in 3D. Data presented as n = 3 ± SEM.

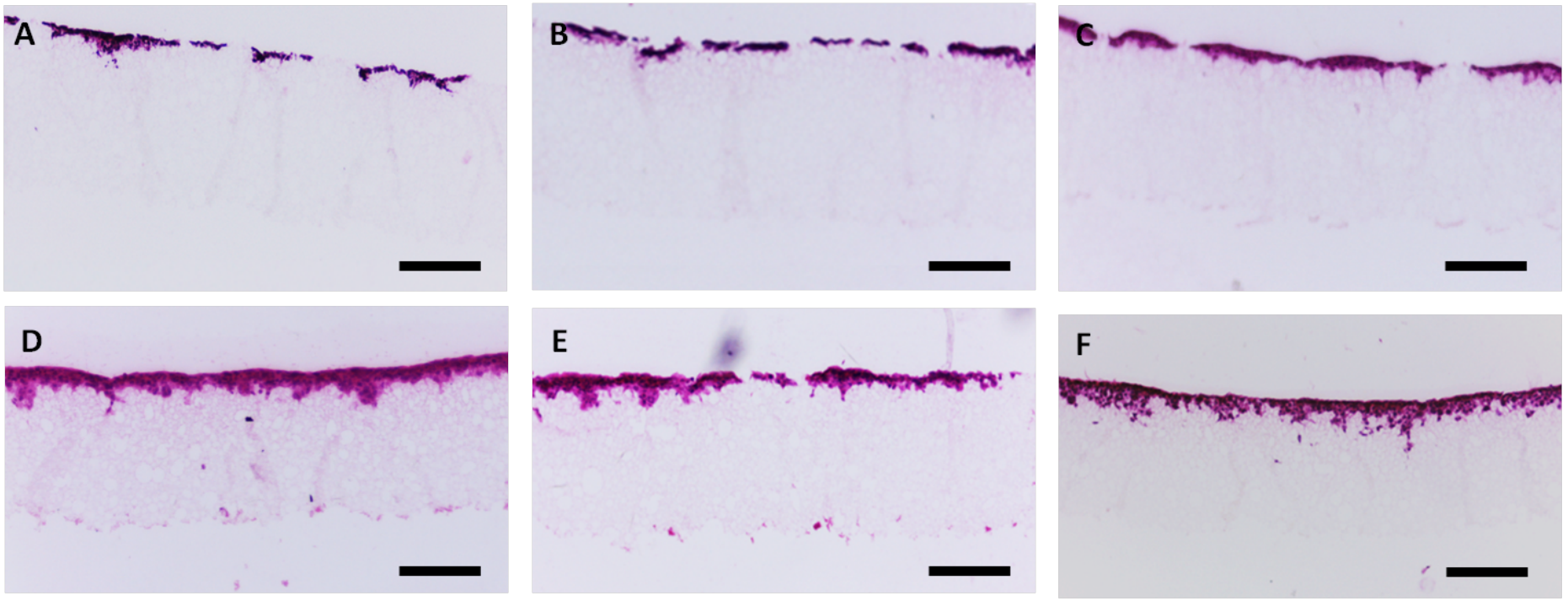

Figure 3.19 The penetrative behaviour of HepG2 cells changes throughout the culture period.

HepG2 cells were grown over 2 weeks at a density of 0.5 x 10^6 cells/disc without media changes. Initially cells grow mostly on the top of the membrane (A-C), however after 7 days in culture, cells begin to penetrate the membrane. Therefore, the optimal time period to grow HepG2 cells in order to facilitate maximal cell retrieval is 5 days. Scale bars = 100µm

However, viability was not the only issue in determining the best growth period for on-going experiments. A key advantage of using Strata for a retrieval and propagation model is that the majority of cells grow on top rather than through the material, meaning that cell removal should theoretically be easier. Thus, it was important to see how cell organisation on the material varied across the growth period (Figure 3.19). Using the same penetration analysis model as with the other cell-lines in Figure 3.15, HepG2 penetration was quantified over the 14 day period. As Figure 3.19 shows, the behaviour of these cells towards the material changes with cell growth. Initially, cells grew in a thin layer right at the surface, only extending a few microns either above or below the surface. However, for the first 5 days, cells began to penetrate less and occupy the space above the membrane, reaching a peak at day 5. Between day 5 and day 7 however, there is a drastic change, with cells beginning to penetrate the material to an extent far outweighing the cells growing on top – this mirrors the period of most exponential growth in Figure 3.18, indicating that rapid growth is accompanied by penetration through the material, possibly due to lack of space. Penetration through the material continues from day to day 14. Therefore to maximise the advantage of membrane-free growth as well as ensuring cell viability is optimal, a growth period of 4-5 days was determined upon for retrieval and re-passage attempts.

3.5.5 Propagating HepG2 cells using Alvetex®Strata

A methodology for the retrieval and re-passaging of HepG2 cells from Strata was developed by the industrial partner for this project, ReproCELL Reinnervate. This methodology drew on the optimised retrieval of cells from Scaffold shown in Figures 3.10 and 3.11, utilising both Trypsin incubation and agitation. At the set up, 1 million HepG2 cells were seeded diffusely and grown for 3-5 days. The cells were grown diffusely in order to promote even growth across the surface of the material, and actively discourage growth downwards throughout the depth material which is often seen when seeding in a concentrated manner. The high cell number was chosen to take into consideration a loss of cells through incomplete retrieval. The media was changed after 2 days, and after 3-5 days the discs were removed from plastic inserts, placed into a fresh 6 well plate and incubated at 37°C for 15 minutes with 2 ml Trypsin-EDTA solution on a rotating platform.

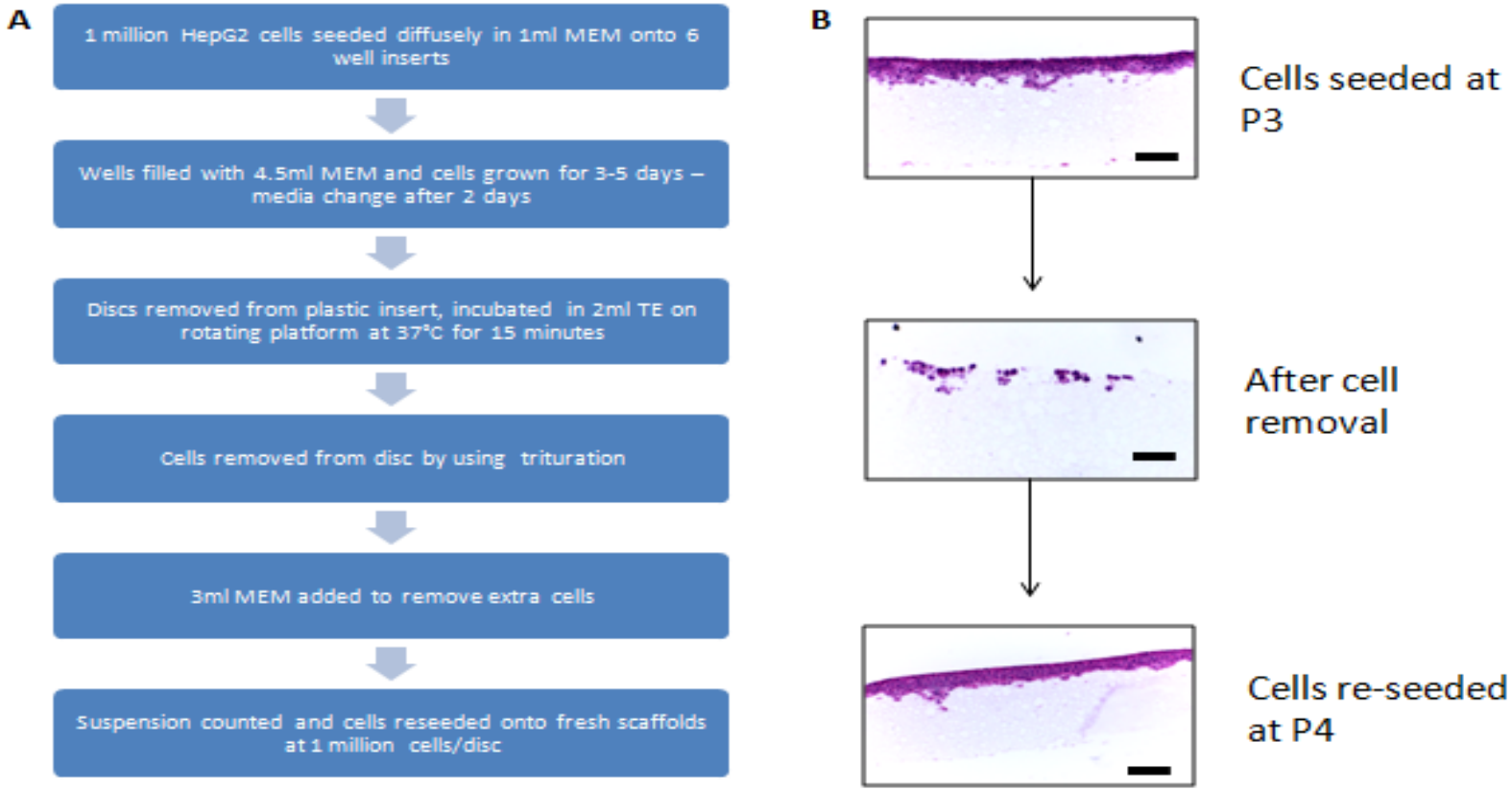

Figure 3.20 Cells can be propagated from one Alvetex®Strata disc to another.

Using data from the industrial partner ReproCELL Reinnervate, a methodology was developed to attempt to grow HepG2 cells on Strata, retrieve these cells, and re-passage onto fresh Strata (A). The H&E images before and after cell removal show that a majority of cells were successfully retrieved. These cells were successfully re-passaged (B). Scale bars = 100µm.

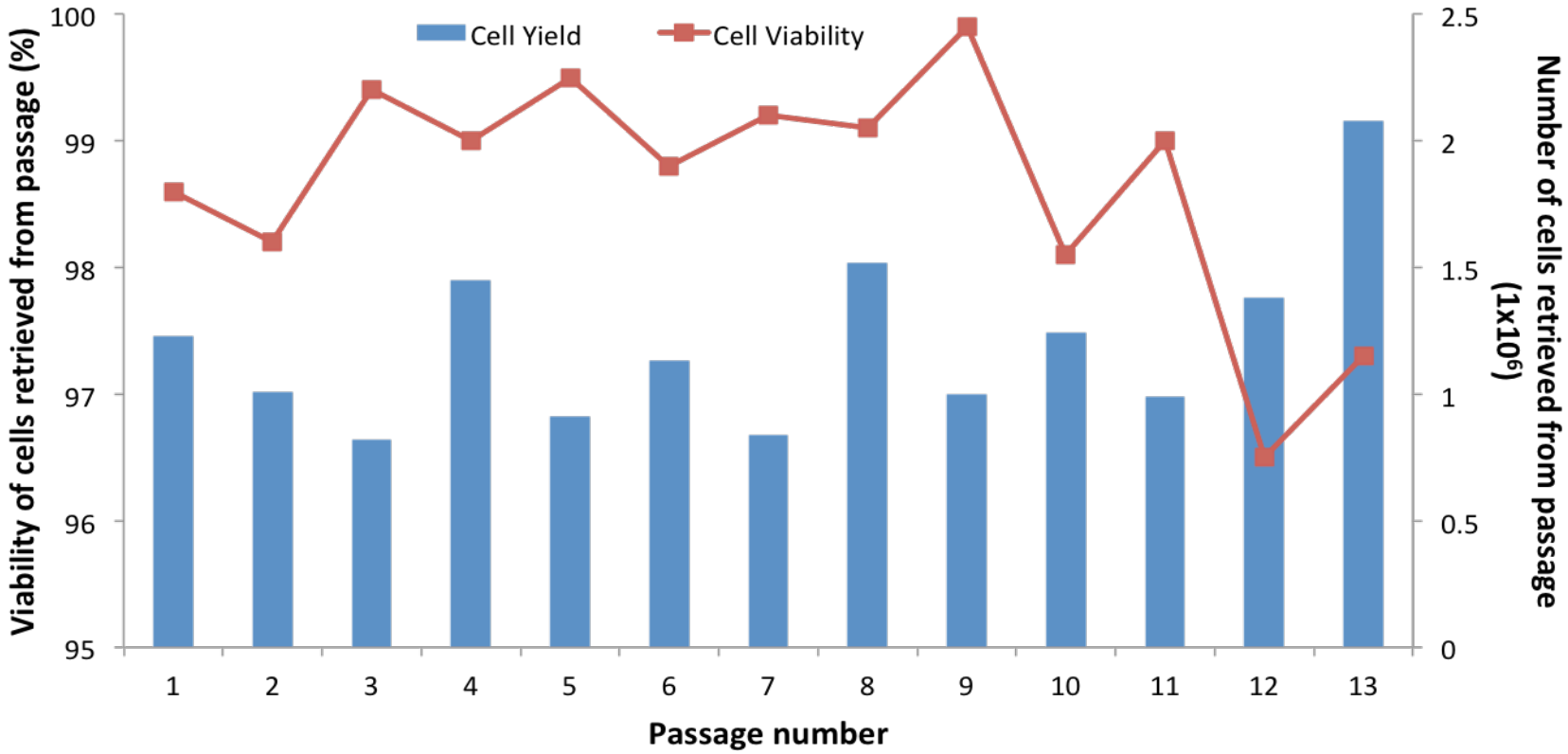

Figure 3.21 Using a newly developed propagation technique, HepG2 cells can be propagated in 3D for 2 months.

Using the methodology in Fig 3.18, cells were propagated for 2 months in 3D. At each passage point, the number of cells retrieved from the membrane was counted and recorded, and 1.0 million cells re-passaged per disc. The dotted line represents this seeding density. A live/dead Trypan Blue Exclusion assay was conducted at each passage point, and the counts expressed as a percentage cell viability. The data shows that cells can be successfully passaged in 3D over a long culture period, but with some inconsistent yields and viability.

The plates were removed from the incubator and then the dissociation solution was triturated using a 5ml pipette for approximately 30 seconds. The dissociation solution containing the released cells was transferred to a centrifuge tube, and additional media was added to the discs to collect any residual cells. This media was too added to the centrifuge tube, and the cells in the suspension were counted and re-passaged onto fresh Strata discs at 1 million cells/disc. This protocol is outlined in Figure 3.20A, and a stereotypical example of a re-passage is shown in Figure 3.20B. As seen from the H&E images, most of the cells from the scaffold were successfully retrieved; the average percentage retrieval was 73.4% using this protocol. This protocol was used to successfully maintain cells in 3D on Strata for 13 passages – the average cell yield and cell viability can be seen in Figure 3.21. Cell yield was calculated by counting the total number of cells retrieved across the number of discs and dividing this by the number of discs seeded. The viability was assessed by a Trypan Blue Exclusion Assay whereby dead cells are identified because their destroyed cell membranes allow dye to be taken up. As the data shows, the cell yield was generally either just above or just below the initial seeding density of 1 million cells per disc. With the exception of passage 13, this protocol does not seem to allow for significant proliferation across the growth period, meaning that the methodology cannot be used to expand cell populations. The viability, though generally high, does not stay consistent across the culture period. This is probably due to the inconsistent time points – at some passage points, cells were grown for 3 days without a media change, and at others they were grown for 4 days with a single media change. This was due to working around experimental and practical constraints.

Taking a few of these observations into consideration, the protocol was redesigned with a few minor modifications. Firstly, the initial seeding density was dropped from 1 million cells per disc to 0.5 million cells per disc. This was to promote proliferation. Secondly, cells were grown consistently for 4 days between passage points, with no media changes. This was to protect against any incidental cell loss that could've occurred during media changes. Thirdly, instead of using trituration to remove detached cells, a cell scraper was used. This was because trituration is known to cause mechanical damage to cells, which could in turn affect their viability. These differences are outlined in the updated protocol flow chart in Figure 3.22A.

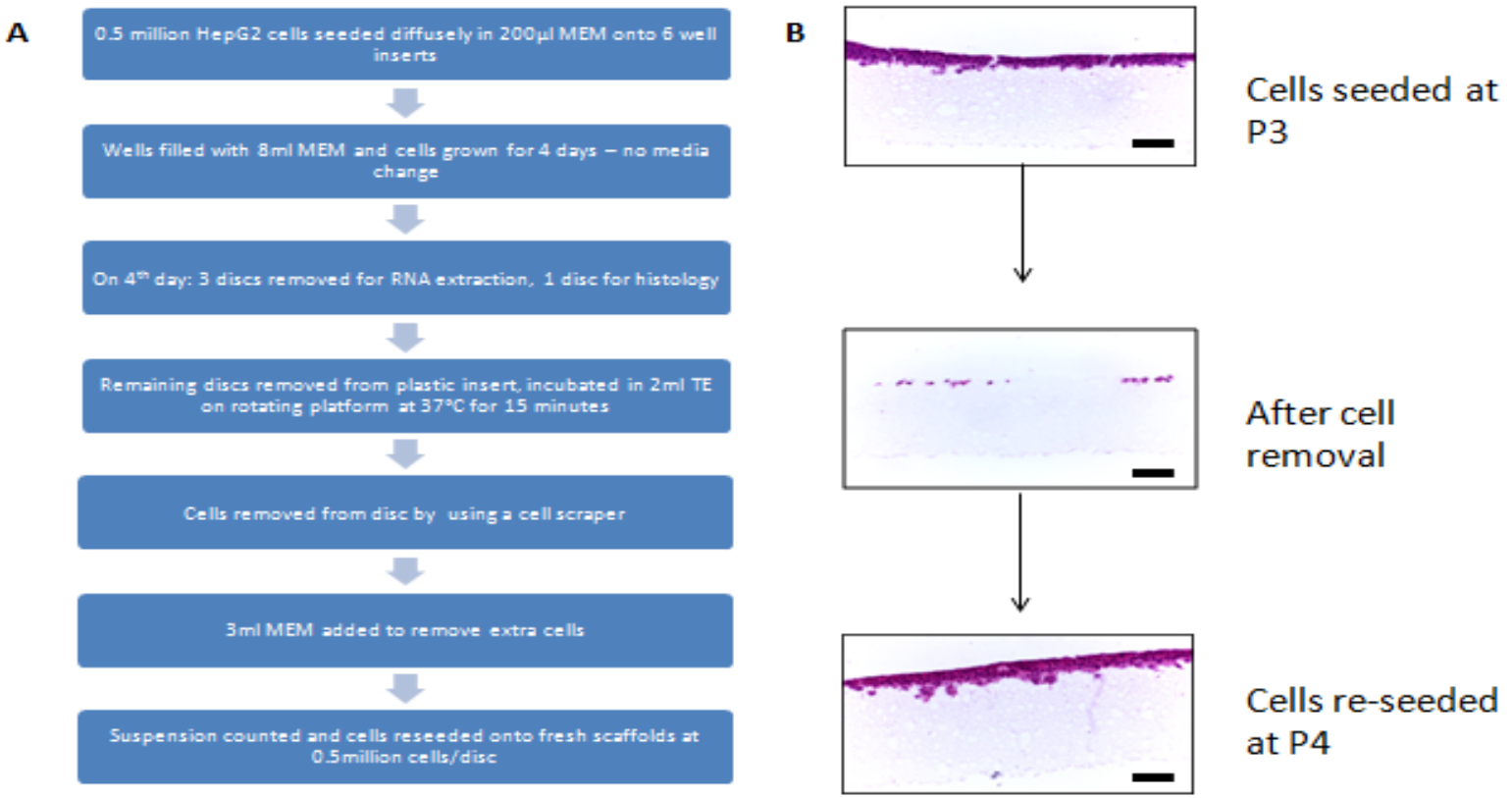

Figure 3.22 A newly optimised propagation technique was developed to optimise cell retrieval and regrowth of HepG2 cells.

Using previously gathered data from the Met4 cell line, as well as data from the industrial partner ReproCELL Reinnervate, the methodology for propagation previously used was optimised (A). The H&E images before and after cell removal show a higher degree of cell retrieval than was seen in Fig 3.19. These cells were successfully re-passaged (B). Scale bars = 100µm.

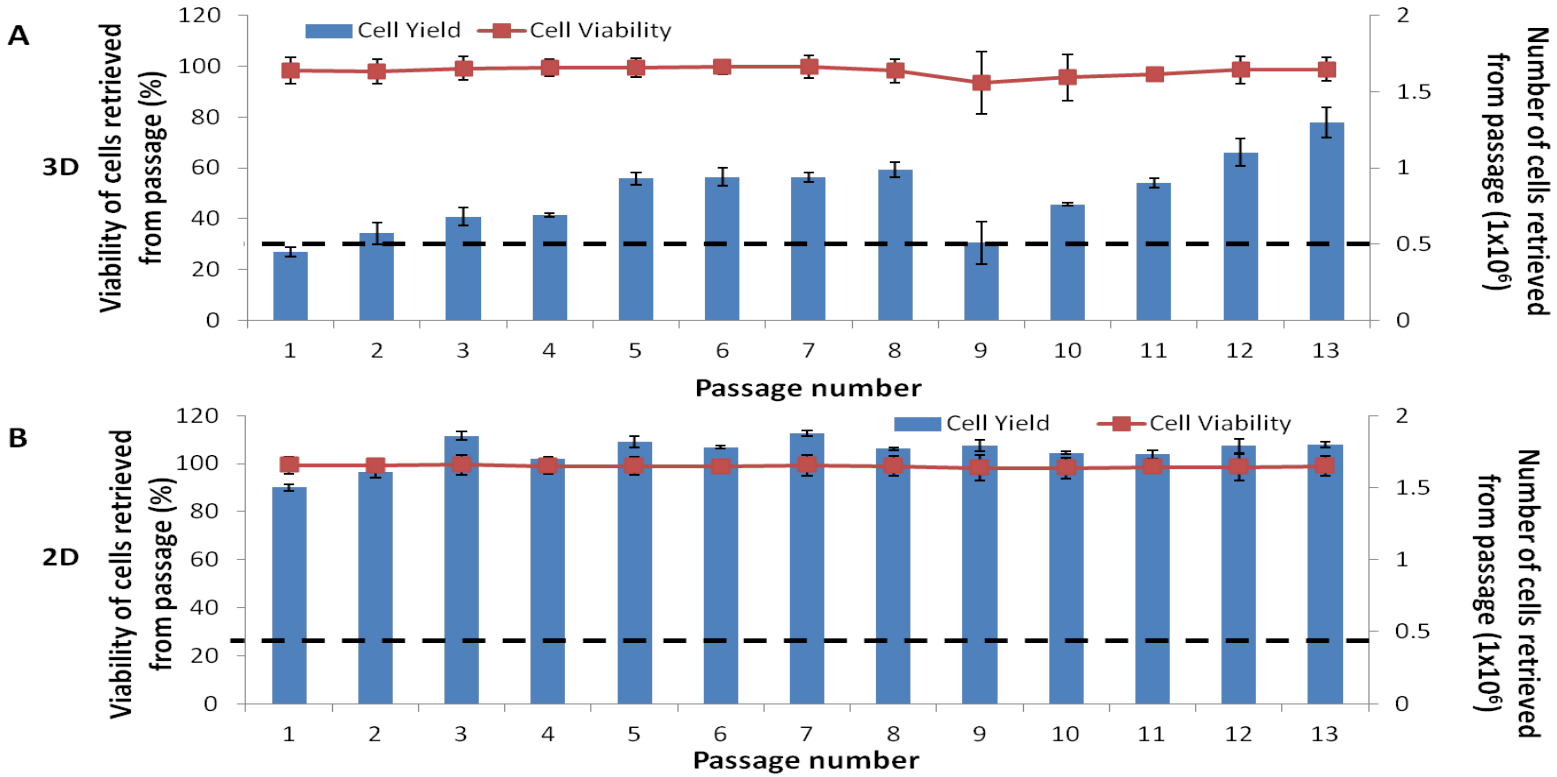

Figure 3.23 An optimised propagation technique allowed cells to be maintained in 3D for 2 months and the growth pattern differs significantly from that seen with 2D cells propagated in parallel.

Using the methodology in Fig 3.20, cells were propagated for 2 months in 3D. At each passage point, the number of cells retrieved from the membrane was counted and recorded, and 0.5 million cells re-passaged per disc. The dotted line represents this seeding density. A live/dead Trypan Blue Exclusion assay was conducted at each passage point, and the counts expressed as a percentage cell viability. The data shows that the optimised protocol results in more consistent yields and viability. (A). In parallel, cells were also propagated for 2 months in 2D using traditional sub-culture technique (B). Data shows that cells in 2D show higher levels of proliferation. Data presented as n = 6 ± SEM.

Comparing the H&E before and after images in Figure 3.22B to those obtained using the unmodified protocol in Figure 3.22B, it is clear that the changes to the cell retrieval protocol resulted in more efficient removal, with an average percentage cell yield of 91.2%. Finally, in order to compare proliferation and viability with that of standard 2D culture methods, cells were maintained in parallel in 2D and 3D for all 13 passages. This data can be visualised in Figure 3.22. Comparing Figure 3.23A to Figure 3.21 the redesigned protocol clearly results in more consistent cell viabilities. The cell yields, while not higher in totality, show more proliferation between passages when the lower initial seeding density is taken into consideration. Excluding the anomalously low yield at passage 9, it appears as though it takes the cells a few passages to fully adapt to the 3D environment, but once this adaptation occurs, cells begin to proliferate and double. The average doubling time before passage 4 is 6.11 days compared to 4.23 days between passages 5 and 9, and 3.71 days between passages 10 and 13. However, cells grown in 2D culture do show significantly higher cell proliferation and equally high viability. This may have indications for the limited use of 3D maintenance techniques for population expansion.

3.6 Discussion

The aim of this chapter was to develop and optimise a model that would enable long-term propagation and maintenance of cells in 3D. Propagation using 3D culture techniques is important for the future of 3D cell culture because most in-depth studies require large numbers of cells to be harvested for downstream analysis; a lack of a fully established protocol for cell expansion in 3D is a bottleneck in this process [138] Another key benefit of having a model that allows for 3D propagation is that cells can be 'primed' to the added dimensionality of the microenvironment prior to use in assays and experiments. This is particularly useful for hepatocytes, which are often used in drug toxicity assays. A priming event prior to toxicity studies would allow the cells to be fully adapted prior to the addition of the drug, and thus are less likely to react aberrantly due to the stress of adaptation.

The primary stages of this work focused on the use of a commercially available porous polystyrene scaffold Alvetex®Scaffold. Due to the compatibility of this scaffold with traditional culture plastic-ware, it represented an attractive model system to work with for 3D maintenance. The first hurdle to using this scaffold for cell passage is the encapsulation that occurs when cells are seeded onto the scaffold surface. Cells migrate into the interior of the scaffold, and inhabit the pores and interconnect within the material. They secrete an ECM and form multi-cell colonies within the interior, and while this is a positive in terms of enabling restraint-free 3D cell growth, it poses a problem for cell retrieval. With this in mind, the first cell-line utilized for model development was the Met-4 squamous cell carcinoma cell-line. These cells are small and semi-adherent, and therefore should be easier to retrieve from the porous topography. The standard protocol for the removal of cells from growth substrates as part of 2D subculture was modified to account for the differences between 2D and 3D growth environments. These modifications included increasing the length of time cells were incubated with trypsin-EDTA, the standard enzymatic solution used to cleave cells from the substratum. Cell retrieval is often damaging to cells – the use of 0.2% trypsin-EDTA solution to remove adherent cells from culture has been associated with changes at the proteome level, with an up-regulation of pro-apoptotic proteins in particular being found with extended exposure to this enzymatic solution [139]. The standard incubation times for 2D cells vary between 2 and 15 minutes. However, it was found that even 30 minutes exposure to Typsin-EDTA wasn't enough to retrieve a sufficient number of cells that were viable enough post-enzymatic treatment for re-passage. Another modification was to cut the scaffold discs into either halves or quarters in order to increase the surface area of cell growth that could be reached by the

enzymatic solution. A consideration of using porous scaffolds is the concept of nutrient and solution diffusion through the material [140], and thus, it is likely that if discs are simply bathed in trypsin, the enzyme solution may not reach the interior zone of the material, leaving a percentage of cells untreated, and thus unable to be disattached and retrieved. By cutting the discs across the diameter, it shortens the diffusion path for the trypsin, hopefully increasing the percentage of cells exposed. However, attempts at doing this did not significantly increase the cell retrieval. Finally, the discs were placed in trypsin and incubated on rotating platforms or orbital shakers in order to add agitation to the system since mechanical agitation has been shown to facilitate enzymatic cleavage using Trypsin [141]. However, added agitation to the incubation process again did not improve cell yields significantly.

Alvetex®Strata differs from the previously used scaffold with smaller pores and interconnect sizes. Research has shown that porosity and the nano-scale architecture of porous scaffolds has a significant impact on cell morphology. Nehrer showed that smaller pore sizes allowed primary chondrocytes to maintain their native shape for longer *in vitro*, as compared to cells grown on larger pore material, which became elongated and fibroblastic after 3hrs [142]. This finding also correlated to pore-size dependent changes in GAG content of intracellular DNA, showing the importance of pore size on cell morphology. However, for the purposes of this project, the major advantage of Alvetex®Strata is that the smaller pore-size allows cells to grow in scaffold-free tissue-like 'slabs' on top of the membrane surface, rather than infiltrating through into the scaffold interior. Because cells are growing on top, they can be more easily removed, and theoretically shouldn't need to be exposed to trypsin for longer than would be required for 2D monolayer subculture. Also, because cells are growing on the surface, the discs should not need to be cut into pieces in order to expose the interior zones of the cell population.

In order to characterise the material, several commonly used cell lines were incubated on the material. One interesting observation was that despite being isolated from a variety of diverse biological tissues, both healthy and cancerous, the cells approached the material in one of three definable fashions: they either populated the entire depth of the material, despite the small pore size, migrated partially through the material, or grew exclusively on top of the membrane. This finding highlighted the importance of the microenvironment on cellular behaviour *in vitro*, in this case migratory behaviour. In the body, the migratory pattern of a cell is determined by the properties of the matrix in which is grows, since this matrix needs to be

negotiated, travelled through, or cleaved in order for cell movement [143]. To further illustrate the importance of the cellular environment on cell behaviour, a representative cell type of each of three classes were grown under identical conditions on both the large pore Alvetex®Scaffold material and the small pore Alvetex®Strata material. Results form this study supported the concepts the Nehrer paper [142] illustrated – namely that porosity has an observable and quantifiable consequence on cell morphology and migration.

The overall results from this detailed study of cell growth on Strata® indicated that this material did indeed provide a more effective scaffold for the retrieval and re-passage of cells than Alvetex®Scaffold. The next step of the project involved comparing the different cell lines in order to determine the best cell-line for optimising a cell propagation methodology. Cell lines from either of the latter 2 classes (partial or full penetration of the material) were excluded since they significantly infiltrate the interior of the material and thus these cells would be as difficult to retrieve as cells from Alvetex®Scaffold. From the cells that grew on top of the membrane, the HepG2 cells were chosen for the next stages of this project. These cells were chosen because they are a well characterised and commonly used cell-line in preclinical drug testing [144]. They're also a good case study for the importance of cell shape on cell function since they exhibit functional polarity that is vital for their tissue specific function [145].

The first stages of designing this methodology involved the optimisation of the growth of HepG2 cells on the Strata material. Once parameters such as the length of time between subculture and the optimal seeding method and density were established, a cell retrieval protocol of 15-minute trypsin incubation with mechanical agitation was trialled. This protocol was found to be effective in releasing a sufficient number of viable cells from the material to allow subculture onto a fresh scaffold. This process was repeated over several generations, allowing cells to be maintained in 3D for 2 months. The initial protocol was found to produce inconsistent cell yields and viabilities, and was thus optimised further. These changes included reducing the initial seeding density to manoeuvre around the issue of over-confluence. The higher the initial seeding density, the thicker the cell layer above the scaffold. This causes issues with necrotic cores in the middle of the cell layer due to the increased diffusion path for nutrients from the media, as well as the excretion of potentially toxic metabolites [146]. Thus, the concern with using a high seeding density was that a percentage of the cells being passaged may be non viable, and this could explain the inconsistent cell viabilities. The optimised protocol led to a more consistent dataset over the 2 month passage period, making

the methodology of 3D propagation more standardisable and an effective alternate to maintaining cells in 2D.

Comparing 2D and 3D propagation directly in terms of proliferation and viability, there are two main conclusions. Firstly, there is no significant difference in viability between cells propagated in 2D and 3D, which validates the potential use of this methodology to routinely maintain cells in 3D. Secondly, cells propagated in 3D show a consistently lower proliferative capacity over the culture period. This lower proliferation rate is more physiological [122]. Several studies have demonstrated that cells grown in monolayers show artificially increased proliferation rates when compared to those seen in native tissue [31, 147, 148]. The finding that 3D cells do not show this exaggerated proliferation indicates that this methodology can be successfully used to maintain a 3D phenotype that more closely resembles the state of cells *in vivo*.

3.7 Conclusions

The following conclusions can be drawn from this Chapter:

- Alvetex®Scaffold provides a permissive environment that allows for routine 3D culture of mammalian cells *in vitro*. However, since the matrix entraps cells within the porous material, these cells are difficult to retrieve in sufficient numbers to allow for population expansion. Without population expansion, it is suboptimal to use this material for continual maintenance of cells in Alvetex®Scaffold.

- Alvetex®Strata differs from Alvetex®Scaffold by having smaller pore and interconnect sizes. This increases its potential use for continual propagation by allowing cells to grow on top of the membrane rather than entrapping them within it.

- Cells grow on Strata in one of three characteristic ways: some cell-lines fully penetrate the entire depth of the material, some cell-lines partially penetrate the top 50% of the material, and some grow almost entirely on top of the membrane, and only penetrate the very upper layers of the material. It is this latter cell-type that shows propagation potential and of these, the HepG2 hepatocyte cell line was used to develop a model.

- HepG2 cells can be easily retrieved from Strata membranes using conventional cell scrapers and standard enzymatic disassociation solutions. These cells can then be seeded onto fresh membranes and expanded further in culture.

- This methodology was used to maintain HepG2 cells in 3D for over 2 months at viabilities above 90%, which is in line with the viability of cells maintained in standard 2D culture. Cells propagated in 3D show lower proliferation rates than those in 2D; this rate of population doubling is closer to that of hepatocytes *in vivo*.

- The data from this chapter suggest that AlvetexStrata enables convenient and routine maintenance of cells in 3D, allowing these cells to be primed to 3D conditions.

With these conclusions in mind, the following chapter looks to use this methodology to compare the effect of 3D propagation on cell morphology.

Chapter 4: Comparing 2D and 3D maintained hepatocytes in terms of cellular morphology

4.1 Introduction

Cell shape plays a role in cell growth, differentiation, and death. Morphological cell events that occur in liver regeneration as well as in angiogenesis, inflammation, embryogenesis, wound repair and tumor metastasis, play a critical role in cell physiology. Morphogenesis, at the cellular level, can be defined as giving shape to, or defining the architecture of a cell. The assembly of the cytoskeleton, including the actin cytoskeleton, is the determining factor in specifying cellular morphogenesis and conferring shape to cells. Specifically in hepatocytes, the actin cytoskeleton is important in regulating cell shape, spreading, and migration and is a crucial determinant of hepatocyte polarity and functions [149,150].

The cytoskeleton of a cell is composed of three main elements: interfilaments, microtubules and microfilaments [151]. Microfilaments are composed of actin, and they function in cytokinesis, amoeboid migration and, importantly for this project, changes in cell shape. Stress fibres are contractile actin bundles found in non-muscle cells. Stress fibers have been shown to play an important role in cellular contractility, providing the necessary force for a diverse range of functions including cell adhesion, migration and morphogenesis. Stress fibers are necessary for the formation of cell-cell and cell-ECM interactions, including adherens junctions, tight junctions and focal adhesions [152,153]. One key paper [154] looked at stress fibres, and actin organisation in hepatocytes by characterising filamentous actin (F-actin) distribution in order to analyse the relative strength of the cell–cell and cell–substratum interactions experienced by hepatocytes. 2D hepatocytes cultured on collagen substratum showed intense stress fibers throughout the cells indicating strong cell–substratum interaction. Hepatocytes cultured as 3D aggregates but allowed to adhere to a rigid 2D substrate had less actin stress fibers than the 2D monolayer on collagen substratum but more stress fibers than the 3D spheroids grown in suspension, indicating an intermediate strength of cell–substratum interaction. The 3D adhered spheroids exhibited cortical F-actin distribution similar to the 3D spheroids in suspension indicating strong cell–cell interaction characteristic of hepatocytes *in vivo*.

Stress fibres are an interesting morphological landmark in this project because they provide a conceptual link between cell shape and cell adhesion in a matrix through the idea of cell spreading. Cell adhesion and motility depend strongly on the interactions between cells and ECM substrates. When plated onto artificial adhesive surfaces, cells first flatten and then deform as they spread. The cytoskeletal re-organisation of the cell that occurs during this spreading has been shown to have direct consequences on cell behaviours ranging from

proliferation and differentiation, to migration and metabolism. Adhesion and interaction with the matrix is required for cell progression through the G1 phase, and it is well established that growth in most normal cells requires cell adhesion and stimulation by growth factors [155-157]. Proliferation of many cells has been shown to be dependent on adhesion and spreading, requiring specific intracellular signaling events. In normal liver tissue, hepatocytes can remain quiescent for lengthy periods of time. However, after tissue disruption of cell-cell contact during cell isolation, the G0/G1 transition takes place [158] This mimics the entry into G1 of proliferating hepatocytes, *in vivo*, in the regenerating liver post liver injury. Research along these lines collectively shows that modulating a cell's cytoskeleton through cell spreading has an effect on complex cell behaviours. Thus, technologies that allow researchers to directly manipulate the cytoskeleton, such as micro-patterning, have contributed to our current understanding of how the geometry of a cell can influence *in vitro* findings.

Cell micro-patterning comprises the fabrication and use of a culture substrate with microscopic features that impose a defined cell adhesion pattern. It is a highly efficient method to investigate the sensitivity and response of a cell to specific micro-environmental cues. Micro-patterning techniques allow researchers to position cells in areas of the growth substratum *in vitro*, enabling the control of cell shape and position [159,160]. All micro-patterning approaches share the common goal of controlling spatial architecture. However this can be accomplished on different scales, ranging from single cell patterns to tissue level patterns depending on the technique used and the size of the adhesive regions on the substrate. Micro-patterns at subcellular to single cell resolution (approx. 5-30μm) limit the extent to which individual cells can spread on the substrate, enabling detailed observation of the effects of geometrical constraints on single cell morphology and behavior. A critical requirement here is that the adhesive areas must be less than the optimal spreading area of the particular cell. By limiting the attachment space available to the cell to below its optimal spreading area, cells can only spread by remodeling their cytoskeleton and overall shape to fill that of the patterned island. This approach has been pivotal in demonstrating the importance of cell shape and cytoskeletal geometry on mechano-transduction [161-163], migratory behavior [164,165], functional polarization [166] and differentiation [167,168].

Since cell shape and geometry has been shown to impact so significantly on cell behavior, it is interesting to consider how 3D propagation could influence these same behaviours. One of the major adaptations that a cell undergoes when being placed in 3D is cytoskeletal remodeling and a reduction in aberrant cell flattening [169]. Ghibaudo plated fibroblasts on chemically

identical substrates composed of micro-patterned pillars [170]. When the dimensions of the pillars (i.e., the diameter, length, and spacing) were manipulated, cells were exposed to alternating flat and rough surfaces that depend on the spacing between the pillars. Cells on micro-pillar substrates exhibited less cell spreading, more elongated and branched cell shapes, and cells with fewer actin stress fibers compared with cells on flat surfaces. Furthermore, this study showed different mechanisms of cell migration, including a persistent type of "3D migration" that depended on the topographical properties of the environment. They concluded that these differences could be attributed to a spatial reorganization of the actin cytoskeleton due to physical constraints placed on the cell by the microenvironment.

Using the model for 3D propagation developed in Chapter 3, pools of 2D and 3D maintained cells were analysed for changes in cell shape and cytoskeletal organisation in order to determine whether cells could be primed to a 3D environment in terms of morphology.

4.2 Aims of Chapter

The aim of this Chapter is to assess 2D and 3D maintained cells for differences in morphology, cytoskeletal flexibility and migratory behaviour. It is hypothesised that cells maintained in 3D will adopt a rounder, more spherical morphology due to a more physiological micro-environment, and that this change in shape will lead to changes in migration that bring the cells closer to a physiological state.

4.3 Objectives

1. Characterise any differences in how 2D and 3D maintained cells self-organise on 2D and 3D growth substrates.
2. Assess differences in individual cell morphology using quantifiable shape descriptors.
3. Use high resolution microscopy to analyse changes in cytoskeletal organisation and flexibility.
4. Characterise any differences in nuclear morphology using the same quantifiable shape descriptors as in (2).
5. Compare differences in 2D and 3D maintained cells back to primary tissue.

4.4 Materials and Methods

4.4.1 Using ImageJ to quantify morphology

ImageJ is a free platform that can be used for image analysis. This software was used to analyse the phase contrast micrographs of cells maintained in 2D and 3D in order to quantify changes in cell shape (see Fig 4.1). All cells to be analysed were seeded at 50,000 cells per coverslip onto PDL-coated glass coverslips in triplicate, left to adhere for 48 hours in an incubator set to 37°C and 5% CO_2, and then fixed in 4% PFA. Images were then in the taken at 4 compass points and centrally across each coverslip using a Leica DFC 310FX microscope at various time-points in order to analyse changes in cell shape. A grid with squares measuring 50μm^2 was placed over the image, and each square designated a number. A random number generator was used to pick 5 cells per field of view, ensuring no selection bias. These were outlined using the wand tool and measured for various cellular parameters using plugins endogenous to the program (formulas given in Figure 4.1B):

1) Cell Area: this was quantified in order to measure the degree of cell flattening. The program calculated cell area in pixels^2, and this was converted into μm^2 using the merged scale bar.
2) Cell Perimeter: this was quantified in order to assess the regularity of cell shape. This program again calculated this in pixels, and the scale bar was used to convert this into µm.
3) Feret's Diameter: this is the measure of a cell's size along a specific direction. When used in cell biology, this figure is applied to projections of 3D objects on 2D planes. It is often used to analyse the size of cells within tissue sections. The value is given arbitrary units.
4) Cell Circularity: this is a number given to denote how round a cell is: the closer the value is to 1, which is a perfect sphere, the more circular a cell is. The value is given arbitrary units.
5) Cell Height: this was quantified from composite Z stack images obtained through high resolution and confocal microscopy. The program again calculated this value in pixels, and a scale bar was used to convert this to µm.

A

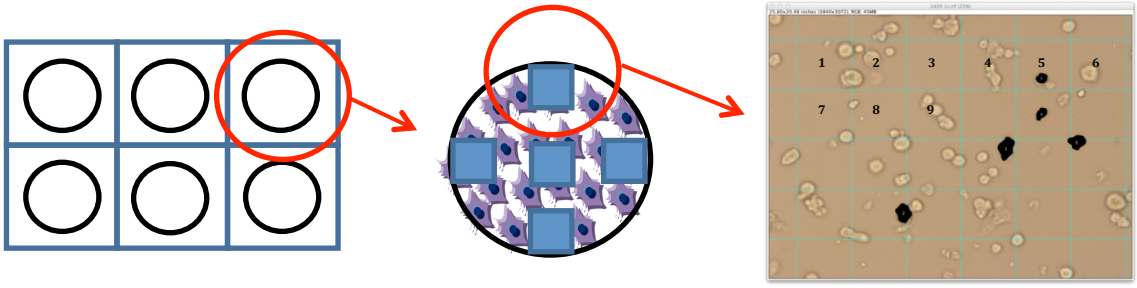

B

$$Cell\ Area\ (A) = \pi r^2$$

$$Cell\ Perimeter\ (P) = 2\pi r$$

$$Feret's\ Diameter = \Sigma < F > \frac{P}{\pi}$$

$$Cell\ Circularity = 4\pi \left(\frac{A}{P}\right)^2$$

Figure 4.1 ImageJ can be used to quantify cell morphology

The schematic shows the experimental set-up for analysing cell shape quantitatively using ImageJ software (A). The determinants of morphology were cell area, perimeter, Feret's diameter and circularity. The formulae for calculating these dimensions are endogenous plug-ins within the software and are given in (B). In order to ensure that there was no selection bias in the cells chosen to analyse, a grid of known measurement was placed over the field of view, and each full square was designated a sequential number. A random number generator was used to chose 5 squares at random. If the square chosen had more than one cell, the cells were numbered and again a random number generator used to chose one cell. If the square did not have a cell in it, another square was chosen. The chosen cells were outlined in black and then measured.

4.4.2 Using Volocity® to quantify morphology

Volocity® is a commercially available software platform specifically designed for 3D image analysis using raw data generated through confocal and high resolution microscopy. In order to use this software to calculate volumes, a measurement protocol needs to be created in order to locate significant fluorescent intensities in a specific channel. This is used to threshold data to select areas of interest, i.e. the cell in question, and exclude objects outside a set criteria, i.e. background fluorescence. To do this, a Z stack file is imported into the software and sliced into individual slices. For each slice, an intensity histogram for the channel of interest is opened, and the gating adjusted so that only intensities above a certain significance are selected. This task also allows the exclusion of objects below a size threshold which will exclude most noise is biological images. Selected objects will be highlighted on the slice, and standard morphological measurements will be displayed below the image in a table. A new measurement item is then created, which allows all the measurements from all slices to be compiled into a table of raw data. This measurement item can then be analysed to find the total labelled volume.

4.5 Results

4.5.1 Creating 2D and 3D maintained cell populations

Having designed and optimised a protocol for the propagation of HepG2 cells in 3D using Strata, the next experimental questions involved comparing 2D and 3D maintained cells in order to determine whether long term culture in 3D would have any effect(s) on cell shape and function. To do this, two populations of cells were created from a common pool of HepG2 cells that had been maintained in the traditional 2D way. Half of these cells were passaged as normal in 2D using T25 culture flasks, and half were seeded onto Strata discs and passaged in 3D using the protocol designed in the previous Chapter. Both populations of cells were seeded at the same number and grown for 4 days with a media change on day 2. This variation from the protocol was introduced because the 2D populations of cells showed signs of entering the stationary phase of growth by day 3 in culture without a media change. On the 5^{th} day, both cell populations were passaged. At each passage, cells were sampled out from both populations for further analysis:

1) 200,000 cells from each suspension were plated into fresh culture plates to observe cell shape changes;
2) One disc/flask was put aside to create lysates for Western blotting and RNA extraction;
3) One disc was put aside and embedded for H&E/immuno-labelling;
4) 100,000 cells from each suspension were plated onto glass coverslips for advanced imaging.

One vial of cells from each passage in either 2D or 3D was also frozen down for cryopreservation. This was carried out over a period of 2 months, and cells were taken to passage 10 in both 2D and 3D. The entire experimental set-up can be seen in the schematic in Figure 4.2.

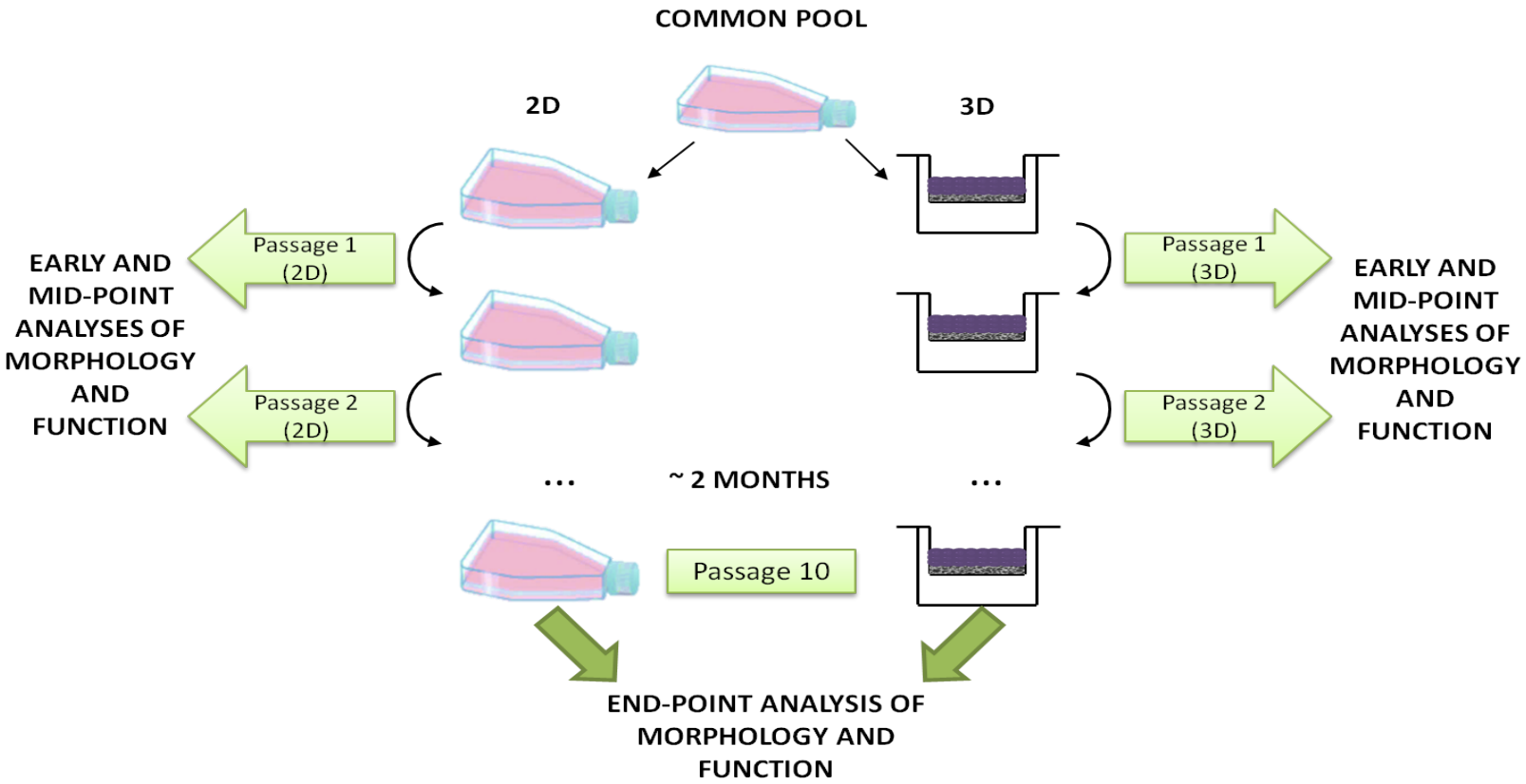

Figure 4.2 Cells were passaged in parallel in 2D and 3D conditions for 2 months to generate two separate cell populations

The schematic shows the experimental set-up that forms the basis of the majority of the results that follow. Cells were plated into 2D or 3D conditions from a common pool of cells at the exact same seeding density (0.5 x 10^6 cells/ml) on either TCP or Alvetex®Strata inserts for 4 days, with a media change on day 2. On Day 5, cells were sampled out for morphological and functional analysis. The rest were counted and re-plated onto either TCP or Strata at the same seeding density as before. This propagation was carried out for both 2D and 3D conditions for approximately 2 months until cells reached Passage 10.

4.5.2 Assessing changes in migration with long term maintenance in 3D

One disc per passage point was embedded, sectioned, and stained with H&E dyes in order to visualise the cells and investigate whether long-term maintenance in 3D alters the penetrative behaviour of the HepG2 cells on Strata material (Figure 4.3). At passage 1, the majority of cells do not grow on top of the membrane, but rather occupy the upper depths of the material. With the exception of a few further migrating cells, the cells in general do not penetrate further than the top 50µm of the membrane, but rather form a thin layer on top of the membrane that is between one and three cells thick. By passage 2, this behaviour is amplified, with the cells migrating, on average, 30µm into the material, and forming layers that are 3-5 cells thick on top of the membrane. The biggest change seen between passage 2 and 6 (Figure 4.3B and D respectively) is a change in cell density; though the cell layer above the surface does not get thicker, the cells appear to pack together more closely, forming a much denser layer. By passage 10, the vast majority of cells do not penetrate the material at all, but instead grow in thick 'islands' across the surface of the material. At the tallest, these islands are between 5 and 10 cells thick, and again show dense packing of cells together, indicated by the darker staining. Finally, by passage 10, the end-point of the experiment, cells form a more consistent tissue-like formation on the surface of Strata. This formation is between 5 and 10 cells thick but the cells do not appear to pack together as closely, thus making the overall structure thicker. These changes in penetration were analysed quantitatively using a penetration analysis, and as visualised in Figure 4.4, the biggest change in cell penetration across the 10 passages was a gradual shift towards more cells growing on top of the membrane and fewer cells penetrating the material. At passage 0, less than 50% of cells grow on top of the membrane – by passage 6, the balance has shifted and just over 50% of cells occupy the space above the surface of the material – by passage 10, this percentage increases to almost 90%. This change in penetrative behaviour during maintenance in 3D culture indicates that cells are actively adapting to the novel microenvironment. To see whether these adaptations are a) temporary and b) specific to Strata, cells at the end-point of the experiment were counted and 0.5 million cells from both the 2D and 3D maintained populations were seeded onto Alvetex®Scaffold and grown for 48 hours. At this point, scaffolds were fixed, embedded, sectioned, and stained with H&E to visualise cells. Figure 4.5 shows a representative example of both populations, and there are clear differences both in penetration and cell morphology.

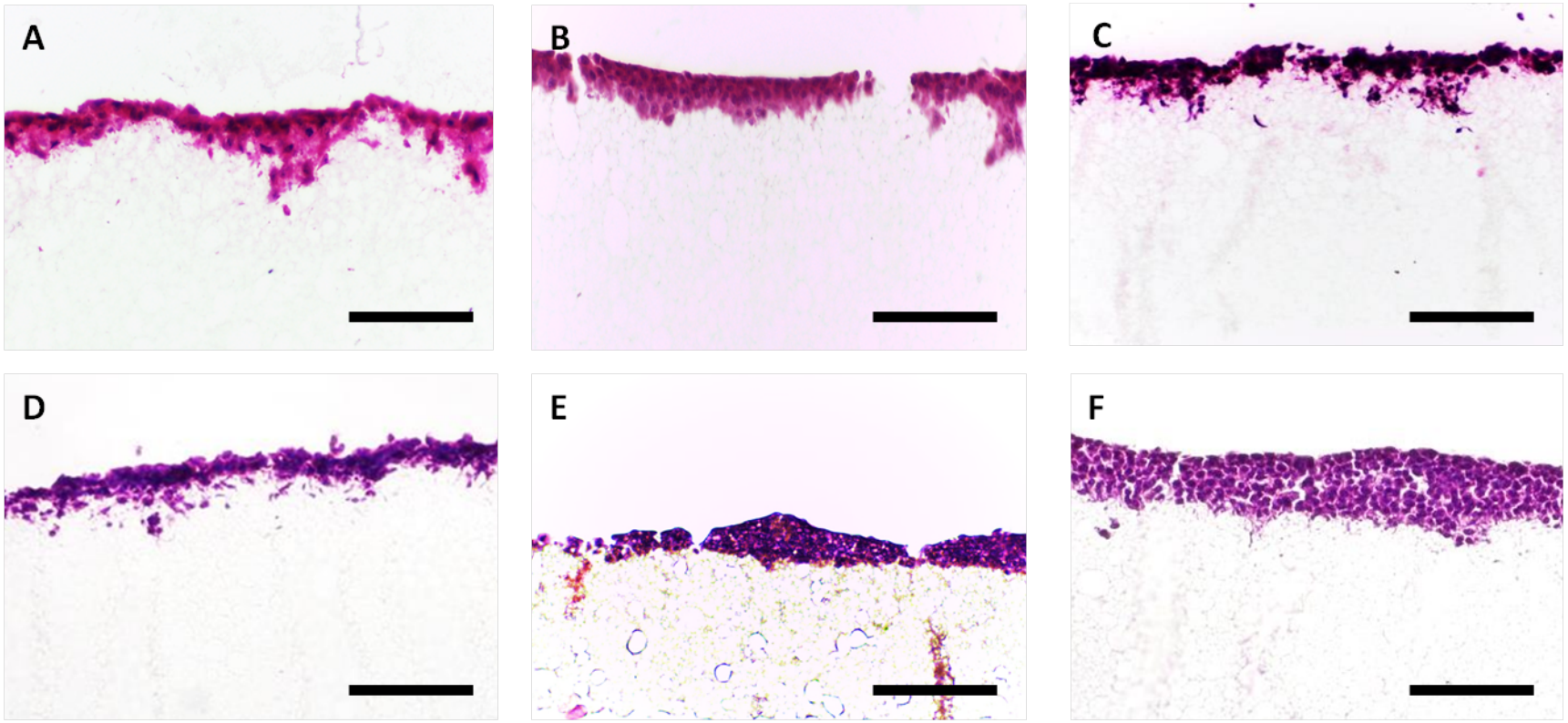

Figure 4.3 3D propagated cells organise themselves into multi-cell thick layers that grow on top of the membrane

Cells were passaged for 10 generations in 3D on Alvetex®Strata, and at each passage point membranes were sectioned and stained for H&E to visualise the cell layers. At passage 1 (A) and 2 (B), the majority of cells occupy the top quarter of the membrane. At mid passages (passages 4 and 6; C & D respectively), cells begin to grow on top of the membrane, and by passage 8, the vast majority of cells do not penetrate the material at all (E). At the end-point of the experiment, passage 10, cells form thick tissue-like formations on top of the scaffold in a membrane-free manner (F). Scale bars = 100µm.

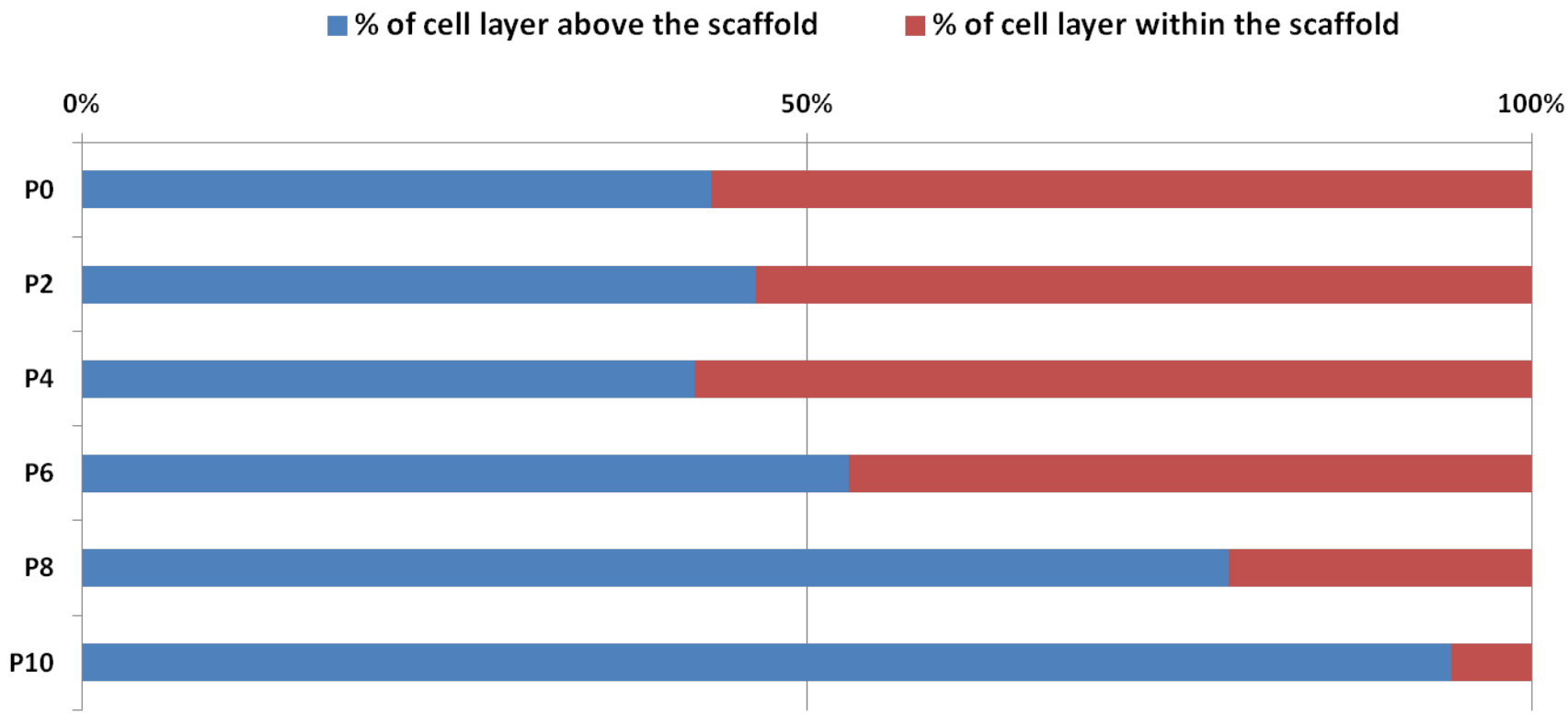

Figure 4.4 As cells are propagated in 3D, the percentage of cells growing on top of the membrane increases

At each passage point, membranes were sectioned and stained for H&E to visualise the cell layers. A penetration analysis was conducted to explore how penetration changes with increased propagation in 3D. At earlier passage points, the majority of cells exist in the top quarter of the membrane. However midway through the propagation period, this reverses, and approximately 55% of cells grow in multi-layer structures above the membrane. By passage 10, this increases to just under 90%.

The cells that had been maintained in 2D for 2 months show flattened morphologies that pack together in a long think layer across the entire diameter of the disc. They do not penetrate further than the upper third of the scaffold, but grow consistently across the entire length (Figure 4.5A). Contrastingly, cells maintained in 3D show small, rounded shapes and rather than growing in thin layers, they clump together in 'islands' that resemble those that were observed at mid-late passages in Strata. These islands grow randomly both across the disc diameter and also throughout the entire depth of the scaffold, occupying mid regions mostly. It is possibly due to their smaller size that they can penetrate the full depth of the scaffold. This change in size may also change their cell-cell contacts, thus explaining their different organisation.

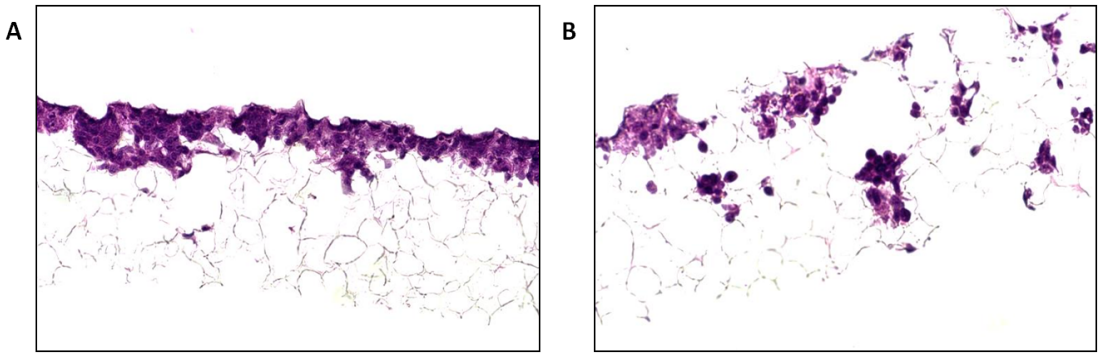

Figure 4.5 Cells at the end-point show a smaller, rounder morphology that allows further penetration through Alvetex®Scaffold

Cells at passage 10 were counted and seeded in a concentrated manner at 0.5 x 10^6 cells/ml onto Alvetex®Scaffold in order to examine changes in penetration. Cells grown in 2D (A) show minimal penetration, with cells growing in long, thin layers across the entire diameter of the scaffold, whereas cells grown in 3D (B) are smaller and grow in 'clumps' randomly across the disc diameter, as well as throughout the entire depth of the scaffold.

Previous research has indicated that cell size may have an inversely proportional correlation with migration speed [171]. In a similar way, cell shape is an important variable when considering the migratory behaviour of a cell through its matrix. In response to the loss or grain of several key intracellular and molecular determinants, drastic adaptation reactions, such as to a change in microenvironment, can modify a cell's shape and thus cause a switch from one form of migration to another [172]. Individual cell migration can be classified as either mesenchymal or amoeboid-like.

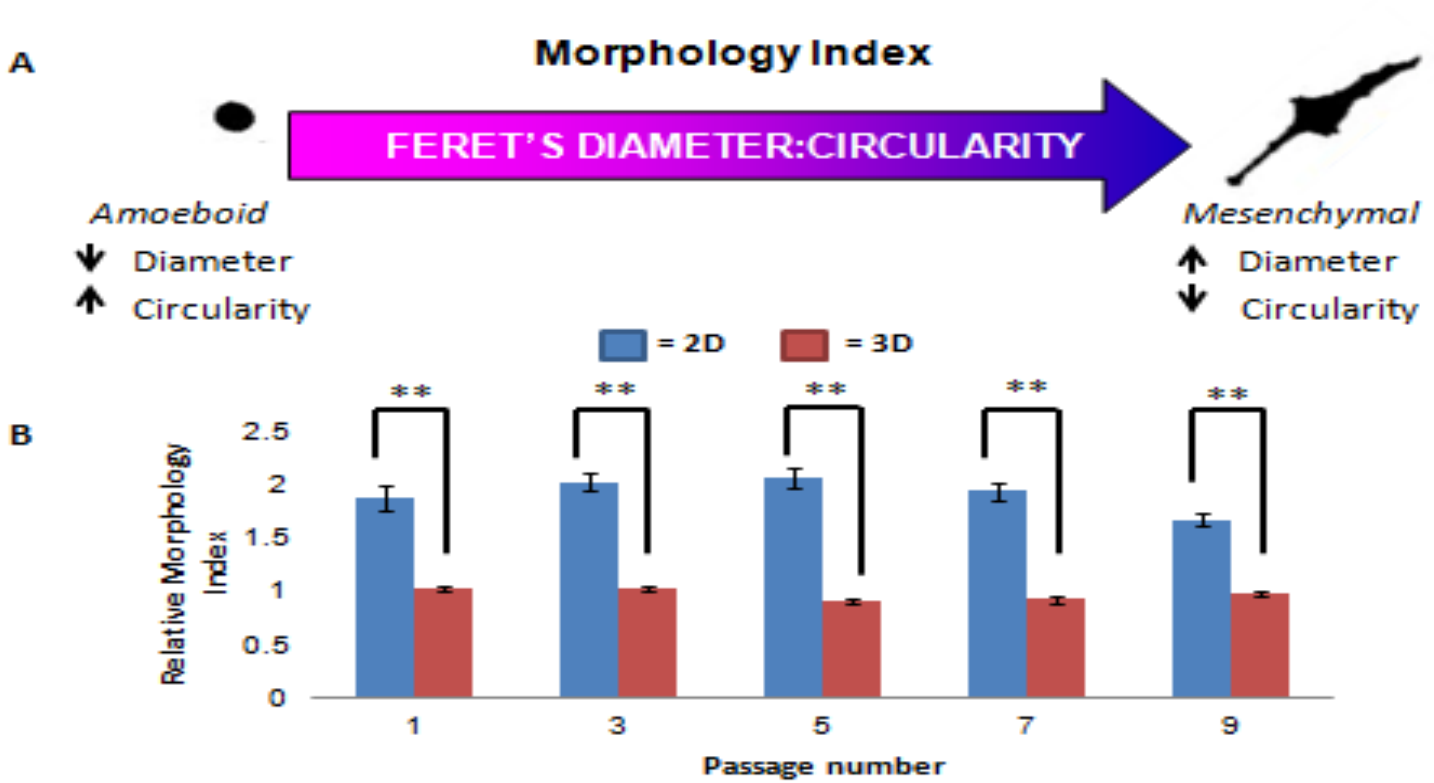

Figure 4.6 The relative morphology index (RMI) can be used to predict a migratory behaviour through cell shape and indicates differences in migration between 2D and 3D cells

Cells at various passages were measured for their Feret's diameter and circularity and these values were put in a ratio to obtain a RMI value [241]. A high RMI value indicates that a cell migrates in a mesenchymal manner, whereas a low RMI value indicates that cells migrate in an amoeboid manner (A). Cells propagated in 3D consistently show a tendency to migrate in an amoeboid manner, befitting their rounder morphology (B). Data presented as n=15. Statistical analysis through ANOVA. ** denotes $p \leq 0.01$

Amoeboid migration refers to the movement of round or ellipsoidal cells that lack mature adhesions and stress fibers. Mesenchymal migration is seen in elongated cells that display high levels of attachment, cytoskeletal contractility, and fibroblastic morphologies [7]. In order to further investigate the observations of Figure 4.4, and tie together cell shape and penetration, a relative morphology index was used to quantify the degree to which cells maintained in 2D and 3D showed mesenchymal or amoeboid-like migration. The relative morphology index (RMI) value is derived from the ratio between a cell's circularity and Feret's Diameter. For instance if a cell has a circularity value of 0.92 and a Feret's Diameter of 1.8, the RMI value would be 1.95. A higher RMI value indicates that a cell tends to migrate using mesenchymal migration, and a lower value indicated a preference for amoeboid-like migration. The RMI values for 2D and 3D maintained cells were calculated and graphed in order to see whether long term 3D maintenance had an effect on migratory profiles – this is visualised in Figure 4.6. As the graph shows, 2D cells are consistently more mesenchymal and 3D cells are consistently more amoeboid. There does not appear to be an amplification of this difference the longer cells are maintained in 3D though.

Migratory mode can also have an impact on how cells spread and organise across a flat surface. In order to examine whether the morphological and migratory changes brought about by 3D propagation would be retained after plating in 2D, 200,000 cells were samples out from each population at each passage point and plated onto the individual wells of a 6 well plate. Phase contrast images were taken every day for 4 days to follow the process – these are captured in Figure 4.7. To describe the changes in cell organisation, colonies were classed as either single-cell (outlined in red), mid-size (yellow) or large (green). At day 1, there is a clear difference in cell spreading and proliferation between 2D and 3D cells even passage 3, but these changes are lost by day 2, as 3D cells at p3 start to resemble the 2D cells. This can be seen by a general decrease in the abundance of single cell colonies, and a concomitant increase in mid-size and large-size colonies. This is probably because the changes brought about by 3D propagation are not hard-wired into the cells at early passages, but rather are transient, and thus when the cells are placed into a 2D environment, the changes are reversed and the cells revert back to a 2D like morphology and migratory mode. By passage 6, however, it appears that propagation in 3D is having a more permanent effect on the cells. Comparing the spreading of cells across the four days between 2D cells and p6 3D cells, there is a clear and maintained difference. The main difference is that the 3D cells exist in single cell and mid size colonies for longer, with large scale colonies only becoming apparent by day 4.

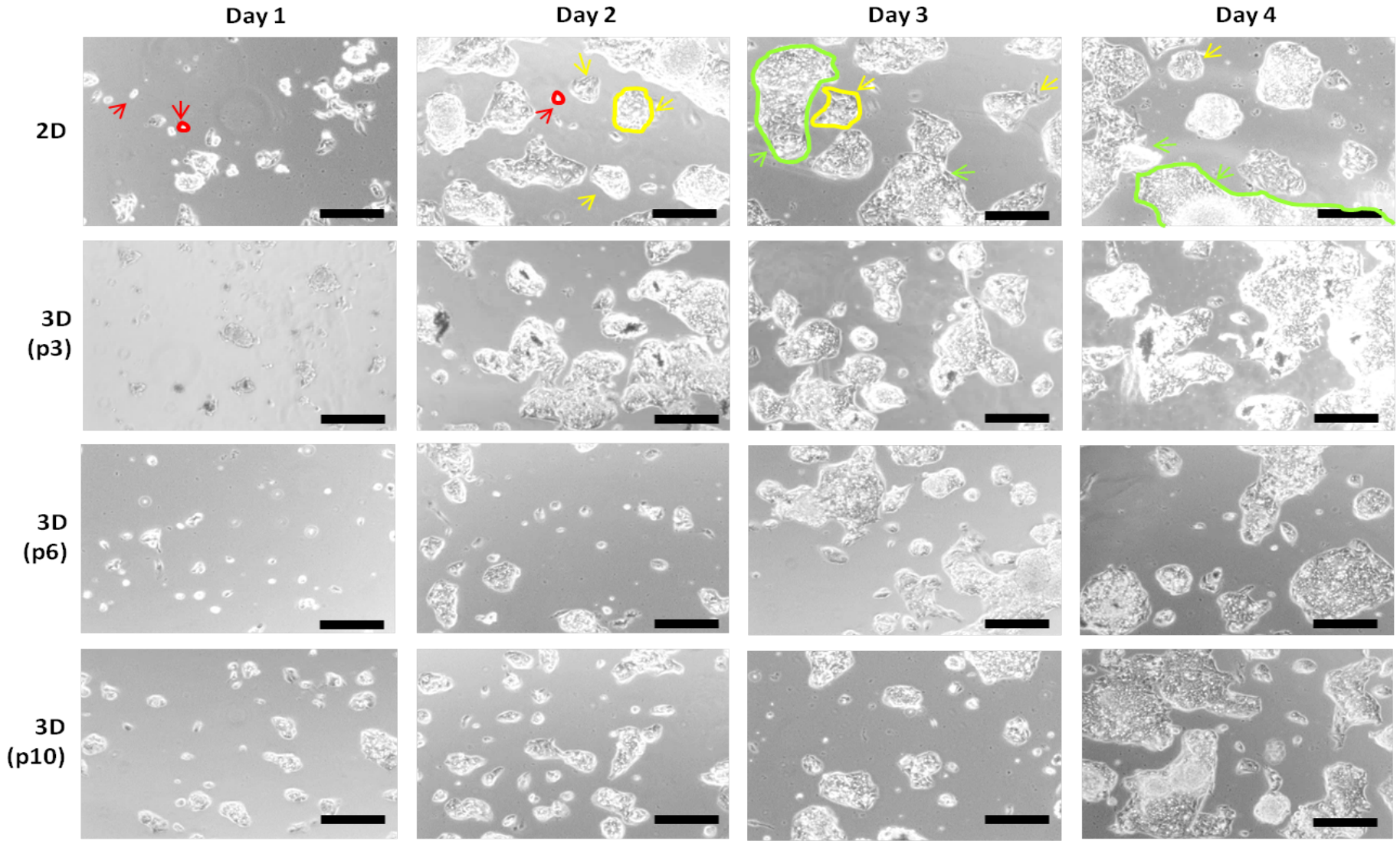
Day 1
Day 2
Day 3
Day 4
2D
3D (p3)
3D (p6)
3D (p10)

Figure 4.7 Phase contrast micrographs of cells maintained in 2D and 3D show that cell-cell organisation differs between the two cell populations

At each passage point, 0.2 million cells were plated onto TCP and photographed every 24 hours for 4 days in order to see whether any morphological changes brought about by a 3D growth environment could be maintained after plating in 2D. Though there is a difference in cell shape, organisation, and proliferation between 2D and 3D samples at early passage, this difference is lost by 2 days as the cells adapt to the 2D growth substrate. This can be shown by a general decrease in single cell colonies (red arrowheads), and an increase in mid-size (yellow) and large (green) colonies. However, as the cells are passaged for longer in 3D, this difference in maintained for longer. This can be indicated by the maintenance of more single cell and mid-size colonies over 4 days, and the absence of large colonies by Day 3. Small, mid-size and large colonies were

In other words, the cells that are maintained in 3D prefer to organise into small clumps or islands rather than large thin layers – this exactly parallels the behaviour seen on both Strata and Scaffold, meaning that 3D propagation results in a global change in cell-cell contact and organisation. The results from this experiment indicate possible involvement of cell adhesion molecules such as cadherins and integrins in the adaptation of cells to a 3D microenvironment.

4.5.3 Assessing changes in individual cell morphology with long term maintenance in 3D

The next experimental step involved a closer examination of individual cellular morphology. For the next set of experiments, it was vital to obtain single cells for imaging purposes. Therefore, to establish the optimal conditions for this, a titration experiment was conducted whereby cells were seeded at three different concentrations and left to adhere and flatten. It was also important to establish the minimum amount of time cells required to adhere to ensure that the cellular morphologies were captured before any aberrant flattening. The results from this can be seen in Figure 4.8. As is clearly demonstrated, cells begin to adhere to PDL coated glass coverslips by hour 1, but by hour 5 there are signs of flattening. At the highest seeding density tested, 100,000 cells per coverslip, there are signs of cell clumping, and it is difficult to isolate single cells for imaging. At the lowest seeding density, 25,000 cells per coverslips, there are signs of membrane blebbing, indicating that the cells are not viable, which could confuse any observations of cell shape. Thus, the optimal conditions were found to be seeding 50,000 cells per coverslip and allowing an adhesion time of 2 hours.

In order to ascertain the main morphological differences between individual cells maintained in 2D and 3D, cells from a mid-passage (p6) were plated onto PDL coated coverslips and stained with Phalloidin and Hoechst-33342. Phalloidin is plant-derived toxin that specifically binds and stabilises filamentous Actin (F-actin). When conjugated to a fluorescent tag, it can be used to visualise F-actin and thus the cytoskeleton of a cell. It is a much smaller molecule than an antibody that would typically be used in labelling cellular proteins for imaging, and thus its use leads to denser labelling and therefore more detailed images can be acquired at higher resolutions. Hoechst 33342 is a synthetic dye that binds to the minor groove of double stranded DNA, and as such is used as a supravital nucleic stain. Together these two dyes were used to determine the major differences in cell morphology between 2D and 3D propagated cells (Figure 4.9).

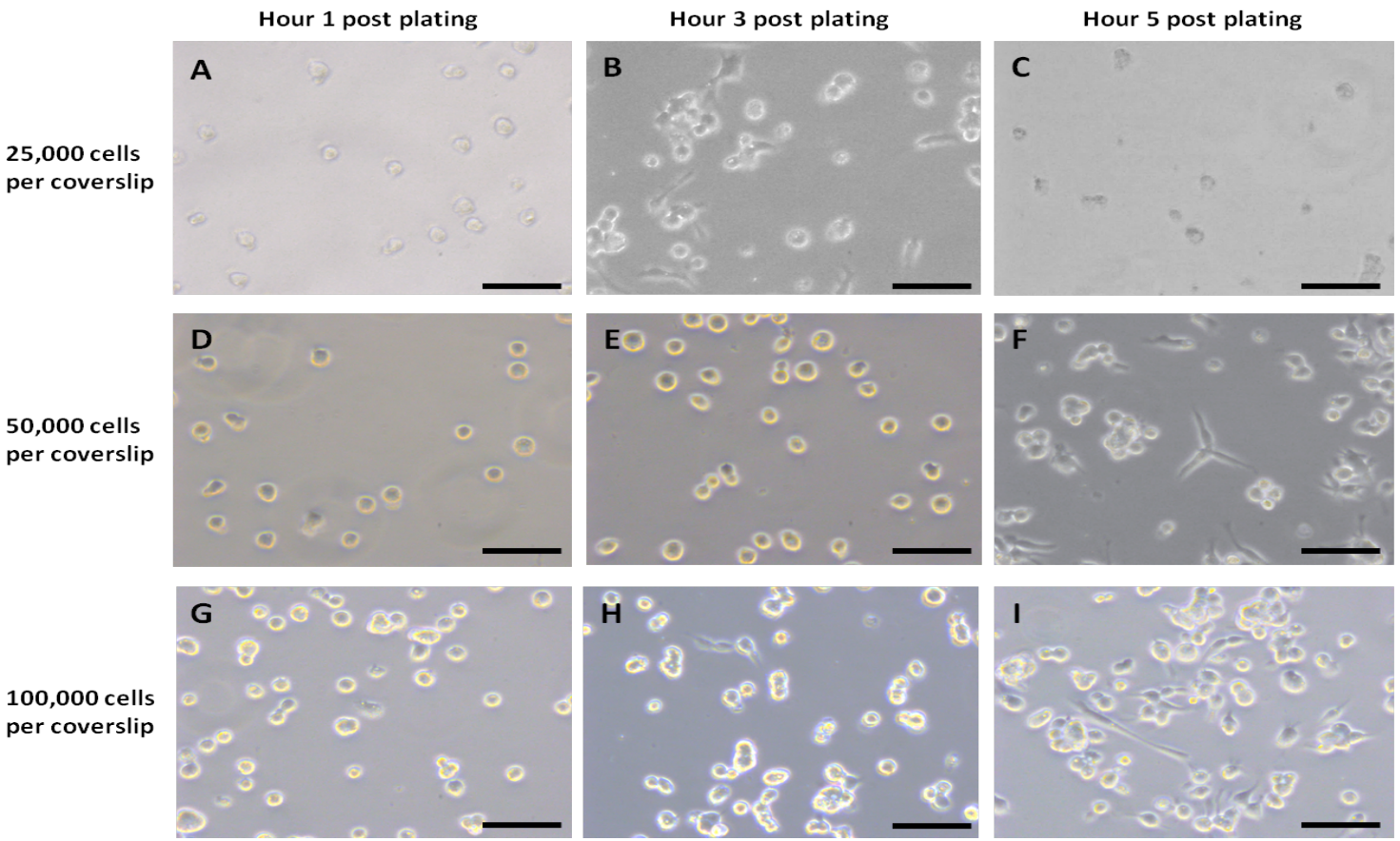

Figure 4.8 Phase contrast micrographs show that the optimal conditions to obtain single cells are 50,000 cells plated on a coverslip for 3 hours

In order to obtain a single cell population for cell measuring and high resolution imaging, cells were plated at different densities for between 1 and 5 hours. The optimal conditions are those that allow adhesion without inducing flattening, and that result in atleast 10 single cells per field of view. These criteria are best met by the conditions imaged in E. Scale bars = 100µm.

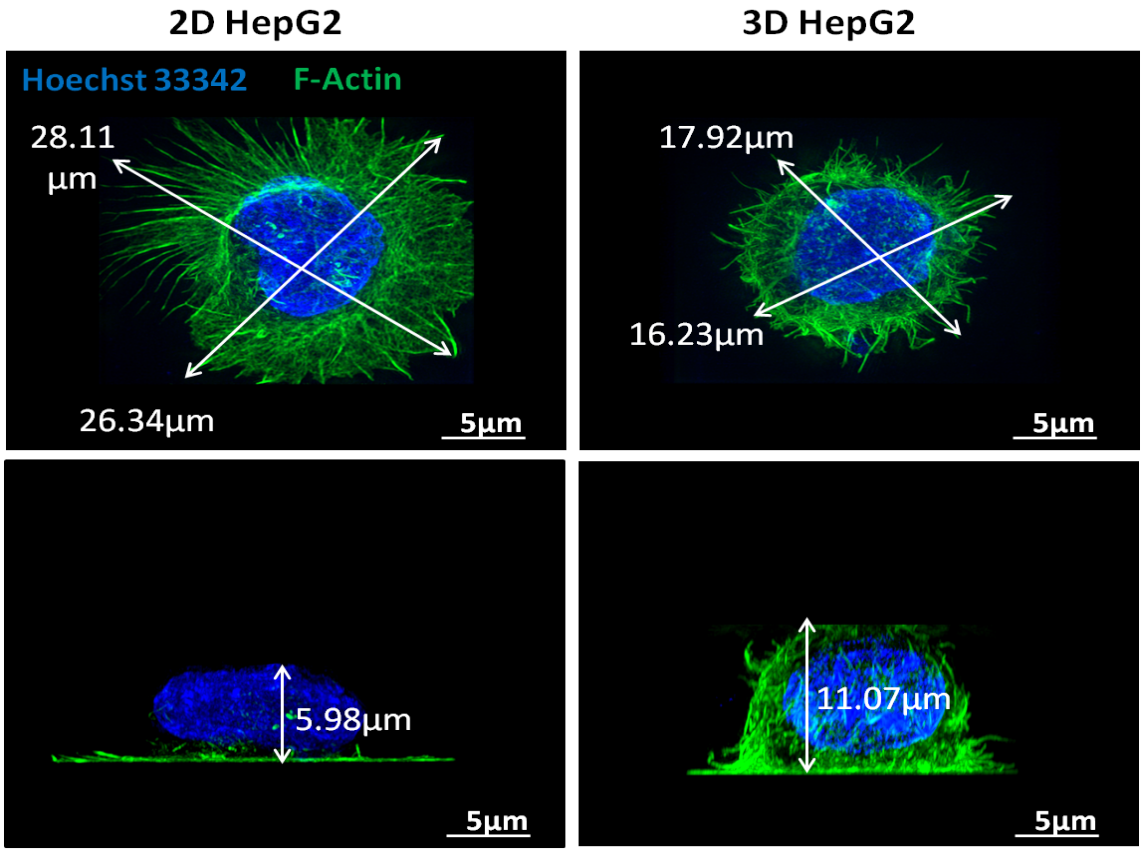

Figure 4.9 High resolution images of 2D and 3D cells show the main morphological differences

Cells were plated on glass coverslips at 50,000 cells per coverslip, stained with Phalloidin (against F-Actin) and DAPI (against nucleic acid and imaged using Structured Illumination Microscopy (SIM). Cells grown in 2D flatten to a greater extent than 3D maintained cells, as shown by a shorter cell height as well as increased stress fibres, which may indicate a more rigid cytoskeleton. The phalloidin staining in 3D cells also shows that the cytoskeleton wraps around the nucleus, rather than lying flat as in 2D cells. Scale bars = 5µm.

The main cellular dimensions, length width and height, were measured at their longest, using ImageJ to quantify changes in cell shape and size. Cells in 2D spread out significantly more than their 3D counterparts, with a 36% larger spread in the X and Y dimensions on average. They also demonstrate a more extensive network of stress fibres, as well as discernibly more lamellipodia and filopodia. Contrastingly, 3D maintained cells show a less complex actin organisation. In terms of the Z dimension, cells maintained in 2D are, on average, 45% flatter. There is also a difference in the cytoskeletal organisation in the Z dimension, with the actin network wrapping itself around the nucleus like a cage in 3D cells, but lying flat in 2D cells, giving them the illusion of a "fried egg" morphology.

Differences in cell morphology brought about by 3D propagation can be quantified using ImageJ software. In order to carry out a thorough investigation into morphological differences between the two cell populations, cells maintained in 2D and 3D were sampled out at several passage points and plated in triplicate at 50,000 cells per coverslip. They were allowed to adhere for 2 hours to enable adhesion but prevent flattening, and then imaged. For statistical validity, images were taken at 5 different fields of view per coverslip at 20x magnification. A $50\mu m^2$ grid overlay was placed on top of each image and each square was designated a number. Using a random number generator to ensure no selection bias, 5 cells were chosen from each field of view. These were outlined using the wand tool and measured for various cellular parameters using plugins endogenous to the program. More details on each of these can be found in Section 4.2. A schematic of the experimental set-up can be seen in Figure 4.10.
One of the main parameters to be examined was cell circularity. From previous findings, one would expect 3D propagation to result in more rounded, regularly shaped cells, which is more physiological than the fibroblastic and irregular cell shapes seen in 2D culture. Figure 4.11A shows representative examples of cells from both populations across the experimental period. The cell outlines show that cells in 2D consistently flatten to irregular and elongated shapes, and that this is independent of propagation. The cells also appear to adopt larger areas than the 3D cells which is indicative of aberrant and extensive cell flattening. Cells in 3D though are consistently smaller and rounder than their 2D counterparts. This change can be seen from passage 1 but also appears to be amplified the longer that the cells are maintained in 3D, as shown by comparing the cell outlines from P1 in 3D to those at P9. These differences can be quantified by the formula given in Figure 4.11B.

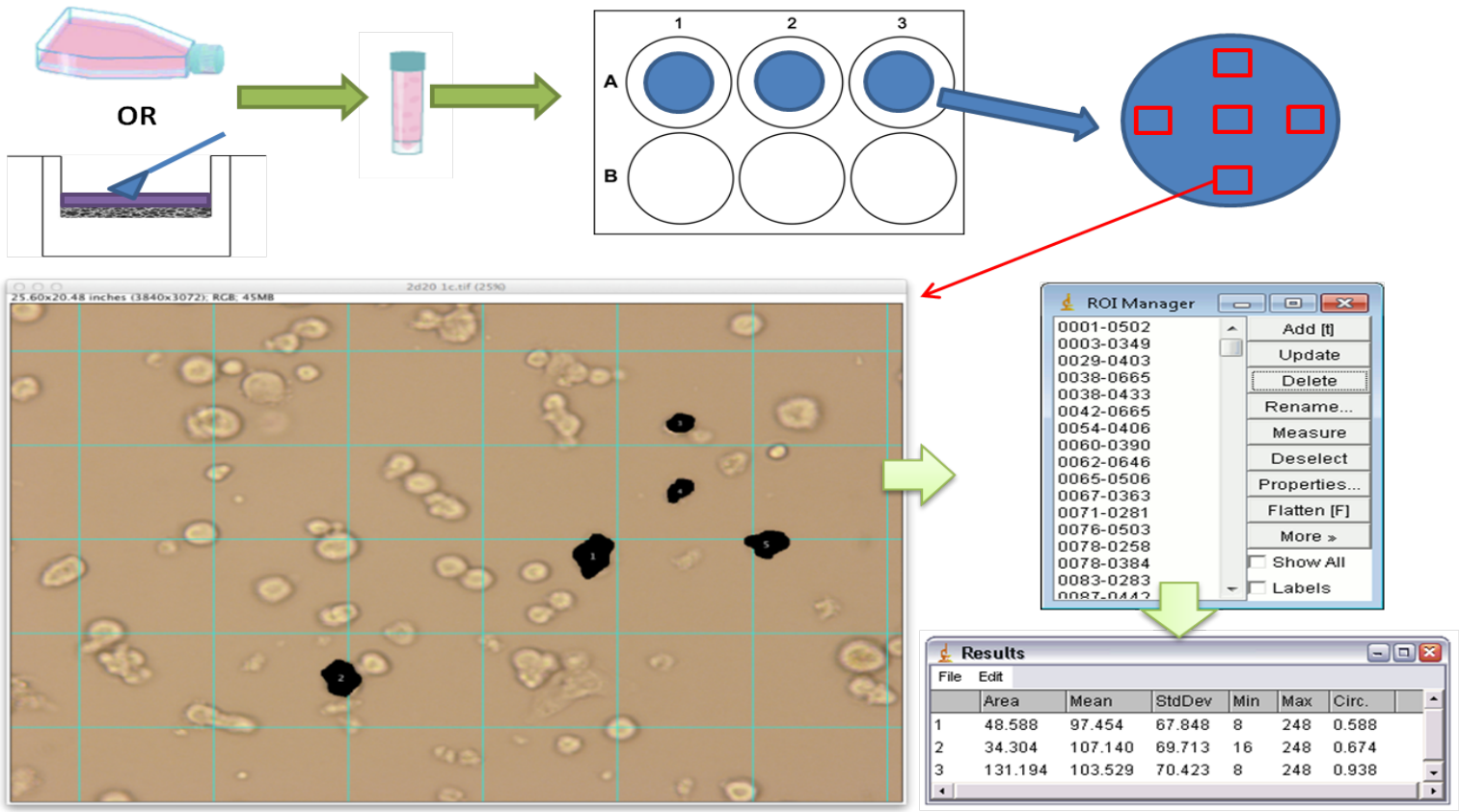

Figure 4.10 ImageJ software can be used to measure cell parameters

In order to quantify morphological changes, certain cell parameters, such as cell area, cell perimeter and circularity were measured using ImageJ software. For each condition, cells were scraped off from either TCP or Alvetex®Strata inserts, counted, and plated in triplicate at 50,000 cells per coverslip. For each coverslip, phase-contrast micrographs were taken at 5 fields of view. Images were opened in ImageJ with a grid overlay to allow random cells to be chosen. Each cell was outlined using the wand tool and measured for various parameters using endogenous plugins.

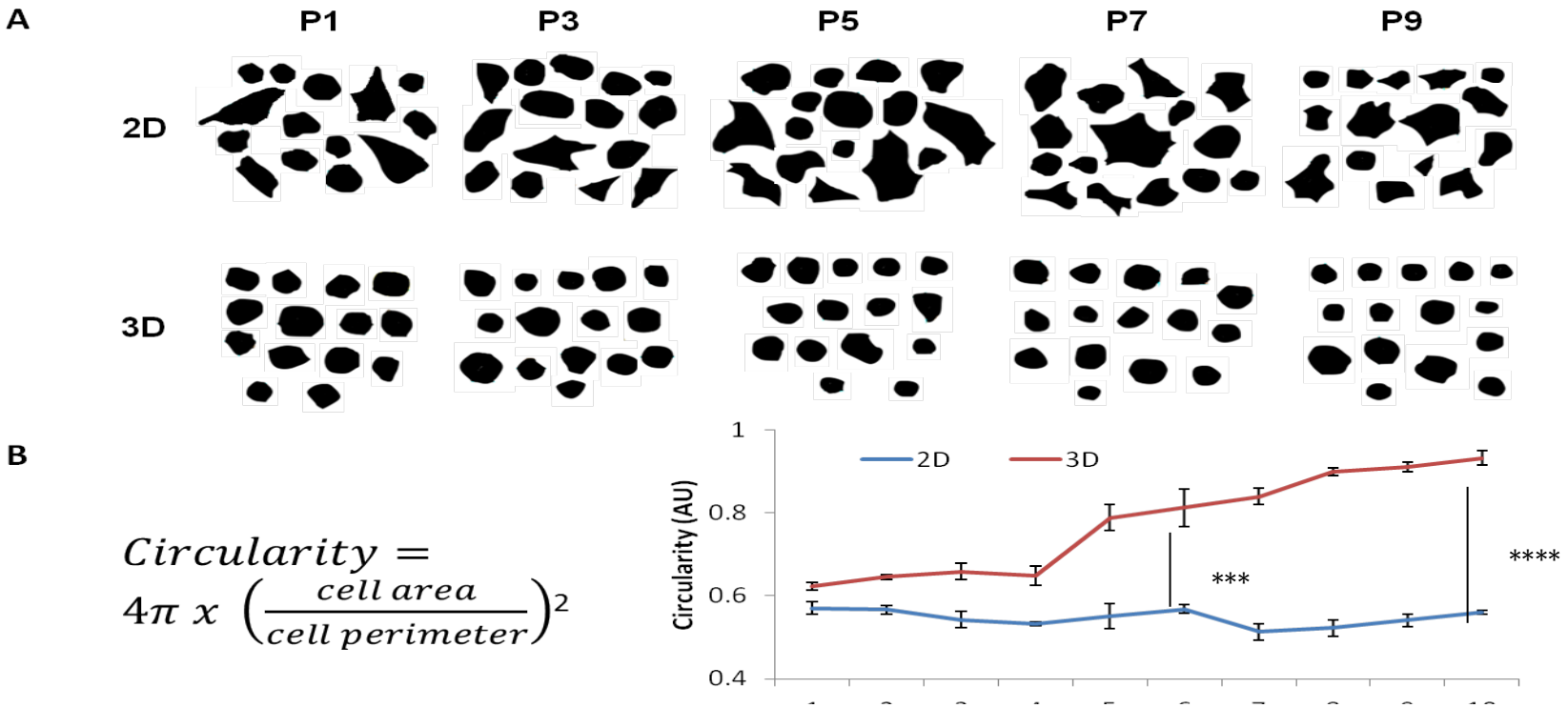

Figure 4.11 Cell outlines from random 2D and 3D maintained cells at chosen passage points show drastic morphological differences

Random cells were selected from 2D and 3D phase contrast micrographs and outlined to show gross morphological differences (A). Data shows that cells in 3D are constantly smaller and rounder than those in 2D. 2D cells appear to flatten into irregular shapes – a behaviour that is not changed with continuous propagation, whereas cells in 3D appear to maintain a more circular form that is resistant to flattening. Though this difference can be seen as early as Passage 1, the differences become amplified the longer cells are maintained in 3D conditions. These differences can be quantified using circularity (C), the equation for which is given in B. Data presented as n=75 ± SEM. Statistical analysis through ANOVA. *** denotes $p \leq 0.001$, **** denotes $p \leq 0.0001$.

The results from this quantification (Figure 4.11C) show that though 3D circularity is constantly higher than 2D circularity, this change becomes greater throughout the experimental period, becoming statistically significant at the mid-passages, as the two populations drift further apart from each other.

To investigate the changes in cell shape further, cells were stained with Phalloidin and Hoechst and examined using Structured Illumination Microscopy (SIM). SIM is a wide-field microscopic technique in which a grid pattern is created through interference of diffraction orders and superimposed onto the specimen during image capture. The grid is rotated 60° between the capture of each image, and the 5 subsets are processed with a specialised algorithm in order to generate a reconstructed image with a lateral resolution approximately twice that of diffraction-limited technique such as laser scanning confocal microscopy [173]. This increased resolution makes SIM perfect for analysing cytoskeletal changes in individual cells at high magnification.

2D and 3D propagated cells at passages 2, 4 and 6 were sampled out, plated at 50,000 cells per coverslip, and imaged using SIM. From these high resolution images, cell outlines were obtained, and these were uploaded into ImageJ in order to calculate cell area and cell circularity. Cell height was calculated on ImageJ using Z stack compositions put together using software from the SIM. This data is shown in Figure 4.12, cells at passage 2 show clear differences in cytoskeletal organisation. From the representative image in Figure 4.12A, and the outlines in Figure 4.12B, it is clear that 3D maintained cells are rounder whereas 2D maintained cells are elongated. This difference is shown in the circularity data in Figure 4.12E. The cells in 3D show less flattening, which can be seen in the lower cell area and higher cell height. By passage 4, these differences become amplified (Figure 4.13). The 3D maintained cells show a regular circular morphology, and a lower area and higher height – these three parameters when taken together suggest a spherical morphology. 2D maintained cells continue to show flattened and irregular shapes, as well as a significantly shorter height. The story remains similar for cells sampled out at passage 6, but the differences do not increase any further, suggesting that by mid passages, cells have fully adapted to their 3D microenvironment (Figure 4.14).

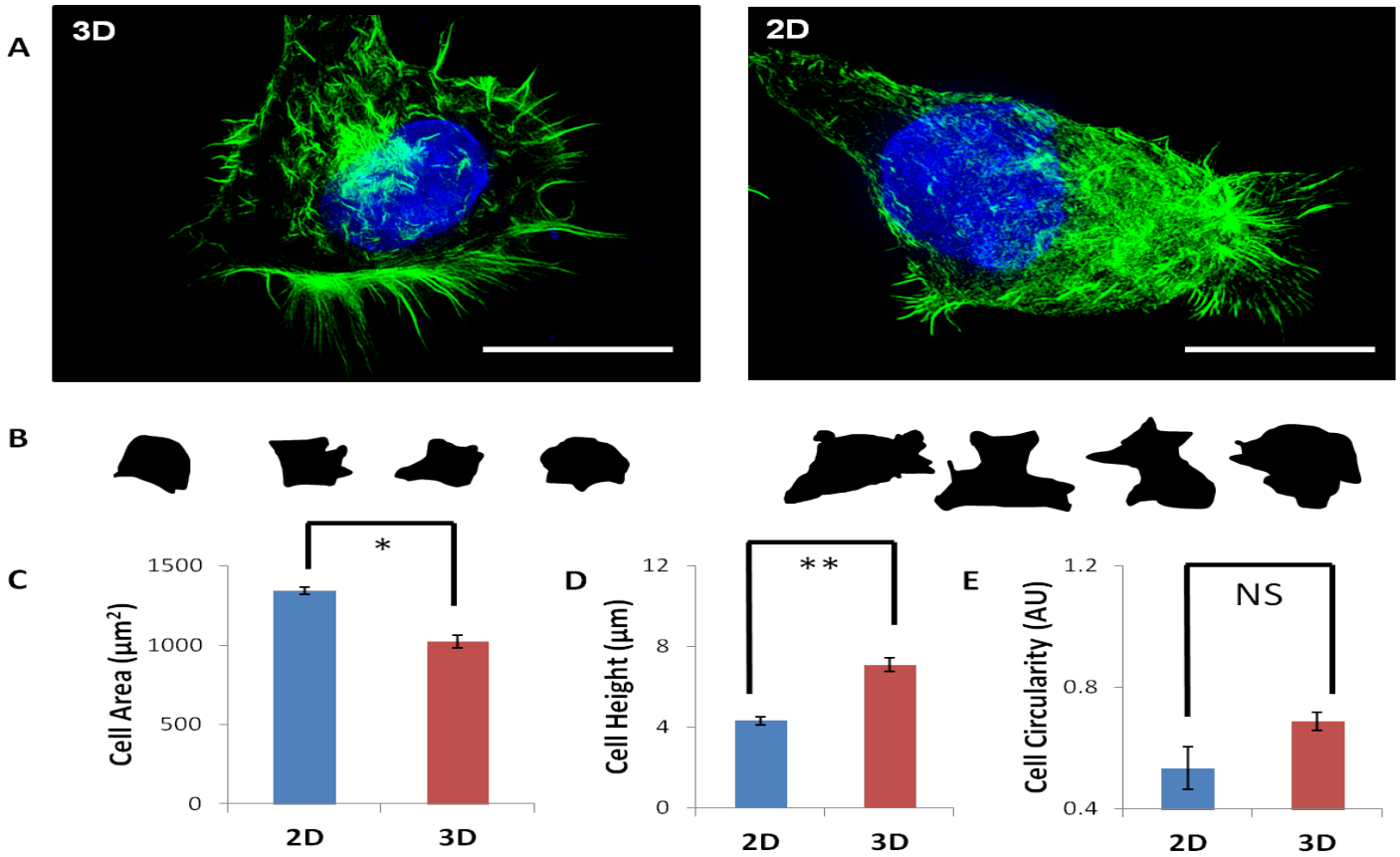

Figure 4.12 Cells grown in 3D for 2 passages show slightly rounder morphologies and flatten less than those grown in 2D for 2 passages

Cells grown in 2D and 3D conditions were sampled out at passage 2 and stained with Phalloidin (against F-Actin) and DAPI (against nucleic acid). (A). Cells in 3D on average show a rounder morphology than those grown in 2D (outlines in B). The cells grown in 2D flatten more on a 2D growth substrate, as shown by a higher area and a lower height, as well as a less circular form. Scale bars = 5µm. Data presented as n=20 ± SEM. Statistical analysis through ANOVA. NS denotes non-significant, * denotes $p \leq 0.05$, ** denotes $p \leq 0.01$

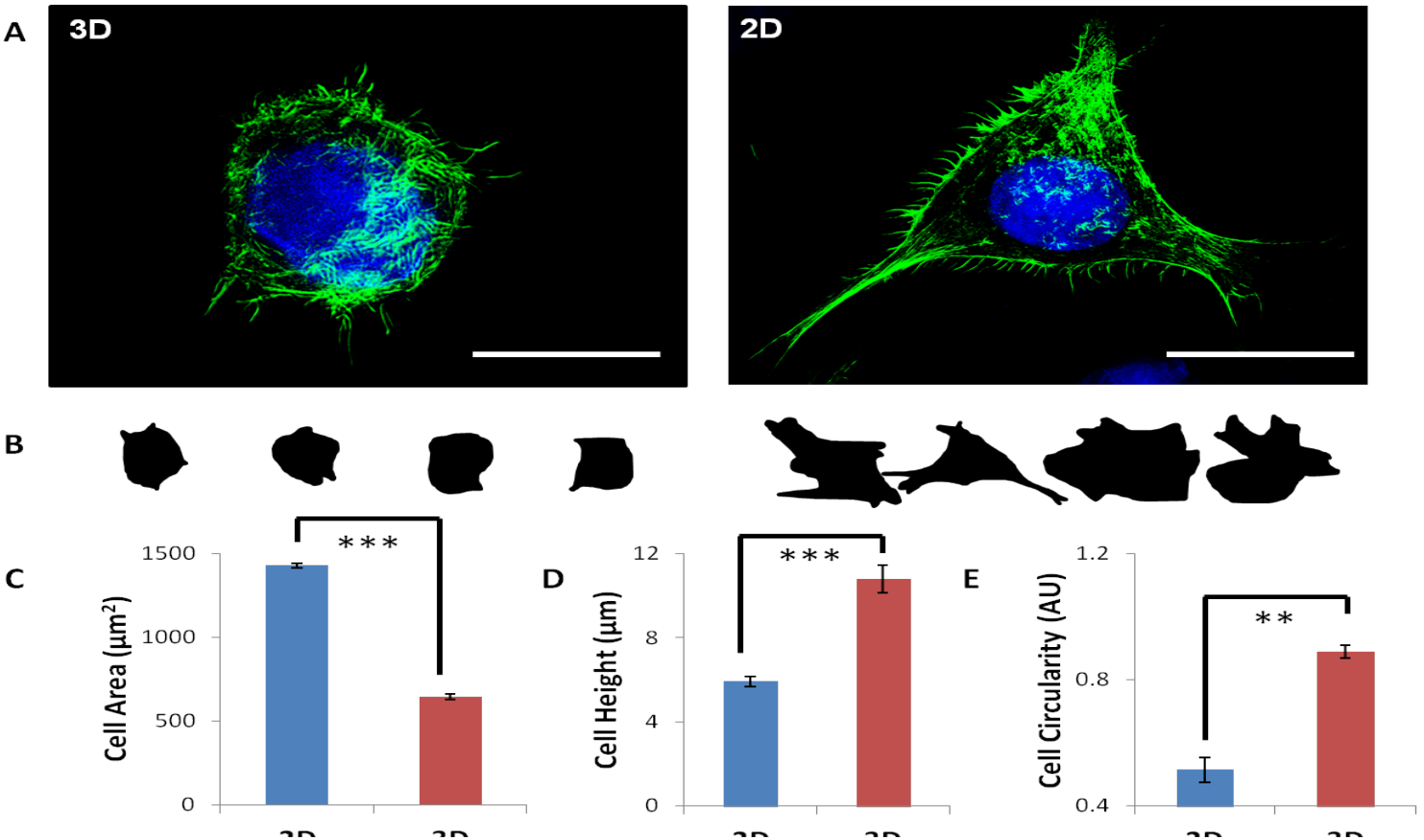

Figure 4.13 Cells grown in 3D for 6 passages show an enhanced circular shape, and a more 3D morphology indicated by a substantially increased height

Cells grown in 2D and 3D conditions were sampled out at passage 6 and stained with Phalloidin (against F-Actin) and DAPI (against nucleic acid). (A). Cells in 3D not only continue to show a rounder morphology than those grown in 2D (outlines in B), but they continue to flatten at a decreased rate when compared to 2D counterparts, as shown by a higher area and a lower height, as well as a less circular form. Scale bars = 5µm. Data presented as n=20 ± SEM. Statistical analysis through ANOVA. ** denotes $p \leq 0.01$, *** denotes $p \leq 0.001$.

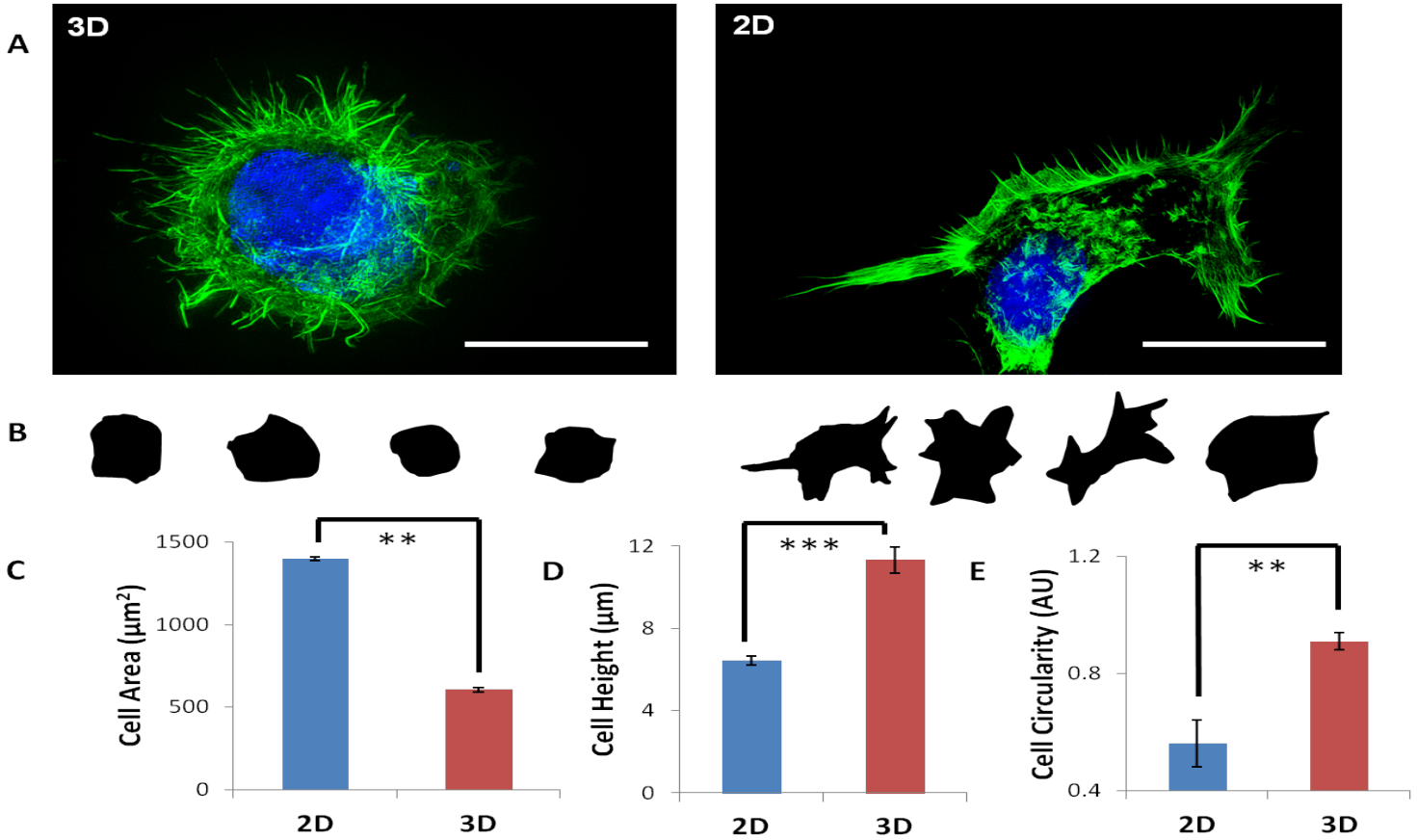

Figure 4.14 Cells at passage 10 maintain a clear difference between 2D and 3D growth

Cells grown in 2D and 3D conditions were sampled out at passage 10 and stained with Phalloidin (against F-Actin) and DAPI (against nucleic acid). (A). The differences previously shown at earlier passages are maintained but do not increase, indicating that cells have fully adapted to a 3D environment and the reduction in flattening has reached a plateau. Scale bars = 5µm. Data presented as n=20 ± SEM. Statistical analysis through ANOVA. ** denotes $p \leq 0.01$, *** denotes $p \leq 0.001$.

4.5.4 Assessing changes in cytoskeletal elements with long term maintenance in 3D

The cytoskeleton of eukaryotic cells is a dynamic structure made of three main proteins: actin microfilaments, tubulin microtubules, and intermediate filaments. Actin microfilaments are the thinnest filaments of the cytoskeleton, and as such are highly versatile, functioning in, among other things, amoeboid movement and changes in cell shape. Stress fibres are contractile actin bundles found primarily in non-muscle cells that play a vital role in cellular tension and contractility, and provide the tensile force for a number of key functions such as adhesion, migration and morphogenesis [174], making them a key cellular element to explore in this project. There are types of stress fibre in the migrating (or spreading) cell – ventral stress fibres, dorsal stress fibres, and transverse arcs [175] – they are visualised in the schematic in Figure 4.15.

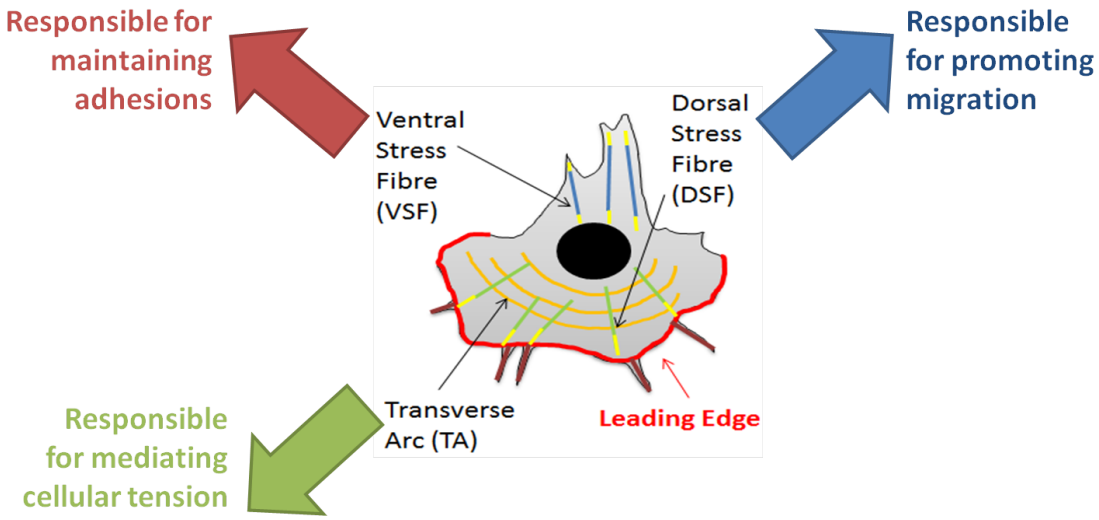

Figure 4.15 A schematic showing the three different types of intracellular stress fibre, each of which is responsible for a different cellular behavior

The actin cytoskeleton of a mammalian cell is made of three different types of stress fibre, classified by their intracellular location and interaction with focal adhesion sites. Dorsal stress fibres (DSF) are capped by adhesions at one end and run towards the leading edge of the cell. Ventral stress fibres (VSF) are capped at both ends by adhesions and run in opposite directions to the leading edge. Transverse arcs (TA) are not associated with adhesions and as such control the overall integrity of the cytoskeleton. Image modified from [179].

Ventral stress fibres are associated with focal adhesions (FAs) on both ends and run in the opposite direction to the leading edge – they function mainly to maintain adhesions to the growth substrate or extracellular matrix [176]. Dorsal stress fibres run towards the leading

edge and are capped with focal adhesions on their polymerising end – they function mostly to promote cellular migration through a matrix or cell spreading across a growth substrate [177]. Transverse arcs are not directly linked with adhesions and typically flow from the leading edge back towards the nucleus – they are responsible for mediating cellular tension and maintaining the overall integrity of the cytoskeleton [178].

One would expect that, given the differences in cell shape and migration brought about by 3D propagation that the balance of these types of stress fibres would differ between 2D and 3D maintained cells. In order to examine this, 50,000 cells from each cell population were seeded onto PDL coated glass coverslips and allowed to adhere for 4 hours. The longer growth period was to ensure that cells were both adhering and beginning to flatten, since the flattening and spreading process mirrors the migratory process cells experience *in vivo* and it is essential that cells are actively spreading in order to see stress fibres forming. Cells were then stained with Phalloidin and imaged using SIM allowing individual stress fibres to be traced using ImageJ. Stress fibres were classified as VSFs, DSFs or TAs using intracellular location. This was confirmed with dual staining using Vinculin, which is a focal adhesion marker. Fibres capped with Vinculin at both ends were classed as VSFs, those with Vinculin at one end were classed as DSFs and those with no associated Vinculin staining were classed as TAs. Given that this is an indirect method of identifying and classifying stress fibres, given the immense number of overlapping stress fibres per cell, and due to the resolution limitations of current microscopy, it was difficult to be certain of the different types of stress fibre. Thus the data that follows serves only to show trends in cytoskeletal remodeling, and further work would be required to confirm these patterns.

Figure 4.16A shows a representative cell from 2D and 3D maintained populations at passage 3, and the calculated number of VSFs, DSFs and TAs is shown in Figure 4.16B. From the immuno-labelled cells, it is clear that 3D cells show a different stress fibre organisation to 2D counterparts: there appear to be more TA fibres running across the entirety of the cell, with relatively fewer VSFs and DSFs. This was confirmed quantitatively. There also appear to be several intracellular actin 'bundles' as indicated by white arrowheads. This suggests that the actin cytoskeleton has a rapid turnover and thus requires intracellular stores of G-Actin ready for fibre assembly, indicative of a more flexible, dynamic cytoskeleton. This would fit with the idea of 3D cells actively adapting their morphology in response to changes in the geometry of their microenvironment. At passage 6, this is no difference in the organisation in the 2D cell, but the 3D cell shows a more complex network of stress fibres, indicating increased

cytoskeletal tension and thus reduced intracellular flexibility (Figure 4.17). In particular, there is a reduction in the number of TAs, confirming a more rigid cytoskeleton. Finally, there also appear to be less intracellular stores of un-polymerised actin, again supporting the idea that the cells have fully adapted to a 3D growth environment by passage 6.

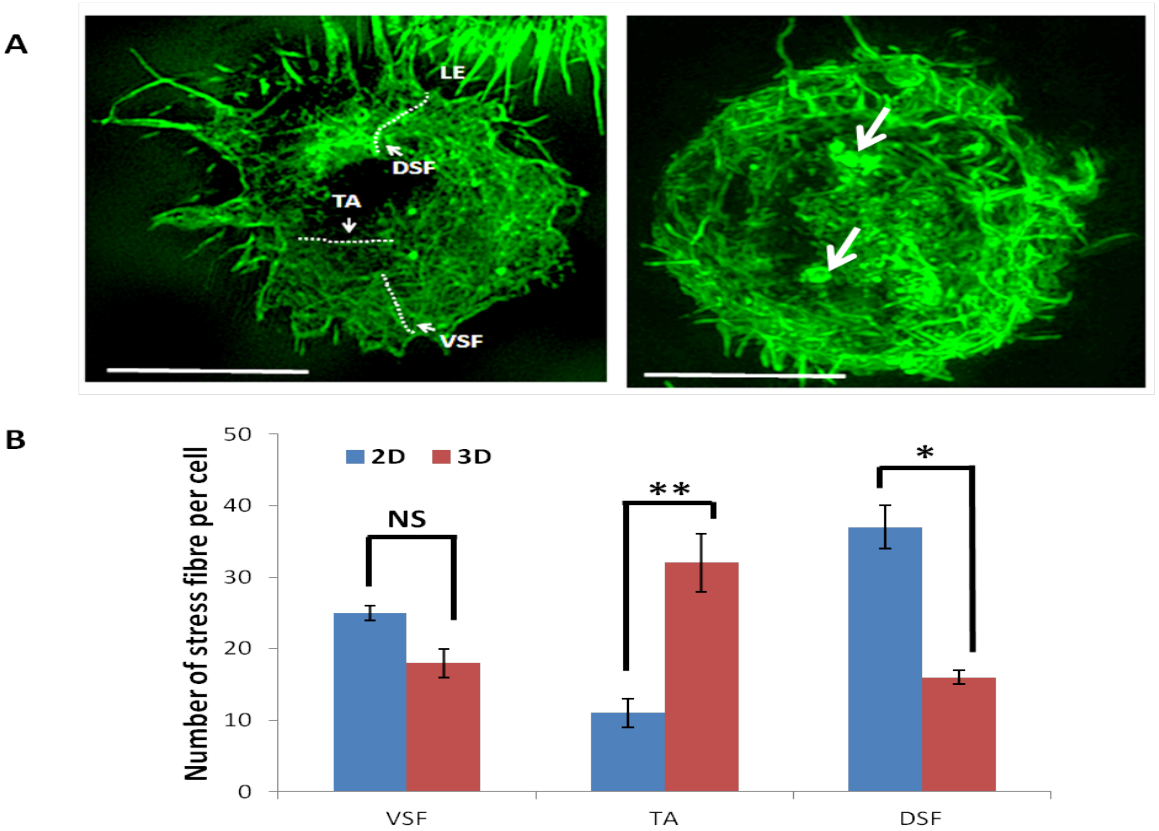

Figure 4.16 Cells grown in 2D and 3D conditions show different types of intracellular stress fibre at passage 3.

Cells grown in 2D and 3D for 3 passages were stained for Phalloidin to monitor the intracellular actin distribution. Cells grown in 2D tend to show significantly more DSF fibres and less VSF fibres, indicating that the cells adhere more than migrate, which in the context of a 2D surface would lead to flattening. The higher numbers of TA fibres indicates a higher degree of cellular flexibility in 3D cells. Scale bars = 5µm. Data presented as n=10 ± SEM. Statistical analysis through ANOVA. NS denotes non-significant, * denotes $p \leq 0.05$, ** denotes $p \leq 0.01$

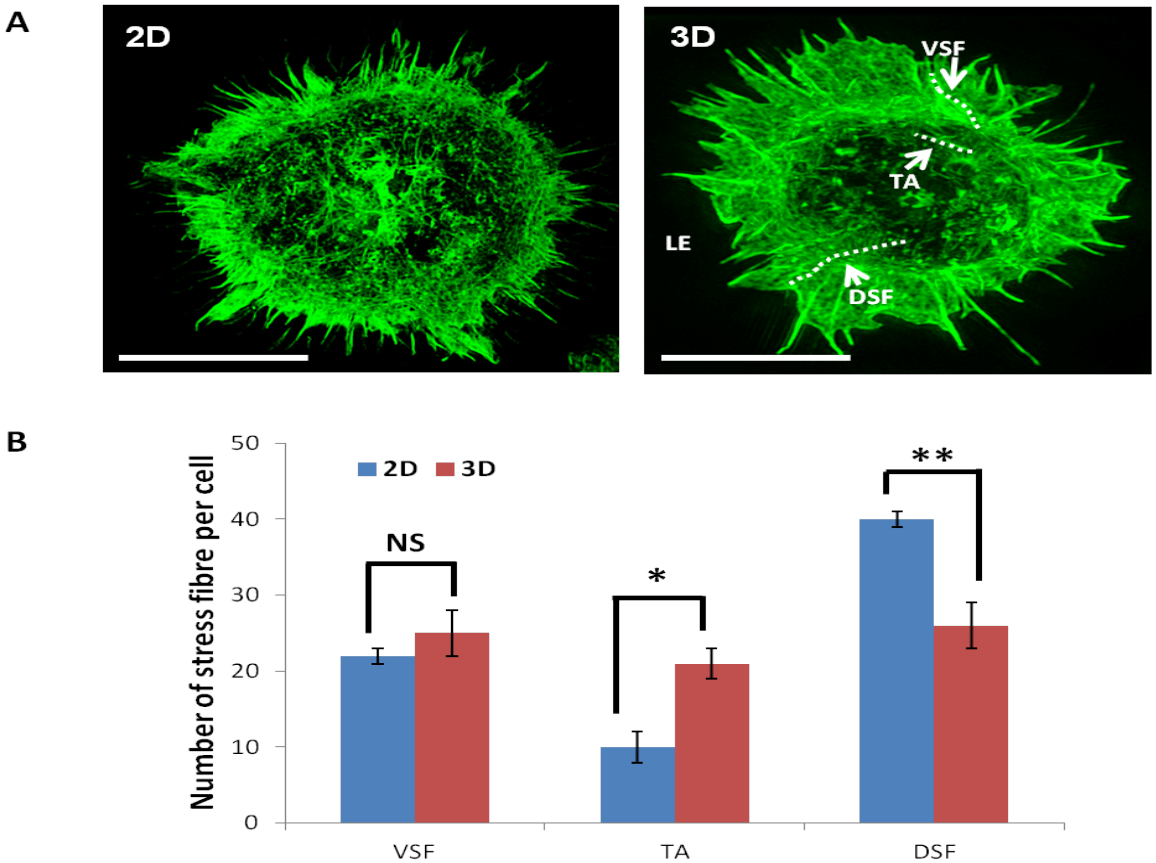

Figure 4.17 Cells in 3D show less cytoskeletal flexibility at passage 8

Cells grown in 2D and 3D for 8 passages were stained for Phalloidin to monitor the intracellular actin distribution. Once cells reach passage 8, cells grown in 3D tend to show reduced intracellular flexibility as indicated by increased sress fibres, and a decrease in the amount of TA fibres in particular. Cells grown in tend to show little difference in cytoskeletal organisation between passage points. Scale bars = 5µm. Data presented as n=10 ± SEM. Statistical analysis through ANOVA. NS denotes non-significant, * denotes $p \leq 0.05$, ** denotes $p \leq 0.01$

4.5.5 Assessing cytoskeletal reorganisation as cells flatten

Having established that the cytoskeleton of 2D and 3D cells appear to differ in the degree of inherent flexibility, cells that were maintained in 2D and 3D were allowed to flatten over a longer period of time in order to see how the adapted cytoskeleton of a 3D primed cell would reorganise when placed on a flat growth substrate. Cells were seeded as before and stained with Phalloidin and Hoechst 33342. Representative cells from both 2D and 3D maintained populations are shown at 4, 6 and 8 hours post plating in Figure 4.18. Looking at the cells 4 hours after plating, the 3D cells are significantly rounder, whereas the 2D cells show signs of a flattened morphology (Figure 4.18a and d respectively). The cells in 2D show extensive actin networks, whereas the 3D cells show fewer distinct stress fibres, indicating cytoskeletal flexibility. The 3D cells do show extensive lamellipodia though, indicating that they are beginning to spread. These differences continue to be seen at cells 6 hours after plating, with the 2D cells spreading even further and the 3D cells maintaining a rounded morphology (Figure 4.18b and e respectively). However, by this time, the 3D cells begin to show more intracellular stress fibres, indicating a less flexible cytoskeleton, and a reversion back to the 2D state. By 8 hours, the 2D cells have completely spread into a fibroblastic shape, which is a completely artificial shape for a hepatocytic cell. In contrast, the 3D cells remains rounded, though there are signs of flattening – namely an increase in stress fibres extending towards the leading edge.

Taking this experiment further, cells were allowed to spread and flatten for 24 hours, and at several time-points, fixed and imaged to allow for quantification of cell area, height and volume. Volume can be calculated by uploading a Z stack into Volocity and thresholding cell area on every slice. These figures are put into an algorithm and an estimate of cellular volume given. This was done for cells at passage 3, 6 and 9 in order to see how 3D propagation affects cytoskeletal flexibility. At early passages, the differences seen in cellular dimensions between 4 and 12 hours, a smaller cell area and larger height, are amplified further between 12 and 24 hours, indicating that cells maintained in 3D show a resistance to flattening (Figure 4.19). This is also seen at cells that have reached passage 6 (Figure 4.20), suggesting that changes seen to the cytoskeleton in previous experiments is hard-wired into the cellular machinery, thereby allowing cells to be primed to a 3D microenvironment. This conclusion is supported in Figure 4.21, which shows very little difference to the previous figure, indicating that by passage 9, cells have fully adapted to the 3D culture system. These cells stay smaller and taller than their 2D counterparts even after 24 hours in a 2D environment.

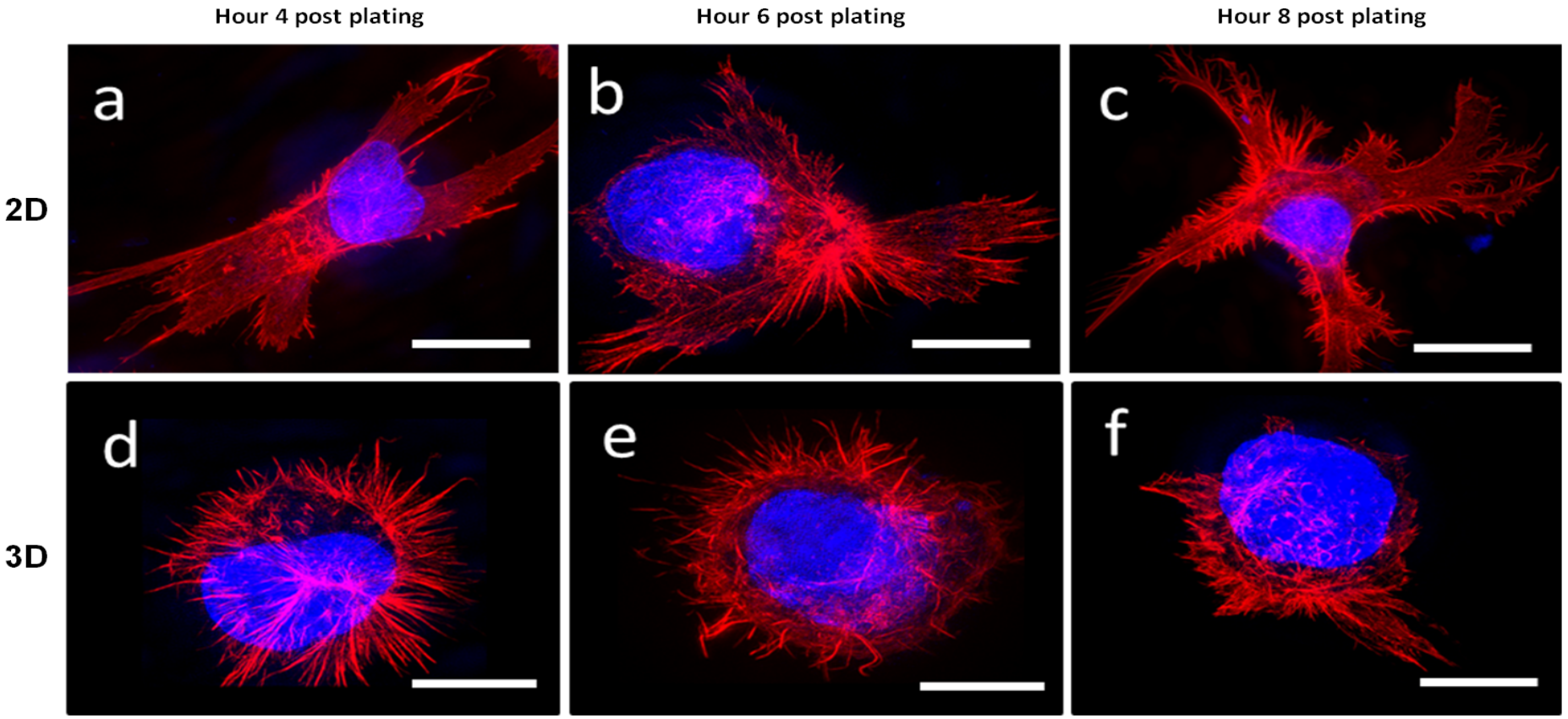

Figure 4.18 Cells in 2D flatten quicker than those grown in 3D, as shown by cytoskeletal labeling

Cells maintained in 2D and 3D for 5 passages were grown on PDL coated glass coverslips and allowed to flatten for 8 hours before being stained for Phalloidin to mark the cytoskeleton. The above images show a typical example. Cells in 2D show signs of a flattened morphology by 4 hours, and they continue to flatten further for the next 4 hours. In sharp contrast, cells grown in 3D maintain a circular shape for up to 8 hours, at which point they show slight flattening in the form of stress fibres extending towards the leading edge. Scale bars = 5µm.

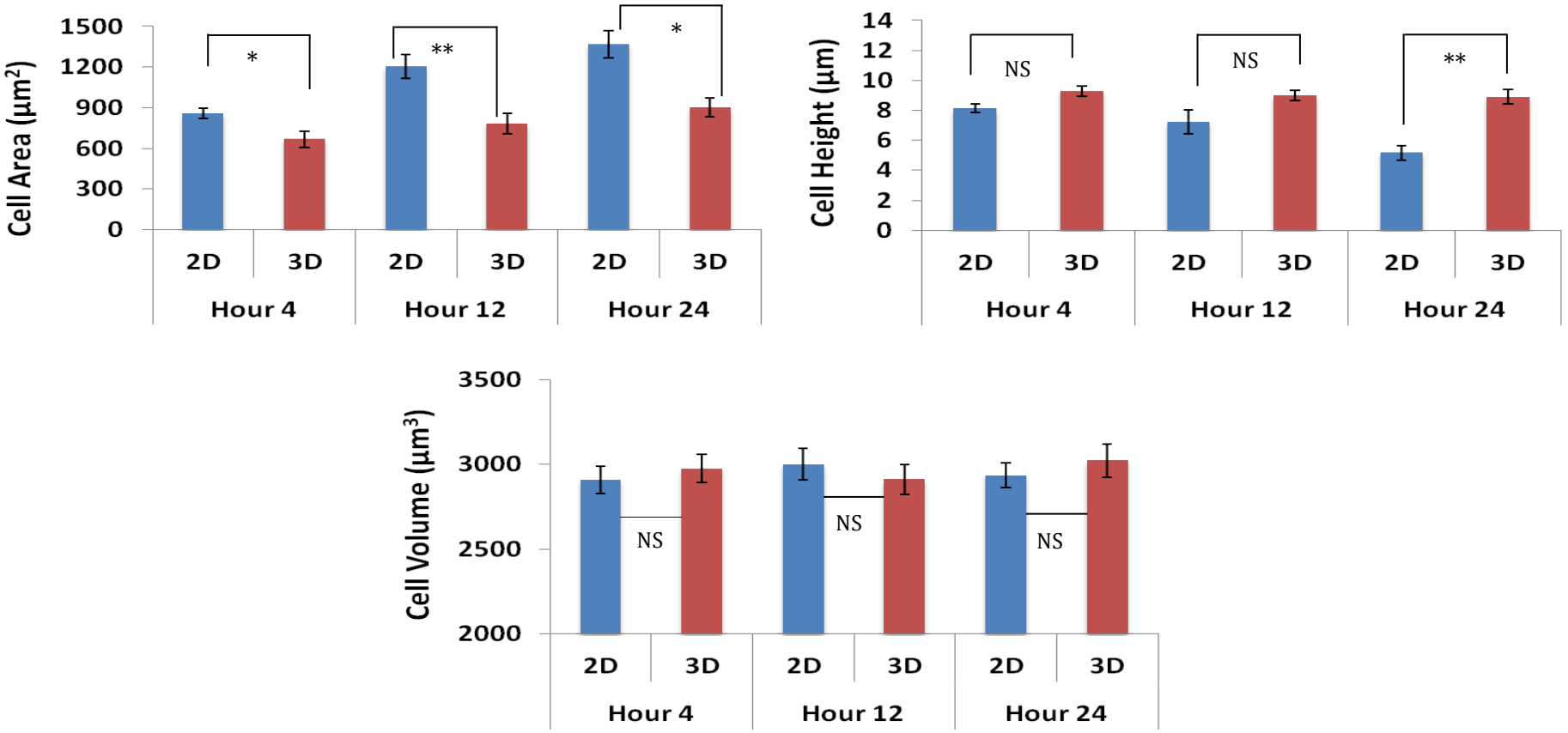

Figure 4.19 Cells grown in 2D and 3D show different cytoskeletal remodelling when placed onto flat growth substrates

Cells maintained in 2D and 3D for 3 passages were transferred to a 2D substrate and allowed to flatten for 24 hours in order to examine morphological adaptation. The differences in cellular dimensions seen at earlier time points are enhanced the longer cells are monitored, indicating that 3D cells show a resistance to flattening. Data presented as n=20 ± SEM. Statistical analysis through ANOVA. NS denotes non-significant, * denotes $p \leq 0.05$, ** denotes $p \leq 0.01$

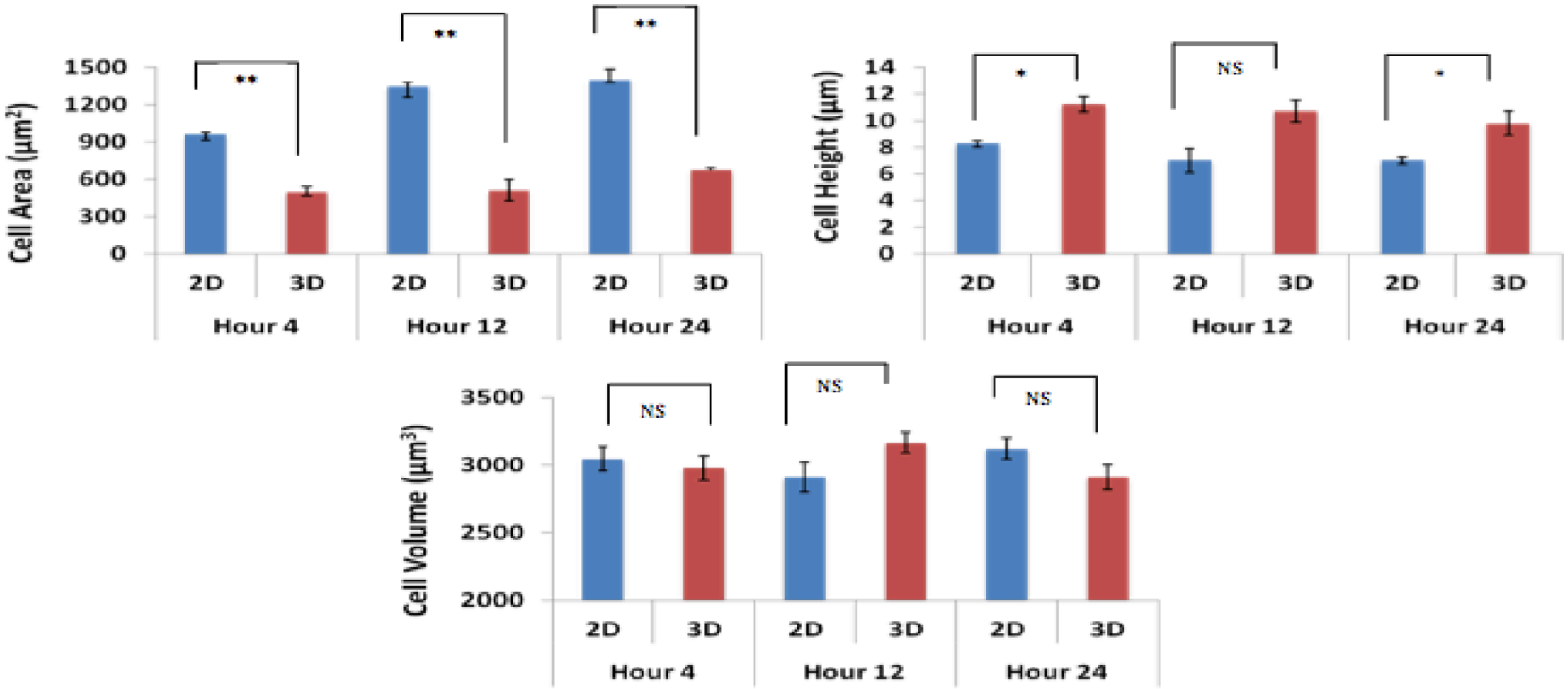

Figure 4.20 Cytoskeletal reorganisation in 3D cells is maintained at higher passages

Cells maintained in 2D and 3D for 6 passages were transferred to a 2D substrate and allowed to flatten for 24 hours in order to examine morphological adaptation. Cells that have propagated in 3D show a resistance to flattening, indicating that the cytoskeletal re-organisation seen in previous experiments is hard-wired into the cellular machinery. Data presented as n=20 ± SEM. Statistical analysis through ANOVA. NS denotes non-significant, * denotes $p \leq 0.05$, ** denotes $p \leq 0.01$

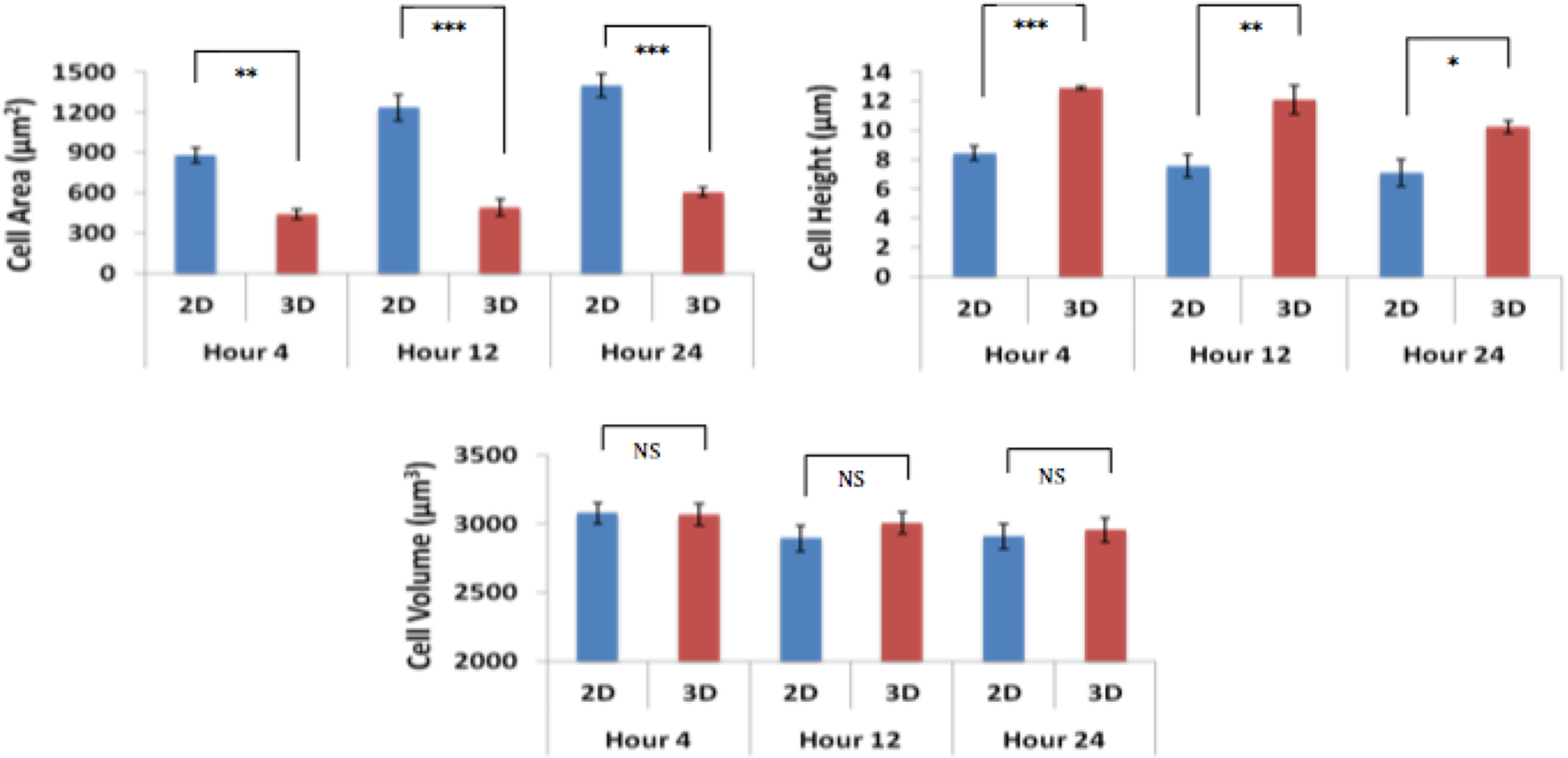

Figure 4.21 Cells maintained in 3D reach a plateau, at which no further adaptation is seen

Cells maintained in 2D and 3D for 9 passages were transferred to a 2D substrate and allowed to flatten for 24 hours in order to examine morphological adaptation. Morphological analysis at this passage closely mirrors that of passage 6, showing that at later passages, cells appear to have fully adapted to a 3D microenvironment. Data presented as n=20 ± SEM. Statistical analysis through ANOVA. NS denotes non-significant, * denotes $p \leq 0.05$, ** denotes $p \leq 0.01$, *** denotes $p \leq 0.001$.

4.5.6 Assessing changes in nuclear shape with long term maintenance in 3D

Despite being one of the most important organelles in mammalian cells, surprisingly little is known about the formation of the nucleus, and in particular what determines its shape and size [8]. The nucleus is usually round or oval, and changes in nuclear shape have been implicated in aging and disease [9]. Also, in specialised cells such as hepatocytes, nuclear shape is vital for proper cell function. There is previous research that shows that changes in cell morphology can have knock-on effects on nuclear morphology [180]. Having built up a solid body of work indicating drastic changes in cell shape brought about by 3D propagation, the hypothesis was that these changes would correlate with changes in nuclear shape.

Cells maintained in 2D and 3D for 5 passages were sampled out and seeded onto glass coverslips at 50,000 per coverslip. The cells were stained with Hoechst 33342 to highlight the nuclei, and imaged though SIM in order to generate high resolution images. Representative examples of these are shown in Figure 4.22. As the larger images on the left show, the nuclei in 3D cells are taller and rounder. They are also more regularly shaped across the smaller examples given on the left. The nuclei in 3D cells, by contrast, flatten into discs rather than maintaining height in the Z dimension. They are also more irregularly shaped.

Using the same parameters as with whole cells earlier these changes in nuclear morphology were quantified in Figure 4.23. The parameters measured were cell area, height and circularity (Figures 4.23A-C). As expected from the images in Figure 4.21, the nuclei in 3D maintained cells appear to flatten out less, as shown by a reduced area and an increased height. They are also rounder, as indicated by a statistically increased circularity figure. Another important factor to consider though is nuclear size. The changes seen in nuclear shape were not reflected in changes to cell volume, which was calculated using Z stack images and Volocity software (Figure 4.23D). This shows that cells that are propagated in 3D actively adapt to their microenvironment though a flexible nucleoskeleton. As with the cytoskeleton, these changes occur through signalling proteins on the nuclear surface, and thus these findings could have implications for lamin signalling at the nuclear lamina, which is worthy of further examination.

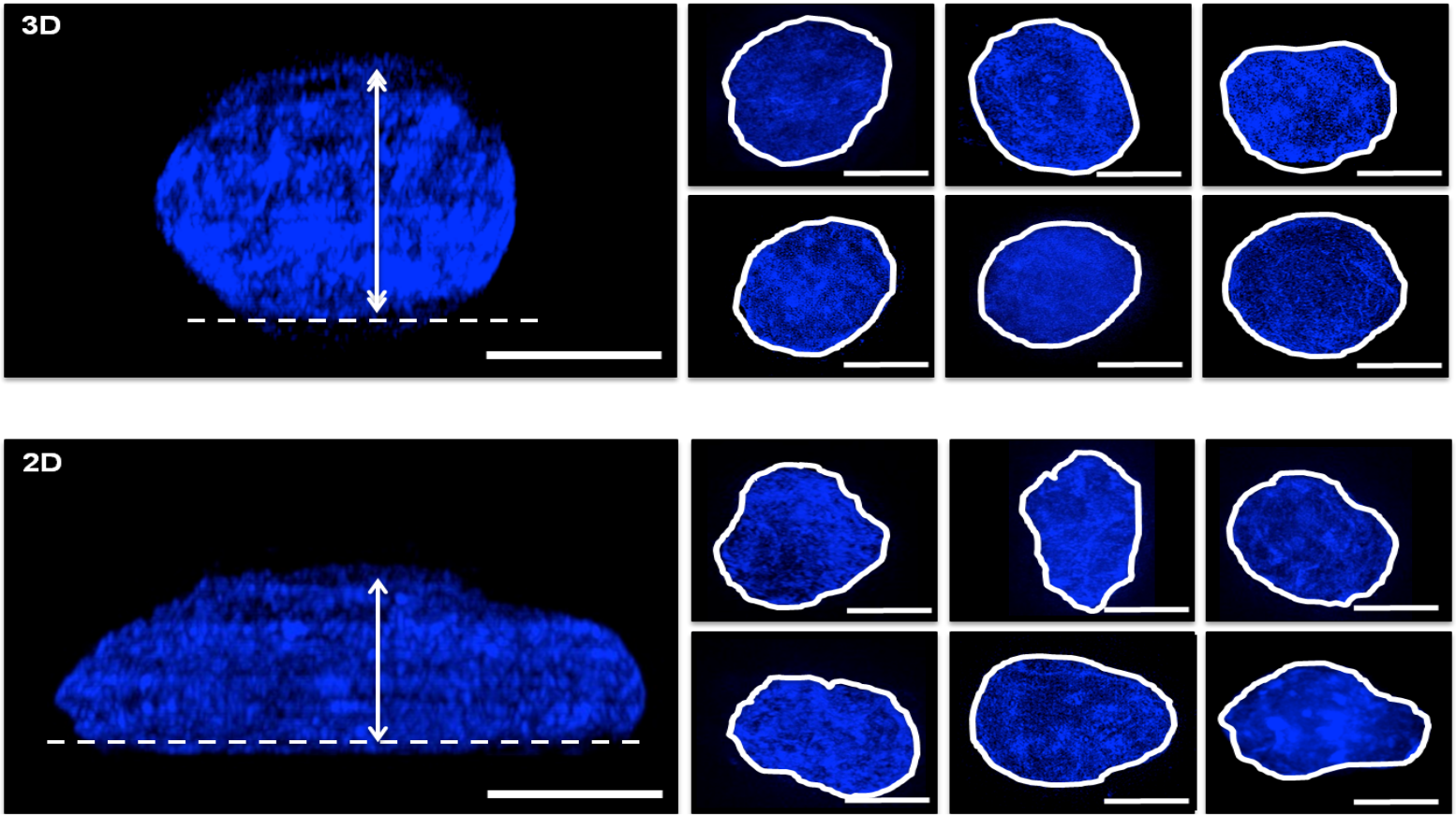

Figure 4.22 The nuclei of cells grown in 2D and 3D conditions show changes in shape and height that mirror those of the cytoskeleton

Cells grown in 2D and 3D conditions stained with DAPI (against nucleic acid). The nuclei in 3D maintained cells are rounder, more regularly shaped, and taller, resulting in a spherical shape that is more physiological than the flattened disc-shape seen in nuclei of the 2D maintained cells. Scale bars = 3µm.

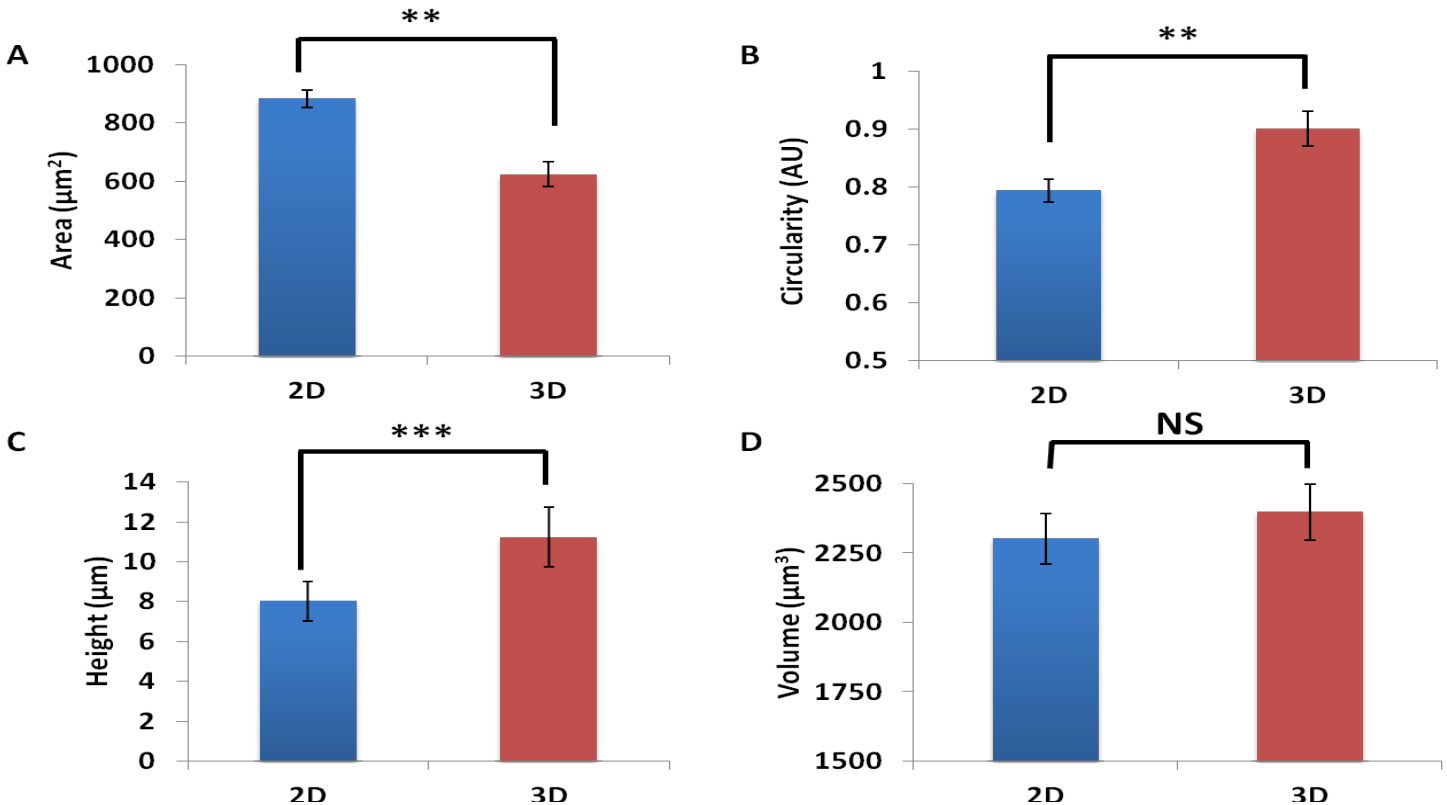

Figure 4.23 The morphological changes in the nuclei of cells grown in 2D and 3D can be quantified

The nuclei in cells grown in 2D are consistently flatter (A), shorter (C) and less circular (B) than the nuclei in 3D counterparts, which brings them closer to the physiological state of hepatocytes. This change in nuclear shape is not mirrored with a change in cell size, as measured by volumetric analysis (D), showing that cells are adapting to the environment through a flexible nucleoskeleton. Data presented as n=20 ± SEM. Statistical analysis through ANOVA. NS denotes non-significant, ** denotes $p \leq 0.01$, *** denotes $p \leq 0.001$

4.5.7 Comparing 2D and 3D cell morphologies with physiological hepatocytes

Having demonstrated that propagating cells in 3D for longer culture periods has far reaching effects on cell shape and cytoskeletal integrity, it was important to show that these changes bring 3D maintained cells closer to the *in vivo* state. In order to answer this question, pre-sectioned slides of primary human liver were obtained from a commercial source and stained with H&E in order to visualise cells (Figure 4.24A). These slides were looked at under high magnification using oil immersion in order to outline individual cells, as shown in Figure 4.24B. These images were uploaded into ImageJ and outlined in a similar way to 2D and 3D maintained cells in previous experiments. These outlines were then used to quantify cell area and circularity, and the values plotted against already established values for 2D and 3D maintained cells (Figures 4.24C and D). Area and circularity measurements show that the 3D cells show values much closer to physiological hepatocytes, whereas the 2D cells are statistically flatter and less circular. These data provide further evidence for the use of 3D propagation for physiologically accurate modelling of hepatocytes

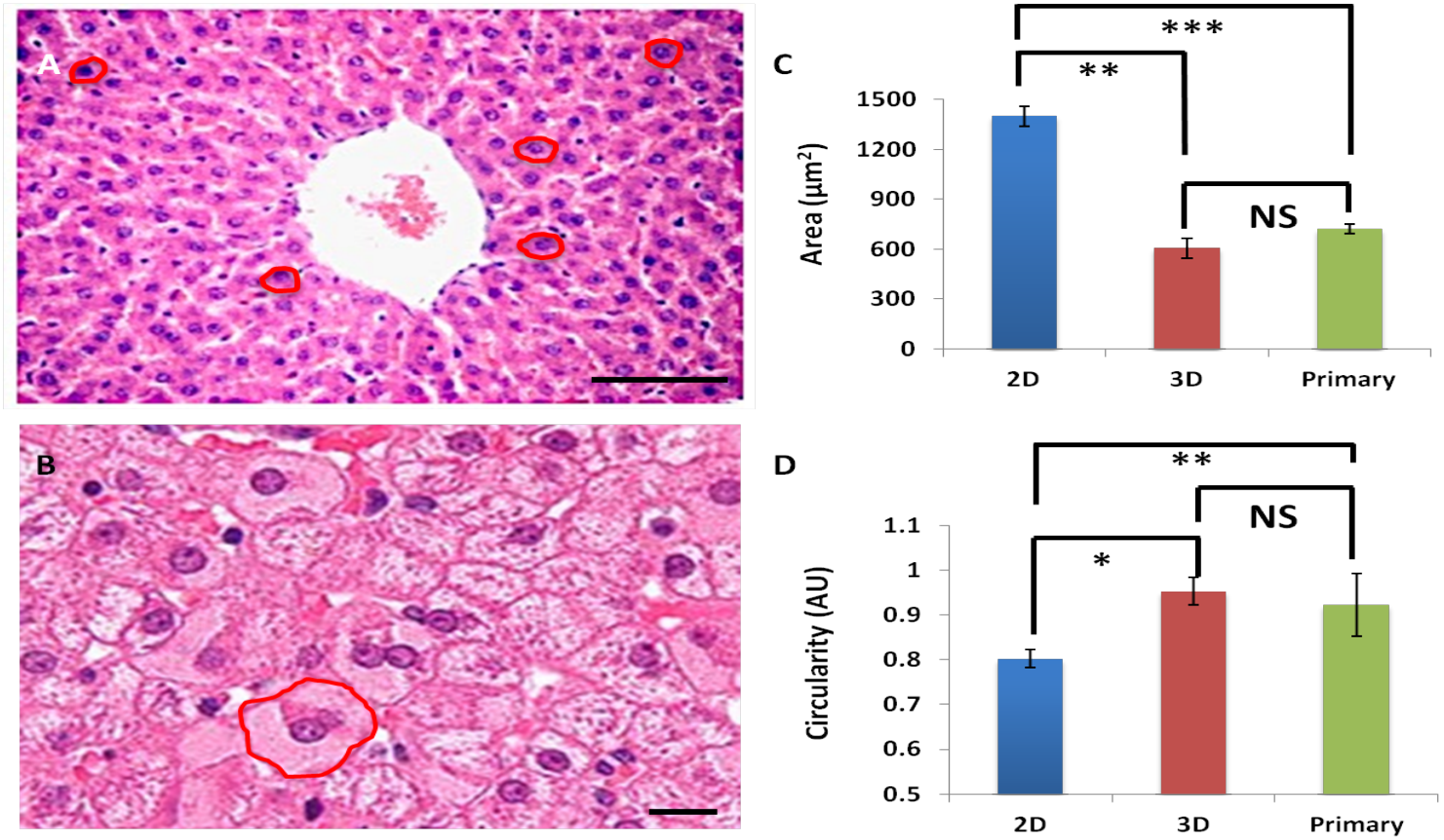

Figure 4.24 Primary human liver sections show morphologies closer to 3D maintained cells than 2D counterparts

Slides of primary human liver were sectioned and stained with H&E in order to visualise the cells (A). High magnification images (B) were taken and 5 individual cells outlined per field of view on 3 sections. Area and circularity measurements (C and D respectively) show that by the end of a 10 passage propagation, cells in 3D are closer to physiological hepatocytes than 2D cells. Data presented as n=15 ± SEM. Statistical analysis through ANOVA. NS denotes non-significant, * denotes $p \leq 0.05$, ** denotes $p \leq 0.01$, *** denotes $p \leq 0.001$.

4.6 Discussion

This chapter was primarily concerned with the comparison of 2D and 3D maintained cells in terms of migration across a planar substrate as well as penetration through a scaffold, cell morphology and cytoskeletal organisation, and nuclear shape.

The first parameter to be examined was cell organisation across a planar 2D substrate. Cells maintained in 2D and 3D were taken out of their respective growth systems and plated onto 2D glass coverslips in order to compare confluency over a set period of time (4 days). It bears mentioning at this point that cells in 3D have been shown in previous experiments to proliferate slower, and this could have impacted on these experiments. However, on the whole, putting aside the number of cells in the field of view, the organisation of these cells with regards to their neighbours does appear to differ both between cells maintained in 2D and 3D and between cells maintained for shorter and longer times in 3D. With 3D propagation, cells form smaller colonies, and retain this organisation for up to 4 days post plating on 2D substrates. This is in direct comparison to 2D cells, which, over the same time period, form much larger colonies that connect to create a confluent monolayer across the planar substrate. This is mirrored by similar differences when these two cell populations are, once again, taken out of their respective growth systems, and this time seeded onto 3D scaffolds. In this case, cells propagated for short periods of time in 3D form thin long and consistent cell layers along the top of the membrane, whereas cells propagated in 3D for longer periods of time form small multi-dimensional 'clumps' or colonies that spread out across and throughout the matrix. In both cases, cells propagated in 3D formed small spheroid-like structures that spread, in contrast to 2D propagated cells that form larger, and flatter sheet-like structures. Presumably, the mechanistic explanation for this is similar to that exploited for the formation of aggregate cultures. 3D cells do not show the same exaggerated adhesion to the growth substrate as 2D cells, but instead share tighter adhesion to each other [181]. As such, instead of flattening into layers or sheets, they form rounded structures.

As well as changes in how the cells interact with each other, these experiments revealed a clear change in cell shape, with 3D propagated cells constantly appearing rounder. This was confirmed by using high magnification images of single cells to calculate various cell descriptors. Cells propagated in 3D were, on average, more circular and less flattened, as measured by cell area over time. Cell shape has been shown to impact on how cells self-

organise on growth substrates, as well as how cells migrate through a matrix, and in this way the findings from cell organisation, penetration through scaffold, and cell shape analysis can be tied together to give a comprehensive view of how cells adapt their cytoskeleton to a changing microenvironment.

The shape of adherent cells is known to have a profound effect on a number of important properties including cytoskeletal structure, growth, and differentiation [182]. In particular, cell shape plays a vital role in regulating the relationship among cell adhesion (both cell-cell and cell-matrix) and contractile force. Recent studies have shown that cell shape regulates the cytoskeleton and subsequently cell stiffness [183]. For example, extensive actin stress fibers have been seen in cells with large spreading area, whereas only diffuse cortical actin was observed with a small spreading area, suggesting that actin stress fiber formation can be affected by cell shape [183]. The cell–matrix interaction and the rigidity of the substrate can also regulate cell shape. For adherent cell types, cell shape is largely determined by the adhesion between cell cytoskeleton and the ECM [184]. Therefore, the dynamic interactions among cell shape, cell adhesion and the associated cell contractile force, as well as the substrate stiffness, are closely interrelated. It has been posited that changes in cell shape bought about by biomechanical cues from the matrix may be transduced into a regulatory signal by several structures at the interior cell membrane, including focal adhesion complexes (FACs) and the intracellular actin cytoskeleton [185]. For cell migration, the changes in cell shape are required by developing an asymmetric pattern of substrate contacts for producing the driving force of migration. Thus the changes seen in the way 2D and 3D maintained cells spread across a planar substrate, and the way they organize within the Alvetex®Scaffold matrix can be directly linked to the changes in cell morphology brought about by propagation in 3D.

Cell morphology is particularly important in culturing hepatocytes due to the importance of correct cell geometry in maintained functional polarization. To study the role of cell shape in control of hepatocyte function, Saramoto developed a system to control the spreading of cultured rat hepatocytes using poly[2-hydroxyethyl methacrylate] [186]. When hepatocytes were cultured in a dish coated with high concentration of this solution, formation of stress fibers was suppressed and cells maintained a spherical shape. In these cells, the ability to metabolise Dexamethasone remained high for longer periods of time, as compared to hepatocytes that were allowed to spread following culture in a control uncoated polystyrene dish. When the hepatocytes that had spread following long-term culture in the polystyrene dishes were treated with Cytochalasin to induce depolymerization of F-actin, the ability of the

cells to metabolise Dexamethasone was recovered, despite their flattened shape. Thus, there is a possibility that it is the kinetics of F-actin polymerisation rather than cell shape that regulates cellular function in primary cultured hepatocytes. However, since these dynamics are irrevocably linked to changes in cell morphology, it could be argued that this is a distinction without significance.

As well as exploring changes in cell morphology, cytoskeletal organisation, and cell organisation bought about by 3D propagation, cells from 2D and 3D maintained pools were also compared for changes in nuclear shape and size. Cells maintained in 2D showed flatter nuclei that sat on top of a flattened cytoskeleton that was fully adhered to the planar substrate. However cells maintained in 3D showed taller, and more circular nuclei, as quantified using ImageJ software. In these cells, the nuclei remained roughly spherical, and the cytoskeleton wrapped itself tightly around on all sides like a cage. This finding was taken to show that culturing cells in 3D allowed the nucleus to adopt a more rounded form, which is the shape the nuclei of native hepatocytes in the liver adopt [187]. In many cell types, altered nuclear shape is due to changes in the nuclear lamina. In some cases, however, the shape of the nucleus is altered by forces that act from the cytoplasm, and which are mediated by the cytoskeleton [188]. Several experimental findings suggest that the expression of A-type lamins, which are found at the nuclear lamin can affect the mechanical properties of the cytoplasm and the organization of cytoskeletal elements such as actin stress fibres [189]. Thus, in the light of the previous data showing signs of changed cytoskeletal organisation in 3D maintained cells, it would fit that this could in turn lead to nuclear changes.

It is still not entirely clear how nuclear shape affects function, although two main hypotheses exist [188]. The first hypothesis suggests that changes in nuclear shape alter the rigidity of the nucleus; this could be beneficial for cells that need to squeeze through tight spaces such as migrating cancer cells, but harmful to more fragile cells that are placed under extreme mechanical stress. The second hypothesis proposes that changes in nuclear shape result in chromatin reorganization and thereby affect gene expression. In this way, it is posited that the nucleus itself acts as a cellular mechanosensor, with changes in nuclear shape causing conformational changes in chromatin structure and organization and directly affecting transcriptional regulation. Studies focusing on nuclear shape and structure have revealed strong correlations between nuclear shape change and changes in cellular phenotype. By controlling the cellular environment with microfabricated patterning, Thomas showed that

collagen synthesis correlated more strongly with nuclear shape than with cell shape. [190]. Studies looking at mammary epithelial cell morphogenesis have demonstrated that altering nuclear organization can modulate the cellular and tissue phenotype [191]. Additionally, mechanical compression studies have been used to manipulate nuclear shape directly. They have shown that induced shapes changes in the nuclei of cultured chondrocytes leads to changes in cartilage composition and density [192].

These findings taken together suggest that propagation of cells in 3D allows them to adopt a 3D morphology and phenotype, and indicates that there is potential for this methodology to be used to enhance hepatic functionality in hepatocytes, a cell type for which morphology is directly linked to functional behavior.

4.7 Conclusions

The following conclusions can be drawn from this Chapter:

- Cells can be propagated in parallel in 2D and 3D culture systems, thus allowing for the formation of two separate pools of cells that have been maintained solely in either 2D or 3D for 2 months. This allows for direct comparison of propagation strategies.

- Cells propagated in 3D show different cell-cell organisation both across a 2D planar substrate and throughout a 3D porous matrix when compared to 2D controls. Namely, 3D maintained cells form small round structures akin to spheroids that spread out across the available growth substrate. This is in contrast to 2D maintained cells, which form long thin 'islands' across the growth substrate.

- 3D maintained cells are quantifiably more circular and regularly shaped, whereas 2D maintained cells form flat irregular fibroblastic shapes. 2D cells show larger cell areas, as well as shorter heights in the Z dimension and more irregular cell perimeters, as measured by circularity. 3D cells in contrast spread less, and so have smaller cell areas, and are taller in the Z dimension.

- Cells in 2D and 3D show different intracellular actin organisation in the form of stress fibres. Cells in 2D on average show more extensive stress fibres, especially VSFs, which are indicative of strong cell-substratum interaction. Contrastingly, cells maintained in 3D show more diffuse cortical actin, and fewer distinct stress fibres spanning the cytoskeleton. This could be a sign of increased cellular flexibility.

- Cells maintained in 2D show flatter disc-like nuclei that sit on top of a flattened actin cytoskeleton, whereas cells maintained in 3D show more spherical nuclei around which the cytoskeleton wraps itself across all dimensions.

The data from this chapter suggest that cells can be primed to a 3D morphology by continual propagation over long term *in vitro* culture. The following chapter will explore whether this is indicative of a more 3D phenotype in terms of metabolism, function, and gene expression.

Chapter 5: Comparing 2D and 3D maintained hepatocytes in terms of enhanced metabolism and liver-specific functionality

5.1 Introduction

5.1.1 Drug metabolism in hepatocytes

One of the key roles of hepatocytes in the liver is to metabolise xenobiotic substances such as drugs, making them crucial in the early stages of *in-vitro* drug discovery [193]. Hepatic metabolism occurs in two phases: phase I and phase II. Phase I metabolism is mediated by the cytochrome P450 enzyme superfamily which are found in the endoplasmic reticulum of hepatocytes [194]. This family has dozens of members, however most common drugs are metabolised by the CYP1, CYP2 and CYP3 families, with CYP3A4 being involved in almost 50% of all drug metabolism [195]. CYP enzymes most commonly act to hydroxylate the drug molecule in order to increase its polarity [196]. Phase II metabolism then usually involves conjugating the drug in order to render the molecule more polar and water-soluble, so as to facilitate renal elimination. The most common Phase II reaction is glucuronidation, in which glucuronic acid is added to a functional group on the drug molecule. Other conjugation mechanisms include the addition of sulphate groups, acetyl groups and glutathione groups.
The precise mechanism by which a drug molecule is metabolised is characterised early on during the drug discovery process, usually using cultured primary hepatocytes grown in 2D culture.

5.1.2. Differences in drug metabolism between 2D and 3D cultured cells

Although 2D cell culture has proven to be a valuable method for cell-based studies, its limitations are being increasingly recognized. Since almost all cells *in vivo* are surrounded by other cells and extracellular matrix (ECM) in a three-dimensional (3D) fashion, 2D cell culture does not adequately take into account the natural 3D environment of cells. As a result, when 2D models of liver tissue are used for preclinical drug testing, these tests sometimes provide misleading and non-predictive data for *in vivo* responses [20,22,197]. Currently, in drug discovery, the standard pipeline runs from the screening of potentially therapeutic compounds with 2D cell culture-based tests, followed by animal model tests, and finally human clinical trials. There is a high attrition rate, with only 10% of compounds progressing successfully through clinical development. Many of the drugs fail during clinical trials, especially during phase III, which is the most expensive phase of clinical development [9,16]. A large proportion of these failures is attributed to aberrant data collected from monolayer culture tests in which

the cellular response to the tested drug is altered due to an unnatural cellular microenvironment. To lower the cost drug development, the cessation of work with ineffective or toxic compounds should happen as early in the pipeline as possible, ideally before animal tests. Therefore, it is imperative to develop *in vitro* cell-based systems that can more realistically mimic the *in vivo* cell behaviors and provide more predictable results to *in vivo* tests. Recently, a growing body of evidence has suggested that 3D cell culture systems, in contrast to the 2D culture system, more accurately represent the native microenvironment that cells experience when they reside in tissues. Thus, the observed behavior of 3D cells is likely more reflective of *in vivo* cellular responses.

The differences in cellular chemo responses between 2D and 3D cultures are primarily due to:

1) Changes in cell spreading due to difference in physical properties between 2D and 3D cultures.

   2D-cultured cells are stretched out to an unnatural degree on a flat substrate, but cells cultured in 3D on a biological or synthetic scaffold material are free to maintain a normal morphology. Gurski *et al*. attributed this
   morphological spread for the differences in response to drug between 2D and 3D cultures [198].

2) Differences in the expression and the spatial organization of surface receptors in 3D and 2D culture.

   Many drugs are designed to target specific receptors on cell surfaces. Because the 3D environment causes changes to the structure, localization, and spatial arrangement of these receptors, as well as potentially modulating their expression levels at the transcriptional stage, the binding efficiency of a drug to these receptors may be different in 3D and 2D cultures [199]. This change in binding efficiency could lead to altered cellular uptake/metabolism of the drug within the cell.

3) Differences in molecular target gene expression levels.

   Cells growing in 2D monolayer are under stress and therefore some genes and proteins being expressed are altered as a result of this unnatural state. These genes and proteins may be engaged in mediating drug actions, or may indeed be the target

of certain drug actions. Thus, changes in the general proteome of the cell could alter the effectiveness of a drug.

4) Heterogeneity of cell stages in 3D.

While cells in 2D culture are mostly proliferating cells, 3D cultures are usually a mixture of cells at different stages. Wen *et al*. indicated that larger spheroids are likely to be heterogeneous, having proliferating cells on the outer region and quiescent cells in the inner region due to lack of nutrients and gas exchange. Active cell proliferation is sometimes required for some drugs to be effective [200]. Examples of drugs that require active proliferation to be effective are 5-fluorouracil (5-FU) and doxorubicin. Tung *et al*. [31] showed that the lack proliferating cells in A431.H9 3D cultures resulted in 100-fold increase in resistance to 5-Fluoruracil. This same pattern was observed to a lesser degree with doxorubicin and endometrial cells. [201].

5) Differences in drug accessibility and waste/metabolite transport.

While drugs diffuse to cells in the 2D monolayer equally, drug diffusion to cells in a 3D culture may be at variable concentrations depending on the depth to where the cells located. Diffusion of molecules and waste metabolites also has causes variable pH levels. Researchers have found that regions of hypoxia may exist due to lack of a transport system to remove waste from the center of spheroids [201]. Swietach *et al*. highlighted the importance of intracellular pH on determining the efficacy of weakly basic chemotherapeutic drugs such as doxorubicin, by showing that a lower pH reduces drug uptake, contributing to drug resistance [202].

These differences indicate that 3D models of drug responses will differ significantly from 2D models. Indeed, research has largely borne this out [198,203,204], as reviewed in Section 1.1.2.3. Given that 3D models have consistently yielded differing drug sensitivities when compared to traditional 2D models, it is hypothesised that 3D propagation will result in enhanced differences. To study this, the pools of 2D and 3D maintained cells generated by the methodolody in Chapter 3 were analysed for differences in metabolism. This involved a study of secondary hepatic metabolic markers such as urea and albumin, drug toxicity profiles, and protein expression levels of key metabolic enzymes.

5.2 Aims of Chapter

The aim of this Chapter is to compare the metabolic profile of 2D and 3D maintained cell populations both as single cell suspensions and as aggregates, as an example of a secondary 3D model. The purpose of this is to observe whether any changes seen in cell behaviour are specific to Alvetex®Strata or the geometry of a 3D microenvironment. A secondary aim is to investigate whether changes in metabolism lead to functional enhancement of immortalised hepatocytes, and whether these changes can be linked to downstream modification of gene expression. These observations will provide validation for the model of long-term propagation of cells in 3D.

5.3 Objectives

1. Use 2D and 3D maintained cells to produce aggregates, and assess differences in the formation and shape of these aggregates
2. Characterise changes in media levels of glucose, albumin and urea between 2D and 3D cells, and aggregates formed from 2D and 3D maintained cells.
3. Expose 2D and 3D maintained cells to several pharmacological agents in order to test for changes in resistance to xenobiotic-induced cytotoxicity.
4. Probe these cell populations for key genes involved in the metabolism of drugs in order to test for changes in gene expression.

5.4 Materials and Methods

5.4.1 Assessing metabolic activity

5.4.1.1 Bradford Assay

A Bradford Assay was conducted using a commercial kit (BioRad, 500-0202) according to instructions. The Bradford assay is a protein determination method that involves the binding of Coomassie Brilliant Blue G-250 dye to all proteins in the sample. The protein-dye conjugate can be detected at 595nm using a standard plate reader. A standard curve was created by using Bovine Serum Albumin (BSA) standards supplied in the kit. Briefly, 5µl of sample/standard are mixed with 250µl of dye reagent in individual wells of a 96 well plate, and incubated at room temperature for 5 minutes. The plate was then loaded into a BioTek ELx800 plate reader and absorbances read and noted.

5.4.1.2 Quant-iT™PicoGreen® Assay

Cell number was quantified using a commercial kit (Life Technologies, P7589). Cell samples were lysed using a standard lysis buffer, and both lysates and scaffold discs (in the case of 3D samples) were transferred to eppendorf tubes and homogenised using a 21G needle. Standards of known cell number were used to create a standard curve using instructions supplied in the kit. Briefly, 1ml of sample lysate was mixed with 1ml of working solution of the Pico Green reagent in a 3ml tube, which was wrapped in foil to protect from light and incubated at room temperature for 5 minutes. Fluorescence was then read at 540nm using a BioTek Synergy H4 plate reader (excitement at 460nm).

5.4.2 Glucose Consumption using GlucCELL™

Glucose levels in culture media were assessed using the GlucCELL system (CESCO Bioproducts, DG1000). This system is made up of a glucose meter, calibration strip, and test strips. Briefly, the meter is calibrated to a known value using the calibration strip. Once the meter is blanked, 10µl of sample media was pipetted to the right of the aperture of the test strip, allowing the sample to fill the confirmation window. A value for the glucose level appears on the screen of the meter. Fresh media pre-warmed to 37°C was also analysed in order to normalise data.

5.4.1.4 Albumin Assay

Secreted albumin in culture media was quantified using a commercial enzyme-linked immunosorbant assay (ELISA) plate (AssayPro, EA3201-1), following instructions provided in the kit. Firstly, a standard curve was created by serially diluting a standard provided in the kit. Briefly, 50µl of either standard or sample was added to the individual wells of the plate, which was then sealed using sealing tape, and incubated at room temperature for an hour. The plates were washed using buffer in the kit, and then 50µl of biotinylated antibody was added per well and the plate was incubated as before for 30 minutes. The plate was washed again and 50µl of SP conjugate was added per well, and the plate was incubated again for 30 minutes. At this point, the plate was washed and 50µl of chromogen substrate was added to each well and incubated for 20 minutes. Finally, 50µl of stop solution was added tro each well, and the plate read immediately at 450nm using a BioTek ELx800 plate reader.

5.4.1.5 Urea Assay

Secreted urea in culture media was quantified using a commercial colorimetric assay (BioAssay Systems, DIUR-500), following instructions provided in the kit. Briefly, 5µl of either water (blank), standard (provided in kit), or sample media were added to the individual wells of a 96 well plate, followed by 200µl of working reagent, and the plates were incubated at room temperature for 15 minutes, and then read at 540nm using a BioTek ELx800 plate reader.

5.4.3 RT-PCR

Cells from 2D and 3D maintained populations were lysed using RLT Lysis Buffer (Qiagen), and homogenised using a 21G needle. A commercial RNA spin-column extraction kit was used to isolate RNA (Qiagen RNeasy® Mini Kit, 74106), and the quality and quantity of this RNA was checked using a Nanodrop Spectrophotometer (NanoDrop ND-1000). RNA was converted into cDNA using a commercial cDNA reverse transcription kit (Applied Biosystems, 4368814) and a thermal cycler (Biometra), and cDNA samples were stored at -20°C prior to RT-PCR. RT-PCR analysis was carried out using the TaqMan® Gene Expression assays (Table 5.1), and assays were normalised against the housekeeping gene GAPDH. Experiments were carried out using the Applied Biosystems 7500 Fast RT-PCR machine, and analysed using the associated software.

Gene	Supplier	Code
CYP2E1	Life Technologies	Hs00559368_m1
CYP3A4	Life Technologies	Hs00604506_m1
GST-1	Life Technologies	Hs02512067_s1
GAPDH	Applied Biosystems	4352934-1001030

Table 5.1 TaqMan® Gene Expression Assays using in RT-PCR

For each gene expression assay run in this chapter, this table lists the gene target, the supplier, and the identifier code. These gene assays were chosen based on previous research conducted in this research group.

5.5 Results

5.5.1. Using 2D and 3D maintained populations to create aggregates

Data from previous chapters has established that 2D and 3D maintained cells behave entirely differently when placed into a 2D environment, and thus one would hypothesise that they would also behave differently when placed into a secondary 3D model system. In order to test this hypothesis, cells were sampled out at different passage points and allowed to aggregate in order to form spheroids. As discussed in Section 1.1.3.1, spheroids are micro-scale, spherical cell clusters that form by self-assembly [200]. They are especially useful 3D models because they exhibit several relevant physiological traits including a more relevant morphology, stronger and more complex cell-cell contacts and signalling, and increased cell survival. Given that maintaining cells in 3D appears to enhance these traits, it would stand to reason that aggregates formed from 3D maintained cells may show greater physiological resemblance.

Cells from a 2D maintained population, and those from early (p3), mid- (p6) and late (p8) passage in 3D were placed in a non-treated petri dish for two weeks and allowed to form aggregates (Figure 5.1). During this time, photos were taken every few days in order to monitor the aggregation process. As seen in Figure 5.1, 2D maintained cells appear to form aggregates faster than early passage 3D cells. However, by mid-passage, this difference is less noticeable, and completely disappears by passage 8. Fast aggregation can be taken as a sign of 'stickier' cells; this indicates a difference in the presence of cell adhesion molecules. This finding suggests that maintenance in 3D has an impact on the molecules expressed at the cell surface. Cells maintained in 2D also form more irregularly shaped aggregates, whereas by passage 6, cells maintained in 3D form rounder, more regularly shaped aggregates. This could be a by-product of the increased circularity seen in individual cells once they're maintained in 3D for several passages.

The qualitative changes seen in Figure 5.1 were quantified using ImageJ parameters previously established in Chapter 4. Namely, the area and circularity of the aggregates were measured and plotted against time in order to characterise any differences in the aggregation process between early, mid- and late passage 2D and 3D maintained cells (Figure 5.2).

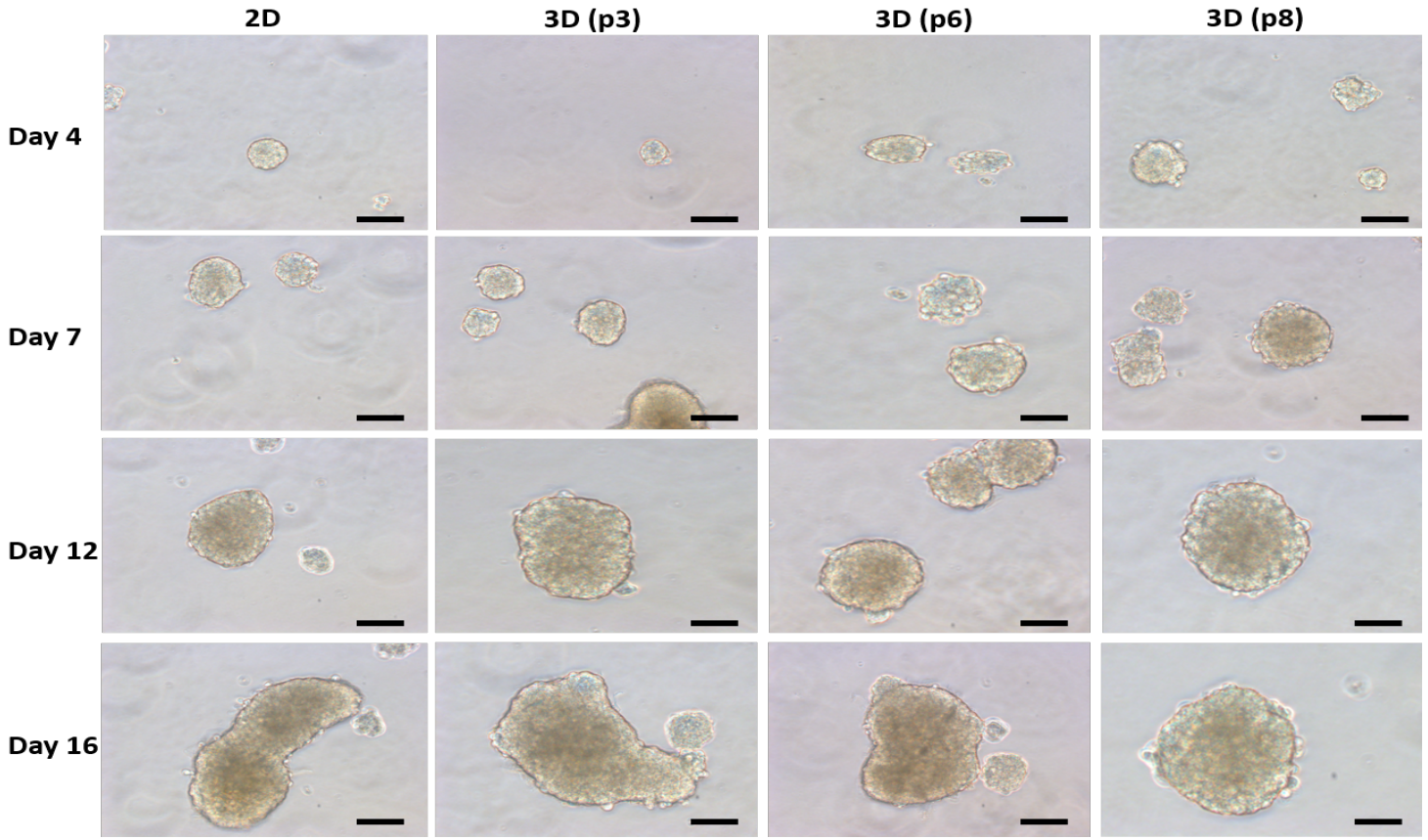

Figure 5.1 Aggregates can be formed from 2D and 3D maintained cells.

Cells maintained in either 2D or 3D were left to form aggregates for 16 days and imaged at several time-points in order to characterise the aggregation process. Cells begin to aggregate quicker in 2D systems than 3D systems at earlier passage points but this change disappears by passage 6. Likewise, cells in 2D form more irregularly shaped aggregates, whereas by passage 6, cells maintained in 3D form rounder, more regularly shaped aggregates. Scale bars = 100µm.

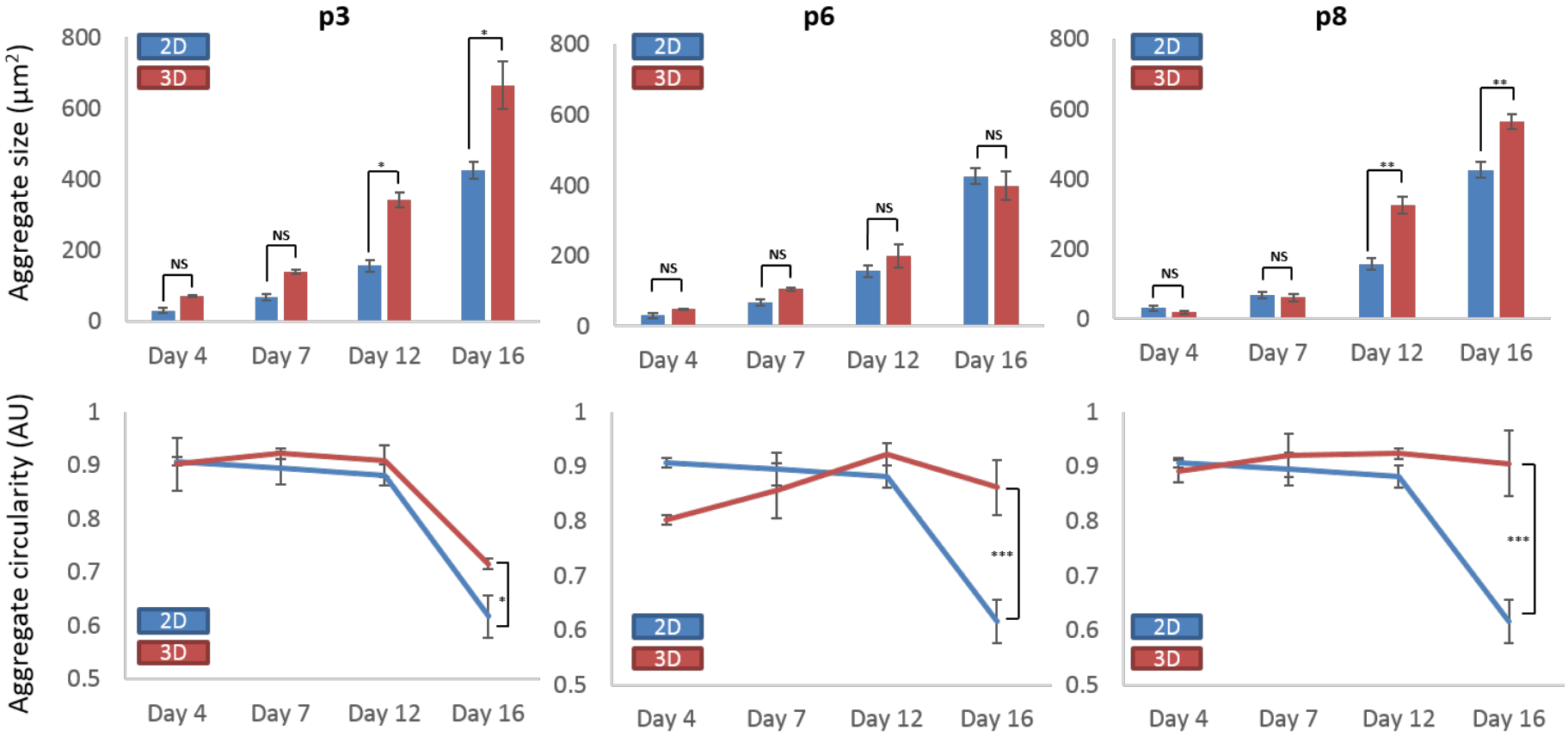

Figure 5.2 Aggregates formed from 3D maintained cells are generally larger and more circular than those formed from 2D maintained cells

By Day 12 in culture, aggregates formed by cells maintained in 3D for 3 passages are larger and more circular than those formed by cells maintained in 2D. This difference in size and circularity is amplified the longer cells are maintained in 3D. Data presented as n=10 ± SEM. Statistical analysis through ANOVA. NS denotes non-significant, * denotes $p \leq 0.05$, ** denotes $p \leq 0.01$, *** denotes $p \leq 0.001$.

Differences in size between 2D and 3D maintained cells do not appear to be significant in the first 7 days of the aggregation process, but become so after 12 days, at which point aggregates formed from 3D maintained cells appear to be bigger. The biggest change seen between the populations though is in circularity – by passage 6, cells maintained in 3D form significantly more circular aggregates by day 16. This change is amplified by passage 8.

The fact that the differences between 2D and 3D maintained cells are not seen in early stages of aggregation but are in later stages suggests that the two cell populations organise themselves differently within the aggregates. In order to test this, 2D and 3D cells from a late stage passage (passage 8) were allowed to form aggregates over two weeks, as before. At several time-points, aggregates were fixed and stained with Hoechst in order to monitor individual cells and characterise the aggregation process (Figure 5.3). As expected, there do not appear to be any clear differences in the aggregates up till day 7. However, by day 12, 3D maintained cells appear to organise into a thin but dense layer towards the exterior zones of the aggregates, and fewer cells occupy the interior zone. Though a similar pattern can be seen in the 2D maintained cells, this layer is thicker and the growth is less dense. This finding could mean one of three things: a) cells are preferentially migrating to the outside of the aggregate, b) newly added cells are not able to migrate through to the centre of the aggregate, or c) cells within the interior zone of the aggregate are dead/non-viable and thus do not stain for DAPI. Out of these options, the most likely is a combination of the latter two: that there is a hypoxic core in the centre of the aggregate, meaning that cells that reside there are not viable, but also that there is a non-permissible environment being created that is forcing cells to aggregate towards the exterior of the aggregate. Hypoxic cores are commonly found in tumours and *in vivo* tissues – they form as a result of metabolic gradients, such as nutrient diffusion. These gradients are aberrantly absent in 2D cultures due to monolayer growth, but are seen in 3D cultures. Specifically, spheroids with radii of 150-200µm will have zones of proliferating cells on the outside and quiescent cells internally, due to diffusional limitations to mass transport of nutrients and oxygen [200]. Spheroids with diameters exceeding 500µm commonly exhibit a concentrically layered structure consisting of a necrotic core, surrounded by a layer of viable quiescent cells and outer rim of proliferating cells. Since aggregates formed from 3D maintained cells grow to larger sizes, it would follow that they would be more likely to exhibit hypoxic cores. However, since they commonly do not exceed 500µm in diameter, they are unlikely to possess necrotic cores.

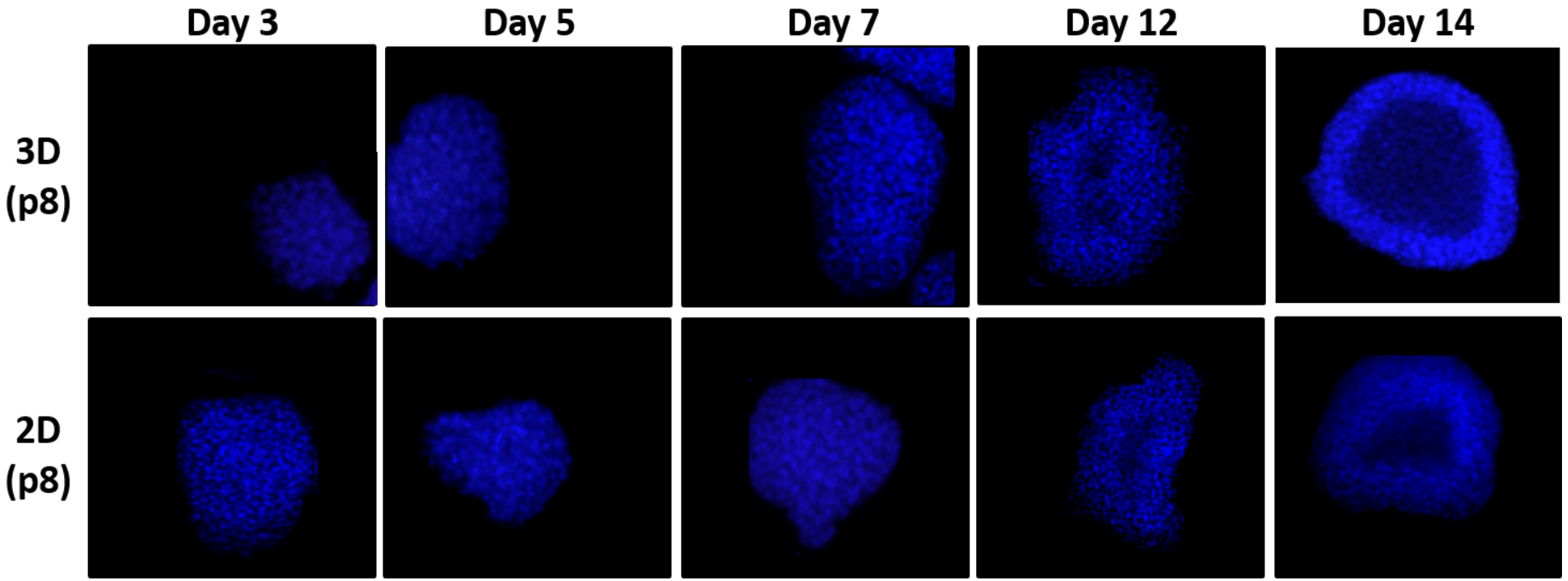

Figure 5.3 3D cells organise themselves differently to 2D cells as they aggregate

Cells maintained in either 2D or 3D were left to form aggregates for 14 days and fixed at several time-points. After fixation, cells were stained with DAPI in order to characterise the aggregation process. 3D maintained cells appear to organise themselves into a thin dense layer around the outside of the aggregate, with fewer cells occupying the interior zone. The same pattern can be seen in 2D maintained aggregates but the layer is thicker and the cell growth is less dense. Scale bars = 100µm.

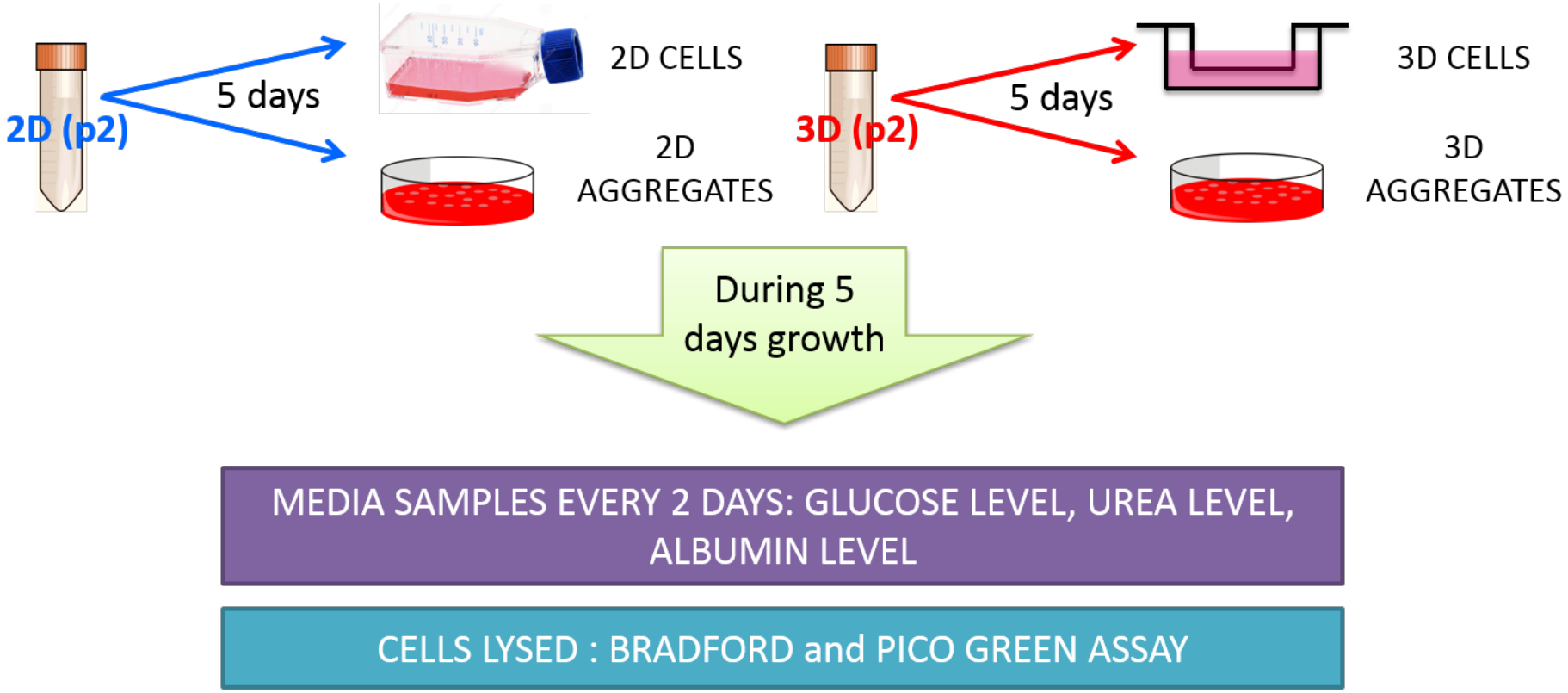

Figure 5.4 Cells were grown in 2D and 3D, and also allowed to form aggregates in order to generate four different cell populations.

Cells that had been maintained in either 2D or 3D for several passages were grown for 5 further days on either TCP, Alvetex®Strata, or in untreated Petri dishes to allow aggregation. This led to the generation of four distinct cell populations: 2D maintained cells, 3D maintained cells, aggregates formed from 2D maintained cells, and aggregates formed from 3D maintained cells. These 5 populations were established over 5 days in culture, and every 2 days media samples were taken out in order to characterise differences in cell metabolism. Cells were also lysed in order to normalise metabolism to protein content and cell number. This was conducted with cells at several different passage points.

This difference in aggregate formation, and subsequently, metabolism, indicates that 3D maintained cells show different metabolic profiles to 2D maintained cells, and presumably, these difference extend to aggregates formed from both populations. The next set of experiments (schematic in Figure 5.4) focuses on examining these differences.

5.5.2. Comparing metabolic profiles of cells and aggregates maintained in 2D and 3D

5.5.2.1 Normalising for differences in proliferation

As illustrated in Figure 5.4, cells maintained in 2D and 3D, as well as aggregates formed from these two populations, were grown for 5 days, during which media samples were analysed for glucose, urea and albumin levels in order to characterise metabolic profiles. Glucose uptake and metabolism is common across all mammalian cells, and represents a vital physiological program that provides cells with energy for proliferation, differentiation, and, importantly to this project, cytoskeletal re-organisation [205]. Urea is the major end product of protein metabolism in mammals [206] and the urea cycle occurs mostly in the liver. Thus, ureagenesis and urea levels can be taken to represent the degree of liver-specific functionality retained by hepatocytes. Finally, albumin is the most abundant extracellular protein and is produced mainly in the liver, and thus again albumin synthesis can be used to measure liver-specific functionality.

In order to accurately compare metabolic rates between the four key cell populations (2D maintained cells, 3D maintained cells, aggregates formed from 2D maintained cells, and aggregates formed from the 3D maintained cells), the levels of glucose, urea and albumin in the media have to be normalised for cell number. One method of doing this is a Bradford assay, which is used to determine protein content, which is correlated with cell number. As shown in Figure 5.5, protein levels in 2D and 3D cells, and aggregates formed from them, vary significantly over 6 days in culture. Expectedly, aggregates show higher protein levels than single cell suspensions, and 3D aggregates show the highest protein levels since they generally grow to larger sizes. 2D and 3D maintained cells show roughly the same protein levels, which correlates well with previous data in Chapter 4 showing that cellular volumes do not vary between 2D and 3D cells.

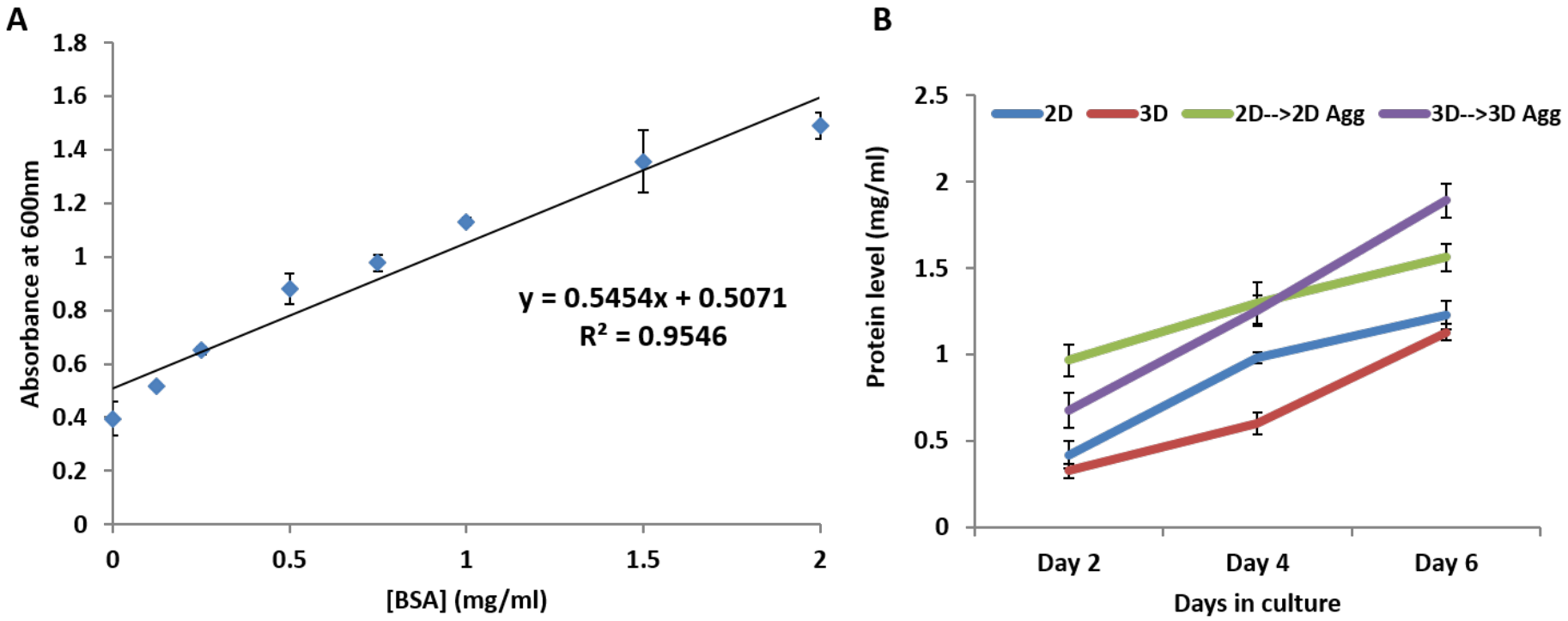

Figure 5.5 Protein levels in 2D and 3D cells and aggregates differ significantly over a 6 day growth period

Cells were grown in 2D and 3D, and also allowed to form aggregates in order to generate four different cell populations. These populations were then tested for protein levels, which were detected using a Bradford assay standard curve (A). As expected, aggregates show higher protein levels than standard cell suspensions (B). Aggregates formed from 3D maintained cells show significantly higher protein levels than those formed from 2D maintained cells. Data presented as n=3 ± SEM.

A more direct way of normalising for cell number is using a Pico Green Assay which, by quantifying double stranded DNA, provides a more accurate measure of actual cell number. As shown in Figure 5.6, the correlation between cell number and fluorescence is incredibly strong. Thus, for future experiments, it was decided that the Pico Green assay would be a better way to normalise media levels for cell number. Therefore, in addition to media samples taken at day 1,3 and 5, cells were also lysed at each of these time points and cell number determined.

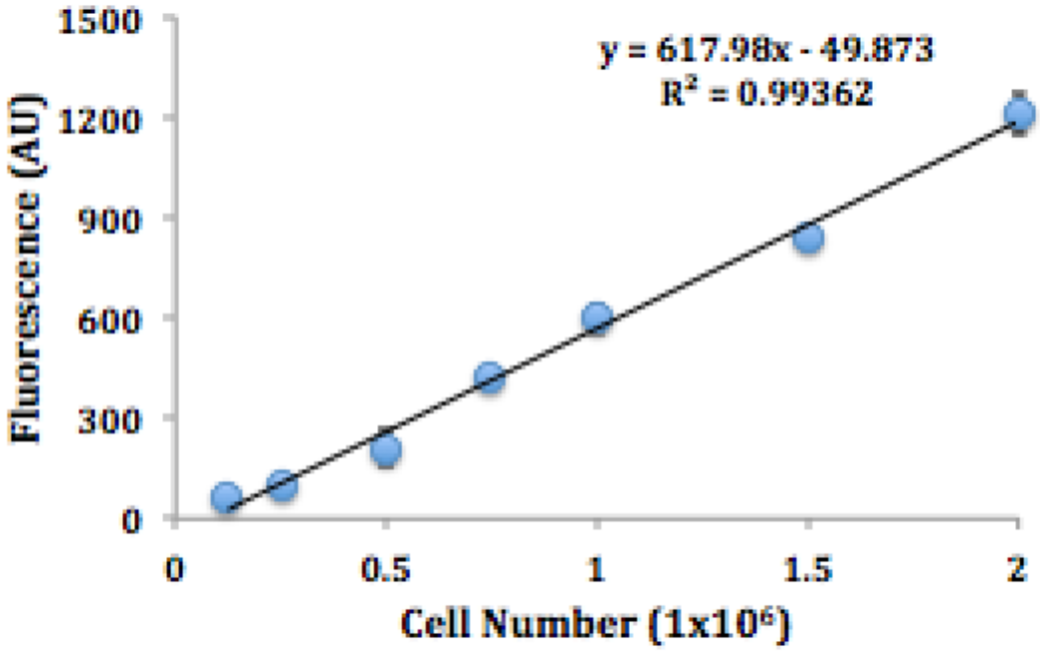

Figure 5.6 The Pico Green assay can be used to determine cell numbers.

The Quant-IT Pico Green dsDNA assay is a commercially available kit that allows for the accurate quantification of cell numbers within a given sample. A standard curve was created from samples of known cell number and this was then used to normalize media sample data according to cell number. Data presented as n=3, +/- SEM.

5.5.2.2 Assessing glucose consumption between 2D cells, 3D cells, and aggregates

Cells maintained in 2D and 3D, as well as aggregates formed from these cells, were assessed for glucose consumption as early (p2), mid (p4) and late (p6) passage points. Glucose consumption was measured using the GlucCELL system, which consists of an electronic glucose meter, and test strips upon which media samples are loaded.

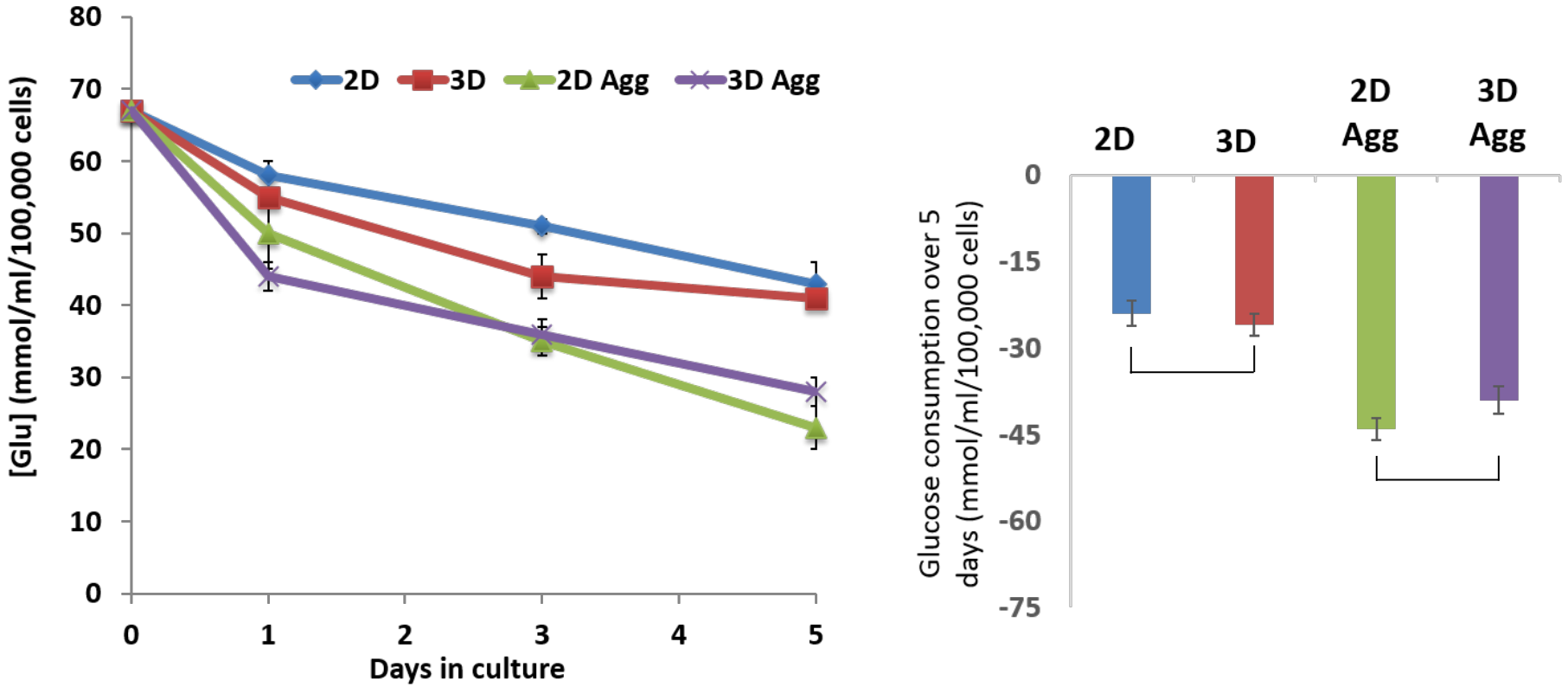

Figure 5.7 Glucose consumption between 2D and 3D derived cell systems is minimal when using cells maintained in 3D for 2 passages

2D and 3D cells were maintained for 2 passages and then allowed to form aggregates for 5 days. Glucose consumption by cells from all 4 populations was quantified by testing media samples for glucose concentration at various time-points and normalising this for cell number. At this early passage point, there are no significant differences between the populations. Data presented as n=3 ± SEM. Statistical analysis through ANOVA. NS denotes non-significant.

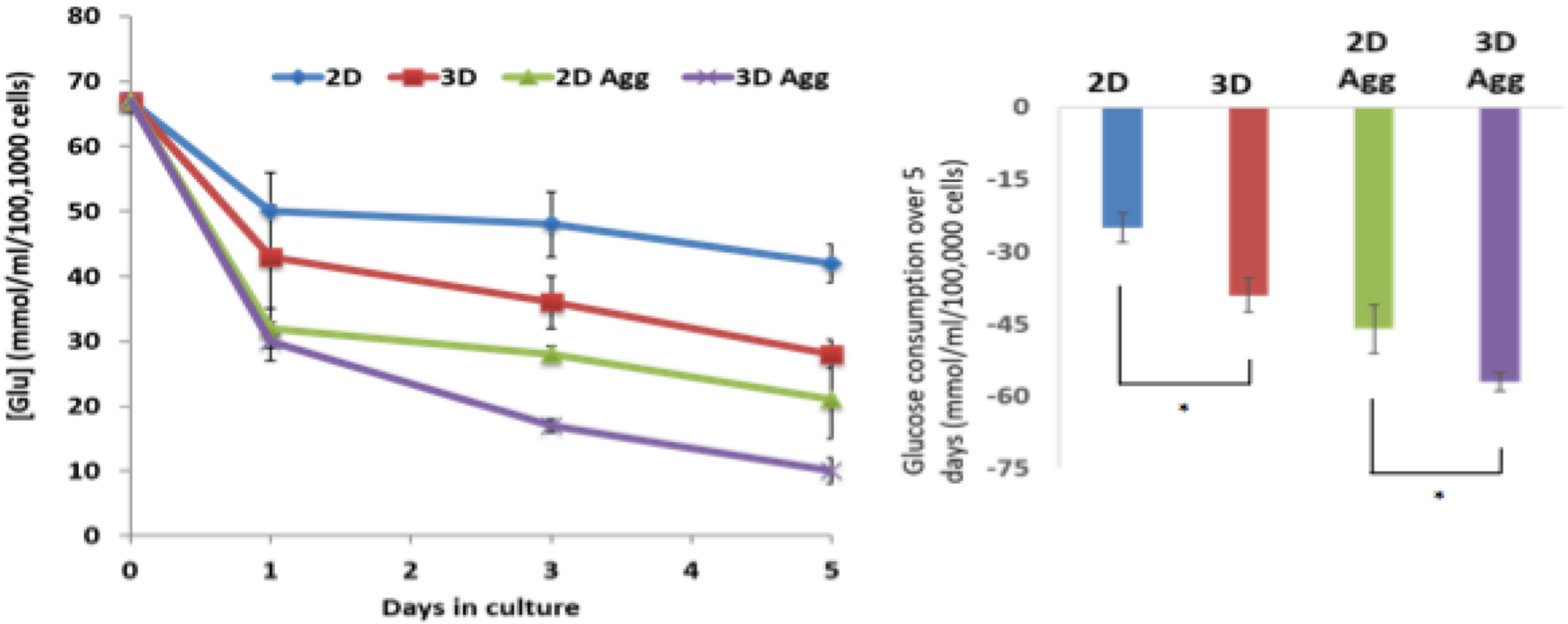

Figure 5.8 Differences in glucose consumption between 2D and 3D cells and aggregates become larger when using cells maintained in 3D for 4 passages

2D and 3D cells were maintained for 4 passages and then allowed to form aggregates for 5 days. Glucose consumption by cells from all 4 populations was quantified by testing media samples for glucose concentration at various time-points and normalising this for cell number. Significant differences between the populations begin to appear when using cells from passage 4. Both 3D cells and 3D aggregates consume significantly more glucose over the 5 day growth period than their 2D counterparts. Data presented as n=3 ± SEM. Statistical analysis through ANOVA. * denotes $p \leq 0.05$

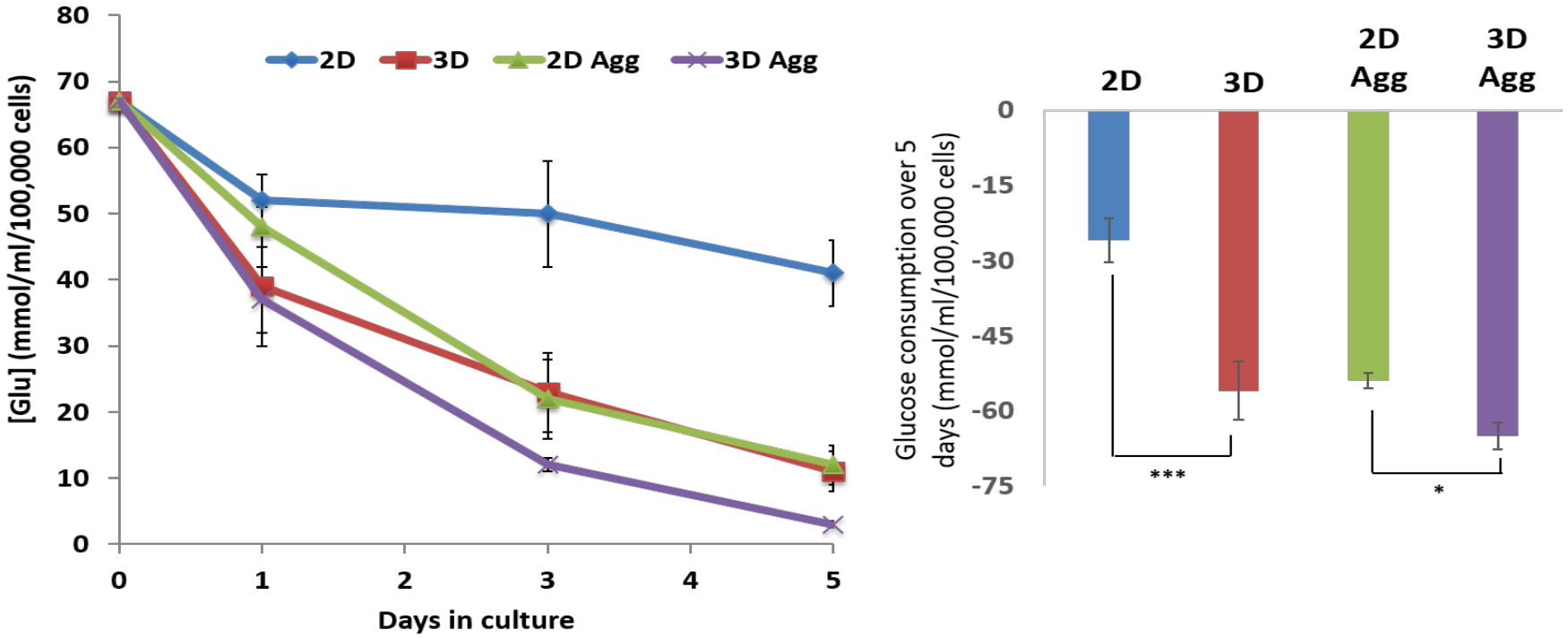

Figure 5.9 Significant differences in glucose consumption between 2D and 3D cells and aggregates are maintained when using cells maintained in 3D for 6 passages

2D and 3D cells were maintained for 6 passages and then allowed to form aggregates for 5 days. Glucose consumption by cells from all 4 populations was quantified by testing media samples for glucose concentration at various time-points and normalising this for cell number. Significant differences between the populations that begun to appear when using cells from passage 4 are maintained when using cells from passage 6. In particular, the difference between 2D and 3D cells is amplified, and 3D cell suspensions begin to consume large quantities of glucose from the media. Data presented as n=3 ± SEM. Statistical analysis through ANOVA. * denotes $p \leq 0.05$, *** denotes $p \leq 0.001$.

At early passage points, the four populations do not show any significant differences in glucose consumption, except that aggregates trend towards a slightly higher consumption of glucose (Figure 5.7). This could be because of energy required for aggregation, or because the aggregates show a more metabolically active behaviour. Differences between 2D and 3D maintained cells begin to become apparent at mid passages. Propagation in 3D has resulted in cells taking up a significantly higher amount of glucose from the media (Figure 5.8). This correlates well with other data that suggests that mid passage points represent a switching point for cells, where transient changes in cytoskeletal organisation become hard-wired into the cell machinery. This requires changes in gene expression and signalling, both of which require large amounts of energy, and thus glucose metabolism. This change is also seen with aggregates formed from 2D and 3D cells, suggesting a maintained higher degree of metabolism in a secondary 3D system. This could either be an amplification of the differences seen on a single cell level, or indicative of the cells co-ordinating in a tissue-like manner, which would require excess energy. These differences are maintained at later passages, as seen in Figure 5.9.

Albumin synthesis was measured using a commercially available ELISA plate and a standard spectrophotometer. Before this kit could be used to accurately measure albumin levels in the media, a standard curve using standards of known albumin concentration had to be drawn (Figure 5.10). As shown in this graph, the absorbance readings obtained correlate strongly to the concentration of albumin in the sample, making this a reliable methodology for characterising albumin synthesis in the four tested populations.

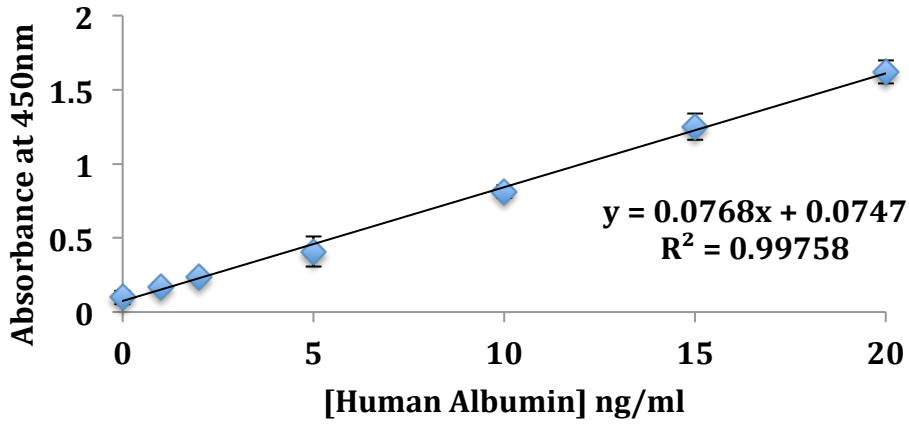

Figure 5.10 Albumin secretion can be determined by using an ELISA assay
Albumin levels in the culture media can be quantified using a commercially available ELISA plate. A standard curve was created from samples of known albumin concentration and this was then used to quantify albumin secretion in unknown samples. Data presented as n=3 ± SEM.

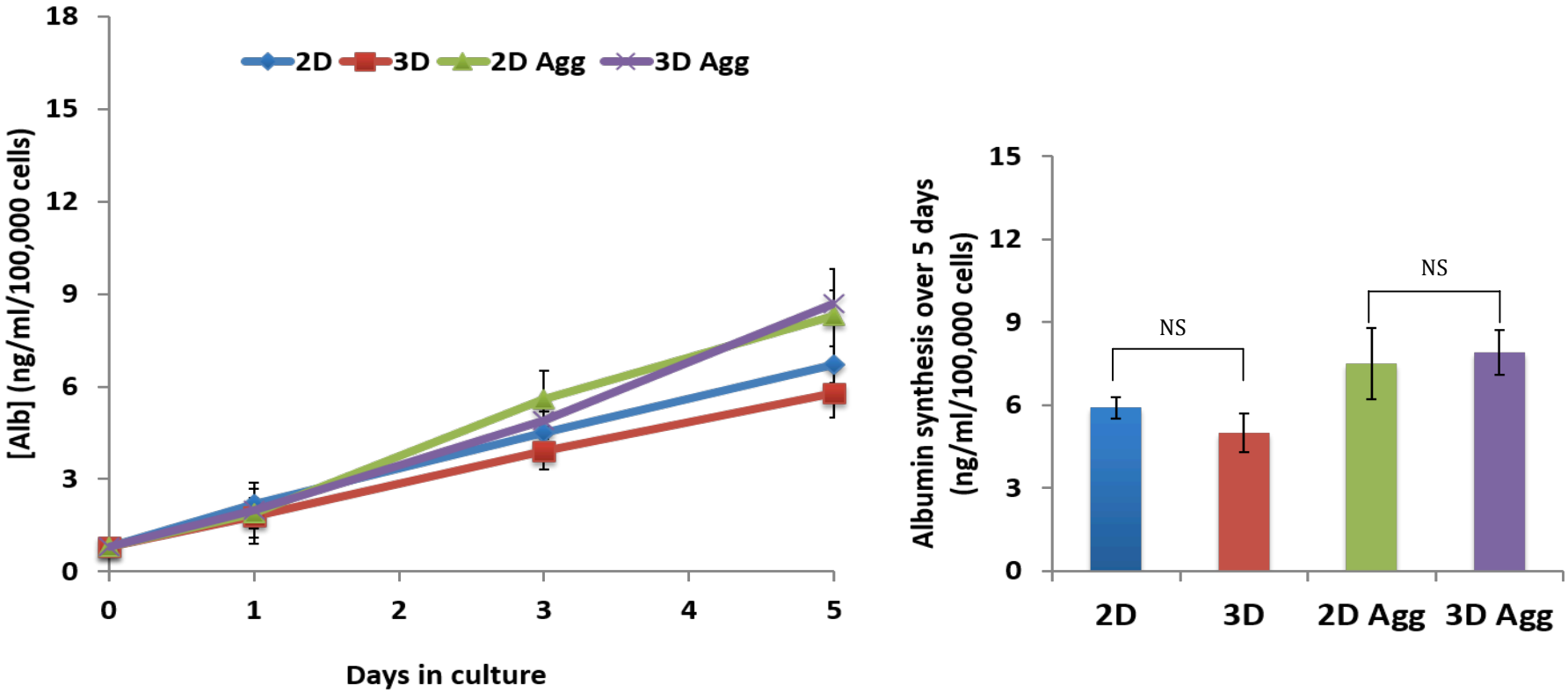

Figure 5.11 Albumin secretion between 2D and 3D derived cell systems is minimal when using cells maintained in 3D for 2 passages

2D and 3D cells were maintained for 2 passages and then allowed to form aggregates for 5 days. Albumin secretion by cells from all 4 populations was quantified by testing media samples for albumin concentration at various time-points and normalising this for cell number. At this early passage point, there are no significant differences between the populations. Data presented as n=3 ± SEM. Statistical analysis through ANOVA. NS denotes non-significant.

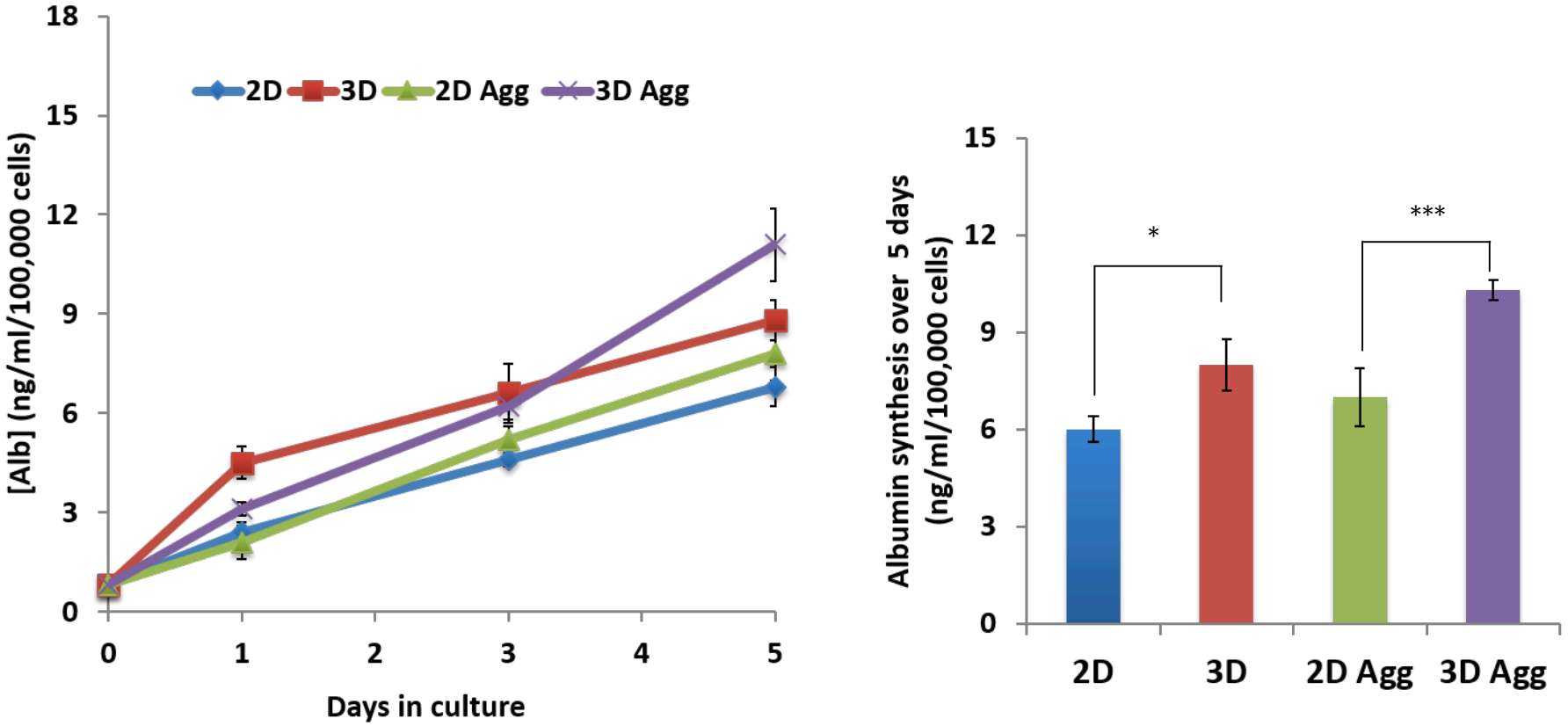

Figure 5.12 Differences in albumin synthesis between 2D and 3D cells and aggregates become larger when using cells maintained in 3D for 4 passages

2D and 3D cells were maintained for 4 passages and then allowed to form aggregates for 5 days. Albumin synthesis by cells from all 4 populations was quantified by testing media samples for albumin concentration at various time-points and normalising this for cell number. Significant differences between the populations begin to appear when using cells from passage 4. Both 3D cells and 3D aggregates produce more albumin over the 5 day growth period than their 2D counterparts. Data presented as n=3 ± SEM. Statistical analysis through ANOVA. * denotes $p \leq 0.05$, *** denotes $p \leq 0.001$.

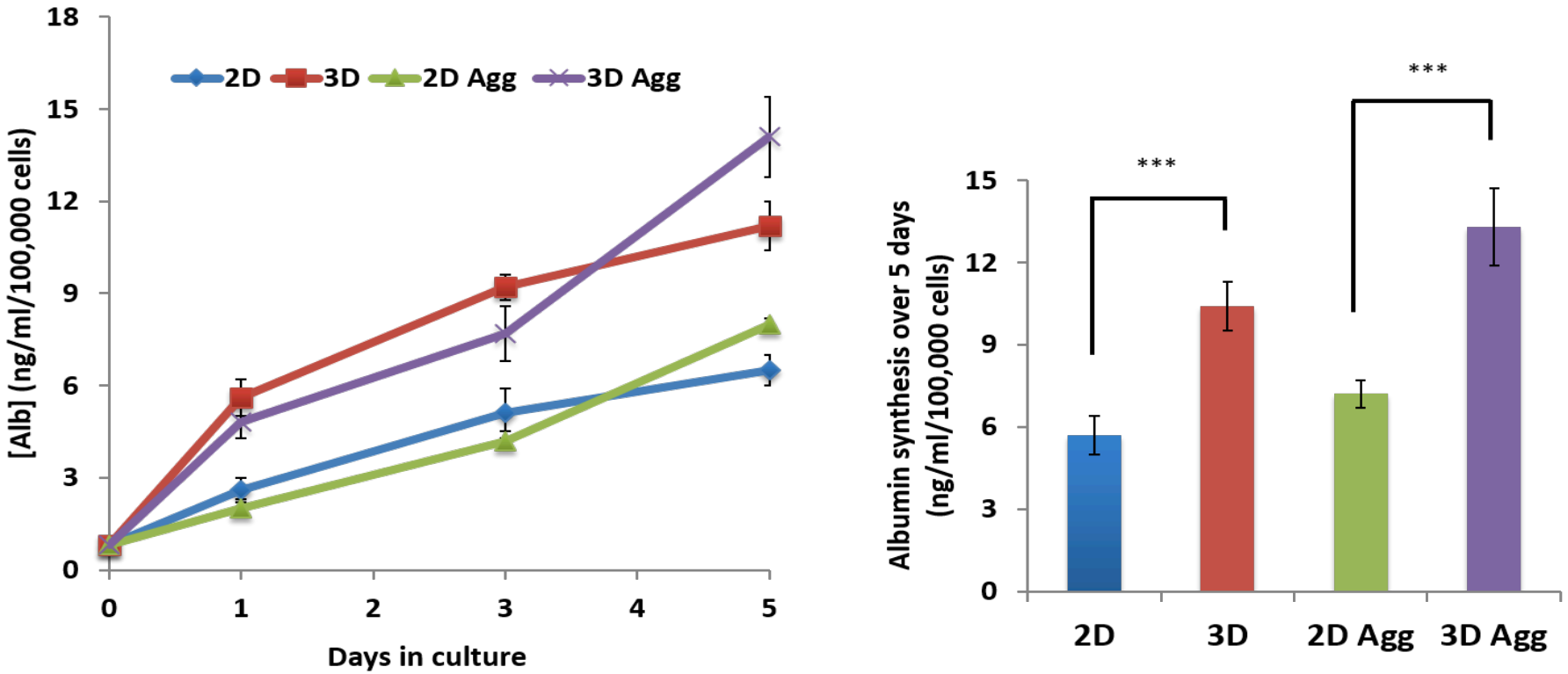

Figure 5.13 Significant differences in albumin synthesis between 2D and 3D cells and aggregates are maintained when using cells maintained in 3D for 6 passages

2D and 3D cells were maintained for 6 passages and then allowed to form aggregates for 5 days. Albumin synthesis by cells from all 4 populations was quantified by testing media samples for albumin concentration at various time-points and normalising this for cell number. Significant differences between the populations that begun to appear when using cells from passage 4 are amplified when using cells from passage 6. Data presented as n=3 ± SEM. Statistical analysis through ANOVA. *** denotes $p \leq 0.001$.

The dataset for albumin synthesis paints a very similar picture of metabolism to that for glucose consumption. At passage 2, cells from all four populations appear to produce almost equivalent levels of albumin when the data is normalised to cell number (Figure 5.11). However, unlike with glucose metabolism, the secretion rates for albumin appear to be consistent over the 5 day period. Comparing Figure 5.11A to Figure 5.7A, where glucose consumption seems to be at a faster rate for the first day and then slower for the next 4 days, albumin synthesis stays at a steady rate throughout the 5 day study period at this early passage point. This changes by passage 4 for the 3D maintained populations (red and purple lines on Figure 5.12A respectively), which appear to be more metabolically active for the first day. This could be due to active adaptation to the environment, an adaptation process that 2D cells do not have to go through. By day 5, there are significant differences between the 2D and 3D maintained populations, both in cell suspensions and aggregates, with the 3D maintained cells secreting more albumin into the media, and thus showing more metabolic activity. Looking at cells maintained in 2D and 3D for 6 passages (Figure 5.13), these patterns appear to be amplified. Again, 2D and 3D maintained populations show different rates of albumin synthesis over the 5 day culture period. However, an interesting observation is that aggregates from both populations appear to enter an exponential period of albumin synthesis between days 3 and 5, indicating perhaps that as the aggregates are getting larger and denser, they are becoming more metabolically active. This may mean that longer culture periods for aggregates could lead to enhanced metabolism and possibly functional activity.

Urea was measured using a commercially available colorimetric assay kit. As with albumin secretion, in order for urea levels to be determined, a standard curve was drawn using standards of known urea concentration. Again, this method proved to be a highly accurate method of determining urea levels in the media, with an R^2 value of above 0.99 (Figure 5.14).

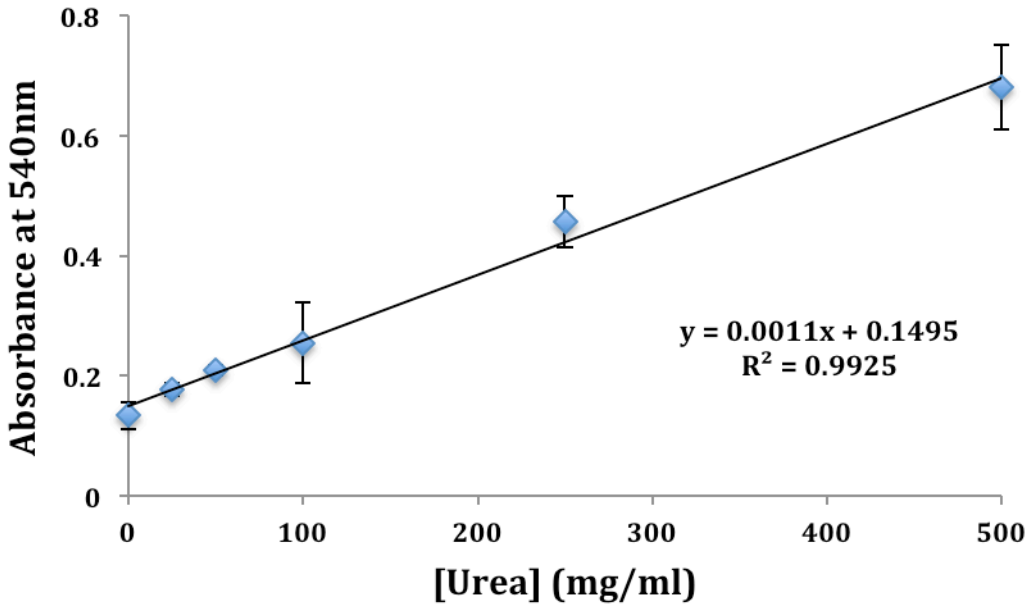

Figure 5.14 Urea secretion can be determined by using a colorimetric assay

Urea levels in the culture media can be quantified using a commercially available colorimetric kit. A standard curve was created from samples of known urea concentration and this was then used to quantify urea secretion in unknown samples. Data presented as n=3 ± SEM.

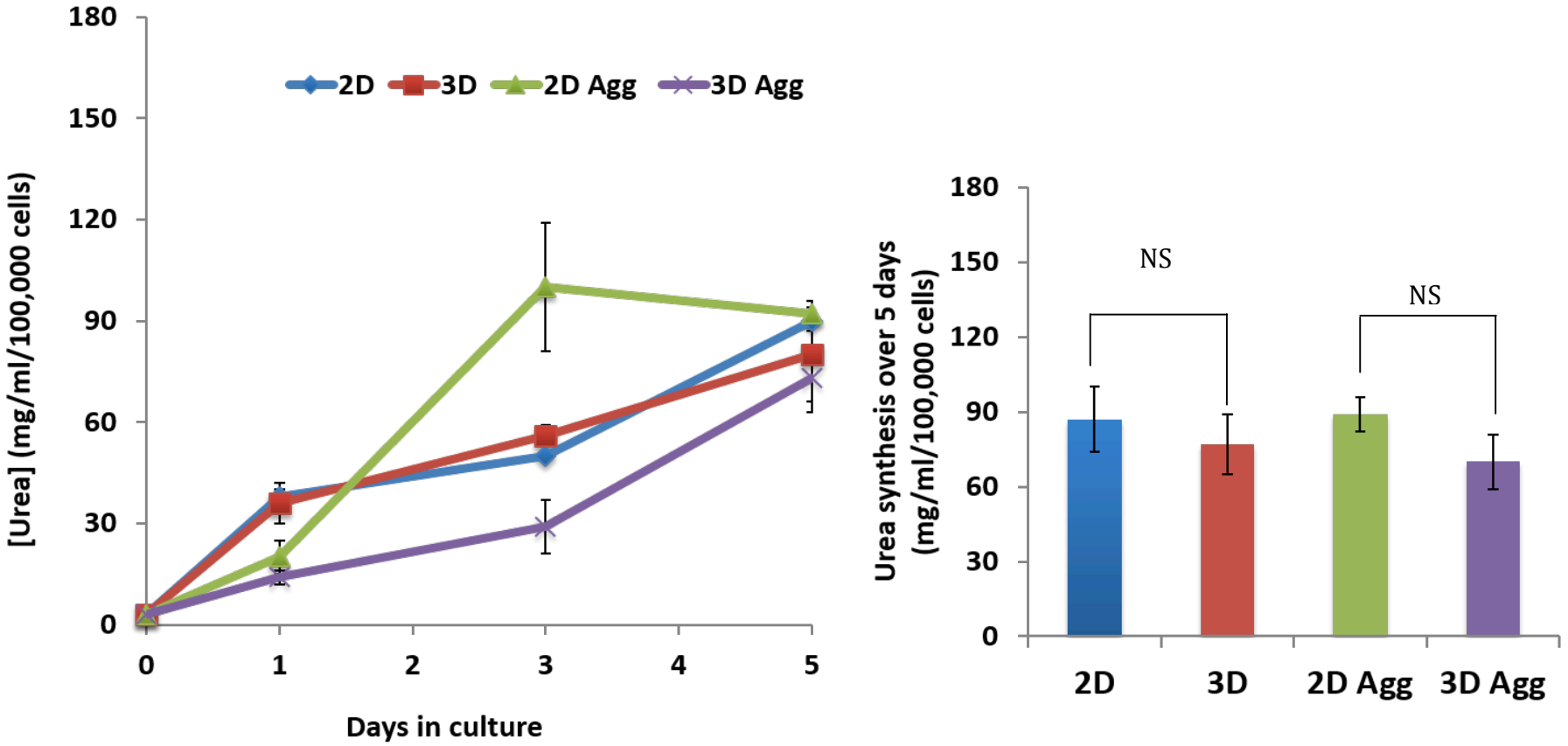

Figure 5.15 Urea secretion between 2D and 3D derived cell systems is minimal when using cells maintained in 3D for 2 passages

2D and 3D cells were maintained for 2 passages and then allowed to form aggregates for 5 days. Urea secretion by cells from all 4 populations was quantified by testing media samples for urea concentration at various time-points and normalising this for cell number. At this early passage point, there are no significant differences between the populations. Data presented as n=3 ± SEM. Statistical analysis through ANOVA. NS denotes non-significant.

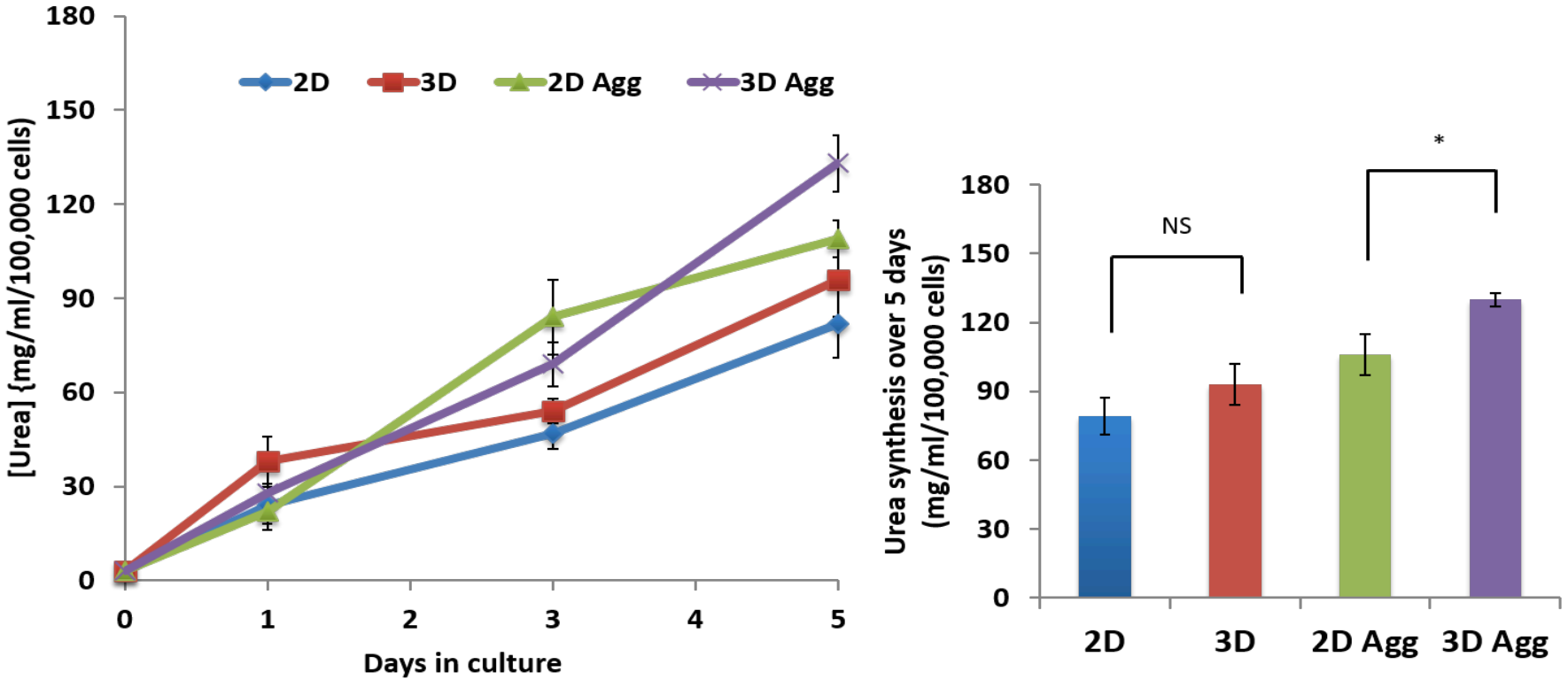

Figure 5.16 Urea synthesis does not differ between 2D and 3D cells at passage 4, but is larger in aggregates formed from cells maintained in 3D for 4 passages

2D and 3D cells were maintained for 4 passages and then allowed to form aggregates for 5 days. Urea synthesis by cells from all 4 populations was quantified by testing media samples for urea concentration at various time-points and normalising this for cell number. Urea synthesis remains similar in 2D and 3D maintained cells, but interestingly is significantly heightened in aggregates formed from 3D maintained cells. Data presented as n=3 ± SEM. Statistical analysis through ANOVA. NS denotes non-significant. * denotes $p \leq 0.05$

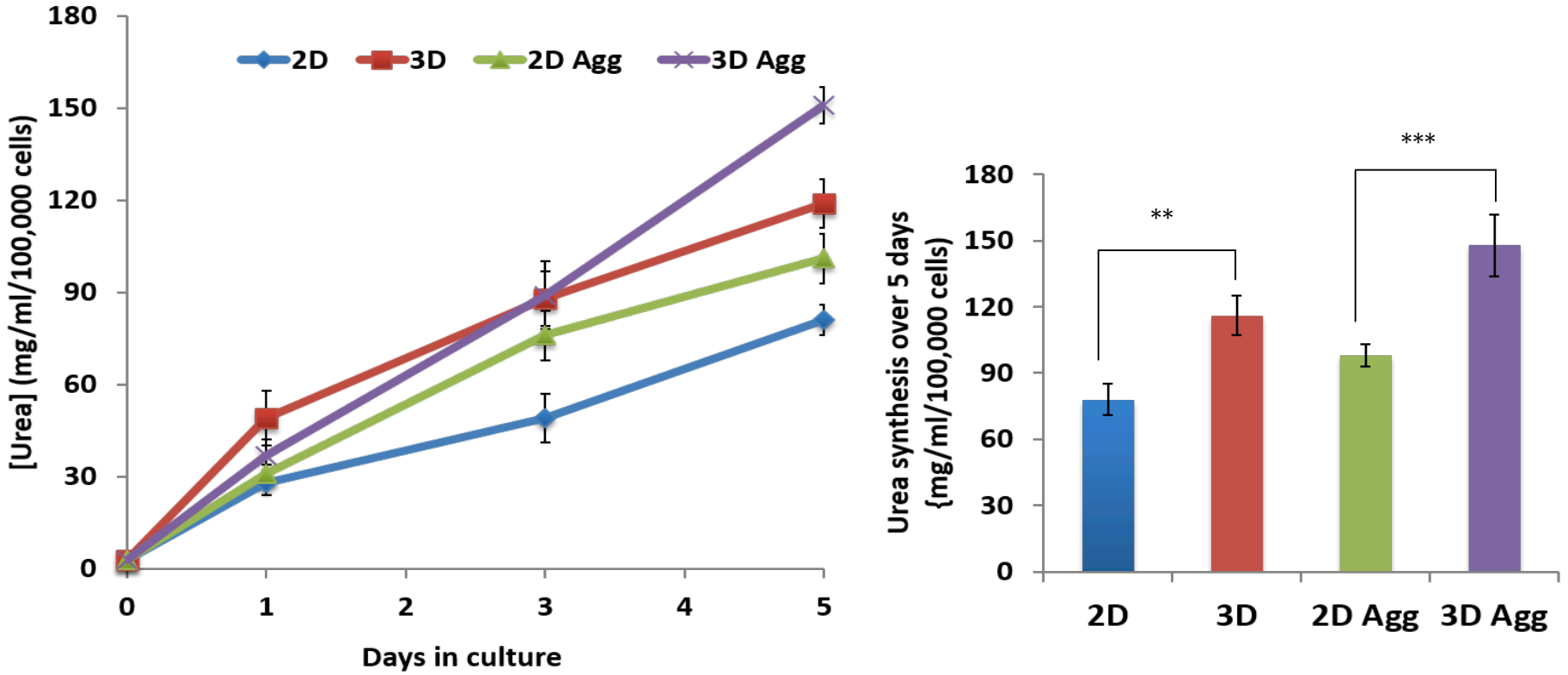

Figure 5.17 Significant differences in urea synthesis between 2D and 3D maintained cells and aggregates appear at passage 6

2D and 3D cells were maintained for 6 passages and then allowed to form aggregates for 5 days. Urea synthesis by cells from all 4 populations was quantified by testing media samples for urea concentration at various time-points and normalising this for cell number. Significant differences between the populations appear when using cells from passage 6. Data presented as n=3 ± SEM. Statistical analysis through ANOVA. ** denotes p≤0.01 *** denotes p ≤0.001.

As Figure 5.15 shows, the four populations of cells actually show quite different patterns of urea synthesis over the 5 day culture period, but the overall levels detected at day 5 remain similar across the board. Generally, urea synthesis appears to be the most similar across the four populations, when compared to glucose consumption and albumin synthesis. Interestingly, there does not appear to be an increased rate of urea synthesis in the aggregates compared to the cell suspensions. This could be because the urea cycle does not play a role in the aggregation process, or that energy is preferentially derived from other metabolic pathways. At passage 4, there is a slight increase in urea synthesis in the aggregate models compared to the suspension models (Figure 5.16), suggesting that enhancement in urea synthesis is due to 3D propagation rather than a by-product simply of 3D culture. This time delay in indicative of changes further downstream of intracellular signalling, and perhaps suggests that increased urea synthesis is a result of increased/altered gene expression rather than a transient metabolic shift. This pattern is further amplified when looking at cells passaged for 6 passages (Figure 5.17). 3D populations show even higher urea synthesis levels than at passages 2 and 4, and 2D populations remain unaltered.

Taken together, the data from the metabolism studies show that 3D maintained cells are consistently more metabolically active than 2D maintained cells, and that this metabolic activity is enhanced when 3D maintained cells are placed into a secondary 3D model. Glucose consumption was three-fold higher in 3D maintained aggregates than in 2D cells, albumin synthesis was 2.6 fold higher in 3D maintained aggregates, and 1.7 fold higher in 3D maintained aggregates. These findings show that 3D maintenance has a positive impact on liver-specific metabolism of cultured cells.

5.5.3. Comparing toxicity profiles of cells and aggregates maintained in 2D and 3D

Given that previous data has shown that 3D maintained HepG2 cells show more hepatocytic morphology and metabolism, the next set of experiments will focus on seeing whether 3D propagation has an effect on drug toxicity. Hepatocytes are the primary anatomical substrate for xenobiotic metabolism and a major function of the liver is to metabolise drugs and toxic agents. One of the best characterised drug metabolic pathways is that of acetaminophen (APAP), shown in the schematic in Figure 5.18. APAP is a common analgesic medication that is metabolised primarily in the liver through three metabolic pathways: glucuronidation (45-55%), sulfation (20-30%) and N-hydroxylation and GSH conjugation (<15%) [207].

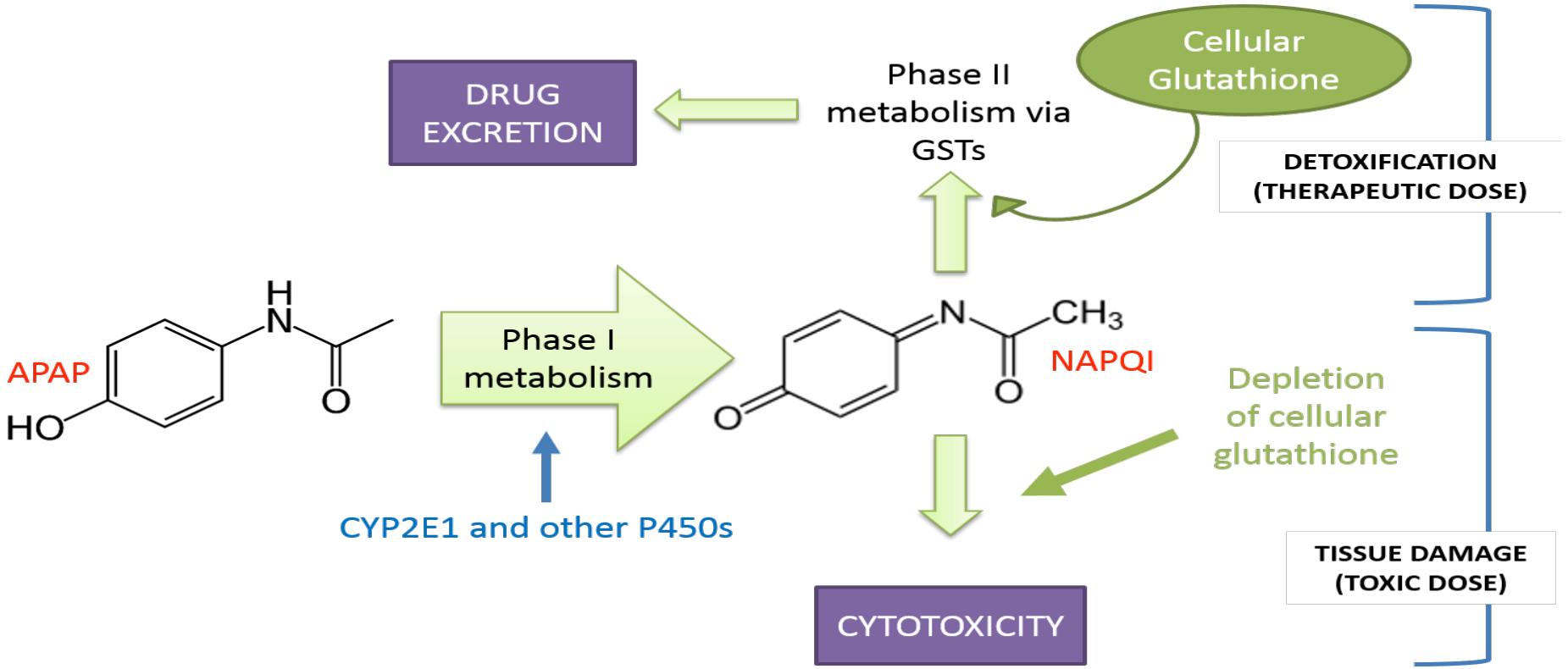

Figure 5.18 Acetaminophen is metabolised by the liver via two main pathways.

The schematic shows how acetaminophen (APAP) can be metabolised by the liver. With sub-lethal doses, APAP is metabolised by phase I enzymes of the CYP450 superfamily into N-acetyl-p-benzoquinone imine (NAPQI); the primary CYP enzyme responsible for APAP detoxification is CYP2E1. NAPQI is then acted on by phase II enzymes such as Glutathione S-transferase (GST). This requires cellular glutathione and leads to excretion of the drug. However, when cellular glutathione stores are depleted, NAPQI is not converted into safe metabolites, and as liver cells undergo necrosis, and tissue damage can occur.

The primary metabolic pathway for APAP is glucuronidation, which yields a non-toxic metabolite, which can be excreted into bile and passed without injury. This occurs with approximately 90% of a therapeutic dose, with the other 10% being metabolised by CYP3A4 and CYP2E1 into NAPQI, which is a strong oxidising agent and thus extremely damaging to liver tissue. Therefore, NAPQI is inactivated by conjugation with glutathione, and this conjugate can be further metabolised by Glutathione-S-Transferase and safely excreted. However, at lethal doses, the glucuronidation pathway becomes saturated and therefore much larger amounts of NAPQI are produced. This leads to depletion of liver stores of glutathione, meaning that NAPQI cannot be inactivated, and cell and tissue damage occur.

In order to see how this metabolic pathway is affected by 3D propagation, cells maintained in 2D and 3D were treated with increasing doses of APAP for 24hrs and then assayed for viability using the MTT assay (Figure 5.19). At the first passage, there is a clear difference in the cell death curve between 2D and 3D maintained cells, with the curve shifting slightly to the right for 3D cells. This means that these cells are more resilient to cell death, and more 3D maintained cells survive at higher doses than 2D maintained cells do at these same doses. This correlates well with metabolic data, which shows that 3D cells are more metabolically active. If the cells are more metabolically active, it means that the toxic agent, APAP, is being metabolised into non-toxic metabolites at a faster/higher rate. Data in 5.3.2 showed that the increase in metabolism seen in 3D maintained cells is a factor of how long the cells are propagated in 3D, and as expected, the shifting of the death curve to the right increases in line with passage number. The two curves become completely distinguishable at passage 3, with significantly less cell death in the 3D population at every dose tested, even the lower doses. The gap between the two curves continues to increase throughout the mid passages, up till passage 7, after which the death curves appear to stay consistent. This would indicate that any adaptation to the 3D environment is complete, and that past passage 6, the cells have become as '3D-like' as possible given the experimental parameters.

Another way of analysing the cytotoxicity profiles shown in Figure 5.19 is to calculate the LD50 values for each cell population at each passage point. The LD50 value is the dose at which 50% of the cell population is dead. This value can be calculated from the cytotoxicity curves by simply reading off the values at 50% normalised cell death, as demonstrated in the schematic

in Figure 5.20A. This was done for both 2D and 3D maintained cells across 10 passages and graphed out in Figure 5.20B.

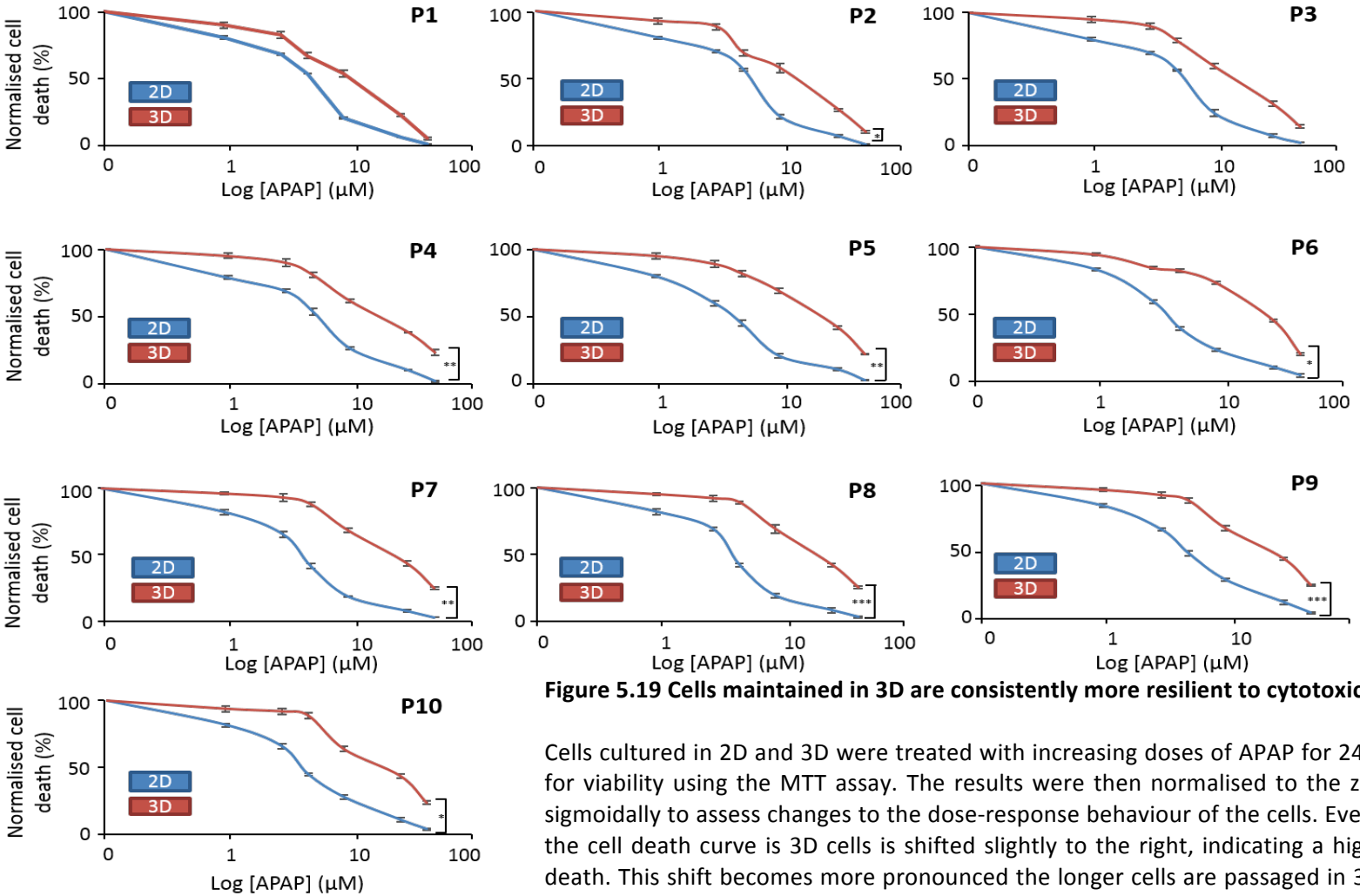

Figure 5.19 Cells maintained in 3D are consistently more resilient to cytotoxic attack by APAP

Cells cultured in 2D and 3D were treated with increasing doses of APAP for 24hrs and then assayed for viability using the MTT assay. The results were then normalised to the zero dose and plotted sigmoidally to assess changes to the dose-response behaviour of the cells. Even at the first passage, the cell death curve is 3D cells is shifted slightly to the right, indicating a higher resistance to cell death. This shift becomes more pronounced the longer cells are passaged in 3D. Data presented as n=3 ± SEM. Statistical analysis through ANOVA. NS denotes non-significant, * denotes $p \leq 0.05$, ** denotes $p \leq 0.01$, *** denotes $p \leq 0.001$.

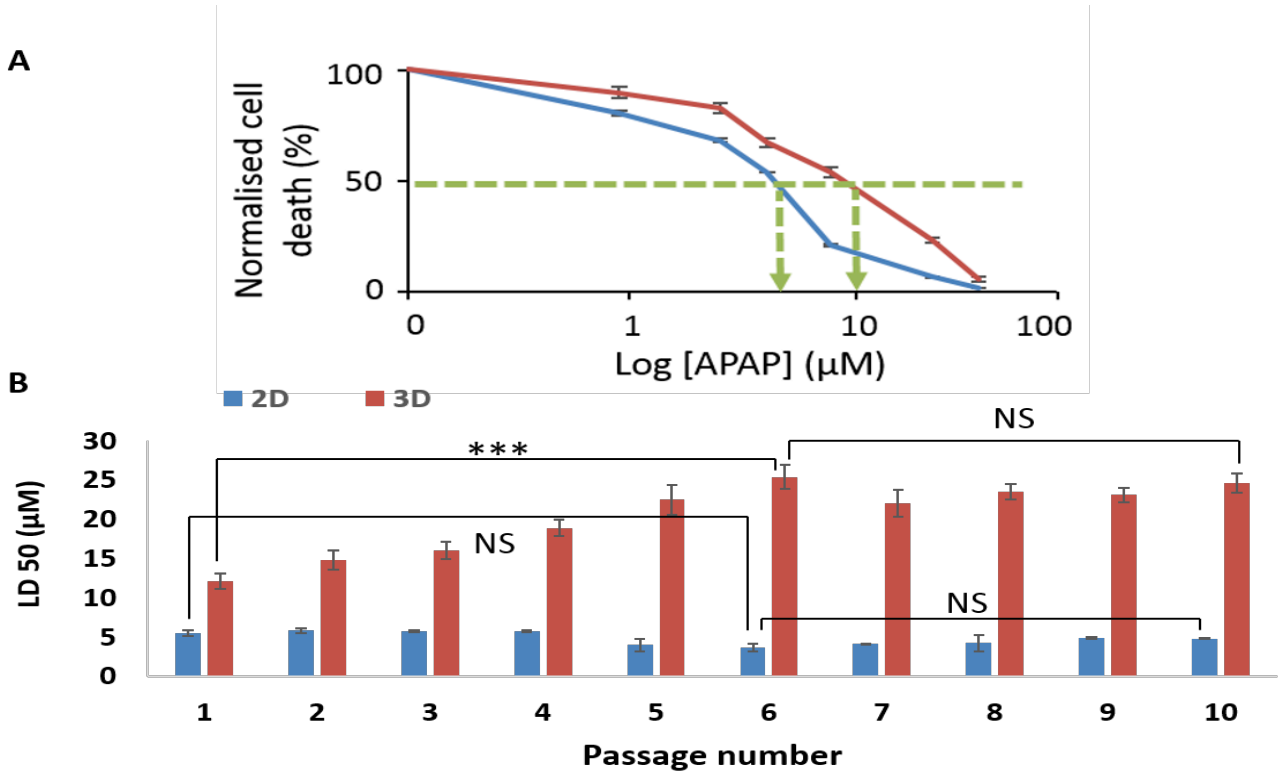

Figure 5.20 Cells maintained in 3D have a significantly higher LD50 for APAP than cells maintained in 2D.

The LD50 value for a given drug represents the dose that kills 50% of the sample – for *in vitro* studies, this is taken to mean the dose that kills 50% of cells. This value can be predicted by reading off cell death curves (A). This value was approximated from the curves in Fig 5.19 and graphed (B). Cells in 3D show a higher LD50 value from the first passage and this difference increases consistently till reaching a saturation point at passage 6. The LD50 values for the 2D samples do not show any significant variation over the same culture period. Data presented as n=3 ± SEM. Statistical analysis through ANOVA. NS denotes non-significant, *** denotes p ≤0.001.

As expected, cells maintained in 3D show a significantly higher LD50 value across all ten passage points, indicating a higher resistance to drug toxicity. For the first 6 passages, this value increases exponentially for 3D maintained cells but there is no significant change for 2D maintained cells. This passage-dependent amplification points to an adaptation of the cells to a 3D microenvironment over time, and the timing correlates well with changes seen in morphology, cytoskeletal flexibility, and metabolism. After passage 6, there are no significant increases in the LD50 values for either population.

In order to confirm that the increased resistance to drug toxicity seen for 3D maintained HepG2 cells was not specific to APAP, another model drug was tested using the same experimental set-up. Gemfibrozil is a peroxisome proliferator-activated receptor alpha (PPARα) agonist that is medically used to lower plasma levels of triglycerides, very-low density lipoproteins (VLDL) and low-density lipoproteins (LDL), and increase high density lipoproteins (HDL). Like with APAP, Gemfibrozil has a very well characterised metabolic pathway shown in Figure 5.21A. The molecules undergoes glucuronidation, followed by further metabolism via the cytochrome P450 system into a hydroxyl compound that can be safely excreted [16]. However, high doses of gemfibrozil saturate the metabolic pathway and the un-metabolised drug can cause cell lysis and death.

To see how this metabolic pathway is affected by 3D propagation, cells maintained in 2D and 3D at early (p1), mid (p4) and late (p7) passage were treated with increasing doses of Gemfibrozil for 24hrs and then assayed for viability using the MTT assay (Figure 5.21B). At passage 1, the cytotoxicity curves at low doses for 2D and 3D cells are very similar. However, at doses above 1µM, the lines begin to diverge, and 2D cells show significantly more cell death than 3D cells. At this passage, there is only a slight difference in LD50 values, with 2D cells showing an average LD50 of 3.68µM, compared to 4.35µM in 2D cells. At passage 4, the lines begin to separate even at low doses, and the LD50 values show this, with 2D cells having an average LD50 of 3.49µM, and 3D cells showing an LD50 of 4.76µM. This enhanced resilience to cytotoxicity is seen also at passage 7, where the cytotoxicity curve for 3D cells is significantly shifted to right. The LD50 values reflect this, with 2D cells showing an average LD50 of 3.42µM, and 3D cells showing an average LD50 of 5.88µM, which is almost twice as high.
This data supports the cytotoxicity data for APAP and indicates that 3D propagation results in enhanced liver-specific functionality in HepG2 cells.

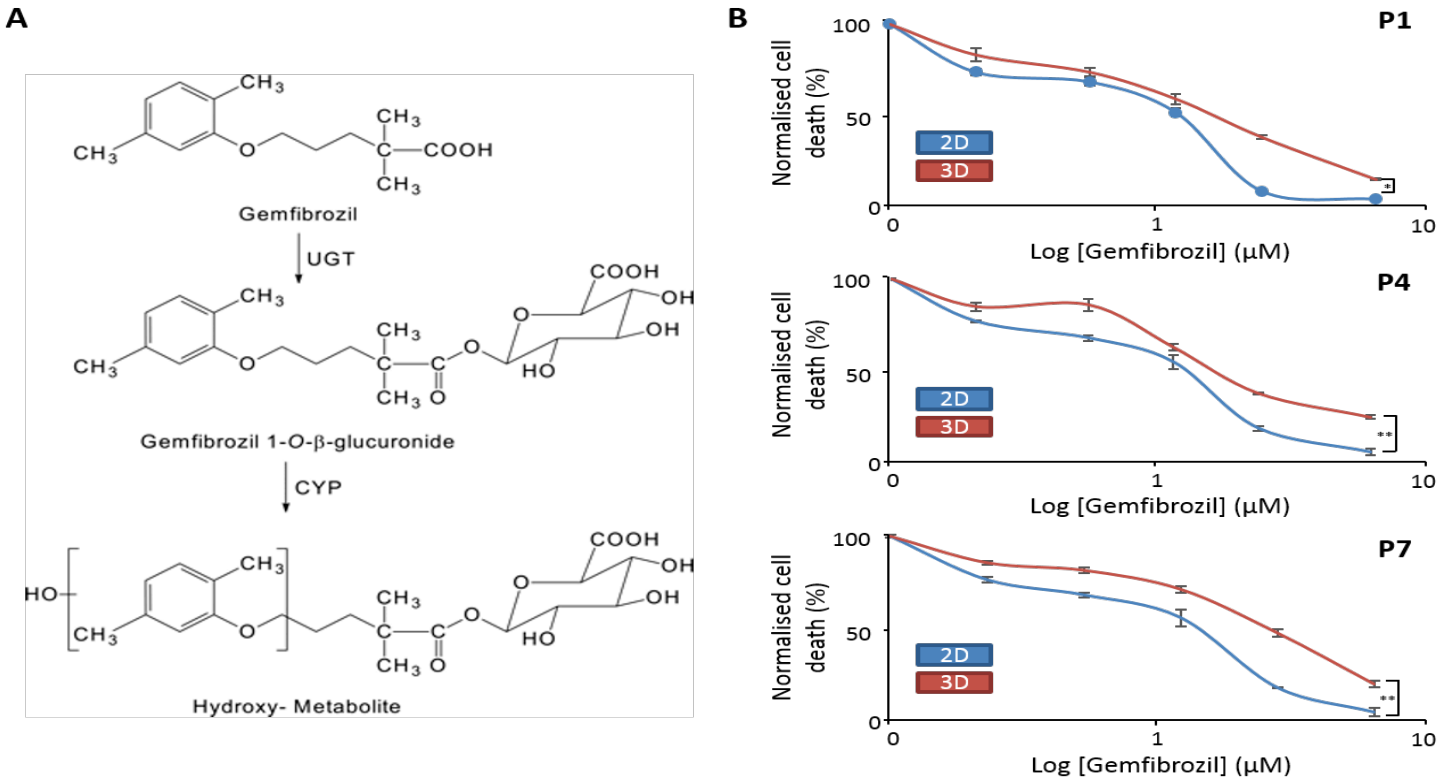

Figure 5.21 Cells maintained in 2D and 3D show different cell death curves when treated with Gemfibrozil.

Gemfibrozil is metabolised in the liver by the CYP450 superfamily of enzymes in a characteristic manner (depicted in A, taken from Ogilvie *et al.*, 2006), and in addition to APAP is often used as a model xenobiotic for investigating liver function. Cells cultured in 2D and 3D were treated with increasing doses of APAP for 24hrs and then assayed for viability using the MTT assay. As seen with APAP, cells grown in 3D show a heightened resistance to cytotoxicity when compared to cells grown in 2D. This difference in enhanced at passage 4 and enhanced even further at passage 7. Data presented as n=3 ± SEM. Statistical analysis through ANOVA. * denotes p≤0.05, ** denotes p ≤0.01.
(A) taken from Ogilvie et.al., 2006.

5.5.4. Comparing cytochrome P450 and Phase II enzyme activity of cells and aggregates maintained in 2D and 3D

Cytochrome P450 (CYPs) enzymes are a superfamily of hemoproteins essential for hormone synthesis and breakdown, cholesterol synthesis, vitamin metabolism and, the metabolism of xenobiotics. CYPs are the major enzymes in the liver responsible for drug metabolism, accounting for approximately 75% of total drug metabolism [208]. They act primarily during Phase I xenobiotic metabolism, and usually introduce reactive and polar groups into drug molecules through oxidation, reduction, hydrolysis, cyclisation, and decyclisation [209]. There are thousands of members of this family, and different drugs are metabolised by different CYPs. The main CYPs involved in xenobiotic metabolism in humans are CYP3A4, responsible for 40-45% of all CYP-mediated drug metabolism, CYP2D6 (20-30%), CYP2E1 (5-10%) and CYP1A2 (5-10%) [210]. In particular, CYP3A4 and CYP2E1 are of importance in this study because they are responsible for the primary metabolism of APAP. Another key component in the metabolism of APAP are Glutathione-S-Transferases (GSTs), a group of enzymes responsible for detoxifying NAPQI. GSTs are a part of Phase II xenobiotic metabolism, during which the activated xenobiotic metabolites produced in Phase I are conjugated with charged species such as glutathione (GST), sulphate and glycine. Both Phase I and Phase II enzymes are continually expressed at low levels in hepatocytes, but upon drug treatment, expression is induced at a much higher copy number, leading to much higher levels of the enzymes in the cytoplasm. These levels return to basal levels after the drug is fully metabolised.

Given that 2D and 3D maintained cells show drastically different toxicological profiles for APAP metabolism, one would hypothesise that the expression and activity of these enzymes would differ between the two populations. To test this theory, 2D and 3D maintained cells at passage 3, 6 and 8 were treated with previously demonstrated toxic doses of APAP for 24 hours, at which point they were lysed and RNA extracted. These samples (termed 'induced' samples), as well as samples extracted prior to APAP treatment (termed 'basal' samples) were converted into cDNA and probed using qt-PCR for three key genes involved in APAP metabolism: CYP2E1, CYP3A4 and GST-1. Expression levels were normalised to a housekeeping gene, GAPDH.

At passage 3 (Figure 5.22), 2D cells show slightly lower basal expression levels of CYP2E1 but this is not significant – basal levels for CYP3A4 and GST-1 are equivalent between the two

populations. With CYP2E1, 2D and 3D maintained cells show similar inducibility, but 3D cells show a significantly higher inducibility for CYP3A4 and GST-1. As Figure 5.23 shows, by passage 6 the differences between the two populations are much larger. Both CYP2E1 and CYP3A4 enzymes show higher inducibility in 3D maintained cells. Interestingly, with CYP2E1, the basal level of expression in 3D cells is almost that of the induced levels in 2D maintained cells. This suggests that there are long-term changes in gene expression occurring as cells are propagated in 3D. Another key observation from this data set is that the changes seen for the CYP system are not reflected in the levels of GST-1 between the two populations. This would indicate that the major changes in drug metabolism by passage 6 cells seen in Figure 5.20 occur during Phase I rather than Phase II metabolism. By passage 8 (Figure 5.24), the patterns of enhanced inducibility seen for CYP2E1 and CYP3A4 are amplified. However, the most significant finding was that at this late passage point, there is now an observable difference in the inducible expression levels of GST-1 between 2D and 3D cells. This would suggest that phase II metabolism is affected by 3D propagation, but only after Phase I enzyme expression in enhanced.

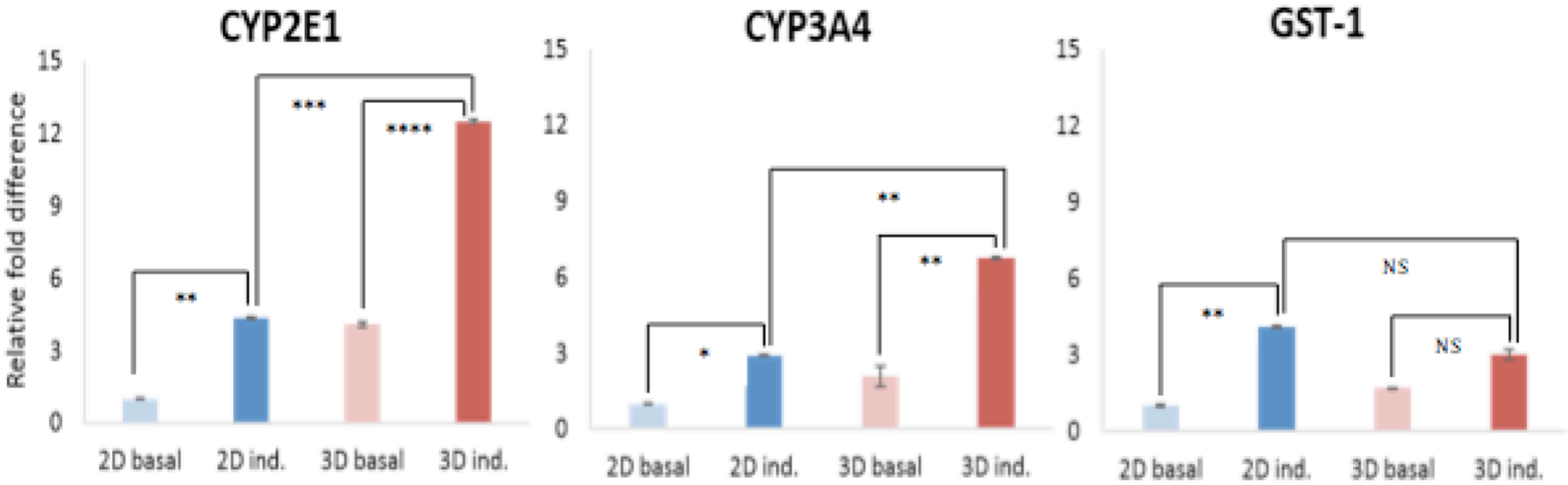

Figure 5.22 Expression and induction of genes associated with drug metabolism differs between cells maintained in 2D and 3D for 3 passages

Cells were grown in 2D and 3D for 3 generations and then treated with toxic doses of APAP. After 24 hours, cells were lysed for RNA extraction. Samples were converted into cDNA using a commercial kit and cDNA samples from untreated (basal) and treated (induced) cells were probed for three key genes involved in APAP metabolism. Though cells maintained in 3D don't show significantly higher basal expression of any of the three genes, they show higher levels of inducibility. Data presented as n=3 ± SEM. Statistical analysis through Student's t-test. NS denotes non-significant,* denotes p≤0.05, ** denotes p ≤0.01, *** denotes p≤0.001

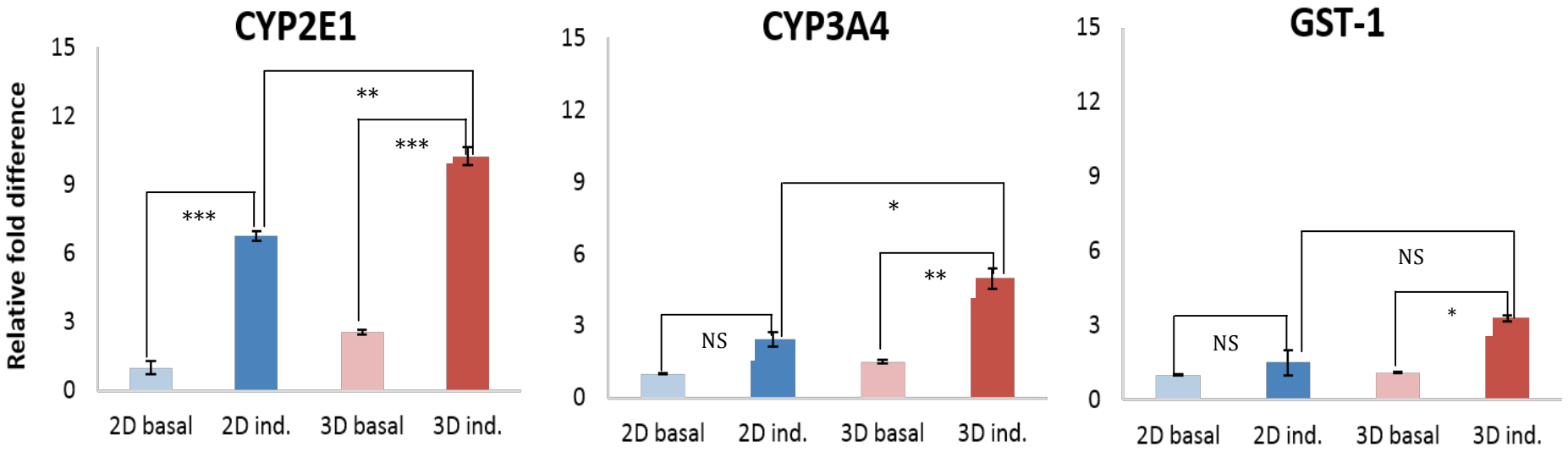

Figure 5.23 CYP450 inducibility increases when cells are maintained in 3D for 6 passages

Cells maintained in 3D for 6 passages show drastically higher expression of CYP2E1 when gene expression is induced through APAP treatment. These cells also show marginally higher basal levels of CYP2E1 expression. This pattern is also seen for CYP3A4 though to a slightly lower extent. There does not appear to be any significant differences in the expression of GST-1 indicating that the major changes in drug metabolism in passage 6 cells seen thus far occur during phase I rather than phase II metabolism. Data presented as n=3 ± SEM. Statistical analysis through Student's t-test. NS denotes non-significant, * denotes p≤0.05, ** denotes p ≤0.01, *** denotes p≤0.001, **** denotes p≤0.0001

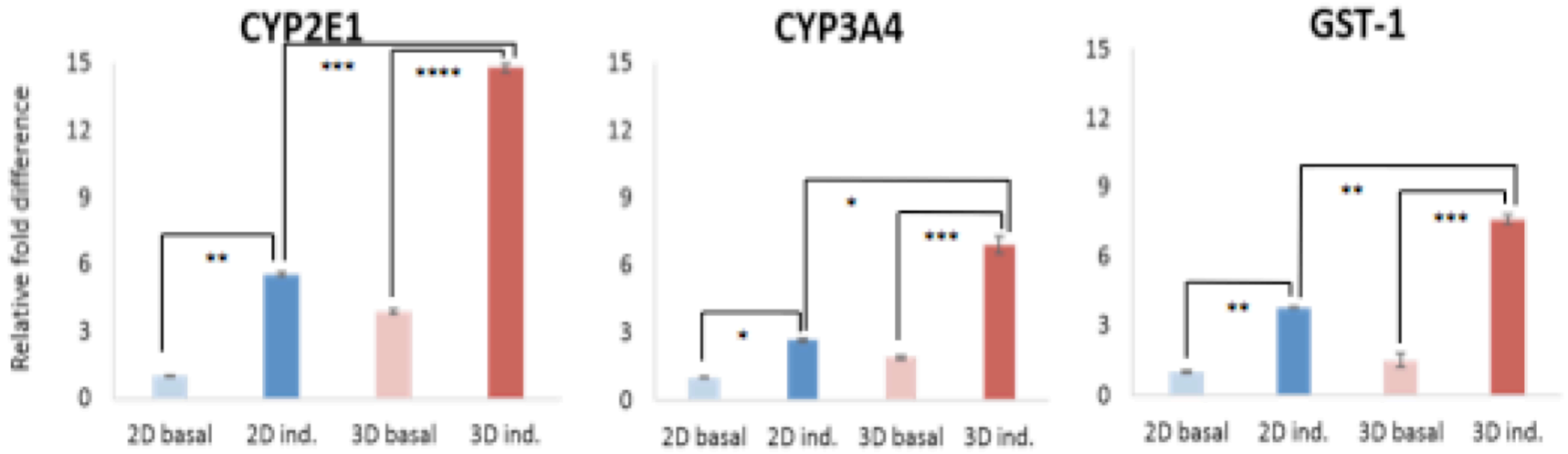

Figure 5.24 Expression and induction of genes associated with phase II drug metabolism differs between cells maintained in 2D and 3D for 8 passages

Cells maintained in 3D for 8 passages maintain the drastically higher expression of CYP2E1 seen at earlier passages, as well as significantly increase CYP3A4 inducibility. However, at this late passage point, there is now an observable difference in expression of GST-1, suggesting that phase II metabolism is increased when cells are maintained in 3D for long culture periods. Data presented as n=3 ± SEM. Statistical analysis through Student's t-test. * denotes p≤0.05, ** denotes p≤0.01, *** denotes p≤0.001, **** denotes p≤0.0001

5.6 Discussion

The liver in general and hepatocytes in particular maintain a wide array of interrelated functions including protein synthesis and xenobiotic intermediary metabolism, and detoxification. Recent work in 3D culture systems has enhanced our knowledge of the factors that permit this range of function be maintained *in vitro* and in particular the complex cell to cell interactions and intracellular signalling in the liver that contribute to this [213]. Understanding the conditions necessary for hepatocytes to express their full functional repertoire is important as translational medicine aims to recreate normality in a diseased liver. This understanding is also fundamental to attempts to establish fully functional *in* vitro cultures of liver cells for preclinical drug testing. The aim of this chapter was to explore whether 3D propagaton results in any changes in hepatocyte metabolism, function and gene expression.

The first set of experiments focussed on placing 2D and 3D maintained cells into a secondary 3D system, aggregate culture. This was to test the concept that maintaining cell in 3D primes them for this novel microenvironment; this 'priming' effect was expected to show itself in a more efficient aggregation process. Efficiency was determined by measuring the speed of aggregate formation and the regularity of aggregate size and shape. The main findings from these experiments showed that at early passage points 2D cells aggregated faster than 3D cells; however after several passages in 3D, the 3D propagated cells catch up, and eventually start forming aggregates at a similar speed. In terms of size and shape, though, 3D aggregates are consistantly rounder and more regularly shaped. This more regular formation could be suggestive of either stronger cell-cell contacts, which hold the aggregate together or the secretion of an ECM which again, would provide structural support to the aggregate.

The next set of experiments took 4 cell populations: 2D maintained cells, 3D maintained cells, aggregates made from 2D maintained cells ("2D aggregates") and aggregates made from 3D maintained cells ("3D aggregates') and compared the metabolic profiles of these distinct groups of cells. A problem traditionally encountered with primary hepatocyte cultures is their rapid dedifferentiation, which is reflected not only in a loss of hepatic morphology (the cells flatten, depolarize, and lose several pivotal surface characteristics

that normal hepatocytes display *in vivo*), but also decreased liver-specific functions such as albumin and urea synthesis and detoxification of drugs [214]. Since data from Chapter 4 revealed that 3D propagation results in HepG2 cells adopting moprhologies that more similar to that of physiological hepatocytes in the native liver than the flattened morphologies these cells usually exhibit in monolayer cultures, the hypothesis was that 3D propagation would enhance hepatic functionality. A secondary hypothesis was that this would be further amplified by the use of a aggregate culture as a secondary 3D model.

This study firstly showed that 3D cells appear to consume more glucose than 2D maintained cells – this was further increased in the aggregate models. Further proprgation in 3D beyond early passages seemed to increase glucose metabolism even further. This could either be explained by an increase in general metabolic activity or more specifically an increase in glycogen synthesis, the latter of which has been demonstrated in 3D culture pvreiously by Chu and colleagues [215]. Further research would be needed to differentiate between these two mechanisms.

As well as glucose metabolism, albumin and urea secretion are key markers of hepatic function. 3D culture has been shown to increase both albumin and urea production in cultured hepatocytes. For example, hepatocytes cultured on the electrispun scaffolds used in [215] showed increased albumin and urea levels when compared to monolayer culture. Tsang used photopatterned hydrogels to embed hepatocytes within a complex multi-layer tissue-mimetic architecture and found that these cells produced higher levels of both albumin and urea compared to control cells [216]. Experiments comparing albumin and urea synthesis across all 4 populations showed similar results – albumin and urea synthesis was significantly increased in 3D propagated cells, and even more so in 3D aggregates. This fits with a body fo work that has demonstrated increased levels of both, for example Miranda et al. [217] showed that several liver-specific functions of hepatocytes, such as albumin and urea secretion and enzymatic activities, were much better maintained in a 3D bioreactor system compared to the standard monolayer culture. More improtantly for the concept of maintenance and propagation in 3D, Miranda found that these several liver-specific functions were maintained for up to 21 days in the 3D bioreactor system compared to only 3–4 days in the monolayer culture. Using the model of 3D propagation, increased albumin and urea production could be seen through till passage 6, which correlates to 30

days *in vitro*. Further work could look at even later passage points to see if levels of metabolism continue to increase or if they stabilise.

In order to test whether this increased metabolism in 3D propagated cells led to differences in drug responses, 2D and 3D maintained cells were exposed to cytotoxic doses of APAP. HepG2 cells propagated in 3D appear to be more resistant to APAP, suggesting an increase in detoxification and/or excretion. To ensure that this wasn't specific to APAP, 3D propagated cells were also exposed to cytotoxic doses of Gemfibrozil. Once again, 3D maintained cells appeared to be more resilient than 2D maintained counterparts. The findings from these experiments are in line with primary literature. Previous studies have shown that 3D cultured cells exhibit different cellular responses for drug toxicities when compared to 2D cells [218-220].

Lastly, gene expression of drug-metabolising enzymes was compared between 2D and 3D maintained HepG2 cultures. It is well known that HepG2 cells have an almost negligible set of cytochrome P450 enzymes [221]. Chang showed that 3D culture leads to an increase in the expression of gene transcripts for CYP450 members [136], and this is supported by a wide range of other studies [222-224]. In addition to probing 2D and 3D maintained cells for the two CYP450 enzymes involved not only in metabolizing APAP and Gemfibrozil, but over 50% of all xenobiotics, these cells were also probed for GST-1, which is a representative Phase II enzymes. The results from these gene expression studies indicated that 3D culture could result in an increase in both CYP450 and Phase II enzyme expression. In particular, the inducibility of these enzymes was tested by comparing expression levels in APAP treated and non-treated cells. This comparison revealed that it is not overall expression levels that are increased upon 3D propagation, but rather the ability of these enzymes to be up-regulated in the case of cytotoxic attack. This distinction is important in the context of preclinical drug testing.

5.7 Conclusions

The following conclusions can be drawn from this Chapter:

- Cells maintained in 2D and 3D can be placed into a secondary 3D aggregate model. 2D maintained cells initially aggregate faster than 3D counterparts; however at later passages, once 3D cells have adapted to the environment, both populations of cells form aggregates at roughly the same time.

- Aggregates from 3D maintained cells are, on average, more circular and regularly shaped than those formed from 2D maintained cells. This suggests that cells can be 'primed' to a 3D microenvironment by continual propagation and maintence under 3D conditions.

- 3D propagation results in HepG2 cells being metabolically more active – this is shown by increased glucose consumption from the media, as well as higher levels of albumin and urea secretion. Since these are well established markers of hepatic function, this data suggests that propagation in 3D allows hepatocytes to retain differentiated functionality.

- 3D cells are more resistant to the cytotoxic effects of both APAP and Gemfibrozil. With both of these drugs, propagation in 3D results in a gradual shift of the cell death curve to the right, indicating resilience to toxicity.

- Cells maintained in 3D do not show significantly higher basal levels of CYP450 enzymes or Phase II enzymes, but they do exhibit a higher degree of inducibility than 2D counterparts. This inducibility increases for Phase I enzymes at early passages, and for Phase II enzymes at later passages.

The data from this chapter suggest that cells can be primed to a 3D phenotype by continual propagation over long term *in vitro* culture. This phenotype exhibits liver-specific functionality often lost in traditional monolayer culture. The following chapter will look at a potential signaling pathway responsible for regulating the relationship between 3D propagation and enhanced functionality.

Chapter 6: Investigating the role of adhesion signalling in the adaptation of hepatocytes during 3D propagation

6.1 Introduction

Cells respond to cues from the matrix by forming multi-protein complexes at the membrane. These complexes are initiated at points along the membrane where integrins cluster in response to binding ligands in the ECM. At this points, focal adhesion complexes (FAC) are formed. These complexes then interact with the cytoskeleton through cytoskeletal regulating proteins, and actin-linking proteins, which are activated after integrin clustering. In this way biomechanical cues are translated into changes in cytoskeletal organisation and cell shape and migration. FACs also signal downstream signaling cascades such as the MAP Kinase pathway and the JNK pathway. These signaling cascades cause the activation and/or inactivation of certain transcription factors, and in this way environmental cues can lead to changes in gene expression. These interactions are outlined in Figure 6.1 below.

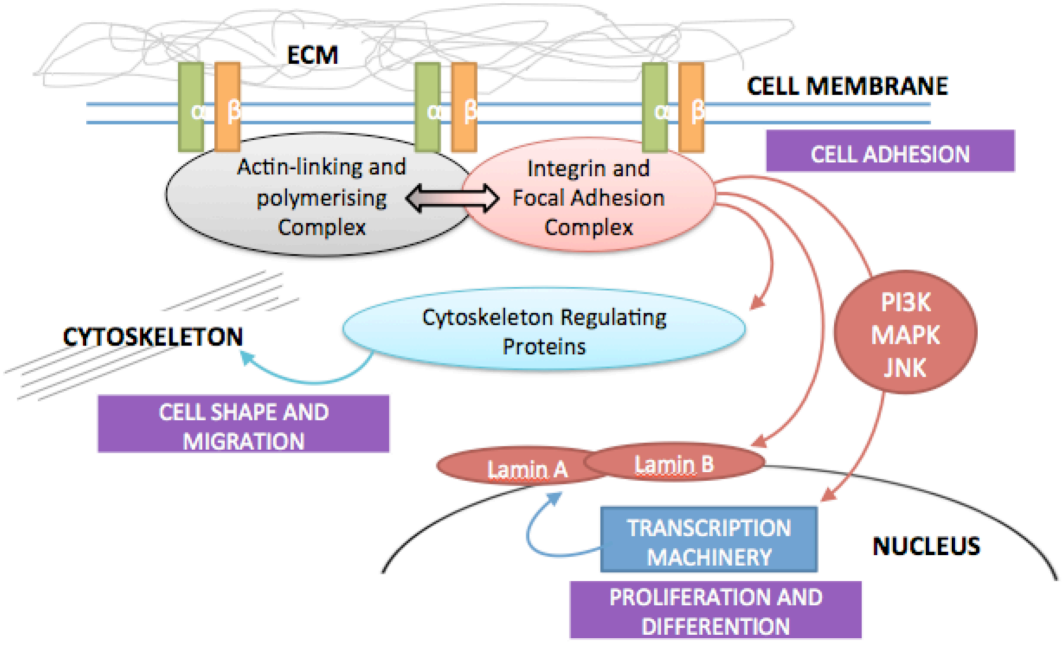

Figure 6.1 Cell behaviour is determined by a number of signalling complexes

Cells are dynamic units of behaviours such as proliferation, adhesion and migration. These behaviours are regulated by various signalling complexes; the cross-talk between these allows for cells to adapt to ever-changing environmental conditions. One of the ways cells adapt is via cytoskeletal re-organisation which is mediated by proteins that themselves are activated by integrin and focal adhesion signalling. This signalling is a direct result of changes in the extracellular matrix (ECM). This biochemical link between the cell's physical environment and biological processes is called mechanotransduction, Data in figure from [225].

Whereas cell adhesion on 2D substrates has been extensively characterized, 3D adhesion is poorly understood because of the physical complexity of the local micro-environment. Beyond the biomechanical regulators known for 2D migration (stiffness, ligand density and chemical composition), a 3D matrix adds ECM micro-architecture, porosity, nanoscale topography and elastic behavior [226]. Research has shown that 2D and 3D cells form different adhesions with the matrix. For example, fibroblasts adherent to a 2D fibronectin matrix will form focal complexes and focal adhesions that are rich in αvβ3. 3D-matrix adhesions contain primarily α5β1, but αvβ3 can be observed at the adhesion periphery. It has been postulated that that different integrin receptors will recruit different cytoplasmic factors and differentially control cell signaling and cellular tension [127]. In this way, it could be that differential integrin expression plays a key mechanistic role in the adaptation of cells to a 3D environment – this is a hypothesis that will be explored further in this Chapter.

With regards to the composition of FACs themselves, 3D matrix adhesions have been suggested to be similar to fibrillar adhesions regarding α5β1 localization; however, 3D-matrix adhesions contain high levels of actin-linker proteins vinculin, α-actinin, and phosphorylated paxillin. An interesting finding of 3D matrices thus far is that levels of FAK Y397 phosphorylation seem to be consistently low in 3D-matrix adhesions, indicating that adhesion signaling can differ substantially in 3D compared to 2D environments [227,228]

Another interesting variable in studies of cell adhesions in 3D involves the physical organization of the matrix itself. Although many studies have focused on relatively homogeneous collagen I gels, some matrices can be quite fibrillar [127,211] and cells follow aligned fibers *in vitro*, just as they migrate along fibres in the ECM *in vivo* [229, 230]. By changing the local physical characteristics of type I collagen gels to mimic the *in vivo* environment, Doyle et al. found that local fibre stiffness could vary by up to 10-fold [231]. These microenvironmental ECM differences altered 3D adhesion protein turnover and overall integrin activation. Thus, there is an argument to be made that to distinguish between the chemical, structural and dimensional elements of 3D culture as they affect matrix adhesions, it would be beneficial to isolate each criterion in turn. Looking specifically at the added Z dimension that 3D culure allows, having a 3D matrix made of the same material as traditional TCP would allow for analysing the specific impact of dimensionality on adhesions. Alvetex®Strata is composed of polystyrene, as are most commercially

available 2D plates and culture flasks – in this way, the developed methodology for 3D propagation in this project is of particular significance in furthering knowledge on the role of adhesion signalling in cell adaptation to 3D systems.

6.2 Aims of Chapter

The aim of this Chapter is to elucidate the intracellular signalling pathways that are responsible for translating changes in cellular microenvironment into biochemical cues within individual cells. Since these pathways regulate the relationship between cell morphology and enhanced cell functionality, it is hypothesised that changes in one or more of these pathways will be seen when cells are propagated in 3D rather than 2D. This Chapter aims to characterise these changes, and mechanistically couple a 3D microenvironment and recovery of liver-specific functionality in immortalised hepatocytes. This would validate the use of long-term 3D propagation in preclinical drug discovery and development.

6.3 Objectives

1. Stain 2D and 3D maintained cells with antibodies against key molecules in the Focal Adhesion Kinase pathway in order to characterise changes in signalling.
2. Investigate the role of differential phosphorylation of FAK in modifying signalling in 3D maintained cells.
3. Use different ECM proteins to see whether changes in intracellular signalling are linked to changes in cell adhesion signalling.
4. Test whether recovery of 2D-like signalling leads to recovery of 2D-like morphology and behaviour.

6.4 Materials and Methods

6.4.1 Functional antibody blocking

A commercially available antibody was used to block the function of both α5β1 and αvβ3 (this is the same antibody used for staining purposes, and details of supplier can be found in Table 2.4). 2D and 3D maintained cells at different passages were plated onto PDL coated glass coverslips at 100,000 cells/disc and allowed to adhere for 2hrs, in 8ml MEM media in an incubator set to 37°C and 5% CO_2. At this point, increasing doses of a commercially available function blocking antibody was added to these cultures in a 1ml solution. To control for the added protein levels, an isotype matched antibody with no functional ability was added in equal volume. The cultures were left for 12 hours and then fixed in 4% PFA before being stained for antibodies against pFAK as per the protocol in Section 2.4.2.3.

6.4.2 Probing the ROCK/RhoA pathway

In order to investigate whether the ROCK/RhoA pathway was involved in cellular adaptation to 3D microenvironments, a set of experiments blocking the action of ROCK were designed. 2D and 3D maintained cells at different passages were plated onto PDL coated glass coverslips at 100,000 cells/disc and allowed to adhere for 2hrs, in 8ml MEM media in an incubator set to 37°C and 5% CO_2. At this point, increasing doses of a commercially available and well characterized ROCK inhibitor, Y27632 were added to these cultures in a 1ml solution. The negative control was PBS in equal volume. The cultures were left for 12 hours and then fixed in 4% PFA before being stained for antibodies against pFAK as per the protocol in Section 2.4.2.3.

6.5 Results

6.5.1. Comparing Focal Adhesion Kinase phosphorylation between 2D and 3D maintained cells

As explained in the introduction, one of the major hypotheses of this Chapter is that phosphorylation of FAK will differ between 2D and 3D systems, and that this difference underpins the more physiological morphology and behaviour seen in 3D maintained HepG2s. To explore this theory, sections of primary mouse liver tissue were stained with antibodies against FAK and phosphorylated FAK (pFAK). In parallel, HepG2 cells grown in 2D on PDL-coated glass coverslips for 48 hours were also stained with the same antibodies, and the pattern of staining compared between the two (Figure 6.3A). In this figure, deep brown regions indicate positive FAK/pFAK staining, and blue indicates positive nuclei staining.

The primary liver tissue showed positive staining for FAK, but negative staining for pFAK. Contrastingly, HepG2 cells grown in 2D showed positive staining for both FAK and pFAK. The finding that positive pFAK staining could be seen in 2D cultured cells but not in native tissue is suggestive that positive pFAK staining is an artifact of the tissue dissociation and/or monolayer culture process. As also clearly shown in this figure, the cell shapes between the primary hepatocytes at this plane of section and 2D HepG2s differ greatly, with primary cells showing rounder morphologies. A typical example is highlighted in red in both images. This could be important in the context of FAK signalling patterns because, looking more closely at the FAK staining in Figure 6.3A, FAK expression appears to be denser at membrane regions in, and points of cell-cell contact in primary cells (as indicated by arrowheads), but appears to be equally expressed across the entire cell in 2D populations. As covered in the introduction, aberrant cell flattening in 2D cells has been shown to affect cell-cell contacts, as well as membrane organisation of the cell, and thus this change in cell shape could be responsible for the change in signalling. Equally so, since cells exhibit bidirectional communication with the ECM, it is also possible that the change in FAK signaling causes cytoskeletal elements to reorganise thus changing cell morphology. It is worth noting at this point that the cells in primary murine tissue can only be taken as hepatocyte-like cells, since specific markers were not used to confirm cell identity. However, the cells in the image display the characteristic shape, size, and cell-cell organisation as hepatocytes are known to adopt in native liver tissue.

Cells grown in 2D and 3D for 28 hours were then stained with the same antibodies to see whether 3D cells show a staining pattern more like 2D cells or more like primary tissues (Figure 6.3B). As seen before, 2D cells show positive pFAK staining, but 3D cells show a staining pattern that resembles the primary tissue samples in that they show positive FAK staining but negative pFAK staining. This provides further data supporting the hypothesis that pFAK staining is an artificial observation of 2D culture

Taking this finding further, 2D and 3D maintained cell populations were allowed to form aggregates, and these were fixed and stained for the same antibodies against FAK and pFAK (Figure 6.4).

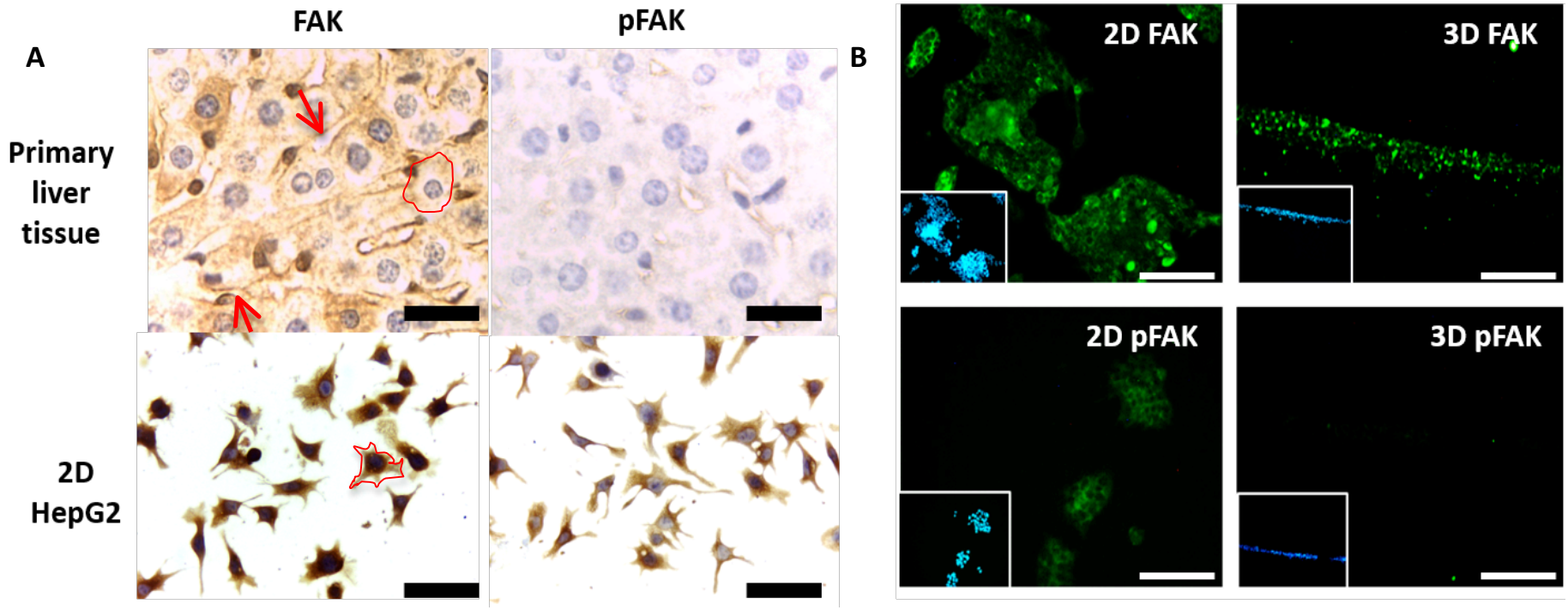

Figure 6.3 Cells propagated in 3D show a drastic reduction in the expression of phosphorylated FAK that mirrors the expression pattern in primary tissue

Sections of murine liver tissue were stained for antibodies against FAK and phosphorylated FAK (pFAK), as were 2D cells grown on coverslips and 3D cells grown on Alvetex®Scaffold. Primary hepatocytes show negative staining for pFAK even though 2D HepG2 cells show positive staining for the same antibody (A). In addition, primary cells show a more membrane-associated staining pattern, as indicated by arrowheads. 2A final difference is in cell morphology, with the average primary cell showing a rounder morphology, as compared to the irregular flattened shapes of the 2D cultured cells. B) 2D and 3D HepG2 cells were stained using the same antibodies and the 3D cells lack positive staining for pFAK that correlates with the staining patterns seen in the primary controls, suggesting that 2D cells show an artificial positive expression of pFAK. Scale bars = 50µm in A; 100µm in B.

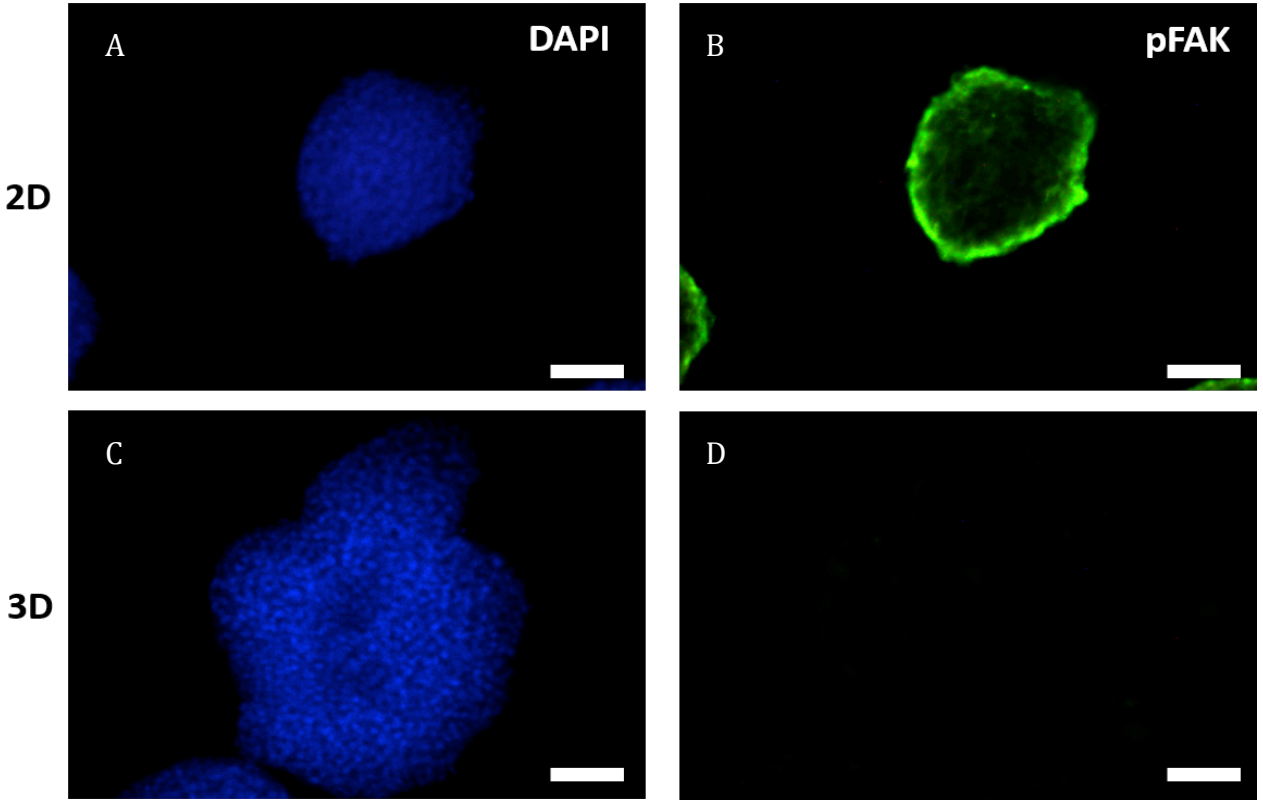

Figure 6.4 Aggregates formed from 3D maintained cells also show a reduction in the expression of pFAK

Cells maintained in 2D and 3D for several passages were allowed to aggregate for 4 days. These aggregates were then transferred to well plates, fixed in 4% PFA, and stained with an antibody against phosphorylated FAK (pFAK) in order to see whether previously shown differences in phosphorylation between 2D and 3D cells would be maintained in a secondary 3D model system. As shown, 3D aggregates show the same absence of pFAK expression as single cells do. Scale bars = 100µm

3D aggregates show a similar staining pattern to that seen in Figure 6.3, showing almost no staining for pFAK. In aggregate culture, cells are surrounded by cells and ECM on all sides, and exist in a microenvironment very similar to that of individual cells in tissue. Therefore, the lack of pFAK expression seen in the aggregate model provides further support for the theory that pFAK expression is a result of monolayer cell culture, which bears very little resemblance to the *in vivo* state of cells within tissue. The fact that 2D maintained aggregates still show positive pFAK expression could be because the cells have yet to adapt to the 3D environment within the aggregate – previous data has shown that full adaptation a 3D like state requires several passages in 3D, whereas the 2D cells in the 2D aggregates in Figure 6.4 have only existed in a 3D environment for 4 days.

In order to test whether the lack of FAK phosphorylation is specific to hepatocytes or consistent across a variety of mammalian cell types, representative cell types used in Chapter 3 (MDA-MB-231 breast carcinoma cells and LN229 glioblastoma cells) were grown alongside HepG2s on Strata for 7 days and stained for FAK and pFAK using the same antibodies as earlier. Scaffolds were embedded, sectioned, and after staining, imaged using laser scanning confocal microscopy (LSCM) so that a high resolution of several cells still within the 3D matrix could be imaged. As Figure 6.5 shows, all three cell types show positive staining for FAK, as expected. While HepG2 cells show a very slight positive staining for pFAK, the other two cell types show absolutely no positive pFAK staining. This shows that the lack of pFAK expression is not cell-type dependent. Thus suggests that a negative staining pattern for FAK is a result of cell geometry within the microenvironment, and provides an interesting foundation for future research into FAK signaling in a 3D context.

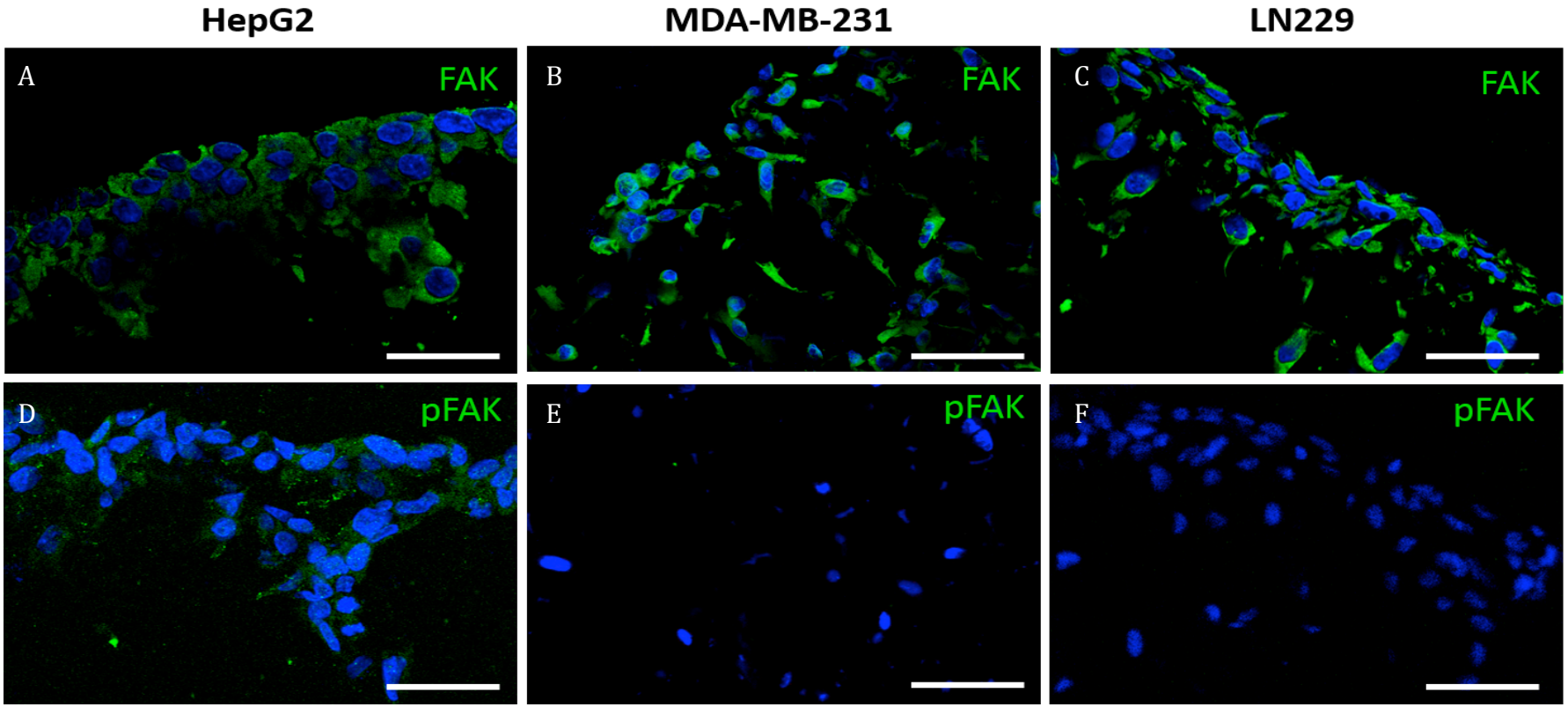

Figure 6.5 The absence of pFAK expression in cells grown in 3D is seen with other cell types on Alvetex®Strata

Cells from each of the three different classes identified in Fig. 3.13 were grown on Alvetex®Strata for 7 days and then fixed and embedded. Sections were stained with antibodies against FAK and phosphorylated FAK (pFAK) and imaged using Laser Scanning Confocal Microscopy (LSCM). As shown above, cells from all three cell lines showed positive FAK expression but were negative for pFAK expression, indicating that this lack of expression is not cell-type dependent but rather a result of cell geometry. Scale bars = 50µm.

6.5.2. Quantifying changes in the phosphorylation of Focal Adhesion Kinase between 2D and 3D cells

The findings from the previous experiments provide a solid argument for the further exploration of the Focal Adhesion Kinase pathway and its role in a cell's adaptation to its microenvironment. In order to fully characterise changes in this pathway, a methodology was developed to quantify the expression of certain key molecules. Cells were pictured at high resolution, and stained with antibodies against proteins of interest as before. Since staining patterns for these molecules is punctate, it was possible to count individual regions of positive staining. These regions were termed 'focal adhesions' (FAs) and designated as either FAK+ or pFAK+ depending on the antibody being tested.

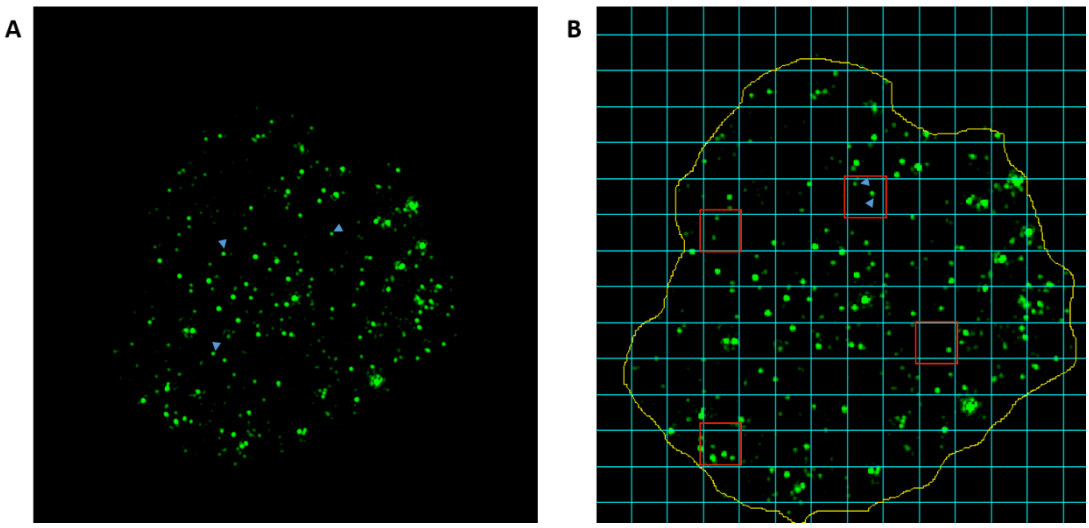

Figure 6.6 Focal Adhesions can be quantified in two ways: total number or density

Cells maintained in 2D and 3D were plated onto PDL-coated glass coverslips and imaged at super resolution using Structured Illumination Microscopy (SIM) to allow visualisation of individual cells and adhesion sites. Staining was quantified by counting the number of positively stained adhesions (green dots). This number can be expressed as a total (A) or a density (B). In the first method, all positive staining (arrowheads) are counted per cell. In the second method, a grid of known size is placed over the cell, and the number of green dots (arrowheads) is counted in several random cells (outlined in red) and averaged to give a density measurement.

Originally, the total number of positive FAs per cell was counted and recorded, as shown in Figure 6.6A. However, this method does not fully account for differences in cell area. Previous data has consistently showed that 3D cells have a smaller area to 2D cells, and so a more accurate way of quantifying staining would be to normalise the data to cell area. To do this, a grid measuring $1\mu m^2$ was placed over each cell, and a random number generator used to pick 10 random squares. The number of positive dots per square is counted and averaged, as shown in the example in Figure 6.6B. To see whether these two methodologies would yield a difference in the results, both methods were used to express the staining patterns of FAK and pFAK in the same 8 cells (four 2D, four 3D) (Figure 6.7). The two methods do appear to show slightly different patterns, though the differences are non-significant. The average standard deviation, though, was much lower when using the density measurement, indicating a higher degree of internal validity. The differences in overall trend were not significantly different between the two methodologies, ensuring that the method of quantification used was not likely to be responsible for observations seen. Thus, the methodology with lower standard deviation, the sample method, was used going forward.

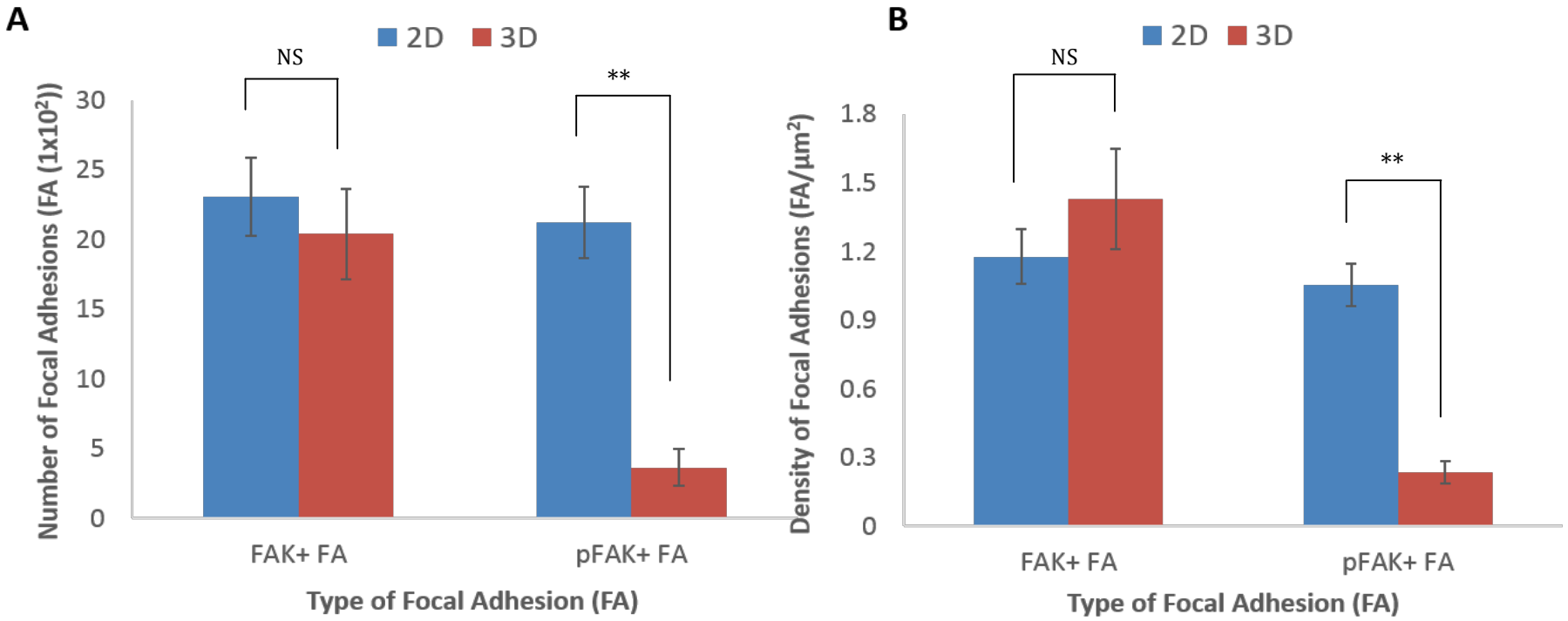

Figure 6.7 The two methods of quantifying focal adhesions result in slightly different results

Staining was quantified by counting the number of positively stained adhesions. This number can be expressed as a total (A) or a density by normalising the total number to cell area quantified using ImageJ (B). When expressed as a total number, it appears as though there is more FAK staining in 2D cells than 3D cells, but when expressed as a density, this pattern is reversed, though it is important to note that these differences are non-significant. Data presented as n=8 ± SEM. Statistical analysis through ANOVA. ** denotes p ≤0.01

6.5.3. Quantifying changes in the FAK pathway between 2D and 3D cells

In order to further explore the differences in the focal adhesion pathway seen earlier, 2D and 3D cells from early (p3) and mid (p6) passage points were plated on PDL coated coverslips and stained with either FAK, pFAK or Paxillin. These coverslips were imaged at high resolution to allow the examination of individual cells, and focal adhesion sites were counted in order to quantify differences.

Figure 6.8 shows the results from examining the expression patterns of FAK. Firstly, the image panel supports previous data that shows that 2D cells exhibit more irregular morphologies. Apart from this, there does not appear to be a significant difference in the level of total FAK expression between cells at high and low passage or between cells in 2D or 3D. Upon close examination of the high-resolution images, there appears to be a slightly different organisational pattern of FAK positive FA sites in 2D and 3D cells. The FAK staining appears to be more evenly distributed across the cell in 2D cells, whereas in 3D maintained cells, the FA clusters appear to be slightly larger – this is indicated with white arrowheads. This observation suggests that the FAK molecules are clustering together in dense FA sites rather than spreading across the entire surface of the cell in more numerous but smaller complexes. This could be a sign that the FAK molecule is interacting with partner proteins and the actin cytoskeleton in a different manner in 3D maintained cells. However this is difficult to quantify due to image resolution constraints, and as such is an observation that for the purposes of this project simply provides an interesting avenue for future focus.

When looking at differences in the expression of pFAK between 2D and 3D cells there is a clear and noticeable difference between the two cell populations (Figure 6.9). The number of pFAK positive FA sites in 3D cells is negligible, and can be taken to indicate negative staining – this decrease in expression, when compared to 2D counterpart cells, is amplified at higher passage points. Looking at distribution of pFAK positive FAs in 2D cells, there is an even distribution across the cell, which is surprising since the expectation would be that there would be a concentration of pFAK positive adhesions at the membrane. One explanation for this could be due to aberrant adhesion to the rigid plastic growth substrate. As shown in Section 4.5.4, 2D cells show a high number of internal stress fibres that run across the surface of the cell that attaches to the substratum. Since these VSF stress fibres

are associated with FAs at both ends, this could explain the positive pFAK staining across the cytoplasm of the cell.

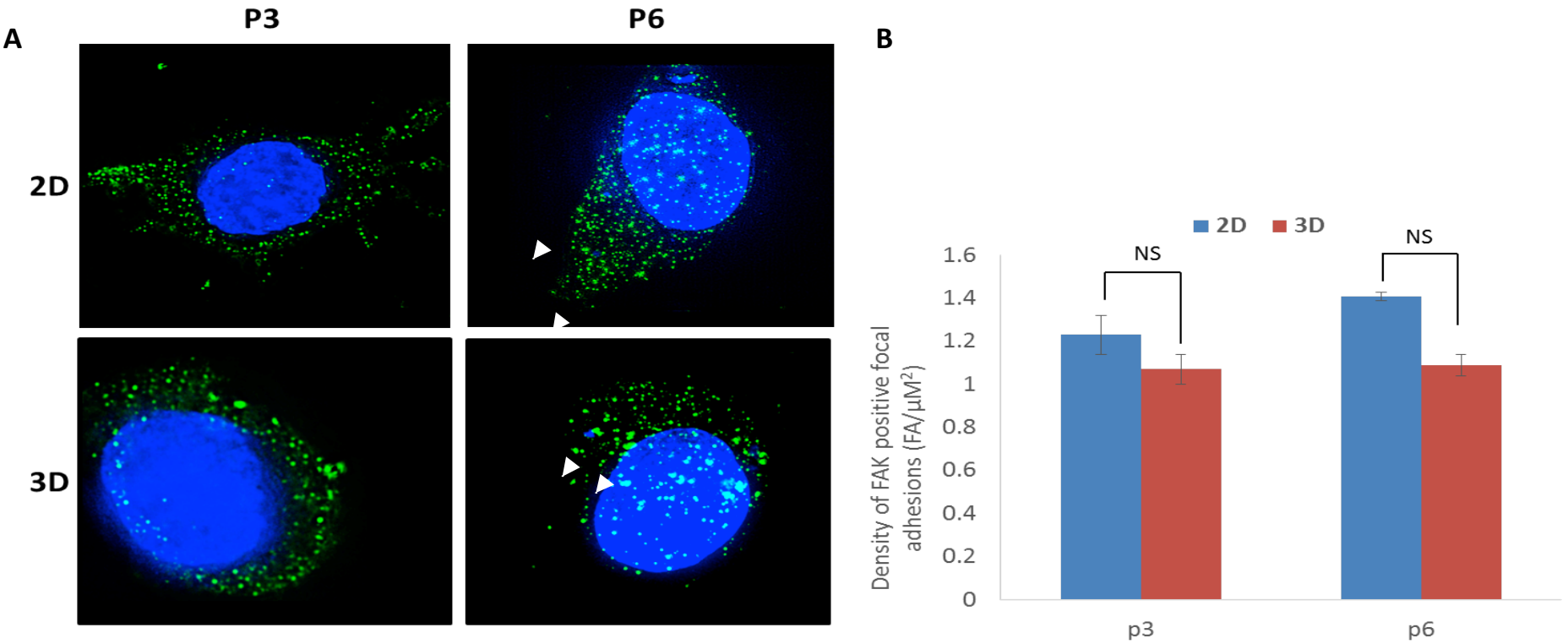

Figure 6.8 Cells in 2D and 3D do not show significant differences in FAK expression

Cells were maintained in 2D and 3D for 3 or 6 passages and then plated onto PDL-coated glass coverslips and imaged at super resolution using Structured Illumination Microscopy (SIM) to allow visualisation of individual cells and adhesion sites. Cells in 2D and 3D do not appear to show any significant differences in FAK expression at either passage. This staining was quantified by counting the number of positively stained adhesions (green dots) and normalising this to cell area quantified using ImageJ. Scale bars = 10µm. Data presented as n=5 ± SEM. Statistical analysis through ANOVA. NS denotes non-significant.

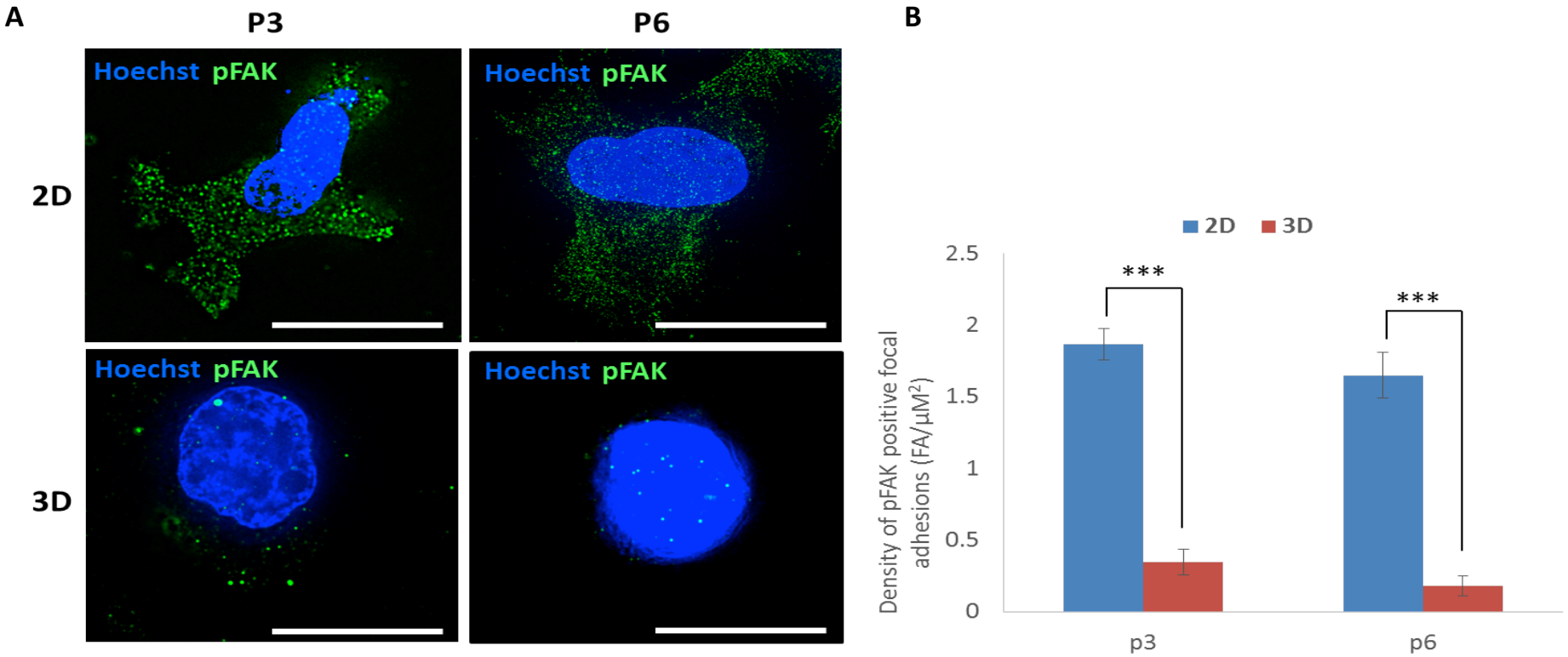

Figure 6.9 Cells in 2D and 3D show significant differences in pFAK expression

Cells were maintained in 2D and 3D for 3 or 6 passages and then plated onto PDL-coated glass coverslips and imaged at super resolution using Structured Illumination Microscopy (SIM) to allow visualisation of individual cells and adhesion sites. Cells in 2D and 3D show significantly different expression patterns of pFAK, with 3D cells showing almost no positive staining. This difference becomes amplified as cells are passaged longer in 3D. This staining was quantified by counting the number of positively stained adhesions (green dots) and normalising this to cell area quantified using ImageJ. Scale bars = 10µm. Data presented as n=5 ± SEM. Statistical analysis through ANOVA . *** denotes P= ≤ 0.001.

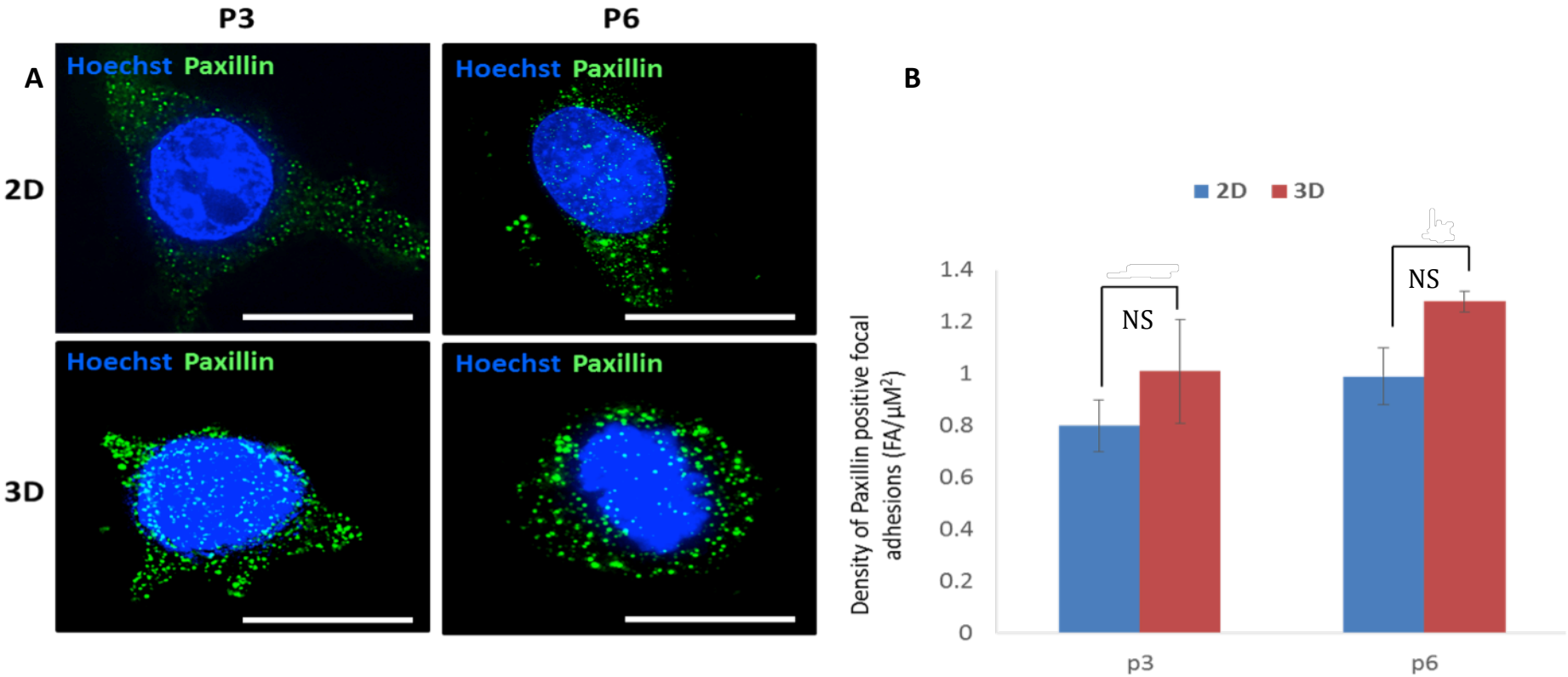

Figure 6.10 Cells in 2D and 3D show slight differences in Paxillin expression

Cells were maintained in 2D and 3D for 3 or 6 passages and then plated onto PDL-coated glass coverslips and imaged at super resolution using Structured Illumination Microscopy (SIM) to allow visualisation of individual cells and adhesion sites. Cells in 2D and 3D show different expression patterns of Paxillin, a key actin-linking protein. Cells maintained in 3D show an elevated level of Paxillin expression, an observation that can be clearly seen at both low and high passage points. This staining was quantified by counting the number of positively stained adhesions (green dots) and normalising this to cell area quantified using ImageJ. Scale bars = 10µm. Data presented as n=5 ± SEM. Statistical analysis through ANOVA. NS denotes non significant.

To further explore the dynamics of the FA sites in 2D and 3D cells, an actin-linking protein, paxillin, was looked at (Figure 6.10). At first glance, there doesn't appear to be a drastic difference in the overall expression between 2D and 3D cells but upon quantification, there are slightly more Paxillin positive FA sites in the 3D cells when compared to the 2D cells, and this difference does increase upon further propagation in 3D. This finding shows that the differential phosphorylation of FAK between 2D and 3D cells leads to differences in the docking sites created for other proteins to bind at FA sites, and has indications for further differences between 2D and 3D signalling downstream of adhesion.

The differences in FAK, pFAK and Paxillin were examined using a secondary form of analysis to confirm the findings seen using immunocytochemistry. Lysates from two different passage points, as well as control lysates from 2D cells, were run on gels and transferred to membrane for immunoblotting. The blot was then quantified using densitometry. The results from this can be seen in Figure 6.11. The results from the immunoblotting experiment generally support the main findings seen with immunocytochemistry; to sum up, 3D propagation causes two major changes in focal adhesion sites, namely a drastic reduction in pFAK expression, and a slight increase in Paxillin expression. Working on the hypothesis that changes in cell function outlined in Chapter 5 are due to these changes, the next set of experiments looked at the differential phosphorylation of FAK.

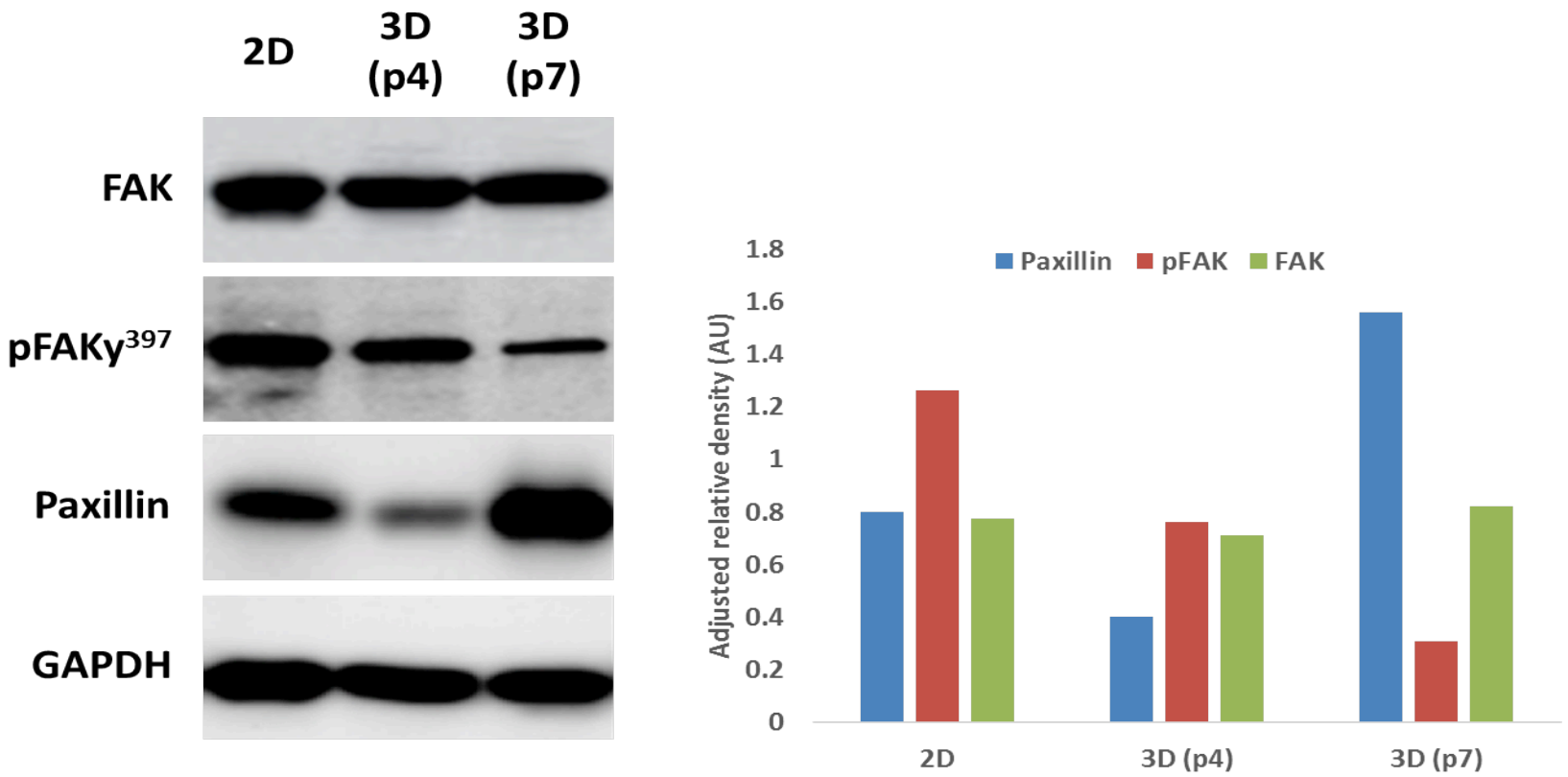

Figure 6.11 Cells in 2D and 3D show different expression levels of certain key FA signalling components

The differences seen in 2D and 3D maintained cells were confirmed using western blotting, and quantified using densitometry calculations in ImageJ software. Cells maintained in 3D show similar levels of FAK expression but reduced expression of phosphorylated FAK and slightly increased levels of Paxillin expression.

6.5.4. Exploring differential phosphorylation of Focal Adhesion Kinase in 3D maintained cells

FAK is a complex molecule with multiple phosphorylation sites, several of which have yet to be fully characterised. Of these, the important ones are highlighted in Figure 6.12.

It has been postulated that the presence of these sites, and their complex regulation, is the mechanism by which FAK can differentially control and regulate such a diverse range of cellular behaviours, ranging from proliferation and differentiation to apoptosis. With this in mind, a major working hypothesis of this project was that differential phosphorylation of FAK occurs in 3D focal adhesions, and that this is associated with the mechanism by which 3D maintained HepG2 cells show a higher degree of functionality as well as more physiological proliferation and migratory behaviour. The focus for the next set of experiments was on a serine residue (Ser732), which is phosphorylated by ROCK. This is because ROCK is well known as a regulator of cytoskeletal rigidity [211], and as such, this phosphorylation site could provide a mechanistic link between cytoskeletal changes, FAK phosphorylation, and the changes in liver-specific functionality seen in the previous chapter. In particular, the phosphorylation of this residue was looked at in the context of the autophosphorylation site Tyr397, since this is the residue suggested in literature to be responsible for the building of FA sites.

To see whether there are any gross differences in the overall expression levels of $pFAK^{S732}$ relative to $pFAK^{Y397}$ between 2D and 3D maintained cells, cells from both populations, both before and after propagation (p0 and p6 respectively) were probed for antibodies against FAK, $pFAK^{Y397}$ and $pFAK^{S732}$ using flow cytometry (Figure 6.13). To clarify, p0 indicates that cells were grown in 2D and 3D respectively for 4 days and then used in the assay. As such they did not go through a sub-culture. As seen before, there were no significant differences between total FAK expression between the tested populations. However, the pattern of expression of $pFAK^{S732}$ was inversely proportional to that of $pFAK^{Y397}$, and there were significantly higher levels of $pFAK^{S732}$ in the 3D populations as compared to the 2D populations. This increase was amplified with propagation. These findings suggest that there is a role for differential phosphorylation of FAK in adaptation to the micro-environment, and that 3D propagation causes a switch in preferential phosphorylation sites.

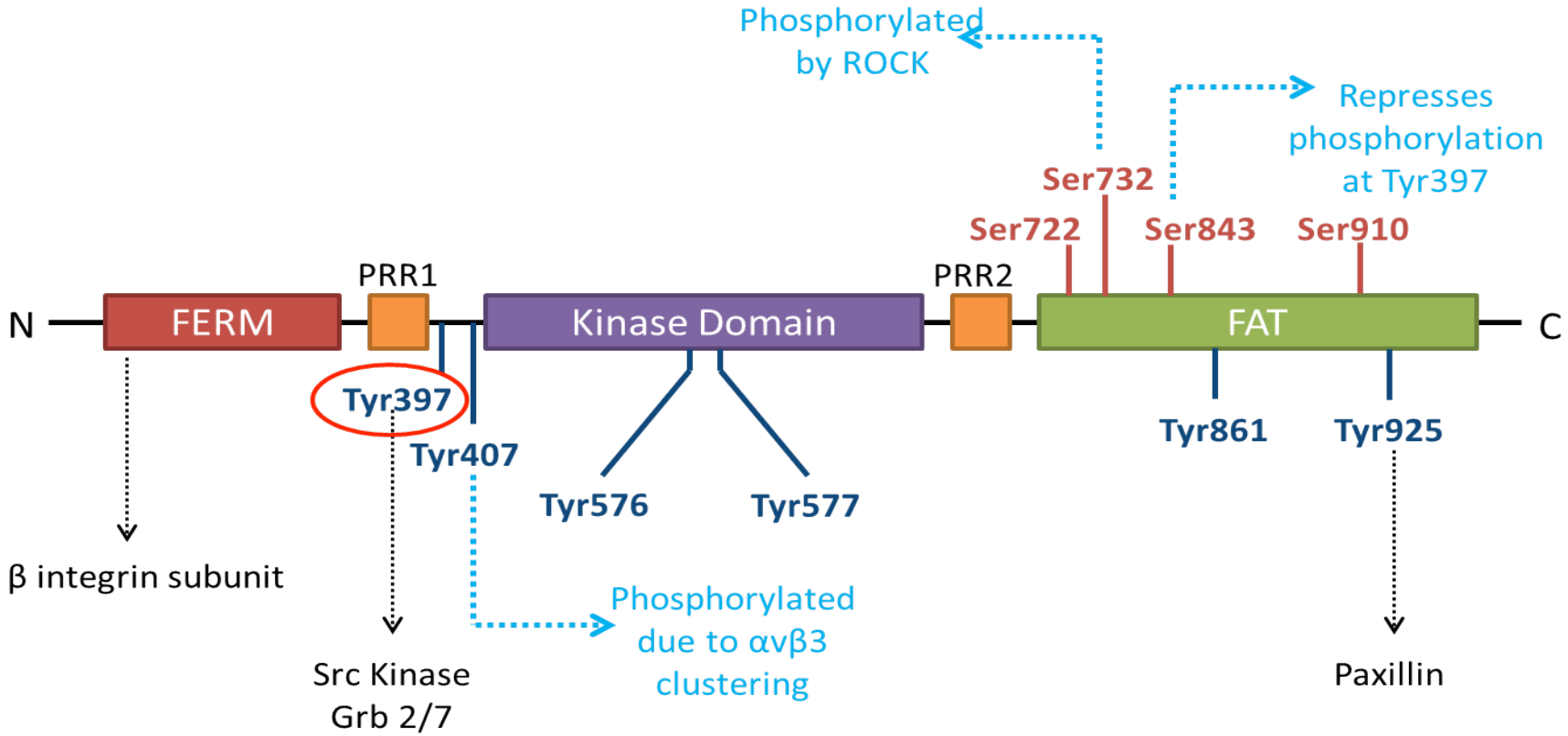

Figure 6.12 Focal Adhesion Kinase has several phosphorylation sites which allow it to regulate various protein-protein interactions

The Focal Adhesion Kinase (FAK) molecule is made up of three main domains – the FERM domain which allows the molecule to localise to the plasma membrane and interact with growth factor receptors, the Kinase domain which regulates catalytic activity and the FAT domain which localises the molecule to adhesion sites. These domains are linked by proline rich regions designated PRR1 and PRR2 respectively. The molecule contains 6 distinct tyrosine phosphorylation sites including the auto-phosphorylation/activation site at Tyr397, and 4 serine phosphorylation sites. Based on [212].

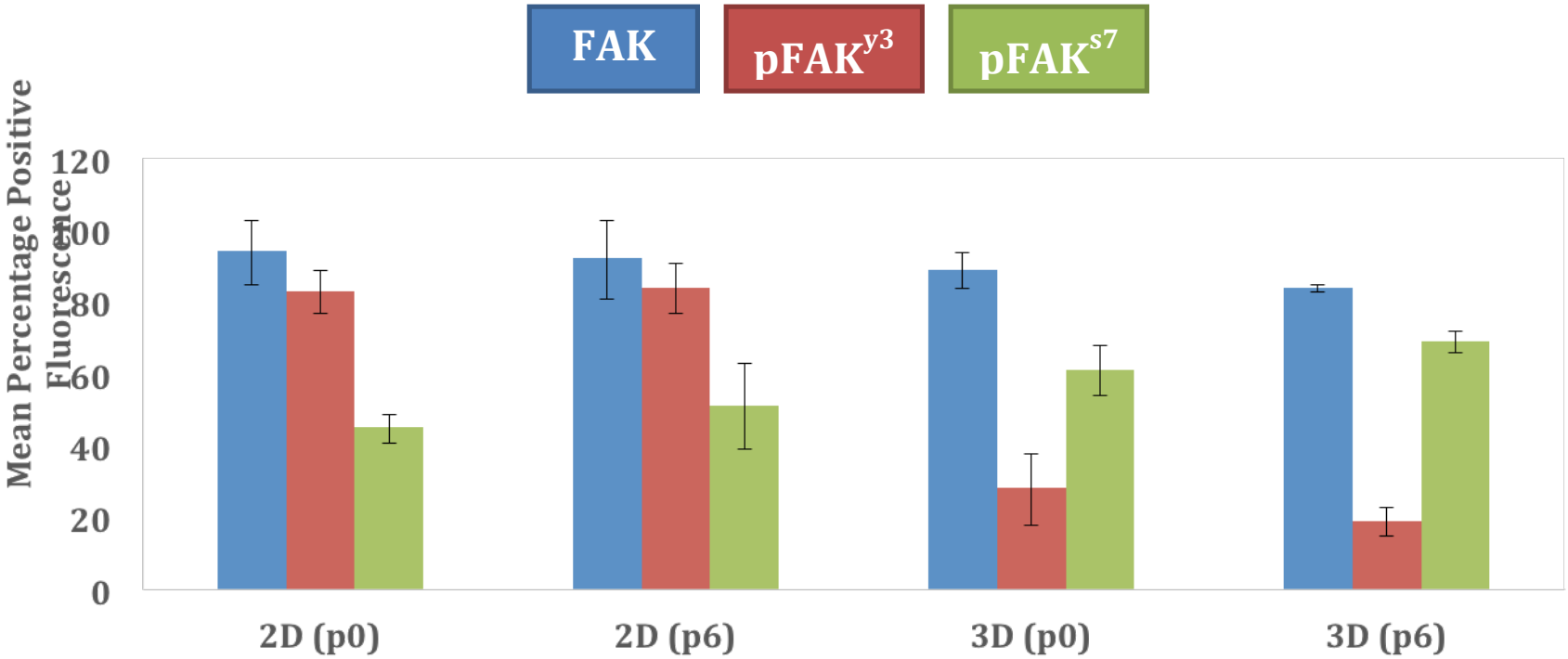

Figure 6.13 Focal Adhesion Kinase has several phosphorylation sites which allow it to regulate various protein-protein interactions

Cells from pre-passage(p0) and post-passage (p6) in 2D and 3D were incubated with antibodies against total FAK, and two differently phosphorylated forms – Y397, the activation site, and S732, a site posited to be activated by ROCK. The samples were then analysed using flow cytometry. As shown above, levels of total FAK remain consistent across samples. 2D cells show high levels of Y397 phosphorylation and relatively low levels of S732 phosphorylation whereas this pattern is reversed in 3D cells. Additionally, the decrease in Y397 expression and increase in S732 expression are both amplified as cells are maintained for longer in 3D, indicating that this change in phosphorylation plays a role in cell adaptation to a novel micro-environment. Data presented as n=3 ± SEM

To test whether the increased pFAK^{S732} phosphorylation seen in 3D is a direct response of increased phosphorylated by ROCK, cells from 2D and 3D populations were treated with a commercial and potent inhibitor of ROCK kinase activity, Y26732 in a dose-dependent manner. As seen in Figure 6.14, with 2D maintained cells, even doses of 10μM Y26732 had no effect on either FAK total expression or FAK^{Y397}, but caused a predictable decrease in pFAK^{S732} levels, confirming that the inhibitor is effective in targeting this phosphorylation event. However, with the 3D maintained cells, as the levels of pFAK^{S732} decrease due to inhibition of ROCK activity, the levels of pFAK^{Y397} begin to increase. This effect is slightly more pronounced at a later passage point. This finding is interesting because it suggests that phosphorylation of FAK at these two sites is reciprocal – an increase in the phosphorylation at one site suppresses phosphorylation at the other site. This dynamism may allow the cell to actively adapt state depending on the geometry of the cell within its environment.

To support the findings of the flow cytometric analysis, 3D cells were treated with increasing doses of Y26732 and then stained with an antibody against pFAK^{Y397} to determine whether the recovery suggested by previous data could be visualised with immunocytochemistry (Figure 6.15). The expression levels were quantified by counting positive FAs in several randomly chosen sections of each cell. To assess the degree of recovery, an untreated 2D cell was also imaged and the degree of pFAK^{Y397} expression quantified. As Figure 6.15 shows, there is a dose-dependent increase in the expression of pFAK^{Y397}, an effect that, at the highest dose of 10μM, leads to a 54.6% recovery of expression, with 100% being represented by the density value of the 2D cell shown. This indicates a probable causal link between the activity of ROCK and phosphorylation of the Y397 site, and provides a potential mechanistic link to cytoskeletal organisation.

As a further validation step for this characterisation of differences in the expression levels of pFAKY397 after ROCK inhibition, the two methodologies of assessing the degree of expression (flow cytometry and immunocytochemistry/FA counting), the results from both were plotted side by side (Figure 6.16). As expected, the two methodologies provide the same information, and show roughly the same trends

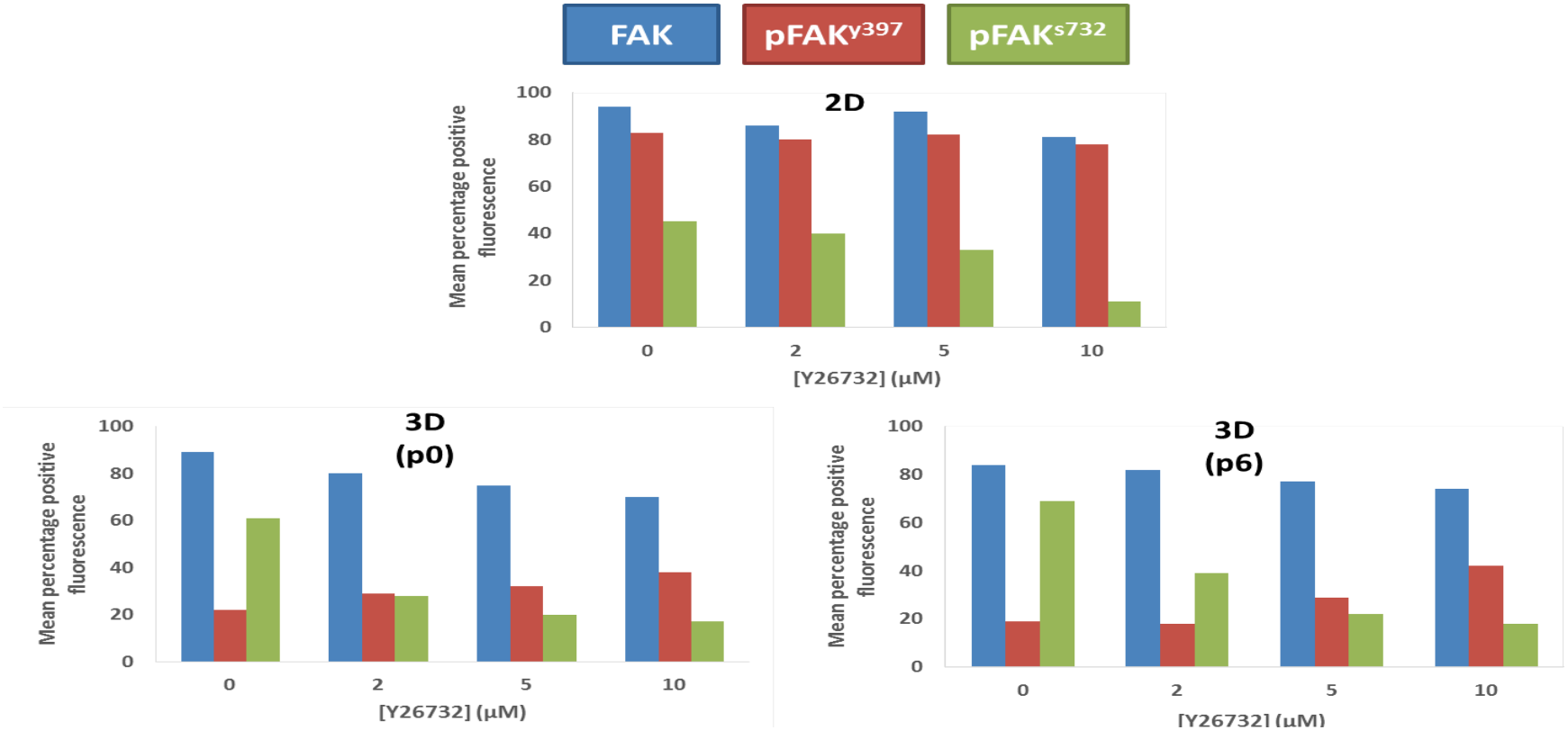

Figure 6.14 Inhibition of ROCK leads to reduced phosphorylation at the S732 site and recovery of phosphorylation at the Y397 site in 3D cells

Cells at low and high passage in 3D, as well as 2D controls, were treated for 24 hours with increasing doses of Y26732, a commercially available ROCK inhibitor to see whether a resultant decrease in phosphorylation at the ROCK activation site S732 would result in concomitant recovery of phosphorylation at Y397. The levels of FAK in either its unphosphorylated, Ser732 or Tyr397 phosphorylation states were determined using flow cytometry. Treatment with even the highest dose tested had little effect on the 2D cells other than to predictably decrease S732 phosphorylation in a dose-dependent manner. In the 3D cells there is clear recovery of Y397 expression that correlates well with the reduction in S732 expression. These results would suggest that these two sites are alternatively phosphorylated depending on the geometric state of the cell.

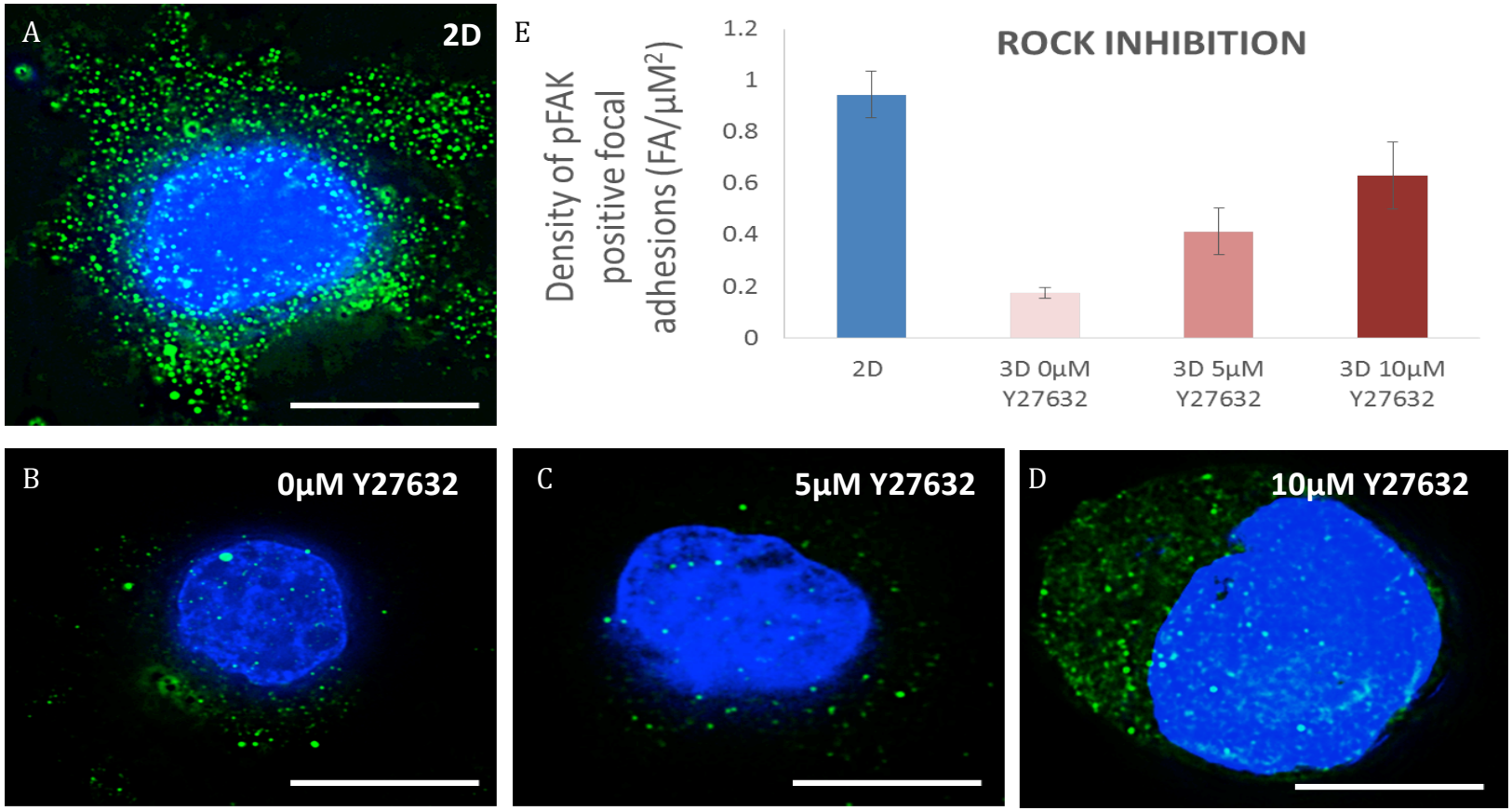

Figure 6.15 Inhibition of ROCK and thus FAK^{S732} phosphorylation results in an increased expression of pFAK^{y397}

3D maintained cells (B-D), as well as 2D controls (A), were treated with increasing doses of Y27632 to inhibit ROCK activation of the S732 phosphorylation site on FAK. They were then fixed and stained with an antibody against Y397. As the dose of the inhibitor increased, so did the expression of Y397, as quantified in (E). Scale bars = 10μm. Data presented as n=5 ± SEM.

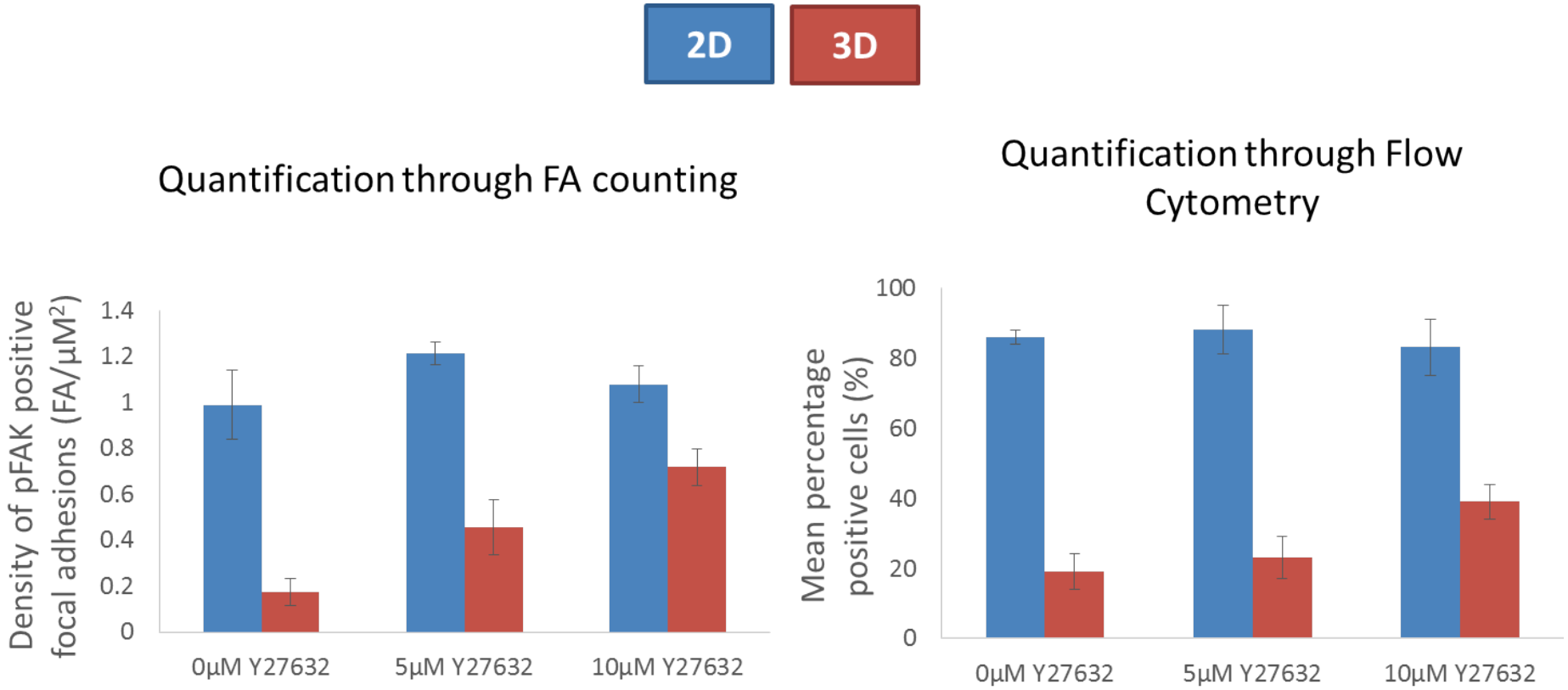

Figure 6.16 The trends seen through counting focal adhesions can be validated using flow cytometry

In order to validate the accuracy of the trends seen in Figs 6.12 and 6.13, cells treated with increasing doses of Y27632 were incubated with an antibody against Y397 and analysed using flow cytometry. As is clear from the above graphs, the patterns produced from both methodologies show close similarity to one another. Data presented as n=3 ± SEM.

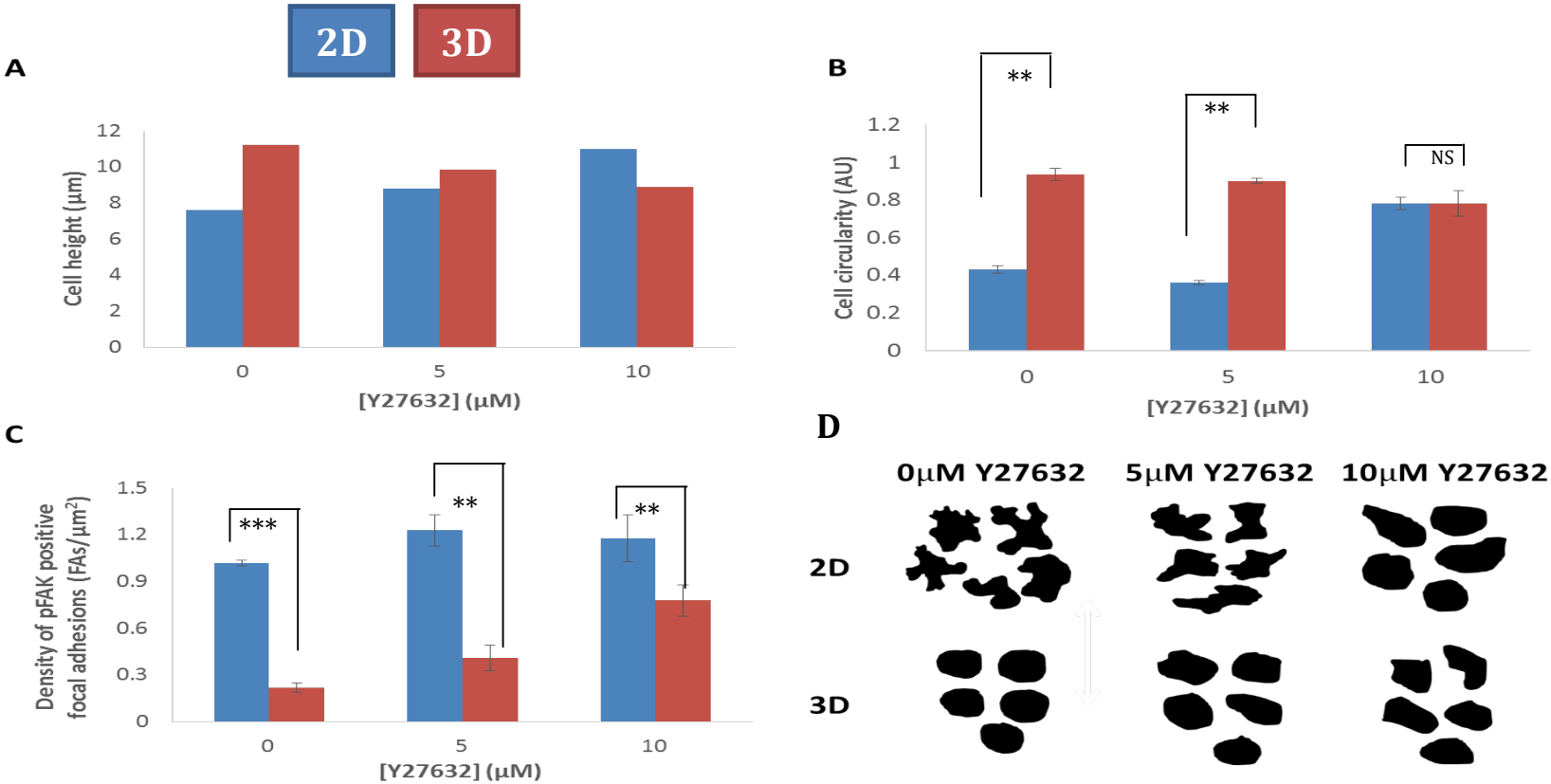

Figure 6.17 Inhibition of FAK^{S732} phosphorylation and resultant increase in pFAK^{Y397} expression leads to adoption of a more 2D like morphology in 3D cells.

3D cells treated with Y27632 show an increase in pFAK^{Y397}-positive focal adhesions (C), and in line with this, the cells become less rounded. This can be seen through the cell outlines in D and quantified using circularity measurements in Image J (B). The cells also flatten slightly (A). These results indicate that cell shape is probably linked to the phosphorylation state of FAK. Data presented as n=1 (A) or n=3 ± SEM (B&C). Statistical analysis through ANOVA. NS denotes non-significant, ** denotes P= ≤ 0.01; *** denotes P= ≤ 0.001.

As mentioned earlier, ROCK is a serine-threonine kinase that acts on the cytoskeleton to regulate the shape and movement of cells. Since the previous set of data provided a mechanism for its involvement in controlling differences in focal adhesion kinetics brought about by 3D propagation, it stands to reason that inhibiting ROCK will have an effect on cellular morphology and control changes in shape due to changes in the topology of the microenvironment. To study this, 2D and 3D cells were treated with increasing doses of Y27632, fixed and imaged to assess cell shape parameters (Figure 6.17). In terms of height, as the degree of ROCK inhibition increases, 3D cells flatten more and become less circular, as indicated in the cellular outlines in Figure 6.16D. This suggests a reversion to a more 2D-like phenotype. This is supported by the increase in $pFAK^{Y397}$. However, surprisingly, there is a slight increase in $pFAK^{Y397}$ in 2D maintained cells as well, but this is matched with an increase in height and circularity. One possible explanation for this is that there is further feedback involved in this pathway, possibly from another signalling pathway that shares a degree of redundancy with adhesion signalling. However, further work would have to be done to see if this is indeed the case, and if so, how this pathway is involved. Another factor may the role that ROCK plays in the formation of stress fibres. Inhibiting ROCK kinase not only reduced the phosphorylation of FAK on S732, it also inhibits the formation of new stress fibres, and at higher doses this may be enough to reduce aberrantly exaggerated adhesion to the planar growth substrate in 2D cells, allowing them to flatten less and maintain a rounder phenotype.

6.5.5. Investigating changes in cell adhesion molecules between 2D and 3D cells

Previous experiments in this Chapter have focused on events that follow cell adhesion, however there may be equally significant changes in the adhesion event itself between 2D and 3D maintained cells. Cells adhere both to each other and their ECM through a variety of cell adhesion molecules (CAMs); one of the most important of these is the integrin family. Integrins are important in any discussion of adhesion sites since it is integrin engagement with ECM ligands that initiates the building of FAs. They also add an extra level of complexity, since there are over 20 different individual integrin receptors, each of which not only engages with a different ligand, but also contains different binding sites for adhesome proteins [97]. It is this complexity that allows cells to dynamically adapt to their microenvironment, and as such it is likely that the change in geometry brought about by 3D

propagation is translated in part through a change in integrin expression and/or binding avidity

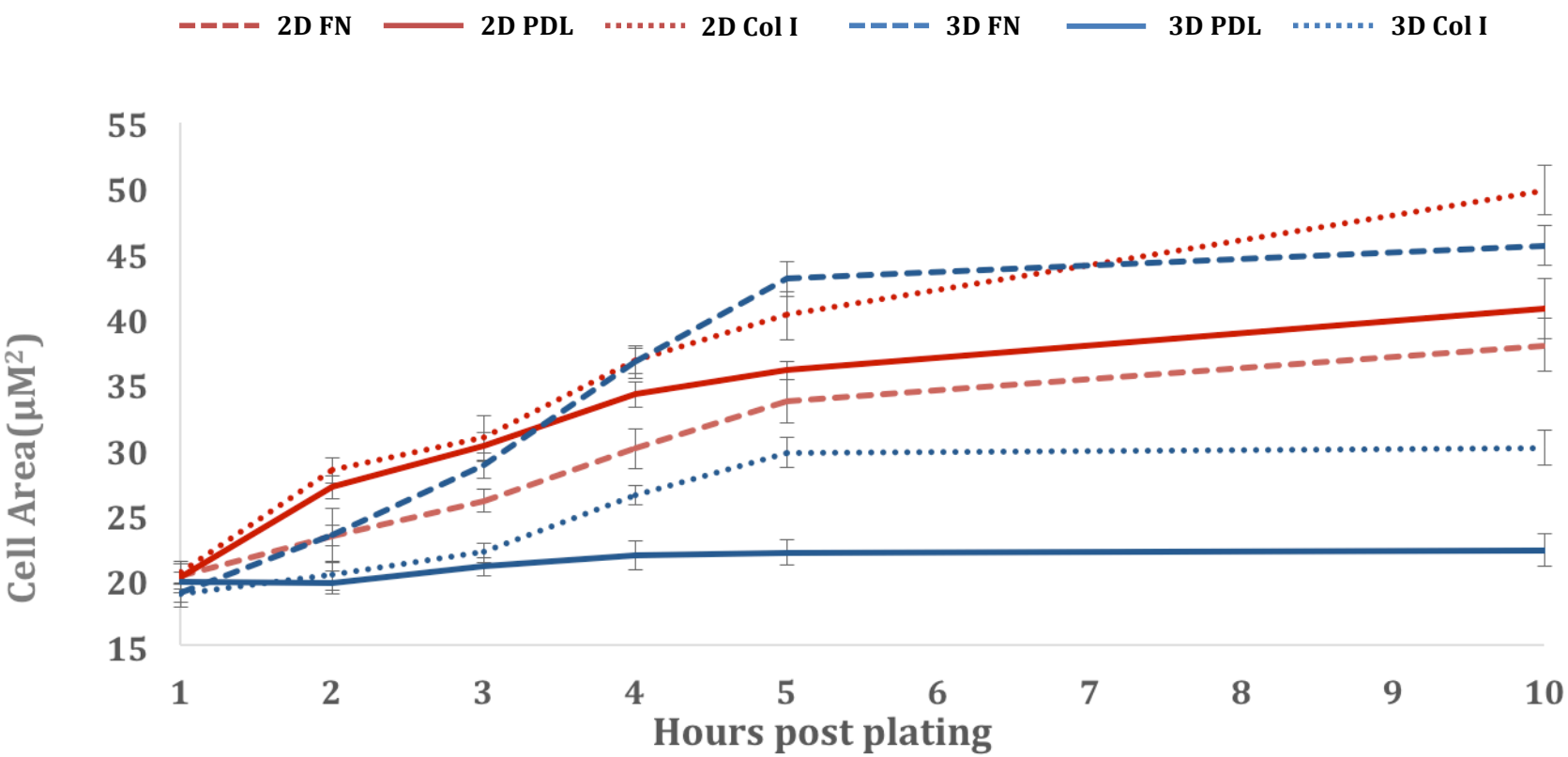

Figure 6.18 Cells maintained in 2D and 3D show different flattening rates when grown on coverslips coated with different ECM ligands.

Cells maintained in 2D and 3D for 4 passages were grown on coverslips coated either with PDL, as an inert control, or collagen I or fibronectin (FN) as ECM components. Cells were allowed to flatten for 10 hours and the cell size monitored as a measure of flattening rate. Since flattening requires cell-substratum interaction, this was taken to be indicative of cell membrane-ligand adhesion strength. Results showed that 2D maintained cells adhere stronger to collagen coated surfaces whereas 3D maintained cells adhere stronger to fibronectin coated surfaces. Data presented as n=3 ± SEM.

To investigate this hypothesis, 2D and 3D maintained cells were seeded onto coverslips coated with either one of two ECM ligands, fibronectin (FN) or Collagen I (Col I), or a synthetic control (PDL) and allowed to flatten for 10 hours. Flattening (measured by an increase in cell area) was taken as an indication of adhesion to the substrate and thus enhanced flattening would mean enhanced integrin avidity. Figure 6.18, shows major differences in integrin avidity between 2D and 3D. Considering attachment to PDL as a control level of attachment, 2D cells appear to flatten more, and thus engage more with a collagen-rich environment; they flatten less, and thus engage less, with a FN-rich environment. In control, 3D cells attach to a greater extent with both FN and collagen, but they show drastically higher engagement with a FN-rich environment when compared to collagen. Since different ECM proteins bind preferentially to different integrins, this could suggest that the cell surface of 2D and 3D cells show different integrin profiles. This would need to be investigated further using specific integrin markers to be certain of this hypothesis though.

Since 2D cells preferentially adhere to collagen-rich substrates and 3D cells preferentially adhere to FN-rich substrates, an integrin known to bind preferentially to each substrate was chosen: αvβ3, though originally discovered as a vitronectin receptor, has been shown to show high affinity for collagen I especially in liver cells [232], and α5β1 is a canonical FN receptor found in high levels within the human liver [233]. Cells maintained in 2D and 3D before (p0) and after (p3) propagation were probed with antibodies against both integrins (Figure 6.19). Fitting in with the findings from the adhesion study, 2D cells before propagation show a higher degree of αvβ3 expression, and a lower degree of α5β1 expression; a pattern almost exactly mirrored by 3D cells. The relative expression levels in 2D cells does not change after 3 passages in 2D culture, but after 3D propagation, 3D cells show an increase in α5β1 and a slight decrease in αvβ3. This last finding is important to note because it indicates that 3D propagation specifically (as opposed to short-term 3D culture) may be responsible for a shift in integrin expression. It is also worth noting that the error bars in this particular set of experiments are particularly high, and the cells show a large degree of intra-sample variability. This may signify a temporal dynamism in integrin expression – cells are constantly trafficking different integrins to the cell surface, and there is a large degree of redundancy amongst different integrin subunits. However, the overall picture shows a clear trend towards an increase in the expression of α5β1 upon 3D propagation.

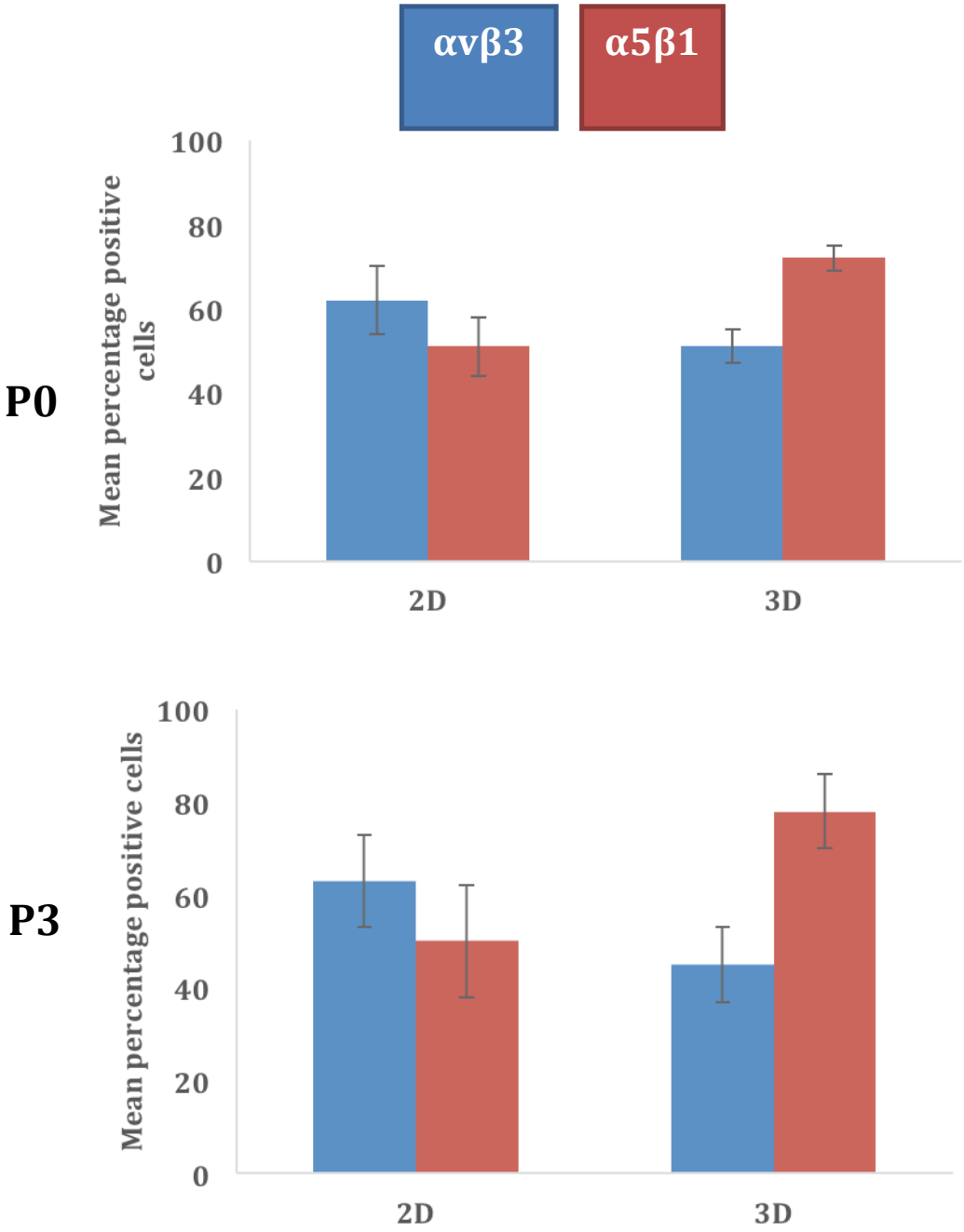

Figure 6.18 Cells maintained in 2D and 3D express different integrins on the cell surface

Cells were grown in 2D or 3D conditions for either 4 days (P0) or 3 passages (P3) and then incubated with antibodies against 2 common integrins found on hepatocytes – α5β1 or αvβ3. The cells were then analysed using flow cytometry. Cells maintained in 2D show higher expression of αvβ3, whereas cells maintained in 3D show higher expression of α5β1. Data presented as n=3 ± SEM. All data deemed non significant after ANOVA.

Cells from 2D and 3D maintained populations were seeded onto glass coverslips and stained with antibodies against both integrins to see if there was a visible difference in the distribution or size of integrin clusters in line with 3D propagation. As Figure 6.20 shows, there is only a slight difference between α5β1 expression between 2D and 3D cells at low passage, with the 3D cells showing slightly higher expression, though this is not statistically significant. There does not appear to be a different in the distribution or size of the adhesion sites though. After several passages propagation, the difference in expression levels is enhanced, and there is an upregulation in the expression of α5β1 in 3D cells compared to 2D cells. The adhesions also seem to be localised mainly to the membranal zone of the cell in 3D cells, but is more evenly distributed across the 2D cells. Integrin expression would not normally be expected within the cytoplasm, since they are membrane-associated proteins. However, the proteins themselves are trafficked to the membrane in vesicles, which remain associated with cytoplasmic volume where they are targeted for ubiquitin-mediated degradation when not needed. Thus a higher degree of membrane expression would suggest active trafficking of the integrin molecules away from the nucleus, to their active location at the cell surface, and a higher degree of cytoplasmic expression would conversely suggest that the integrins are not required for surface signalling. In this manner, the relatively high membrane distribution in 3D cells indicates that 3D propagation is promoting trafficking of the α5β1 integrin to the membrane.

The differences between 2D and 3D maintained cells are more significant when looking at αvβ3 (Figure 6.21). Even at passage 3, it is clear that there is a higher degree of expression for αvβ3 in the 2D cells, and only nominal staining in the 3D cells This difference is maintained through till passage 6, but does not show the same amplification with propagation as seen with α5β1. This would suggest that the down-regulation of αvβ3 occurs at an earlier time point in the adaptation process than α5β1, and this in turn could indicate that the trafficking of αvβ3 away from the nucleus in response to the cell sensing a 3D environment acts as a cue for the up-regulation/ trafficking of α5β1 to the membrane.

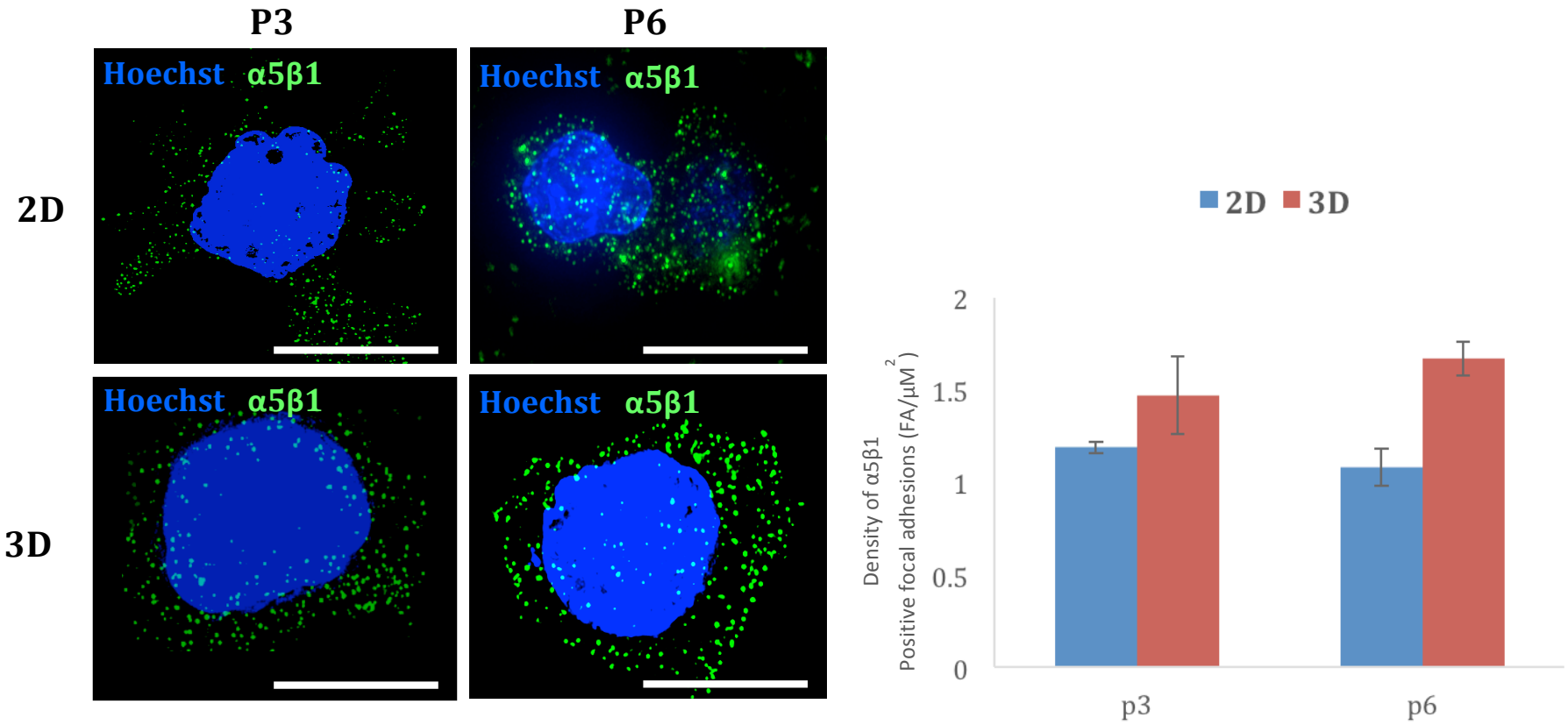

Figure 6.20 Cells increase their expression of α5β1 the longer they are maintained in 3D conditions

Cells were maintained in 2D and 3D for 3 or 6 passages and then plated onto PDL-coated glass coverslips and imaged at super resolution using Structured Illumination Microscopy (SIM) to allow visualisation of individual cells and adhesion sites. Cells in 2D and 3D show significantly different expression patterns of α5β1, with 3D cells showing more positive staining. This difference becomes amplified as cells are passaged longer in 3D. This staining was quantified by counting the number of positively stained adhesions (green dots) and normalising this to cell area quantified using ImageJ. Scale bars = 10μm. Data presented as n=5 ± SEM. Data found to be non significant.

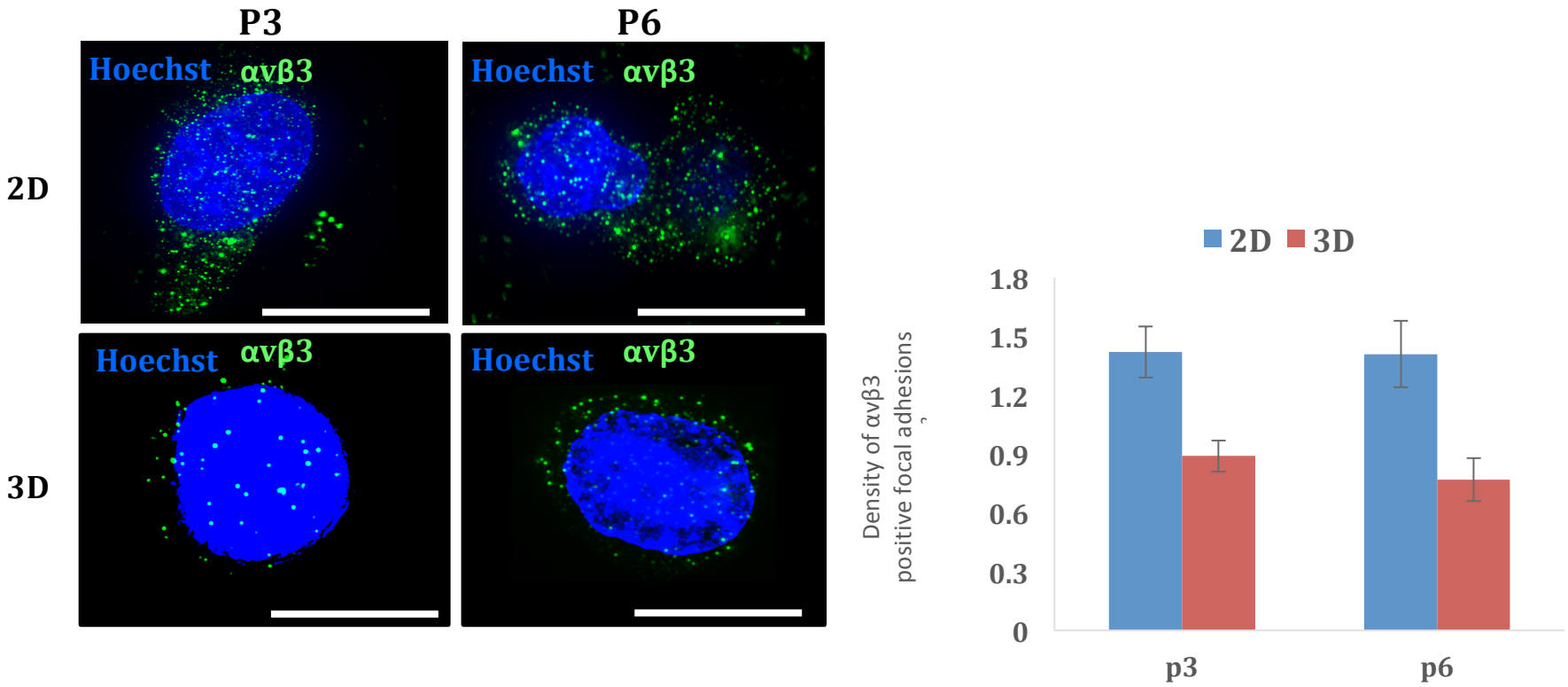

Figure 6.21 Cells decrease their expression of αvβ3 the longer they are maintained in 3D conditions

Cells were maintained in 2D and 3D for 3 or 6 passages and then plated onto PDL-coated glass coverslips and imaged at super resolution using Structured Illumination Microscopy (SIM) to allow visualisation of individual cells and adhesion sites. Cells in 2D and 3D show significantly different expression patterns of αvβ3, with 2D cells showing more positive staining. This difference appears to be independent of the time cells are maintained in 3D. This staining was quantified by counting the number of positively stained adhesions (green dots) and normalising this to cell area quantified using ImageJ. Scale bars = 10µm. Data presented as n=5 ± SEM

To test whether the increased trafficking and clustering of α5β1 plays a causal role in the changes in pFAK expression seen in 3D cell culture, a blocking antibody was used to neutralise integrin activity (Figure 6.22). As with the ROCK inhibition assay (Figure 6.15), 3D cells were exposed to increasing doses of the blocking antibody in order to test for a dose-dependent effect on pFAK staining. Expression patterns were compared back to a control 2D cell in order to estimate recovery of $pFAK^{Y397}$ expression. As expected, at low doses of the blocking antibody, α5β1 activity is still sufficient to suppress auto-phosphorylation of FAK. However, at the highest dose tested, 10μM, there is a drastic increase in positive pFAK staining. Compared to the 2D control, this dose of α5β1 blocking antibody resulted in almost 80% recovery. This indicates a strong role for integrins in controlling the degree of pFAK expression. Since earlier data has shown that abolishing $pFAK^{Y397}$ staining leads to the adoption of a 3D phenotype, in terms of cell flattening, and circularity, the working hypothesis based on this data was that by blocking α5β1, and recovering pFAK expression, one could manipulate 3D cells into reverting to a 2D morphology. To test this, cells maintained in 2D and 3D were treated with a range of doses of α5β1 blocking antibody and then imaged in order to quantify cell parameters.

In terms of height, as the degree of α5β1 suppression increases, 3D cells flatten and become less circular, as indicated in the cellular outlines in Figure 6.23D. This suggests a reversion to a more 2D-like phenotype. This is supported by the increase in $pFAK^{Y397}$. However, surprisingly, there is a slight increase in $pFAK^{Y397}$ in 2D maintained cells as well, but this is matched with an increase in height and circularity. This could indicate that there is further feedback involved in this pathway, possibly from another signalling pathway that shares a degree of redundancy with adhesion signalling. Another factor in play could be the redundancy of integrin expression. Since the family is so diverse, there is often a heterogeneous mix of integrins expressed on an individual cell surface, and each of these triggers intracellular signalling. There is a degree of overlap between these pathways and this could explain this data.

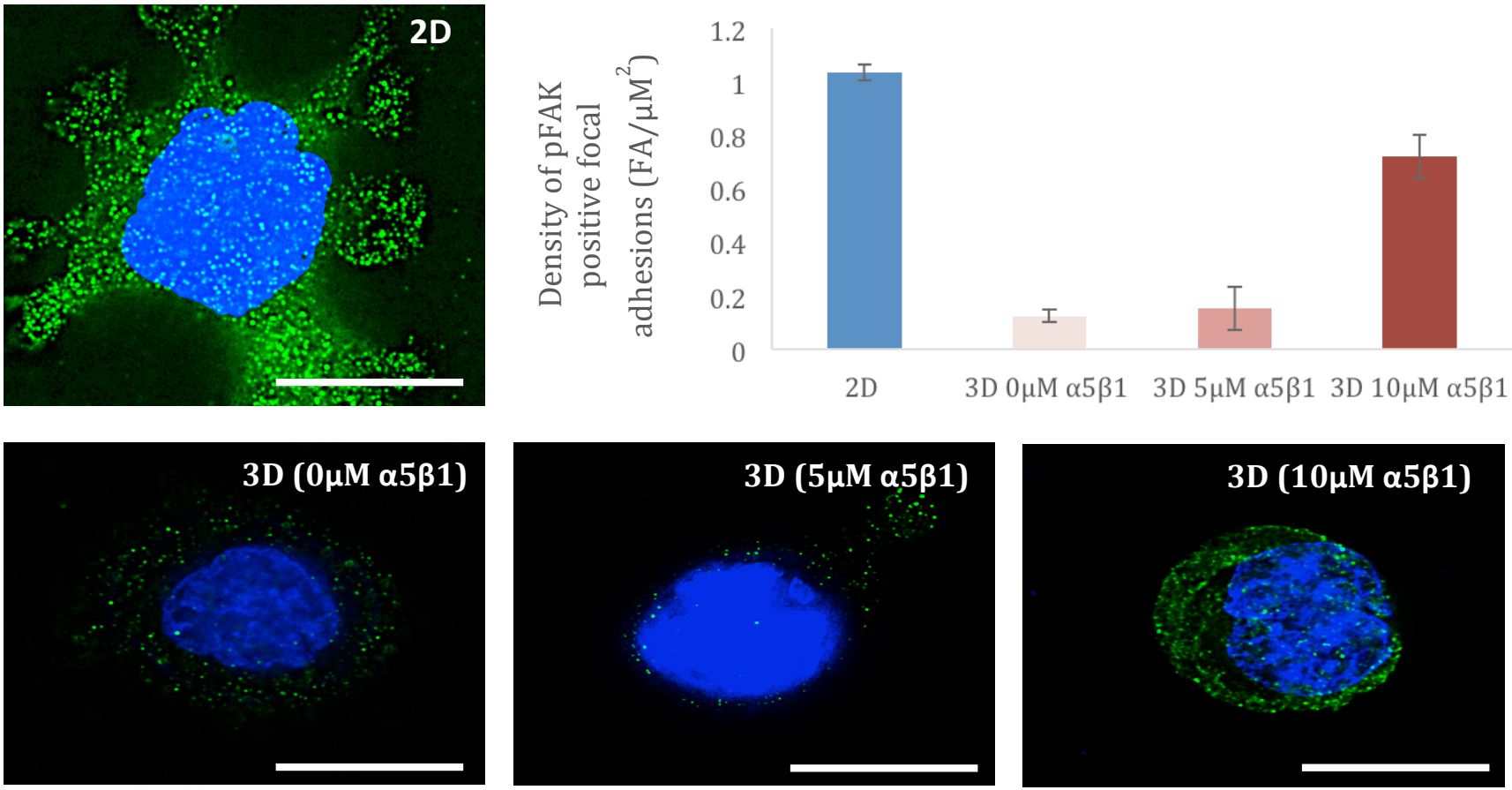

Figure 6.22 Blockade of α5β1 activity results in an increased expression of pFAK^{Y397}

3D maintained cells at passage 4, as well as 2D controls, were treated with increasing doses of a blocking antibody against α5β1 to see if this would lead to a reversion to 2D-like pFAK signalling patterns, and thus recovery of Y397 phosphorylation. As the dose of the blocking antibody increased, so did the expression of Y397 in 3D cells that had previously shown very little positive pFAK staining. Scale bars = 10μm. Data presented as n=5 ± SEM.

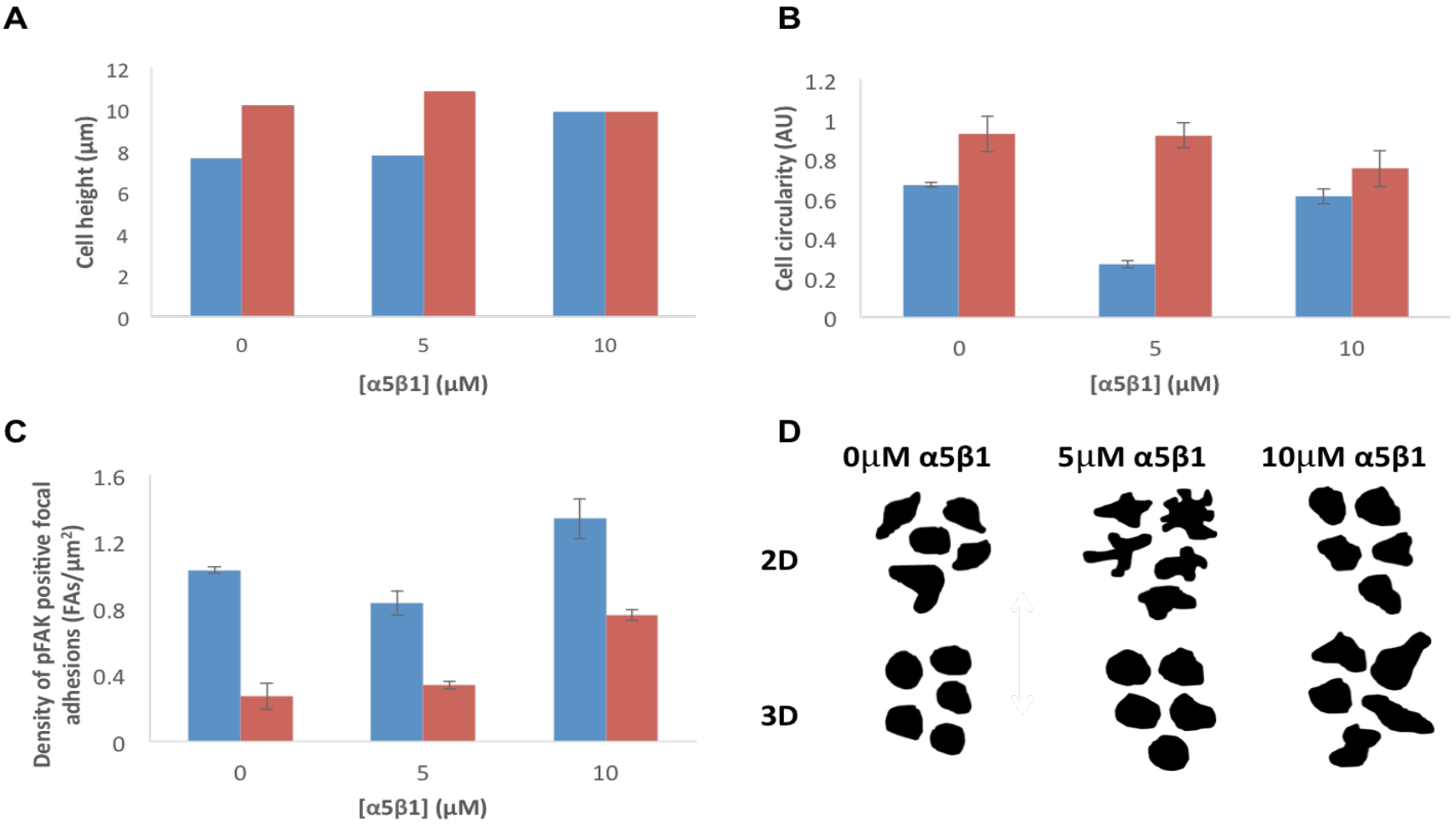
A
Cell height (μm)
12
10
8
6
4
2
0
0
5
10
[α5β1] (μM)
B
Cell circularity (AU)
1.2
1
0.8
0.6
0.4
0.2
0
0
5
10
[α5β1] (μM)
C
Density of pFAK positive focal adhesions (FAs/μm²)
1.6
1.2
0.8
0.4
0
0
5
10
[α5β1] (μM)
D
0μM α5β1
5μM α5β1
10μM α5β1
2D
3D

Figure 6.23 Blocking α5β1 activity results in recovery of pFAK expression, and a concurrent reversion to 2D morphology in 3D maintained cells

3D cells at passage 4 were treated with a blocking antibody against α5β1 show an increase in $pFAK^{Y397}$-positive focal adhesions (C), and in line with this, the cells become less rounded. This can be seen through the cell outlines in D and quantified using circularity measurements in Image J (B). The cells also flatten slightly (A). These results indicate that cell shape is tightly and dynamically linked to the phosphorylation state of FAK. Data presented as n=1 (A) or n=3 ± SEM (B&C). Statistical analysis through ANOVA. NS denotes non-significant, * denotes P= ≤ 0.05, ** denotes P= ≤ 0.01; *** denotes P= ≤ 0.001.

Since integrins are heterodimers, it is possible that the differences seen between 2D and 3D maintained cells could be due to a single monmeric subunit. Since the focus of this work is on adhesion signalling, it would make sense for the β subunit to be responsible for the differences seen thus far, since it is the subunit that binds the majority of adhesion signalling molecules. In particular, the β subunit binds paxillin, a vital actin-linker that is a major component of adhesions in both 2D and 3D systems. Earlier experiments in this Chapter showed that there is a slight increase in the expression of paxillin in 3D propagated cells, as compared to 2D controls. In order to see whether β1 expression is also increased in 3D maintained cells, cell lysates from 2D cells, as well 3D early and late passage cells, were probed for antibodies specific to β1 and blotted. The blot was then quantified with densitometry (Figure 6.24).

As this Figure shows, there does appear to be an increase in β1 subunit expression in 3D cells when compared to 2D controls. Surprisingly though, this difference is reduced with further 3D propagation. This could indicate that the increase in β1 is involved in active adaptation to a changin microenvironment, but that once cells have adapted fully and are no longer under stress, that the integrin changes stabilise. It is worth noting that this experiment was not replicated and so this finding is a trend that deserves further work before any conclusions can be reliably drawn.

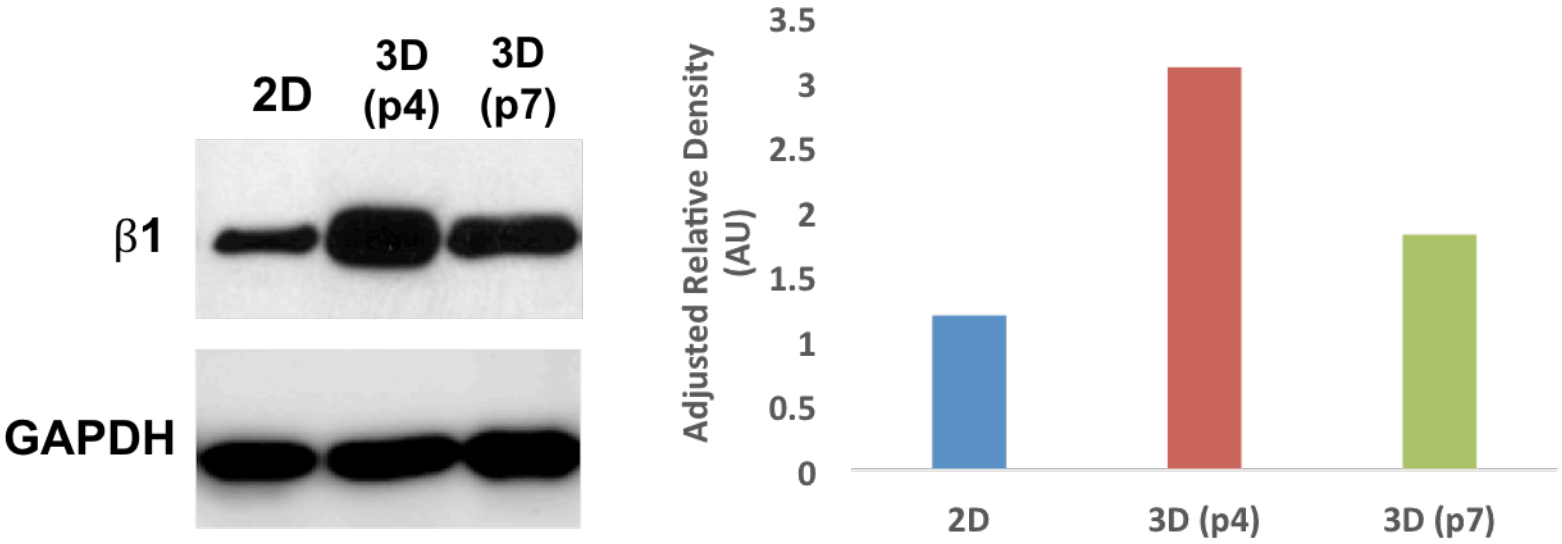

Figure 6.24 Cells maintained in 3D show higher levels of β1 subunit expression

The differences in integrin expression seen in 2D and 3D maintained cells were confirmed using western blotting, and quantified using densitometry calculations in ImageJ software. Cells maintained in 3D show increase expression of the β1 integrin subunit.

6.6 Discussion

This Chapter aimed to explore the differences in adhesion signalling between 2D and 3D propagated cells with the hypothesis that this signalling pathway was pivotal in the adapation cells undergo in 3D culture systems.

Data in this Chapter showed that 3D propagated cells show different signalling patterns at FACs compared to 2D maintained counterparts. There appears to be a significant reduction in the expression of the autophosphorylated form of FAK in 3D cells, as well as an increase in the actin linker protein Paxillin. This reduction in FAK phosphorylation on the Y397 residue has previously been reported in a variety of 3D systems including collagen gels [234] and hydrogels [127]. This discrepancy in signaling in 2D versus 3D contexts is specific to the FAK level of adhesion formation since paxillin has been shown to be equally phosphorylated at tyrosine 31 in both 3D-matrix adhesions and focal adhesions [235]. Differences in adhesion signaling processes have also been reported in cells suspended in relaxed 3D collagen gels when compared to 2D cultures [236-238], or under different loading conditions in mechanically-contracted collagen gels [239,240]. The important take-home message from these studies is that investigation of adhesion signaling in monolayer culture may lead to misleading observations: cells appear to display different signaling responses when they exist in 3D microenvironments that mimic *in vivo* conditions more closely. Future studies of cell interactions with extracellular matrix and signal transduction should therefore be conducted in advanced 3D models, especially if these interactions are in the context of hepatocyte culture given the importance of accuracy in preclinical testing.

Focal adhesions are most commonly visualized in 3D using immunofluorescence staining [244]. By this method, several groups have reported the existence of focal adhesions in metastatic human breast cancer cell line, MDA-MB-231, either cultured in Matrigel [245] or type I collagen matrix [246]. However, one major limitation of imaging focal adhesions in live cells in 3D culture is background fluorescence [241]. Having saturated all available association sites, excess fusion proteins accumulate in the cytoplasm resulting in diffuse background signal. In cells on 2D substrates, this cytoplasmic background is less misleading because of the thinness of the lamellae in migrating cells. Moreover, background fluorescence can be reduced in 2D studies by using TIRF (total internal reflection fluorescence) microscopy, which excludes fluorescence above approximately 100 nm from

the substrate. In contrast, cellular protrusions formed on 3D matrices may be thicker [242] and must therefore be visualized using wide-field, confocal or multi-photon microscopy, all of which section a minimum thickness of 500–800 nm [243] Therefore, overexpression of an adhesion-specific fluorescently tagged protein can be more detrimental to imaging in 3D than in 2D and result in diffuse cytoplasmic fluorescence that masks the signal of molecules localized to adhesions. However, imaging of adhesions in 3D can be optimised by strict fixation and processing protocols as well as the use of advanced high-resolution imaging such as TIRF and SIM.

The findings of this Chpater appear to point to a significant role for FAK as a decision point for cells, in terms of the convergence of biomechanical cues. In particular, it appears as though the lack of autophosphorylation of FAK is a signal to the cell of a novel microenvironment. This could then be the molecular switch that then allows the cell to adopt a more functional 3D phenotype. Indeed, this suggestion is supported by other researchers in the field. Li and colleagues [234] suggest that decreased cell spreading and consequent lack of autophosphorylation of FAK lead to the up-regulation of p21, and this may be responsible for the lower proliferation rate in 3D cultured cells often reported inliterature, and found in Chapter 3. They go further to also suggest that FAK may function as a molecular switch between the cell proliferation and matrix synthesis phenotypes i.e. that the decrease of autophosphorylation of FAK in 3D matrices decreases cell proliferation and increases collagen synthesis. This is an interesting finding that correlates well with some of the findings of this thesis and could be a potential avenue for future work.

As well as looking at FAK phosphorylation, this Chapter also explored changes in integrin expression. Cukierman [106] suggested that 2D and 3D adhesion matrices differ not only in the phosphorylation state of FAK, but also in the predominnant integrin expressed in mature adhesions. This paper suggested that while αvβ3 is expressed preferentially in 2D focal adhesions, 3D adhesions more closely resemble fibrillar adhesions in that they often express higher levels of α5β1 at the expense of αvβ3. This is a finding well supported by the data in this Chapter, which found that 3D propagated cells show a higher surface expression of α5β1 and a down-regulated expression of αvβ3 – a pattern almost exactly mirrored in 2D cells. This change appeared to be propagation specific, with the difference in expression levels widening the longer cells were propagated in 3D. Looking more specifically at the indidivual subunits, it appeared from preliminary research that it is the β1

subunit that is increased in 3D propagated cells. Though a comparison with the α5 subunit should be conducted to support this conclusion. The finding of up-regulated β1 correlates well with previous findings of increased Paxillin in 3D cultures. Wozniak [104] showed that Paxillin is recruited to adhesions primarily by the β1 cytoplasmic tail and so it would make sense that an increase in β1 would allow for a denser expression of Paxillin at focal adhesions. Costa and colleagues [247] showed via FRET biosensors that cells lacking β3 integrins, through genetic knockdowns, not only show more invasive behaviour but this can be coupled with reduced activation of FAK via autophosrylation. This paper outlines an invasive phenotype in MDA-MC-231 cells that consists of both an up-regulation β1 integrin and a down-regulation of pFAK, therefore supporting the notion of these two molecular findings being part of a wider mechanism to control the biomechanics of cell interaction with complex ECM environments. However, as of yet, studies into differential integrin expression in 2D and 3D systems are still in their infancy, and the studies that do exist have mostly been focussed on cancer research, and in particular the role of integrins in metastasis. It would be interesting to explore the role of integrin expression specifially in the context of cell moprhogenesis, and the transduction of mechanical cues from complex 3D environments into changes in gene expression.

In the context of this study, and in particular, hepatocyte cell culture, the influence of the cellular environment on cell survival in the presence of cytotoxic agents was noted several decades ago, when it was observed that multicellular spheroids of tumor cells were more resistant to anticancer agents than the corresponding monolayer cultures, and that these differences were not solely due to a compromised ability of the drug to penetrate the spheroids [248] Similar findings have been reported in many different experimental systems [249,250]. Although the exact mechanisms of “cell–cell adhesion-mediated resistance” are still unknown, it has been shown that E-cadherin, a cell–cell adhesion protein, can mediate G1 arrest and increased resistance to xenobiotic-induced apoptosis through increase of the cyclin-dependent kinase inhibitor p27KIP1 [251]. These findings, though not directly related to this research, provide an interesting context for the importance of establishing the role of integrin-mediated adhesion in 3D systems before such systems are routinely used for hepatocyte models in drug discovery and development.

6.7 Conclusions

The following conclusions can be drawn from this Chapter:

- 3D matrix adhesions of HepG2 cells show a different protein composition to adhesion complexes characterised in 2D cells. These differences are:

  ⇒ A reduction in the expression of pFAK – Y397
  ⇒ A slightly elevated level of Paxillin
  ⇒ An increase in the expression of pFAK – S732
  ⇒ An increase in the expression of α5β1 integrin
  ⇒ A decrease in the expression of αvβ3 integrin

- The differences seen in 2D and 3D adhesion complexes is best visualised using SIM microscopy which allows for high resolution imaging of single cells. The findings from immunocytochemistry can be further supported using flow cytometry and Western Blotting, both of which validated the differences outlined above.

- In addition to differences in the expression key signalling molecules, 2D and 3D maintained cells also show different flattening rates on collagen and fibronectin which indicates that the difference in integrin expression seen through immunocytochemistry is also seen on a functional level through changes in the way cells interact with ECM ligands.

- Phosphorylation of pFAK on the autophosphorylation site Y397 can be partially recovered in 3D cells by blocking the function of the α5β1 integrin. This suggests that changes in the expression of integrins may play a causal role in the adapttaion of cells to a 3D microenvironment by regulating the phosphorylation of FAK which in turn modifies the expression and function of actin-linking proteins and through this alters the cytoskeleton.

- This recovery of $pFAK^{Y397}$ can also be seen by inhibiting ROCK, suggesting a role for thr RhoA/ROCK pathway in mediating the phosphorylation of FAK and downstream adhesion signalling.

Chapter 7: Discussion and Future Work

7.1. Discussion

The overarching aim of this project was to determine the mechanism by which cells adapt to the 3D environment, and to assess the impact of long term propagation on this adaptation process in terms of cell moprhology, function and adhesion signalling.

The first set of experiments involved designing and developing a model that would allow for the continual propagation of cells in 3D. To do this, Alvetex®Scaffold and Alvetex®Strata, two highly porous polystyrene scaffolds, were characterised in terms of cell growth and potential cell retrieval. Met4 squamous carcinoma cells were grown on Alvetex®Scaffold and retrived from their encapsulated state using various optimised protocols involving enzymatic dissociation and mechanical agitation. However, these attempts were unsuccessful and so the model was revised to use Alvetex®Strata instead, since the smaller pore size of this material should allow for cells to grow on top rather thran through the matrix. Using this material, HepG2 immortalised hepatocytes were successfully retrieved and subcultured over several generations with maintained viability and physiological proliferation rates.

The second set of experiments used this methodology to propagate cells in parallel in 2D and 3D culture systems for 2 months. This created two pools of cells that had adapted to either a 2D or 3D environment respectively, allowing direct comparison of cellular morphologies. The data from this chapter showed that 2D and 3D cells show significantly different morphologies, with 3D maintained cells adopting rounder, more spherical morphologies while 2D maintained cells flattened and lost their differentiated hepatic shape. This change in cell shape was associated with a change in intracellular actin distribution, with 2D cells showing a more extensive network of actin stress fibres, mostly adhereing the cell to the substratum, and 3D cells showing fewer distinct stress fibres, with a diffuse cytoplasmic expression of F-Actin. This could be indicative of differences in cytoskeletal tension between the cell populations, and is likely a response of the cell to the artificial rigidity of TCP in monolayers. This Chapter also showed that 3D cells maintained these morphological differences even after being plated in 2D conditions for several hours, before succumbing to the mechanical cues of the substrate and flattening. The maintenance of the morphology for a brief period of time indicates the possibility that 3D propagation could be used to allow hard-wired changes ot occur to cells enabling a ‘priming’ effect. This could be utilised in toxicity studies as part of preclinical

pharmaceutical testing, since it would allow cells to have fully adapted to 3D conditions prior to cytototic attack.

The third set of experiments looked further at this 'priming' effect in the context of enhancing hepatic metabolism and function. Cells from 2D and 3D maintained lineages were placed into aggregates as a secondary 3D model system to test the concept of priming. The results from these experiments indicated that cells can be adapted to a 3D environment which then allows them to adapt quicker and more efficiently to novel microenvironments. Cells propagated in 3D were metabolically more active than their 2D counterparts, and were also more resistent to cytotoxic doses of two different well characterise model drugs. These findings suggested that propagaton in 3D results in changes to the cell beyond moprhology, and based on this, cell lysates from 2D and 3D maintained cells were analysed for genes expressing key metabolic enzymes. Findings showed that there were differences in the expression and inducibility of CYP450 enzymes and a Phase II enzyme called GST-1. These findings taken together show the beneficial use of 3D propagation in maintaining both a differeniated morphology and phenotype of hepatocytes *in vitro* – this could have consequences for the future use of hepatocytes in drug testing.

The final set of experiments looked at a possible mechanistic explanation for the effect of 3D propagation on enhanced hepatocyte function – the Focal Adhesion Kinase pathway. Key differences in this signalling pathway were identified between 2D and 3D maintained cells. Namely, there was a significant decrease in the phosphorylation of FAK on the Y397 residue, a concomittant increase in the phosphorylation of FAK on the S732 reside, a slight increase in the expression of Paxillin, and increased expression of the β1 integrin subunit in 3D adhesions when compared to adhesion complexes in 2D cells. These differences correlate well with the literature, and indicate that adhesion signalling plays a significant role in the adaptation of cells to a novel 3D microenvironment.

The data from this thesis supports the initial hypothesis that hepatocytes propagated in 3D for long culture experiments will show a more physiological morphology, which in turn results in enhanced liver-specific metabolism and function. These changes are

underpinned by changes in adhesion signalling, which provides a potential mechanism by which mechanical cues from the 3D physical microenvironment are translated into *in vivo*-like cell behaviours.

7.2. Future Work

There are several potential avenues for further investigation based on the findings and methodologies developed in this thesis. These include:

1. *Microarray analysis*

   This project touched briefly on the effect of 3D propagation on gene expression in Chapter 5, with Phase I and II metabolic enzymes. These findings, along with the genomic analysis in [136] provide a solid foundation for the concept of 3D culture having a significant effect on the genomic profile of cells. Thus, it would be interesting to conduct a full microarray analysis of cell lysates from different passages in 2D and 3D to characterise the changes in gene expression caused by propagation.

2. *Propagation of other cell types*

   Findings from Chapter 3 showed that there are several cell-types that show potential for propagation by means of their growth and penetration patterns on Strata. This thesis focussed specifically on HepG2s because of their charactertistic shape and functional polarisation, however some of the other cell types that could be appropriate for propagation studies include the MCF-7 carcinoma cell line. Propagation was shown to impact on cell shape, cell migration/penetration and integrin expression - all three of these have strong indications as being important in the progression of cancer, especially in the field of metastasis. Thus, propagation could be used to see how priming cells to a 3D microenvironment prior to migration assays impacts on the observations.

3. *Role of propagation in directed differentiation of iPSCs*

   Another cell type that grows exclusively on top of Strata is the Tera2.sp12 cell line – a stem cell population. This poses a question as to the use of propagation in directing the differentiation of induced pluropotent stem cells (iPSCs). Previous work in this area by other members of the lab group have shown that propagation does have an impact on the expression of several key markers of differentiation. Thus, it could be interesting to see if propagation can be used/modified to direct differentiation of pluripotent stem cells down a chosen lineage.

4. *Nucleotransduction*

While this study focussed on mechanotransduction at the cell membrane, certain findings touched on the important of nucleotransduction/nuclear events. Data from Chapter 4 showed that 3D propagation has an impact on nuclear shape, allowing nuclei to remain spherical. Literature indicates that the shape of the nucleus has improtant consequences for gene expression through controlling chromatin structure and function. Furthermore, it is well characterised that the nucleus is tightly integrated into the structural network of the cell through so-called LINC (linker of the nucleoskeleton and cytoskeleton) complexes, which facilitate the transmission of forces between the nucleus and cytoskeleton [252]. This physical connection between the nucleus and the cytoskeleton is essential for a broad range of cellular functions, including intracellular nuclear movement and positioning, cytoskeletal organization, cell polarization, and cell migration. A recent paper indicated that forces transmitted from the ECM to the nucleus via the cytoskeleton may also directly contribute to the cell's ability to negotiate and adapt to its mechanical environment by triggering force-induced changes in nuclear structures [253]. Thus, propagation could be explored with a focus on the changes that occue to structures on the nuclear lamina such as the lamins.

Chapter 8: References

[1] Xu, R., Boudreau, A. & Bissell, M.J. (2009). Tissue architecture and function: dynamic reciprocity via extra-and intra- cellular matrices. In Cancer Metastasis Reviews, **28(1-2):**167-176

[2] Petersen, O.W., Ronnov-Jessen, L., Howlett, A.R. & Bissell, M.J. (1992). Interaction with basement membrane serves to rapidly distinguish growth and differentiation pattern of normal and malignant human breast epithelial cells. In *Proceedings of the National Academy USA,* **89**: 9064-9068

[3] Biolac-Sage, P., Le Bail, B. & Balabaud, C. (2008). Liver and Biliary Tract Histology. In *Textbook Of Hepatology,* Blackwell Publishing Ltd: 9-19

[4] Harrison, R.G. et al. (1907) Observations of the living developing nerve fiber. In *Anatomical Record*, **1**: 116–128

[5] Harrison, R.G. (1910) The outgrowth of the nerve fiber as a mode of protoplasmic movement. In *Journal of Experimental Zoology*, **9**: 787–846

[6] Carrel A., Burrow M.T. (1911). Cultivation of tissues *in vitro* and its technique. In *Journal of Experimental Medicine,* **13**: 387-396

[7] Masters, J.R. (2002). HeLa cells 50 years on: the good, the bad and the ugly. In *Nature Reviews Cancer,* **2:** 315-319

[8] Eagle, H. (1959). Amino acid metabolism in mammalian cell cultures. In *Science,* **130 (3373)**: 432-437

[9] Breslin, S. & O'Driscoll, L. (2013). Three-dimensional cell culture: the missing link in drug discovery. In *Drug Discovery Today*, **18 (5/6):** 240-249

[10] Li F., Vijayasankaran N., Shen A., Kiss R., Amanullah A. (2010). Cell culture processes for monoclonal antibody production. In *MAbs*, **2(5):** 466-477.)

[11] Hughes, J.P., Rees, S., Kalindjian, S.B. & Philpott, K.L. (2011). Principles of early drug discovery. In *British Journal of Pharmacology,* **162(6):** 1239-1249

[12] Arrondeau, J. et al. (2010) Development of anti-cancer drugs. In *Discovery Medicine,* **10:** 355– 362

[13] Hait, W.N. (2010) Anticancer drug development: the grand challenges. In *Nature Reviews Drug Discovery*, **9**, 253–254

[14] Hopkins, A.L. (2008) Network pharmacology: the next paradigm in drug discovery. In *Nature Chemical Biology*, **4:** 682–690

[15] Kola, I. (2008) The state of innovation in drug development. In *Clinical Pharmacology & Ther*apeutics **83**, 227–230

[16] DiMasi, J.A. and Grabowski, H.G. (2007) Economics of new oncology drug development. J. Clin. Oncol. 25, 209–216

[17] Mazzoleni, G. (2009) Modelling tissues in 3D: the next future of pharmaco- toxicology and food research? In *Genes & Nutrition*, **4**, 13–22

[18] Mazzoleni, G. et al. (2009) Modelling tissues in 3D: the next future of pharmaco-toxicology and food research? In *Genes & Nutrition***, 4**, 13–22

[19] Kunz-Schughart, L.A. et al. (2004) The use of 3-D cultures for high-throughput screening: the multicellular spheroid model. In *Journal of Biomolecular Screening***, 9**, 273–285

[20] Bhadriraju, K. and Chen, C.S. (2002) Engineering cellular microenvironments to improve cell-based drug testing. In *Drug Discovery Today* **7**, 612–620

[21] Bissell, M.J. (2003) Tissue architecture: the ultimate regulator of breast epithelial function. In *Current Opinion in Cell Biology* **15**, 753–762;

[22] Weaver, V.M. et al. (1997) Reversion of the malignant phenotype of human breast cells in three-dimensional culture and in vivo by integrin blocking antibodies. In *Journal of Cell Biology*, **137**: 231–245

[23] Debnath, J. and Brugge, J.S. (2005) Modelling glandular epithelial cancers in three-dimensional cultures. In *Nature Reviews Cancer* **5,** 675–688

[24] Yamada, K.M. and Cukierman, E. (2007) Modeling tissue morphogenesis and cancer in 3D. In *Cell* **130**: 601–610

[25] Howlett, A.R., Bailey, N., Damsky, C., Petersen, O.W., & Bissell, M.J. (1995). Cellular growth and survival are mediated by B1 integrins in normal human breast epithelium but not in breast carcinoma. In *Journal of Cell Science,* **108**: 1945-1957

[26] Abbott, A. (2003). Biology's new dimension. In *Nature,* **424**: 870-872

[27] Danen, E.H.J. (2013). Integrin signaling as a cancer drug target. In *ISRN Cell Biology,* 2013: Article ID 135164 (14 pages)

[28] Slamon, D.J., Godolphin, W., Jones, L.A., Holt, J.A., Wong, S.G., Keith, D.E., Levin, W.J., Stuart, S.G., Udove, J. & Ulrich, A. (1989) Studies of the HER-2/neu proto-oncogene in human breast and ovarian cancer. In *Science* **244**, 707–712

[29] Pickl, M. & Ries, C.H. (2008) Comparison of 3D and 2D tumor models reveals enhanced HER2 activation in 3D associated with an increased response to trastuzumab. In *Oncogene* **28,** 461–468

[30] Toh, Y.C., Zhang, C., Zhang, J., Khong, Y.M., Chang, S., Samper, V.D., van Noort, D., Hutmacher, D.W. & Yu, H. (2007) A novel 3D mammalian cell perfusion-culture system in microfluidic channels. In *Lab on a Chip* **7**, 302–309

[31] Tung, Y.C., Hsiao, A.Y., Allen, S.G., Torisawa, Y.S., Ho, M. & Takayama, S. (2011) High-throughput 3D spheroid culture and drug testing using a 384 hanging drop array. In *The Analyst* **136**, 473–478

[32] Li, A.P., Colburn, S.M. & Beck, D.J. (1992). A simplified method for the culturing of primary adult rat and human hepatocytes as multicellular spheroids. In *In Vitro Cellular and Developmental Biology-Animal,* **28**: 673-677

[33] Keller, G.M. (1995). In vitro differentiation of embryonic stem-cells. In *Current opinion in Cell Biology,* **7(6):** 862-869

[34] Takabatake, H., Koide, N. & Tsuji, T. (1991). Encapsulated multicellular spheroids of rat hepatocytes produce albumin and urea in a spouted bed circulating culture systems. In *Artificial Organs,* **15**: 474-480

[35] Yuasa, C., Tomita, Y., Shono, M., Ishimura, K. & Ichihara, A. (1991). Importance of cell-aggregation for expression of liver functions and regeneration demonstrated with primary cultured hepatocytes. In *Journal of Cellular Physiology,* **156:** 522-530

[36] Satai, Y., Yamagami, S. & Nakazawa, K. (2010). Comparative analysis of gene expression in rat liver tissue and monolayer and spheroid cultured hepatocytes. In *Cells, Tissues & Organs,* **191:** 281-288

[37] Tostoes, R.M., Leite, S.B., Serra, M., Jensen, J., Bjorquist, P., Carrondo, M.J.T., Brito, C. & Alves, P.M. (2012). Human liver cell spheroids in extended perfusion bioreactor culture for repeated-dose drug testing. In *Hepatology,* **55**: 1227-1236

[38] Tong, J.Z., Delaguise, P., Furlan, V., Cresteil, T., Bernard, A. & Alvarez, F. (1992). Long term culture of adult rat hepatocyte spheroids. In *Experimental Cell Research,* **200:** 326-332

[39] Kim, J.B. (2005). Three-dimensional tissue culture models in cancer biology. In *Seminars in Cancer Biology,* **15(5):** 365-377

[40] Kim. J.B., Stein, R. & O'Hare, M.J. (2004). Three-dimensional *in vitro* tissue culture models of breast cancer – a review. In *Breast Cancer Research and Treatment,* **85**: 281-291

[41] Kunz-Schughart, L.A. (1999). Multicellular tumor spheroids: intermediates between monolayer culture and *in vivo* tumor. In *Cell Biology International,* **23(3):** 157-161

[42] Lin, R. & Chang, H. (2008). Recent advances in three-dimensional multicellcular spheroid culture for biomedical research. In *Biotechnology Journal,* 3(9-10): 1172-1184

[43] Thoma, C.R., Zimmermann, M., Agarkova, I., Kelm, J.M. & Krev, W. (2014). 3D cell culture systems modeling tumor growth determinants in cancer target discovery. In *Advanced Drug Delivery Research,* **69-70**: 29-41

[44] Horman, S.R., To, J., Orth, A.O., Slawny, N., Cuddihy, M.J. & Caracino, D. (2013). High content analysis of three-dimensional tumor spheroids: investigating signaling pathways using small hairpin RNA. In *Nature Methods,* **10**: application notes

[45] Tostoes, R.M., Leite, S.B., Serra, M., Jensen, J., Bjorquist, P., Carrondo, M.J.T., Brito, C. & Alves, P.M. (2012). Human liver cell spheroids in extended perfusion bioreactor culture for repeated-dose drug testing. In *Hepatology,* **55**: 1227-1236

[46] Panorchan, P., Lee, J.S.H., Kole, T.P., Tseng, Y. & Wirtz, D. (2006). Microrheology and ROCK signaling of human endothelial cells embedded in a 3D matrix. In *Biophysical Journal,* **91(9**): 3499-3507

[47] Tibbitt, M.W. & Anseth, K.S. (2009). Hydrogels as extracellular matrix mimics for 3D cell culture. In *Biotechnology and Bioengineering,* **103(4**): 655-663

[48] Zimmermann, H., Shirley, S.G. & Zimmermann, U. (2007). Alginate-based encapsulation of cells: past, present and future. In *Current Diabetes Report,* **7(4):** 314-320

[49] Weaver, V.M. et al. (1997). Reversion of the malignant phenotype of human breast cells in three-dimensional culture and in vivo by integrin blocking antibodies. In *Journal of Cell Biology*, **137**: 231–245].

[50] Wang, F., Weaver, V.M., Petersen, O.W., Larabell, C.A., Dedhar, S., Briand, O., Lupu, R. & Bissell, M.J. (1998). Reciprocal interactions between beta-1 integrin and epidermal growth factor receptor in three-dimensional basement membrane breast cultures: a difference perspective in epithelial biology. In *Proceedings of the National Academy of Sciences USA,* **95:** 14821-14826

[51] Zhu, J. (2010). Bioactive modification of poly(ethylene glycol) hydrogels for tissue engineering. In *Biomaterials,* **31(17**): 4639-4656

[52] Ise H., Takashima S., Nagaoka M., Ferdous A. & Akaike T (1999). Analysis of cell viability and differential activity of mouse hepatocytes under 3D and 2D culture in agarose gel. In *Biotechnology letters*, **21**:209–213

[53] Shen C, Zhang G, Qiu H & Meng Q. (2006). Acetaminophen-induced hepatotoxicity of gel entrapped rat hepatocytes in hollow fibers. In *Chemico- Biological Interactions* **162:** 53–6

[54] Lu Y, Meng Q, Zhang G & Bei X. (2008). Clozapine-induced hepatotoxicity in rat hepatocytes by gel entrapment and monolayer culture. In *Toxicology In Vitro*, **22**:1754–1760.

[55] Cornwell, D.J. & Smith, D.K. (2015). Expanding the scope of gels: combining polymers with low-molecular-weight gelators to yield modified self-assembling smart materials with high-tech applications. In *Materials Horizons,* **2**: 279-293

[56] Zhang, X.H., Reagen, M.R. & Kaplan, D.L. (2009). Electrospun silk biomaterial scaffolds for regenerative medicine. In *Advanced Drug Delivery Reviews,* **61(12):** 988-1006

[57] Yu, C.C. (2013). Electrospun scaffolds composing of alginate, chitosan, collagen and hydroxyapatite for applying in bone tissue engineering. In *Materials Letters,* **93:** 133-136

[58] Guex, A.G. (2012). Fine-tuning of substrate architecture and surface chemistry promotes muscle tissue development. In *Acta Biomaterialia,* **8(4):** 1481-1489

[59] Zhang, Y.Z. (2005). Electrospinning of gelatin fibers and gelatin/PCL composite fibrous scaffolds. In *Journal of Biomedical Materials Research Part B – Applied Materials,* **72B(1):** 156-165

[60] Kim, K. (2004). Incorporation and controlled release of a hydrophilic antibiotic using poly(lactide-co-glycolide)-based electrospun nanofibrous scaffolds. In *Journal of Controlled Release,* **98(1):** 47-56

[61] Xie, J.W. & Wang, C.H. (2006). Electrospun micro- and nanofibers for sustained delivery of paclitaxel to treat C6 glioma *in vitro*. In *Pharmaceutical Research,* **23(8):** 1817-1826

[62] Chia, K.N., Lim, W.S., Zhang, P.C., Lu, H.F., Wen, J., Ramakrishna, S., Leong, K.W. & Mao, H.Q. (2005). Stable immobilization of rat hepatocyte spheroids on galactosylated nanofiber scaffold. In *Biomaterials,* **26:** 2537-2547

[63] Feng, Z.Q., Chu, X.H., Huang, N.P., Wang, Y.C., Shi, X.L., Ding, Y.T., Gu, Z.Z. (2009). The effect of nanofibrous galactosylated chitosan scaffolds on the formation of rat primary hepatocyte aggregates and the maintenance of liver function. In *Biomaterials,* **30**: 2753-2763

[64] Ghaedi, M., Soleimani, M., Shabani, I., Duan, Y.Y, Lotfi, A.S. (2012). Hepatic differentiation from human mesenchymal stem cells on a novel nanofiber scaffold. In *Cell Molecular Biology Letters,* **17:** 89-106

[65] Sun, T. (2007). Investigation of fibroblast and keratinocyte cell-scaffold interactions using a novel 3D cell culture system. In *Journal of Materials Science-Materials in Medicine,* **18(2):** 321-328

[66] Freed, L.E., Marquis, J.C., Nohria, A., Emmanual, J., Mikos, A.G. & Langer, R. (1993). Neocartilage formation in vitro and in vivo using cells cultured on synthetic biodegradable polymers. In *Journal of Biomedical Materials Research,* **27:** 11-23

[67] Mikos, A.G., Bao, Y., Cima, L.G., Ingber, D.E., Vacanti, J.P. & Langer, R. (2000). Preparation of poly(glycolic acid) bonded fiber structures for cell attachment and transplantation. In *Journal of Biomedical Materials Research,* **27:** 183-189

[68] Ma, P.X. & Choi, J.W. (2001). Biodegradable polymer scaffolds with well-defined interconnected spherical pore network. In *Tissue Engineering,* **7(1):** 23-33

[69] Levenberg, S. (2003). Differentiation of human embryonic stem cells on three-dimensional polymer scaffolds. In *Proceedings of the National Academy of the Sciences USA,* **100(22):** 12741-12746

[70] Bokhari, M., Carnachan, R., Cameron, N.R. & Przyborski, S.A. (2007). Culture of HepG2 liver cells on three dimensional polystyrene scaffolds enhances cell structure and function during toxicological challenge. In *Journal of Anatomy,* **211(4):** 567-576

[71] Carnachan, R.J., Bokhari, M., Przyborski, S.A. & Cameron, N.R. (2006). Tailoring the morphology of emulsion-templated porous polymers. In *Soft Matter,* **2 (7):** 608-616

[72] Maltman, D.J. & Przyborski, S.A. (2010). Developments in three-dimensional cell culture technology aimed at improving the accuracy of *in vitro* analyses. In *Biochemical Society Transactions,* **38(4):** 1072-1075

[73] Hayman, M.W. (2004). Enhanced neurite outgrowth by human neurons grown on solid three-dimensional scaffolds. In *Biochemical & Biophysical Research Communications,* **314(2):** 483-488

[74] Hayman, M.W. (2005). Growth of human stem-cell derived neurons on solid three-dimensional polymers. In *Journal of Biochemical and Biophysical Methods,* **62(3):**231-240

[75] Bokhari, M., Carnachan, R., Cameron, N.R. & Przyborski, S.A. (2007). Novel cell culture device enabling three-dimensional cell growth and improved cell function. In *Biochemical and Biophysical Research Communications,* **354(4):** 1095-1100

[76] Klaunig, J.E., Goldblatt, P.J., Hinton, D.E., Lipsky, M.M., Knipe, S.M. & Trump, B.F. (1982). Morphologic and functional studies of mouse hepatocytes in primary culture. In *The Anatomical Record,* **204(3):** 231-243

[77] Maher, J.J. & Bissell, D.M. (1993). Cell-matrix interactions in liver. In *Seminars in Cell Biology,* **4**: 189-201

[78] Underhill, G.H., Khetani, S.R., Chen, A.A. & Bhatia, S.N. (2009). Tissue engineering of the liver. In *The Liver,* John Wiley & Sons Ltd: 933-953

[79] Braiterman, L.T., & Hubbard, A.L. (2009). Hepatocyte surface polarity: its dynamic maintenance and establishment. In *The Liver,* John Wiley & Sons Ltd, 73-105

[80] Dancygier, H. (2009). Microscopic Anatomy. In *Clinical Hepatology: Principles and Practice of Hepatobiliary Diseases,* Terry Michael Hynds: 15-47

[81] Klassen, C.D. & Watkins, J.B. (1984). Mechanisms of bile formation, hepatic uptake and biliary excretion. In *Pharmacology Reviews,* **36:** 1-67

[82] Leibold, E. & Schwartz, L.R. (1993). Intercellular communication in primary cultures of putative preneoplastic and normal hepatocytes. In *Carcinogenesis,* **14:** 2127-2129

[83] Hamilton, G.A., Jolley, S.L., Gilbert, D., Coon, D.J., Barros, S. & Lecluyse, E.L. (2001). Regulation of cell morphology and cytochrome p450 expression in human hepatocytes by extracellular matric and cell-cell interactions. In *Cell Tissue Research,* **306:** 85-99

[84] Ben-Ze'ev, A., G. S. Robinson, N. L. R. Bucher, & S. R. Farmer. 1988. Cell-cell and cell-matrix interactions differentially regulate the expression of hepatic and cytoskeletal genes in primary cultures of rat hepatocytes. In *Proceedings of the National Academy of the Sciences USA* **85**:2162-2165.

[85] Reid, L. M., M. Narita, M. Fujita, Z. Murray, C. Liverpool, & L. Rosenberg (1986). Matrix and hormonal regulation of differentiation in liver cultures, p. 225-258. In A. Guillouzo and C. Guguen-Guillouzo (ed.), Isolated and cultured hepatocytes. John Libbey Eurotext Ltd., INSERM, Paris, France.

[86] Schuetz, E. G., D. Li, C. J. Omiecinski, U. Muller-Eberhard, H. K. Kleinman, B. Elswick, & P. S. Guzelian. (1988). Regulation of gene expression in adult rat hepatocytes cultured on a basement membrane matrix. In *Journal of Cell Physiology,* **134:** 309-323.

[87] Clayton, D. F., & J. E. Darnell, Jr. (1983). Changes in liver- specific compared to common gene transcription during primary culture of mouse hepatocytes. In *Molecular Cell Biology* **3**:1552-1561.

[88] Weaver, V.M., Lelievre, S., Lakins, J.N., Chrenek, M.A., Jones, J.C., Giancotti, F., Werb, Z.& Bissell, M.J. (2002). Beta4 integrin-dependent formation of polarized three dimensional architecture confers resistance to apoptosis in normal and malignant mammary epithelium. In *Cancer Cell,* **2(3**): 205-216

[89] Meyers, J., Craig, J & Odde, D.J. (2006). Potential for control of signaling pathways via cell size and shape. In *Current Biology,* **16**:1685-1693

[90] Frantz, C., Stewart, K.M. & Weaver, V.M. (2010). The extracellular matrix at a glance. In *Journal of Cell Science,* **123:** 4195-4200

[91] Rozario, T. & DeSimone, D.W. (2010). The extracellular matrix in development and morphogenesis: a dynamic view. In *Developmental Biology,* **341**: 126-140

[92] Wise, S.G. & Weiss, A.S. (2009). Tropoelastin. In *International Journal for Biochemistry and Cell Biology,* **41**: 494-497

[93] Smith, M.L., Gourdon, D., Little, W.C., Kubow, K.E., Eguiluz, R.A., Luna-Morris, S. & Vogel, V. (2007). Force-induced unfolding of fibronectin in the extracellular matrix of living cells. In *PLoS Biology,* **5**: e268

[94] Martinez-Hernandez, A. & Amenta, S. (1993). The hepatic extracellular matrix I. Components and distribution in normal liver [editorial]. In *Virchows Archiv,* **423**:1-11

[95] Rodriguez-Boulan, E. & Nelson, W.J. (1989). Morphogenesis of the polariseed epithelial cell phenotype. In *Science,* **245:** 718-725

[96] Musat, A.I., Sattler, C.A., Sattler, G.L. & Pitot, H.C.(1993). Reestablishment of cell polarity of rat hepatocytes in primary culture. In *Hepatology,* **18**: 198-205

[97] Faull, R.J. & Ginsberg, M.H. (1996). Inside-Out Signalling through integrins. In *Journal of American Society Nephrology*, **7**: 1091-1097

[98] Campbell, I.D. & Humphries, M.J. (2011). Integrin structure, activation and interactions. In *Cold Spring Harbor Perspectives in Biology,* **3**: a004994

[99] Brown, P.J. & Juliano, R.L. (1985). Selective inhibition of fibronectin-mediated adhesion by monoclonal antibodies to a cell surface glycoprotein. In *Science,* **228**: 1448-1451

[100] Carter, W.G., Ryan, M.C. & Gahr, P.F (1991). Epiligrin, a new cell adhesion ligand for integrin α3β1 in epithelial basement membranes. In *Cell,* **65:** 599-610

[101] Takada, Y., Murphy, E., Pil P., Chen, C., Ginsberg, H. & Hemler, M.E. (1991). Molecular cloning and expression of the cDNA for alpha3 subunit of human alpha3/beta 1 (VLA3) an integrin receptor for fibronectin, laminin and collagen. In *Journal of Cell Biology,* **115:** 257-266

[102] Hall, D.E., Reichard, L.F., Crowley, E,. Holley, B., Moezzi, A., Sonenberg, A. & Damsky, C.H. (1990). The α1/β1 and α1/β1 integrin heterodimers mediate cell attachment to distinct sites on laminin. In *Journal of Cell Biology,* **110**: 2175-2184

[103] Elices, M.J., Urry, L.A. & Hemler, M.E. (1991). Receptor functions for the integrin VLA-3: Fibronectin, collagen and laminin binding are differentially influenced by ARG-GLY-ASP peptide and by divalent cations. In *Journal of Cell Biology,* **112**:169-181

[104] Wozniak, M.A., Modzelewska, K, Kwong, L & Keely, P.J. (2004). Focal adhesion regulation of cell behavior. In *Biochimica et Biophysica Acta – Molecular Cell Research,* **1692(2-3)**: 103-119

[105] Geiger, B., Bershadsky, A., Pankov, R. & Yamada, K.M. (2001). Transmembrane Extracellular matrix-cytoskeleton crosstalk. In *Nature Reviews Molecular Cell Biology,* **2**: 793-805

[106] Cukierman, E., Pankov, R. & Yamada, K.M. (2002). Cell interactions with three-dimensional matrices. In *Current Opinion in Cell Biology,* **14:** 633-639

[107] Sastry, S.K. & Burridge, K. (2000). Focal Adhesions: A nexus for intracellular signaling and cytoskeletal dynamics. In *Experimental Cell Research,* **261**: 25-26

[108] Zaidel-Bar, R. & Geiger, B. (2010). The switchable integrin adhesome. In *Journal of Cell Science,* **123:** 1385-1388

[109] Zaidel-Barm R, Milo, R., Kam, Z. & Geiger, B. (2007). Functional atlas of the integrin adhesome. In *Nature Cell Biology,* **9**: 858-867

[110] Shen, Y. & Schaller, M.D. (1999). Focal adhesion targeting: the critical determinant of FAK regulation and substrate phosphorylation. In *Molecular Biology of the Cell,* **10**: 2507-2518

[111] Frame, M.C., Patel, H., Serrels, B., Lietha, D. & Eck, M.J. (2010). The FERM fomain: organizing the structure and function of FAK. In *Nature Reviews Molecular Cell Biology,* **11**: 802-814

[112] Polte, T.R. & Hanks, S.K. (1995). Interaction between focal adhesion kinase and Crk-associated tyrosine kinase substrate p130Cas. In *Proceedings of the National Academy of the Sciences U.S.A.,* **92:** 10678-10682

[113] Harte, M.T., Hildebrand, J.D., Burnham, M.R., Bouton, A.H. & Parsons, J.T. (1996). p130, a substrate associated with v-Src and v-Crk, localizes to focal adhesions and binds to focal adhesion kinase. In *Journal of Biological Chemistry,* **271**: 13649-13655

[114] Turner, C.E. (2000). Paxillin and focal adhesion signaling. In *Nature Cell Biology,* **2**: E231-E236

[115] Calaib, M.B., Polte, T.R. & Hanks, S.K. (1995). Tyrosine phosphorylation of focal adhesion kinase at sites in the catalytic domain regulates kinase activity: a role for Src family kinases. In *Molecular Cell Biology,* **15:**954-963

[116] Schlaeper, D.D., Hanks, S.K., Hunter, T., van der Geer, P. (1994). Integrin-mediated signal transduction linked to Ras pathway by GRB2 binding to focal adhesion kinase. In *Nature,* **372:** 786:791

[117] Mitogen-Activated Protein (MAP) Kinase Pathways: Regulation and Physiological Functions. In *Endocrine Reviews,* **22(2**): 153-183

[118] Volberg, T., Romer, L,. Zamir, E. & Geiger, B. (2001). pp60(c-src) and related tyrosine kinases: a role in the assembly and reoganisation of matrix adhesions. In *Journal of Cell Science,* **114:** 2279-2289

[119] Ilic, D., Furata, Y., Kanazawa, S, Takeda, N., Sobue, K., Nakatsuji, N., Nomura, S., Fujimoto, J., Okada, M. & Yamamoto, T. (1995). Reduced cell motility and enhanced focal adhesion contact formation in cells from FAK-deficient mice. In *Nature,* **377(6549):** 539-544

[120] Ren, X.D., Kiosses, W.B., Sieg, D.J., Otey, C.A., Schlaepfer, D.D. & Schwartz, M.A. (2000). Focal adhesion kinase suppresses Rho activity to promote focal adhesion turnover. In *Journal of Cell Science,* **113(20):** 3673-3678

[121] Reig, G., Pulgar, E., Concha, M.L. (2014). Cell migration: from tissue culture to embryos. In *Development,* **141:** 1999-2013.

[122] Antoni, D., Burckei, H., Josset, E. & Noel, G. (2015). Three dimensional cell culture: A breakthrough *in vivo.* In *International Journal of Molecular Science,* **16(3):** 5517-5527

[123] Edmondson, R., Broglie, J.J., Adcock, A.F., Yang, L. (2014). Three-dimensional cell culture systems and their applications in drug discovery and cell-based biosensors. In *Assay and Drug Development Technologies,* **12(4)**: 207-218

[124] Fraley, S.I., Feng, Y., Krishnamurthy, R., Kim, D.H., Celedon, A., Longmore, G.D., & Wirtz, D. (2010). A distinctive role for focal adhesion proteins in three-dimensional cell motility. In *Nature Cell Biology,* **12(6):** 598-604

[125] Khetan, S. & Burdick, J.A. (2010). Patterning network structure to spatially control cellular remodeling and stem cell fate within 3-dimensional gels. In *Biomaterials,* **31**: 8288-8234

[126] Benino, K.A., Dembo, M. & Wang, Y.L. (2004). Responses of fibroblasts to anchorage of dorsal extracellular matrix receptors. In *Proceedings of the National Academy of the Sciences USA,* **101:** 18024-18029

[127] Cukierman, E., Pankov, R., Stevens, D.R. & Yamada, K.M. (2001). Taking Cell-Matrix Adhesions to the Third Dimension. In *Science,* **294**: 1708-1712

[128] Hakkinen, K.M., Harunaga, J.S., Doyle, A.D. & Yamada, K.M. (2010). Direct comparisons of the morphology, migration, cell adhesions and actin cytoskeleton of fibroblasts in four different three-dimensional extracellular matrices. In *Tissue Engineering Part A.,* **17(5-6):** 713-724

[129] Baker, B.M. & Chen, C.S. (2012). Deconstructing the third dimension – how 3D culture microenvironments alter cellular cues. In *Journal of Cell Science,* **125(13**): 3015-3024

[130] Proby, C.M., Purdie, K.J., Sexton, C.J., Purkis, P., Navsaria, H.A., Stables, J.N. & Leigh, I.M. (2000). Spontaneous keratinocyte cell lines representing early and advanced stages of malignant transformation of the epidermis. In *Experimental Dermatology,* **9(2):** 104-117

[131] Nyberg, S.L., Remmel. R.P., Mann, H.J., Peshwa, M.V., Hu, W.S. & Cerra F.B. (1994). Primary hepatocytes outperform HepG2 cells as the source of biotransformation functions in a bioartificial liver. In *Annals of Surgery,* **220(1):** 59-67

[132] Carnachan, R.J., Bokhari, M., Przyborski, S.A. & Cameron, N.R. (2006). Tailoring the morphology of emulsion-templated porous polymers. In *Soft Matter,* **2 (7):** 608-616

[133] Baharvand H., Hashemi S.M., Kazemi Ashtiani S. & Farrokhi A. (2006). Differentiation of human embryonic stem cells into hepatocytes in 2D and 3D culture systems *in vitro*. In *International Journal of Developmental Biology*, **50**:645–652

[134] Benya P.D. & Shaffer J.D. (1982). Dedifferentiated chondrocytes reexpress the differentiated collagen phenotype when cultured in agarose gels. In *Cell*, **30**:215–224

[135] Nelson C.M. & Bissell M.J. (2005). Modeling dynamic reciprocity: engineering three-dimensional culture models of breast architecture, function, and neoplastic transformation. In *Seminars in Cancer Biology*, 2005;**15**:342–352

[136] Chang, T.T. & Highes-Fulford, M. (2009). Monolayer and Spheroid Culture of Human Liver Hepatocellular Carcinoma Cell Line Cells Demonstrate Distinct Global Gene Expression Patterns and Functional Phenotypes. In *Tissue Engineering Part A*, **15(3**):559-567

[137] Roth, A. & Singer, T. (2014). The application of 3D cell models to support drug safety assessment: Opportunities & challenges. In *Advanced Drug Delivery Reviews,* **69-70**: 179-189

[138] Lei, Y. & Schafer, D.V. (2013). A fully defined and scalable 3D culture system for human pluripotent stem cell expansion and differentiation. In *Proceedings of the National Academt of the Sciences USA,* **110(52):** E5039-E5048

[139] Huang, H.L. (2010). Tryspin-induced proteome alteration during cell subculture in mammalian cells. In *Journal of Biomedical Science,* **17**

[140] Kim, S.S., Utsunomiya, H., Koski, J.A., Wu, B.M., Cima, M.J., Sohn, J., Mukai, K., Griffith, L.G. & Vacanti, J.P. (1998). Survival and function of hepatocytes on a novel three-dimensional synthetic biodegradable polymer scaffold with an intrinsic network of channels. In *Annals of Surgery,* **228(1):** 8-13

[141] Rinderknecht, H., Silverman, P., Geokas, M.C. & Haverback, B.J. (1970). Determination of trypsin and chymotrypsin with remazolbrilliant blue-hide. In *Clinica Chimica Acta,* **28(2):** 239-246

[142] Nehrer, S., Breinan, H.A., Ramappa, A., Young, G., Shortkroff, S., Louie, L.K., Sledge, C.B., Yanna, I.V. & Spector, M. (1997). Matrix collagen type and pore size influence behavior of seeded canine chondrocytes. In *Biomaterials*, **18(11**):769-776

[143] Charras, G. & Sahai, E. (2014). Physical influences of the extracellular environment on cell migration. In *Nature Reviews Molecular Cell Biology,* **15(12):** 813-824

[144] Soldatow, V.Y., LeCluyse, E.L., Griffith, L.G. & Rusyn, I. (2014). *In vitro* models for liver toxicity testing. In *Toxicology Research,* **2(1):** 23-39

[145] Gissen, P. & Arias, I.M. (2015). Structural and functional hepatocyte polarity and liver disease. In *Journal of Hepatology,* **63(4):** 1023-1037

[146] Lovett, M., Lee, K., Edwards, A. & Kaplan, D.L. (2009). Vascularization strategies for tissue engineering. In *Tissue Engineering Part B: Reviews,* **15(3):** 353-370

[147] Harma, V., Virtanen, J., Makela, R., Happonen, A., Mpindi, J., Knuuttila, M., Kohonen, P., Lotjonen, J., Kallioniemi, O. & Nees, M. (2010). Comprehensive panel of three-dimensional models for studies of prostate cancer growth, invasion and drug responses. In *PLOS One,* DOI: 10.1371/journal.pone.0010431

[148] Lama, R., Zhang, L., Naim, J.M., Williams, J., Zhou, A. & Su, B. (2013). Development, validation and pilot screening of an in vitro multi cellular three dimensional cancer spheroid assay for anti-cancer drug testing. In *Bioorganic & Medicinal Chemistry,* **21:** 922-931

[149] Ezzell, R.M., Toner, M., Hendricks, K., Dunn, J.C., Tompkins, R.G., & Yarmush, M.L. Effect of collagen gel con- figuration on the cytoskeleton in cultured rat hepatocytes. In *Experimental Cell Research* **208**, 442, 1993

[150] Mooney, D.J., Langer, R., and Ingber, D.E. Cytoskeletal filament assembly and the control of cell spreading and function by extracellular matrix. In *Journal of Cell Science,* **108(6):** 2311, 1995

[151] Kreis, T.E. & Birchmeier, W. (1980). Stress fiber sarcomeres of fibroblasts are contractile. In *Cell* **22** (2): 555–561

[152] Braga, V.M.M. (1997). The Small GTPases Rho and Rac Are Required for the Establishment of Cadherin-dependent Cell-Cell Contacts. In *The Journal of Cell Biology* **137** (6): 1421–1431.

[153] Ridley, A.J. & Hall, A. (1992). The small GTP-binding protein rho regulates the assembly of focal adhesions and actin stress fibers in response to growth factors. In *Cell* **70** (3): 389–399

[154] Du, Y., Chia, S., Han, R., Chang, S., Tang, H. &Yu, H. (2006). 3D hepatocyte monolayer on hybrid RGD/galactose substratum. In *Biomaterials* **27(33):** 5669–5680

[155] Assoian, R.K. (1997). Anchorage-dependent cell cycle progression. In *Journal of Cell Biology,* **136(1):** 1-4

[156] Giancotti, F.G. (1997). Integrin signaling: specificity and control of cell survival and cell cycle progression. In *Current Opinion in Cell Biology,* **9(5):** 691-700

[157] Bottazzi, M.E., Zhu, X., Bohmer, R.M. & Assoian, R.K. (1999). Regulation of P21cip1 expression by growth factors and the extracellular matrix reveals a role for transient ERK activity in G1 phase. In *Journal of Cell Biology,* **146(6):** 1255-1264

[158] Etienne, P.L., Baffet, G., Desvergne, B., Boisnard-Rissel, M., Glaise, D. & Guguen-Guillouzo, C. (1988). Transient expression of c-fos and constant expression of c-myc in freshly isolated and cultured normal adult rat hepatocytes. In *Oncogene Research* **3**: 255–262.

[159] Whitesides, G.M., Ostuni, E., Takayama, S., Jiang, X. & Ingber, D.E. (2001) Soft Lithography in Biology and Biochemistry. In *Annual Review of Biomedical Engineering* **3**:335-73.

[160] McNulty, J.D., Klann, T., Sha, J., Salick, M., Knight, G.T., Turng, L.S. & Ashton, R.S. (2014). High-precision robotic micro-contact printing (R-µCP) utilizing a vision guided selectively compliant articulated robotic arm. In *Lab on a Chip* **14**:1923-30.

[161] Parker, K.K., Brock, A.L., Brangwynne, C., Mannix, R.J., Wang, N., Ostuni, E., Geisse, N.A. & Adams, J.C. (2002). Directional control of lamellipodia extension by constraining cell shape and orienting cell tractional forces. In *The FASEB Journal* **16:**1195-1204.

[162] Chen, C.S., Mrkisch, M., Huang, S., Whitesides, G.M. & Ingber, D.E. (1998). Micropatterned surfaces for control of cell shape, position, and function. In *Biotechnology Progress* **14**:356-363.

[163] Wang, N., Ostuni, E., Whitesides, G.M. & Ingber, D.E. (2002). Micropatterning tractional forces in living cells. In *Cell Motility and the Cytoskeleton* **52:**97-106.

[164] Brock, A., Chang, E., Ho, C., Leduc, P., Jiang, X., Whitesides, G.M. & Ingber, D.E. (2003). Geometric determinants of directional dell motility revealed using microcontact printing. In *Langmuir* **19:**1611-1617.

[165] Jiang, X., Bruzewicz, D.A., Wong, A.P., Piel, M. & Whitesides, G.M. (2005). Directing cell migration with asymmetric micro-patterns. In *Proceedings of the National Academy of the Sciences USA* **102:**975-978

[166] Maduram, J.H., Goluch, E., Hu, H., Liu, C. & Mrkisch, M. (2008). Subcellular curvature at the perimeter of micropatterned cells influences lamellopodial distribution and cell polarity. In *Cell Motility and the Cytoskeleton* **65**:841-52.

[167] Kilian, K.A., Bugarija, B., Lahn, B.T. & Mrksich, M. (2010). Geometric cues for directing the differentiation of mesenchymal stem cells. In *Proceedings of the National Academy of the Sciences USA* **107**:4872-7.

[168] Béduer, A., Vieu, C., Arnauduc, F., Sol, J.C., Loubinoux, I. & Vaysse, L. (2012). Engineering of adult human neural stem cells differentiation through surface micropatterning. In *Biomaterials* **33:**504-14.

[169] Ghibardo, M., Di Meglio, J.M., Hersen, P. & Ladoux, B. (2011). Mechanics of cell spreading within 3D micropatterned environments. In *Lab on a Chip*, **11:** 805-812

[170] Ghibardo, M., Trichet, L., Le Digabel, J., Richert, A., Hersen, P. & Ladoux, B. (2009). Substrate topography induces a crossover from 2D to 3D behavior in fibroblast migration. In *Biophysical Journal,* **97(1):** 357-368

[171] Friedl, P., Zanker, K.S. & Brocker, E.B. (1998). Cell migration strategies in 3D extracellular matrix: differences in morphology, cell matrix interactions and integrin function. In *Microscopy Research and Technique,* **43:** 369-378

[172] Friedl, P. (2004). Prespecification and plasticity: shifting mechanisms of cell migration. In *Current Opinion in Cell Biology,* **16:** 14-23

[173] Gustafsson, M.G.L. (2000). Surpassing the lateral resolution limit by a factor of twp using structured illumination microscopy. In *Journal of Microscopy,* **198(2):** 82-87

[174] Pellegrin, S. & Mellor, H. (2007). Actin stress fibres. In *Journal of Cell Science,* **120:** 3491-3499

[175] Small, J.V., Rottner, K., Kaverina, I. & Anderson, K.I. (1998). Assembling an actin cytoskeleton for cell attachment and movement. In *Biochemica Biophysica Acta,* **1404:** 271-281

[176] Burridge, K. (1986). Substrate adhesions in normal and transformed fibroblasts: organisation and regulation of cytoskeletal, membrane and extracellular matrix compoenents at focal contacts. In *Cancer Reviews,* **4:** 18-78

[177] Heath, J.P. & Dunn, G.A. (1978). Cell to substratum contacts of chick fibroblast and their relation to the microfilament system. A correlated interference-reflexion and high voltage electron microscope study. In *Journal of Cell Science,* **29:** 197-212

[178] Heath, J.P. (1983). Behaviour and structure of the leading lamella in moving fibroblasts. I: Occurrence and centripetal movement of arc-shaped microfilament bundles beneath the dorsal cell surface. In *Journal of Cell Science,* **60:** 331-354

[179] Hotulainen, P. & Lappalainen, P. (2006). Stress fibres are generated by two distinct actin assembly mechanisms in motile cells. In *Journal of Cell Biology,* **173:** 383-394

[180] Dahl, K.N., Ribeiro, A.J.S. & Lammerding, J. (2008). Nuclear shape, mechanics and mechanotransduction. In *Circulation Research,* **102:** 1307-1318

[181] Lau, T.T., Wang, C., Png, S.W., Su, K. & Wang, D. (2011). Genipin-crosslinked microcarriers mediating hepatocellular aggregates formation and functionalities. In *Journal of Biomedical Materials Research Part A,* **96(1):** 204-211

[182] Rape, A.D., Guo, W. & Wang, Y. (2011) The regulation of traction force in relation to cell shape and focal adhesions. In *Biomaterials* **32:** 2043–51

[183] Tee, S.Y., Fu, J., Chen, C.S. & Janmey P.A. (2011). Cell shape and substrate rigidity both regulate cell stiffness In *Biophysical Journal* **100:** L25–27

[184] Kanchanawong, P., Shtengel, G., Pasapera, A. M., Ramko, E. B., Davidson, M. W., Hess, H.F. & Waterman, C.M. (2010). Nanoscale architecture of integrin-based cell adhesions In *Nature* **468:** 580-584

[185] McBeath, R., Pirone, D.M., Nelson, C.M., Bhadriraju, K. & Chen, C.S. (2004). Cell shape, cytoskeletal tension, and RhoA regulate stem cell lineage commitment. In *Development of the Cell* **6:** 483–95

[186] Sawamoto, K. & Takahashi, N. (1997). Modulation of hepatocyte function by changing the cell shape in primary culture. In *In vitro cellular and developmental biology - Animals,* **33(7):** 569-574

[187] Jagoe, R., Sowter, C. & Slavin, G. (1984). Shape and texture analysis of liver cell nuclei in hepatomas by computer aided microscopy. In *Journal of Clinical Pathology,* **37(7):** 755-762

[188] Webster, M., Witkin, K.L. & Cohen-Fix, O. (2009). Sizing up the nucleus: nuclear shape, size and nuclear-envelope assembly. In *Journal of Cell Science,* **122:** 1477-1486

[189] Nikolova, V., Leimena, C., McMahon, A.C., Tan, J.C., Chandar, S, Jogia, D., Kesteven, S.H., Michalicek, J., Otway, R., Verheyen, F., Rainer, S., Stewart, C.L., Martin, D., Feneley, M.P. & Fatkin, D. (2004). Defects in nuclear structure and function promote dilated cardiomyopathy in lamin A/C-deficient mice. In *Journal of Clinical Investigation*, **113:** 357–369.

[190] Thomas, C.H., Collier, J.H., Sfeir, C.S. & Healy, K.E. (2002). Engineering gene expression and protein synthesis by modulation of nuclear shape. In *Proceedings of the National Academy of the Sciences USA*, **99:** 1972–1977.

[191] Lelièvre, S.A, Weaver V.M., Nickerson, J.A., Larabell, C.A., Bhaumik, A., Petersen, O.W. & Bissell, M.J. (1998). Tissue phenotype depends on reciprocal interactions between the extracellular matrix and the structural organization of the nucleus. In *Proceedings of the National Academy of the Sciences USA* **95:** 14711–14716

[192] Guilak, F. (1995). Compression-induced changes in the shape and volume of the chondrocyte nucleus. In *Journal of Biomechanics*, **28:** 1529–1541

[193] Hewitt, N.J., Lechon, M.J.G., Houston, J.B., Halifax, D., Brown, H.S., Maurel, P., Kenna, J.G., Gustavsson, L., Lohmann, C., Skonberg, C., Guillouzo, A., Tuschl, G., Li, A.P., LeCluyse, E., Grootuis, G.M.M. & Hengstlr, J.G. (2007). Primary hepatocytes: current understanding of the regulation of metabolic enzymes and transporter proteins and pharmacetucal practical for the use of hepatocytes in metabolism, enzyme induction, transporter, clearance and hepatotoxicity studies. In *Drug Metabolism Reviews,* **39:** 159-234

[194] Derelanko, M.J. & Hollinger, M.A. (1995). Metabolism and Toxicokinetics of Xenobiotics. In *Handbook of Toxicology,* 1st Ed, Crc Press, New York.

[195] Wrighton, S.A Stevens, J.C. (1992). The human hepatic cytochromes-P450 involves in drug metabolism. In *Critical Reviews in Toxicology,* **22:** 1-21

[195] Guengerich, F.P. (2001). Common and uncommon cytochrome P450 reactions related to metabolism and chemical toxicity. In *Chemical Research in Toxicology,* **14:** 611-650

[196] Birgersdotter A., Sandberg R. & Ernberg I. (2005). Gene expression perturbation *in vitro*—a growing case for three-dimensional (3D) culture systems. In *Seminars in Cancer Biology*, **15:** 405–412

[197] Bhadriraju K. & Chen C.S. (2002). Engineering cellular microenvironments to improve cell-based drug testing. In *Drug Discovery Today* **7**:612–620

[198] Gurski L., Petrelli N., Jia X. & Farach-Carson M. (2010). Three-dimensional matrices for anti-cancer drug testing and development. In *Oncology Issues* **25:** 20–25

[199] Luca AC., Mersch S. & Deenen R (2013). Impact of the 3D microenvironment on phenotype, gene expression, and EGFR inhibition of colorectal cancer cell lines. In *PLoS One* **8**:e59689

[200] Wen Z., Liao Q., Hu Y., You L., Zhou L. & Zhao Y. (2013) A spheroid-based 3-D culture model for pancreatic cancer drug testing, using the acid phosphatase assay. In *Brazilian Journal of Medical Biology Research* **46:** 634–642

[201] Chitcholtan K., Sykes P. & Evans J. (2012). The resistance of intracellular mediators to doxorubicin and cisplatin are distinct in 3D and 2D endometrial cancer. In *Journal of Translational Medicine* **10**:1–16

[202] Swietach P., Hulikova A., Patiar S., Vaughan-Jones RD., Harris AL.: Importance of intracellular pH in determining the uptake and efficacy of the weakly basic chemotherapeutic drug, doxorubicin. PLoS One 2012 ;**7**:e35949

[203] Serebrisiskii, I., Castello-Cros, R., Lamb, A., Golemis, E.A. & Cukierman, E. (2008). Fibroblast-derived 3D matrix differentially regulates the growth and drug-responsiveness of human cancer cells. In *Matrix Biology,* **27(6):** 573-585

[204] Hongisto, V., Jernstrom, S., Fey, V., Mpindi, J.,Sahlberg, K.K., Kallioniemi, O. & Perala, M. (2013). High-Throughput 3D Screening Reveals Differences in Drug Sensitivities between Culture Models of JIMT1 Breast Cancer Cells. In *PLOS One,* DOI: 10.1371/journal.pone.0077232

[205] Zhao, Y., Wieman, H.L., Jacobs, S.R & Rathmell, J.C. (2008). Mechanisms and Methods in Glucose Metabolism and Cell Death. In *Methods in Enzymology*, **442**: 439-457

[206] Zawada, R.J.X., Kwan, P., Olszewski, K.L., Llinas, M. & Huang, S. (2010). Quantitative determination of urea concentrations in cell culture medium. In *Biochemical Cell Biology,* **87(3):** 541-544

[207] Prescott, L.F. (1980). Kinetics and metabolism of paracetamol and phenacetin. In *British Journal of Clinical Pharmacology* **10(S2**): 291S-198S

[208] Guengerich, F.P. (2008). Cytochrome P450 and Chemical Toxicology. In *Chemical Research in Toxicology,* **21(1):** 70-83

[209] Schlichting, I., Berendzen, J., Chu, K., Stock, A.M., Maves, A.S., Benson, D.E., Sweet, R.M., Ringe, D., Petsko, G.A. & Sligar, S.G. (2000). The catalytic pathway of cytochrome P450cam at atomic resolution. In *Science,* **287 (5458):** 1615-1622

[210] Singh, K.B. (2007). Cytochrome P450 enzyme isoforms and their therapeutic implications: An update. In *Indian Journal of Medical Science,* **61**: 102-116

[211] Provenzano, P.P & Keely, P.J. (2011). Mechanical signaling through the cytoskeleton regulates cell proliferation by coordinated focal adhesion and Rho GTPase signaling. In *Journal Of Cell Science,* **24(8):** 1195-1205

[212] Mitra, S.K., Hansan, D.A. & Schlaepfer, D.D. (2005). Focal Adhesion Kinase: in command and control of cell motility. In *Nature Reviews Molecular Cell Biology,* **6:** 56-68

[213] Selden, C., Khalil, M. & Hodgson, H.J.F. (1999). What keeps hepatocytes on the straight and narrow? Maintained differentiated function in the liver. In *Gut,* **44:** 443-446

[214] Anterburn, L.M., Zurlo, J., Yager, J.D. Overton, R.M. & Heifetz, A. H. (1995). A morphological study of differentiated hepatocytes *in vitro.* In *Hepatology,* **22(1):** 175-187

[215] Chu, X.H., Shi, X.L., Feng, Z.Q., Gu, Z.Z. & Ding, Y.T. (2009). Chitosan nanofiber scaffold enhances hepatocyte adhesion and function. In *Biotechnology Letters,* **31:** 347-352

[216] Tsang, V.L., Chen. A.A., Cho, L.M., Jadin. K.D., Sah, R.L., DeLong, S., West, J.L. & Bhatia, S.N. (2007). Fabrication of 3D hepatic tissues by additive photopatterning of cellular hydrogels. In *FASEB Journal,* **21(3):** 790-801

[217] Miranda J.P., Leite, S.B., Muller-Vieira, U., Rodrigues, A., Carrondo, M.J. & Alves, P.M. (2008). Toward extended functional hepatocyte *in vitro* culture. Tissue Eng Part C Methods.

[218] Meng Q. (2010) Three-dimensional culture of hepatocytes for prediction of drug-induced hepatotoxicity. Expert Opin. Drug Metab. Toxicol. 6:733–746

[219] Rimann M., Graf-Hausner U. (2012) Synthetic 3D multicellular systems for drug development. In *Current Opinion In Biotechnology.* **23**:803–809

[220] Ramaiahgari S.C., den Braver M.W., Herpers B., Terpstra V., Commandeur J.N., van de Water B., Price L.S. (2014) A 3D *in vitro* model of differentiated HepG2 cell spheroids with improved liver-like properties for repeated dose high-throughput toxicity studies. In *Archives of Toxicology*, **88:** 1083–1095.

[221] Westerwink, W.M.A.. & Schoonen, W.G.E.J (2007). Cytochrome p450 enzyme levels in HepG2 cells and cryopreserved primary human hepatocytes and their induction. In *Toxicology In Vitro*, **21:** 1581-1591

[222] Nakamura, K., Kato, N., Aizwara, K., Mizutani, R., Yamauchi, J. & Tanoue A. (2011). Expression of albumin and cytochrome P450 enzymes in HepG2 cells cultured with a nanotechnology-based culture plate with microfabricated scaffold. In *Journal of Toxicological Studies,* **36(5):** 625-633

[223] Guinness, P., Mueller, D., Shevchenko, V., Heinzle, E., Ingelman-Sundberg, m> & Noor, F. (2013). 3D Organotypic Cultures of Human HepaRG Cells: A Tool for In Vitro Toxicity Studies. In *Toxicological Sciences,* **133(1):** 67-78

[224] Thomas, R.J., Bhandari, R., Barrett, D.A., Bennett, A.J., Fry, J.R., Powe, D., Thomson, B.J. & Shakesheff, K.M. (2005). The Effect of Three-Dimensional Co-Culture of Hepatocytes and Hepatic Stellate Cells on Key Hepatocyte Functions *in vitro*. In *Cells Tissues Organs,* **181:** 67-79

[225] Lee-Thiedeck, C. & Spatz, J.P. (2014). Biophysical regulation of hematopoietic stem cells. In *Biomaterials Science,* **2:** 1548-1561

[226] Doyle, A.D., Petrie, R.J., Kutys, M.L. & Yamada, K.M. (2013). Dimensions in cell migration. In *Current Opinion in Cell Biology*, **25:** 642–649

[227] Zamir, E. & Geiger, B. (2001). Molecular complexity and dynamics of cell-matrix adhesions. In *Journal of Cell Science,* **114(20):** 3583-3590

[228] Miyamoto, S., Katz, B.Z., Lafrenie, R.M. &
, K.M. (1998). Fibronectin and integrins in cell adhesion, signaling, and morphogenesis. In *Annals of the New York Academy of Sciences,* **23 (857):** 119-129

[229] Nakatsuji, N. & Johnson, K.E. (1984). Experimental manipulation of a contact guidance system in amphibian gastrulation by mechanical tension. In *Nature,* **307:** 453-455

[230] Sidani, M., Wyckoff, J., Xue, C., Segall, J.E., & Condeelis, J. (2006). Probing the microenvironment of mammary tumors using multiphoton microscopy. In *Journal of Mammary Gland Biology & Neoplasia,* **11:** 151-163

[231] Doyle, A.D., Carvajal, N., Jin, A., Matsumoto, K. & Yamada, K.M. (2015). Local 3D matrix microenvironment regulates cell migration through spatiotemporal dynamics of contractility-dependent adhesions. In *Nature Communications,* **6:** doi:10.1038/ncomms9720

[232] Zhou, X., Murphy, F.R., Gehdu, N., Zhang, J., Iredale, J.P. & Benyon, R.C. (2004). Engagement of alphavbeta3 integrin regulates proliferation and apoptosis of hepatic stellate cells. In *Journal of Biological Chemistry,* **279(23):** 23996-24006

[233] Bonus, M., Sommerfield, A., Haussinger, D. & Gohlke, H. (2013). a5b1 integrins in hepatocytes act as receptors for bile acids with a (nor)ursodeoxycholane scaffold. In *European Journal of Medical Research,* **19(S1):** S13

[234] Li, S., Lao, J., Chen, B.P.C., Li, Y.S., Zhao, Y., Chu, J., Chen, K., Tsou, T.C., Peck, K. & Chien, S. (2003). Genomic analysis of smooth muscle cells in 3-dimensional collagen matrix. In *FASEB Journal,* **17:** 97-99

[235] Yamada, K.M., Pankov, R. & Cukierman, E. (2003). Dimensions and dynamics in integrin function. In *Brazilian Journal of Medical and Biological Research,* **36(8):** 959-966

[236] Ishii, I., Tomizawa, A. & Kawachi, H. (2001). Histological and functional analysis of vascular smooth muscle cells in a novel culture system with honeycomb-like structure. In *Atherosclerosis*, **158**: 377-384.

[237] Ravanti, L., Heino, J., Lopez-Otin, C. & Kahari V.M. (1999). Induction of collagenase-3 (MMP-13) expression in human skin fibroblasts by three-dimensional collagen is mediated by p38 mitogen-activated protein kinase. In *Journal of Biological Chemistry*, **274:** 2446-2455.

[238] Vaalamo, M., Mattil,a L., Johansson, N., Kariniemi, A.L., Karjalainen-Lindsberg, M.L., Kahari, V.M. & Saarialho-Kere U. (1997). Distinct populations of stromal cells express collagenase-3 (MMP-13) and collagenase-1 (MMP-1) in chronic ulcers but not in normally healing wounds. In *Journal of Investigative Dermatology*, **109:** 96-101

[239] Halliday, N.L. & Tomasek JJ (1995). Mechanical properties of the extracellular matrix influence fibronectin fibril assembly *in vitro*. In *Experimental Cell Research*, **217**: 109-117.

[240] Grinnell F. (2000). Fibroblast-collagen-matrix contraction: Growth-factor signalling and mechanical loading. In *Trends in Cell Biology*, **10**: 362-365.

[241] Kubow, K.E. & Horwitz, A.R. (2011). Reducing background fluorescence reveals adhesions in 3D matrices. In *Nature Cell Biology,* **13(1):** 3-7

[242] Friedl, P. & Brocker, E.B. (2000). The biology of cell locomotion within three-dimensional extracellular matrix. In *Cellular and Molecular Life Sciences,* **57(1):** 41-64

[243] Hell, S.W. (2003). Toward fluorescence nanoscopy. In *Nature Biotechnology,* **21(11):** 1347-1355

[244] Harunaga, J.S. & Yamada, K.M. (2011). Cell-matrix adhesions in 3D. In *Matrix Biology,* **30(7-8):** 363-368

[245] Yu, X.Z., Machesky, L.M. (2012) Cells Assemble Invadopodia-Like Structures and Invade into Matrigel in a Matrix Metalloprotease Dependent Manner in the Circular Invasion Assay. In *PLoS One* **7.** doi: 10.1371/journal.pone.0030605

[246] Deakin, N.O., Turner, C.E. (2011) Distinct roles for paxillin and Hic-5 in regulating breast cancer cell morphology, invasion, and metastasis. In *Molecular Biology of the Cell* **22:** 327–341.

[247] Costa, P., Scales, T.M.E., Ivaska, J. & Parsons, M. (2013). Integrin-Specific Control of Focal Adhesion Kinase and RhoA Regulates Membrane Protrusion and Invasion. In *PLoS ONE,* DOI: 10.1371/journal.pone.0074659

[248] Durand, R.E. & Sutherland, R.M. (1972). Effects of intercellular contact on repair of radiation damage. In *Experimental Cell Research,* **71:** 75-80

[249] dit Faute, M.A., Laurent, L., Plotin, D., Poupon, M.F., Jardellier, J.C. & Bobichon, H. (2002). Distinctive alterations of invasiveness, drug resistance and cell–cell organization in 3D-cultures of MCF-7, a human breast cancer cell line, and its multidrug resistant variant. In *Clinical Experiments of Metastasis,* **19:** 161-168

[250] St Croix, B. & Kerbel, R.S. (1997). Cell adhesion and drug resistance in cancer. In *Current Opinion in Oncology,* **9:** 549-556

[251] St Croix, B., Florenes, V.A., Rak, J.W., Flanagan, N., Bhattacharya, N. & Slingerland, J.M. (1996). Impact of the cyclin-dependent kinase inhibitor p27Kip1 on resistance of tumor cells to anticancer agents. In *Nature Medicine,* **2:** 1204-1210

[252] Isermann, P. & Lammerding, J. (2013). Nuclear mechanics and mechanotransduction in health and disease. In *Current Biology,* **23(24):** R1113-1121

[253] Wang, N., Tytell, J.D. & Ingber, D.E. (2009). Mechanotransduction at a distance: mechanically coupling the extracellular matrix with the nucleus. In *Nature Reviews Molecular Cell Biology,* **10(1):** 75-82